THE UNIVERSITY OF QUEENSLAND

AUSTRALIA

Engineering the ribbon isomer of α-conotoxins in the drug design application

Xiaosa Wu

BSc, MSc

A thesis submitted for the degree of Doctor of Philosophy at

The University of Queensland in 2019

Institute for Molecular Bioscience

Abstract

This PhD project focused on investigating the structure-activity relationships (SARs) of the ribbon isomer of α-conotoxins, providing the basis for using α-conotoxin ribbon isomers as scaffolds in drug design to target nicotinic acetylcholine receptors (nAChRs). Chapter 1 provides an introduction to the structure and function of nAChRs and to α-conotoxins, as well as introducing the concept of disulfide isomers of α-conotoxins. Chapters 2 to 5 describe the engineering of ribbon isomers of α-conotoxins for drug design application, as summarised below.

Chapter 2 describes a strategy to improve the yield of synthesis of a ribbon conotoxin, enabling the creation of mutants for SAR studies. The three-disulfide isomers of αO-conotoxin GeXIVA, *i.e.* the globular, ribbon and beads isomers, have similar potency at the α9α10 nAChR, which is considered to be a pain target. Owing to its potent activity, GeXIVA prompts further studies to investigate its analgesic potential. Unfortunately, the directed folding using orthogonal protection of cysteine residues is difficult for GeXIVA because it has a long sequence and has poor assembly yields arising from numerous Arg residues. Chapter 2 of this thesis shows that the folding of the ribbon GeXIVA could be achieved directly using rationally designed backbone cyclising linkers instead of using an orthogonal protection strategy. Additionally, backbone cyclisation of the ribbon GeXIVA was shown to improve peptide stability in human serum and have comparable activity as the parent peptide.

Chapter 3 focuses on the determination of the binding mode of an α-conotoxin, AuIB, which is an essential step for structure-based design of ribbon α-conotoxins. The ribbon isomer of α-conotoxin AuIB has 10-fold higher potency than the wild-type globular isomer at inhibiting nAChRs in rat parasympathetic neurons, and unlike its globular isoform, ribbon AuIB targets a specific stoichiometry of the α3β4 nAChR subtype. This specificity for a particular stoichiometry is remarkable and suggests that the ribbon isoform of α-conotoxins has potential applications in drug design. In Chapter 3, the binding mode and SAR of ribbon AuIB were investigated to determine the features that underpin its specific activity using a combination of molecular modelling and electrophysiology recording. An alanine scan showed that positions 4 and 9 of ribbon AuIB are the main determinants of the interactions with rat $(\alpha3)_3(\beta4)_2$ nAChR. Computational models indicated that the first loop of ribbon AuIB bound in the "aromatic box" of the acetylcholine orthosteric binding site. In contrast, the second loop and the termini of the ribbon isomer had different orientations and interactions in the binding sites than those of the globular isomer.

In Chapter 4, several computation methods for predicting mutational energies of α-conotoxins were compared, and the optimal method could be used for rational computational design. Binding free energy predictions are potentially an important tool for designing selective inhibitors based on globular and ribbon α-conotoxins but these computational methods need to be benchmarked to assess their accuracy in the context of nAChR/conotoxin systems. Computational free energy predictions are especially sensitive to the accuracy of the structural models; ultimately they should be used with high-resolution experimental structures. Unfortunately, there is so far no crystal structure of nAChR in complex with α-conotoxin. By contrast, the acetylcholine binding proteins (AChBPs), which are structurally homologous to the extracellular domains (ECDs) of the nAChRs, can be relatively easily crystallised and studied using X-ray crystallography. The crystal structures of AChBP/α-conotoxin complexes provide important information on the binding mode of the α-conotoxin. In Chapter 4, we evaluated four mutational energy prediction methods (BeAtMuSic, Foldx, MMPBSA/MMGBSA, and coarse-grained umbrella sampling) using the crystal structure of the complex between AChBP and α-conotoxin LsIA and between AChBP and LvIA, and associated experimental affinity change of these complexes after mutations. Foldx was identified as the most reliable method for mutational energy prediction. Notably, this method was successful at predicting variations with increased or decreased affinities.

Chapter 5 combined results from the two previous chapters to the study of the binding mode of the α-conotoxin GID with the α4β2 nAChR. The α4β2 nAChR is linked to a range of diseases and disorders including nicotine addiction, epilepsy, and Parkinson's and Alzheimer's diseases. Designing α4β2 nAChR selective inhibitors could help refine the role of α4β2 nAChR in disease states. In Chapter 5, we aimed to modify globular and ribbon α-conotoxin GID to selectively target the α4β2 nAChR through competitive inhibition of the α4(+)β2(−) or α4(+)α4(−) interfaces. The binding modes of the globular α-conotoxin [Gla4E]GID with rat α3β2, α4β2 and α7 nAChRs were built using computational methods, and they were validated using published experimental data. The binding mode of globular [Gla4E]GID at α4β2 nAChR can rationally explain the experimental mutagenesis data, suggesting that it could be used to design GID variants rationally. The predicted mutational energy results showed that globular [Gla4E]GID seemed to be already optimal for binding to α4β2 nAChR and its activity cannot further be improved through amino-acid substitutions. The cryo-electron microscopy structure of $(\alpha4)_3(\beta2)_2$ nAChR has been recently released, providing an optimal template to build the binding mode of the ribbon GID with $(\alpha4)_3(\beta2)_2$ nAChR using information on the binding mode of ribbon AuIB studied in Chapter 3. The Foldx predicted the

mutational energies of ribbon [Gla4E]GID at α4(+)α4(−) interface, and a number of ribbon [Gla4E]GID mutants were suggested to have desirable properties to inhibit $(\alpha4)_3(\beta2)_2$ nAChR.

Chapter 6 provides an overview of my findings and highlights the major conclusions of the thesis, as well as suggesting ideas for future studies in this field. In summary, my PhD thesis has shown that ribbon α-conotoxins can be used in the design of specific nAChR inhibitors.

Declaration by author

This thesis is composed of my original work, and contains no material previously published or written by another person except where due reference has been made in the text. I have clearly stated the contribution by others to jointly-authored works that I have included in my thesis.

I have clearly stated the contribution of others to my thesis as a whole, including statistical assistance, survey design, data analysis, significant technical procedures, professional editorial advice, financial support and any other original research work used or reported in my thesis. The content of my thesis is the result of work I have carried out since the commencement of my higher degree by research candidature and does not include a substantial part of work that has been submitted to qualify for the award of any other degree or diploma in any university or other tertiary institution. I have clearly stated which parts of my thesis, if any, have been submitted to qualify for another award.

I acknowledge that an electronic copy of my thesis must be lodged with the University Library and, subject to the policy and procedures of The University of Queensland, the thesis be made available for research and study in accordance with the Copyright Act 1968 unless a period of embargo has been approved by the Dean of the Graduate School.

I acknowledge that copyright of all material contained in my thesis resides with the copyright holder(s) of that material. Where appropriate I have obtained copyright permission from the copyright holder to reproduce material in this thesis and have sought permission from co-authors for any jointly authored works included in the thesis.

Publications included in this thesis

Wu, X., Huang, Y. H., Kaas, Q., and Craik, D. J. (2016) Cyclisation of disulfide-rich conotoxins in drug design applications. *Eur. J. Org. Chem.* **2016**, 3462-3472

Wu, X., Huang, Y. H., Kaas, Q., Harvey, P. J., Wang, C. K., Tae, H. S., Adams, D. J., and Craik, D. J. (2017) Backbone cyclization of analgesic conotoxin GeXIVA facilitates direct folding of the ribbon isomer. *J. Biol. Chem.* **292**, 17101-17112

Wu, X., Tae, H.-S., Huang, Y.H., Adams, D. J., Craik, D. J., and Kaas, Q. (2018) Stoichiometry dependent inhibition of rat α3β4 nicotinic acetylcholine receptor by the ribbon isomer of α-conotoxin AuIB. *Biochem. Pharmacol.* **155**, 288-297

Submitted manuscripts included in this thesis

No manuscripts submitted for publication

Other publications during candidature

Peer-reviewed papers

Hamdaoui, Y. E., **Wu, X**. **(Co-first author)**, Clark R., Garibaldi, J., Anangi, R., Craik, D., King, G., Dutertre, S., Kaas, Q., Herzig, V., and Nicke, A. Periplasmic expression of 4/7 α-conotoxin TxIA analogues in E. coli favours ribbon isomer formation – suggestion of a binding mode at the α7 nAChR. (In press)

Conference abstracts

Wu, X., Tae, H.-S., Huang, Y.H., Adams, D. J., Craik, D. J., and Kaas, Q. (2018) Stoichiometry dependent inhibition of rat α3β4 nicotinic acetylcholine receptor by the ribbon isomer of α-conotoxin AuIB. 5th EMBL Australia Postgraduate Symposium, Brisbane, Australia.

Wu, X., Huang, Y. H., Kaas, Q., Harvey, P. J., Wang, C. K., Tae, H. S., Adams, D. J., and Craik, D. J. (2017) Backbone cyclization of analgesic conotoxin GeXIVA facilitates direct folding of the ribbon isomer. 19th World Congress of the International Society on Toxinology, Haikou, China.

Wu, X., Huang, Y. H., Kaas, Q., Harvey, P. J., Wang, C. K., Tae, H. S., Adams, D. J., and Craik, D. J. (2017) Backbone cyclization of analgesic conotoxin GeXIVA facilitates direct folding of the ribbon isomer. 12th Australian Peptide Conference, Noosa, Australia.

Wu, X., Kaas, Q., Huang, Y. H., and Craik, D. J. (2015) Investigating structure-activity relationships and improving the biopharmaceutical properties of αO-conotoxin GeXIVA through backbone cyclisation. Third International Conference on Circular Proteins, Moreton Island, Australia.

Craik, D. J, **Wu, X.**, Huang, Y. H., and Kaas, Q. (2018) Cyclisation of conotoxins as an engineering tool to modulate folding, analgesic potency and biopharmaceutical properties. 10th International Peptide Symposium, Kyoto, Japan

Kaas, Q., **Wu, X**., Tae, H.-S., Huang, Y.H., Adams, D. J., and Craik, D. J. (2018) Inhibition of nicotinic acetylcholine receptor subtypes by the ribbon isomers of α-conotoxins. 35th European Peptide Symposium, Dublin, Ireland.

Contributions by others to the thesis

Chapter 2

- Olivier Cheneval carried out peptide synthesis using an automatic peptide synthesiser (Symphony®, Protein Technologies, Inc. USA)
- Dr Yen-Hua (Crystal) Huang taught me skills in peptide cleavage, cyclisation, oxidation and purification, and serum stability.
- Dr Quentin Kaas designed the linkers for cyclisation
- Dr Han-Shen Tae carried out the electrophysiological assays
- Dr Peta J. Harvey calculated the 3D structure of cGeXIVA_GG
- Dr Conan K. Wang carried out NMR relaxation measurements

Chapter 3

- Olivier Cheneval carried out peptide synthesis using an automatic peptide synthesiser (Symphony®, Protein Technologies, Inc. USA)
- Dr Han-Shen Tae carried out the electrophysiological assays
- Dr Yen-Hua (Crystal) Huang assisted with structural characterisation
- Dr Quentin Kaas taught me skills in homology modelling and molecular dynamics simulation

Statement of parts of the thesis submitted to qualify for the award of another degree

No works submitted towards another degree have been included in this thesis

Research Involving Human or Animal Subjects

All research involving human or animal subjects in this thesis was conducted by Professor David Adams's laboratory at The University of Wollongong.

Acknowledgements

First and foremost, I sincerely thank Professor David Craik, Dr Quentin Kaas and Dr Yen-Hua Huang. I thank Professor David Craik for giving me the opportunity to undertake my PhD in his laboratory and for his constant support. The skills and knowledge I learnt in his laboratory will benefit my future career. I would also like to thank my co-supervisor Dr Quentin Kaas for guiding me in computational modelling and opening me to the world of peptide design and for his patience in improving my academic writing and great supervision of my PhD projects. I also extend my appreciation to my co-supervisor Dr Yen-Hua (Crystal) Huang for teaching me numerous experimental skills as well as helping me settle in Brisbane when I first arrived three years ago. Her supervision in many aspects was beyond science.

I would like to acknowledge the following people who supported and helped during my PhD: Mr Olivier Cheneval for help with peptide synthesis; Dr Peta Harvey for help with NMR spectroscopy and Dr Conan Wang for help with NMR relaxation measurements; Professor David Adams for giving me the opportunity to visit his laboratory at the University of Wollongong for electrophysiological assays of my peptides and Dr Han-Shen Tae for his help with electrophysiological assays; Dr Meng-Wei Kan for the support she offered, both academically and personally; Mrs Robyn Craik for her valuable assistance in the application of IMB travel funding and the revision of my PhD thesis; Ms Ashlin Turner for her assistance in the revision of my PhD thesis; and Dr Amanda Carozzi for her administration support and help with my scholarship. I would also like to thank present and past members of the Craik lab for their friendship and assistance in the laboratory. Special thanks go to Mr Thomas Dash, who has supported and motivated me during my PhD and gave me huge help both academically and personally.

Finally, I would like to thank my wife, Junqiao Du, for her understanding, support and advice during my PhD, and my parents, Mingliu Wu and Meijuan Wu, for their endless love, never-ending support and encouragement through these years of studies. They helped me get a good education and inspired me to pursue my dreams.

Financial support

This research was supported by the Australian Research Council (DP150103990)

Keywords

α-conotoxin, ribbon isomer, nicotinic acetylcholine receptor, stoichiometry, homology modelling, molecular dynamics simulation, binding energy, biological activity, drug design

Australian and New Zealand Standard Research Classifications (ANZSRC)

ANZSRC code: 030402, Biomolecular Modelling and Design, 25%
ANZSRC code: 030406, Proteins and Peptides, 50%
ANZSRC code: 060112, Structural Biology (incl. Macromolecular Modelling), 25%

Fields of Research (FoR) Classification

FoR code: 0304, Medicinal and Biomolecular Chemistry, 75%
FoR code: 0601, Biochemistry and cell biology, 25%

Table of Contents

Lists of Figures

List of Tables

List of Abbreviations

ACh	Acetylcholine
AChBP	Acetylcholine binding protein
Acm	S-acetamidomethyl
Boc	Tert-butoxycarbonyl
Ca_v	Voltage-dependent calcium channel
CG_US	Coarse-grained umbrella-sampling
ΔΔG	Mutational energy
ECD	Extracellular domain
EM	Energy minimisation
Fmoc	9-Fluorenylmethoxycarbonyl
gAuIB	Globular AuIB
gGID	Globular GID
gGID*	[Gla4E] globular GID
GPCR	G protein-coupled receptor
HSQC	Heteronuclear single quantum coherence
ICK	Inhibitor cystine knot
ICD	Intracellular domain
IC_{50}	Half-maximal inhibitory concentration
K_v	Voltage-gated potassium channels
MD	Molecular dynamics
MNP	Marine natural product
nAChR	Nicotinic acetylcholine receptor
Na_v	Voltage-gated sodium channel
NCL	Native chemical ligation
NET	Norepinephrine transporter
NMR	Nuclear magnetic resonance
NOESY	Nuclear overhauser effect spectroscopy
PMF	Potential of mean force
rAuIB	Ribbon AuIB
rGID	Ribbon GID
rGID*	[Gla4E] ribbon GID
RMSD	Root-mean-square deviations

RP-HPLC	Reversed-phase high performance liquid chromatography
SAR	Structure-activity relationship
SPPS	Solid-phase peptide synthesis
TMD	Transmembrane domain
TFA	Trifluoroacetic acid
TOCSY	Two-dimensional total correlation spectroscopy
Trt	Trityl
US	Umbrella-sampling

Chapter 1: Introduction

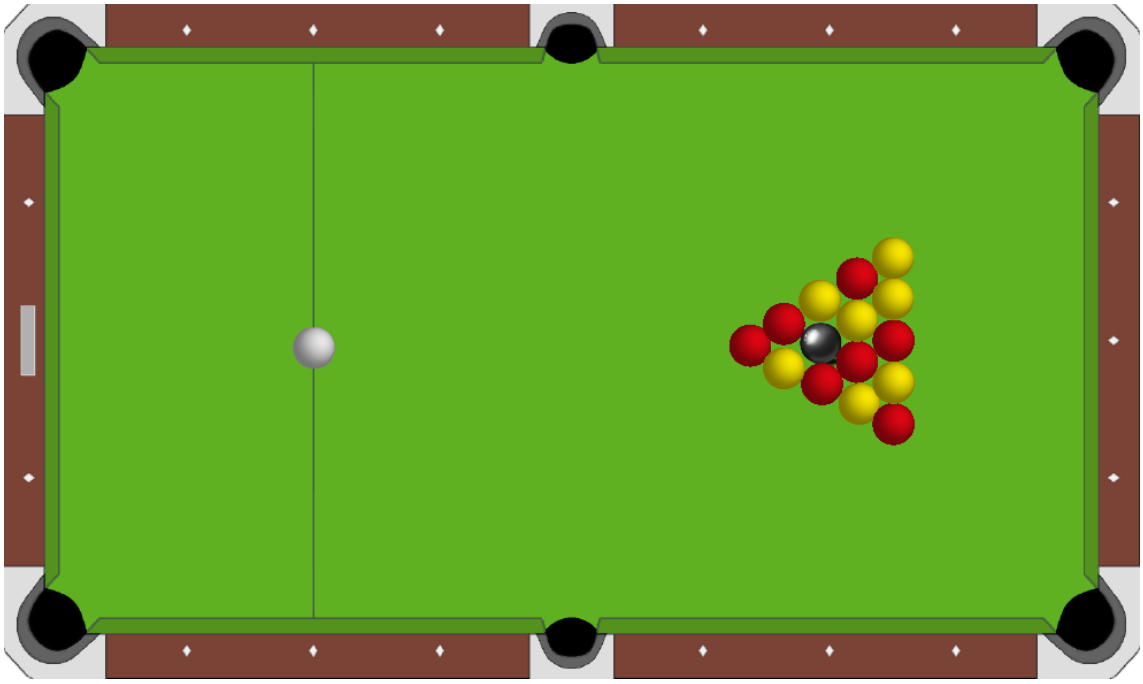

Publications included in this chapter

1. **Wu, X.**, Huang, Y. H., Kaas, Q., and Craik, D. J. (2016) Cyclisation of disulfide-rich conotoxins in drug design applications. *Eur. J. Org. Chem.* **2016**, 3462-3472

Contributions

Xiaosa Wu was responsible for the following work:

- 60% of conception and design
- 100% of data collection
- 70% analysis of data
- 90% drafting and writing

1.1 Overview

The marine environment provides plenty of habitats that support life, with the biodiversity of marine species accounting for half of the global species (1). Marine organisms produce many kinds of bioactive marine natural products (MNPs) whose activity significantly differs from bioactive compounds obtained from terrestrial environments, making them interesting from a pharmacological perspective (2). Thousands of new MNPs have been characterised over past years (3,4), providing a valuable source for many pharmaceutical companies positioning themselves to reap the benefit by developing MNP-based novel drugs. More than 30 MNP-based drugs are in clinical trials to treat various diseases (5,6), such as pain and cancer. The FDA has approved three MNPs: Prialt®, a disulfide-rich peptide from *Conus magus* that is used to treat neuropathic pain (7,8); Adcetris®, an antibody-drug conjugate medication used to treat relapsed or refractory Hodgkin lymphoma and systemic anaplastic large cell lymphoma. It was derived from a peptide isolated from a mollusk associated cyanobacteria (9); and Yondelis®, a drug initially isolated from *Ecteinascidia turbinate* and used to treat soft tissue sarcoma and recurrent platinum-sensitive ovarian cancer (10). Hence, the potential of MNPs to be developed into therapeutics is substantial.

The disulfide-rich conopeptides from the venom of the marine cone snails is a large class of MNPs, and several compounds from this class are drugs or drug leads, such Prialt®, Vc1.1, RgIA and MrIA (11). This thesis focuses on conopeptides and their potential in drug design, specifically the α-conopeptide or α-conotoxin, which target the pharmacologically important nicotinic acetylcholine receptors (nAChRs). This chapter will introduce the general background on nAChRs and conopeptides along with the aims and scope of this thesis.

1.2 nAChRs

nAChRs belong to the pentameric Cys-loop family receptors and are integral allosteric membrane proteins. They can be divided into muscle-type and neuronal-type nAChRs, and are involved in a broad range of physiological processes (12-14). Five subunits (α1, β1, δ, γ and ε) form the muscle-type nAChRs, and 12 subunits are known to assemble to form neuronal-type nAChRs. The 12 neuronal subunits are further classified into two superfamilies, namely the α subunits (α2-α10) and the β subunits (β2-β4). The subunits are expressed in the nervous system and cochlea as well as in some non-neuronal tissues (13).

The combinatorial assembly of nAChR subtypes into homo- and hetero-pentamers creates a large number of nAChR subtypes, which are involved in different physiological aspects and thus are connected with various pathologies (15). α1β1εδ AChRs are involved in the treatment of amyotrophic lateral sclerosis therapy (16). The nAChR subtypes displaying two or three α3 subunits (α3-containing nAChRs) are engaged in a wide range of diseases, including chronic pain, cancer and cardiovascular diseases (17). The α4β2 nAChR subtype is a potential target for several pathologies, such as nicotine addiction, depression, and Parkinson's and Alzheimer's diseases (18-20). Some α6-containing nAChRs have been implicated in the development of neuropathic pain (21) and addiction to nicotine or alcohol (22). The homomeric α7 nAChR is involved in memory and cognitive functions, and is a potential target for Alzheimer's disease (20). The α9α10 is present in outer hair cells (23) and lymphocytes (24,25) and is a potential target for the treatment of neuropathic pain (26,27). The different physiological involvement of each subtype emphasises the importance of developing selective probes for each nAChR subtype.

1.2.1 Structure of nicotinic receptor subtypes

The first glimpse of the structure of a nAChR came from a low resolution (4 Å) electron microscopy structure of a fish muscle-type nAChR (PDB: 2BG9) (28), which shows that the five subunits are arranged symmetrically around a central pore. The nAChR structures are divided into three domains: a hydrophilic extracellular domain (ECD), a transmembrane domain (TMD), which consists of four mainly hydrophobic transmembrane segments (M1-M4) in each subunit, and a hydrophilic intracellular domain (ICD) (Figure 1.1A). Higher-resolution structural information on nAChRs has recently become available with the determination of the X-ray crystal structure of the ECD of the human homomeric α2 nAChR in complex with the agonist epibatidine at 3.2 Å (PDB: 5FJV) (29); the X-ray crystal structure of the human heteromeric $(\alpha4)_2(\beta2)_3$ nAChR in complex with the agonist nicotine at 3.9 Å (PDB: 5KXI) (30) and the cryo-electron microscopy structure of $(\alpha4)_3(\beta2)_2$ nAChR with the agonist nicotine at 3.9 Å (PDB: 6CNK) (31). In these structures, the agonists are deeply buried in the orthosteric ACh binding site located at the α-β interface in the ECD (orthosteric ACh binding site; Figure 1.1B). The interaction of the agonists with the ECD triggers the opening of the channel in the TMD (29-31).

In neuronal nAChRs, each subunit in the ECD is composed of one α-helix, which lines the pore, and two β-sheets made of 10 β-strands (Figure 1.1A and B). The ACh binding site in

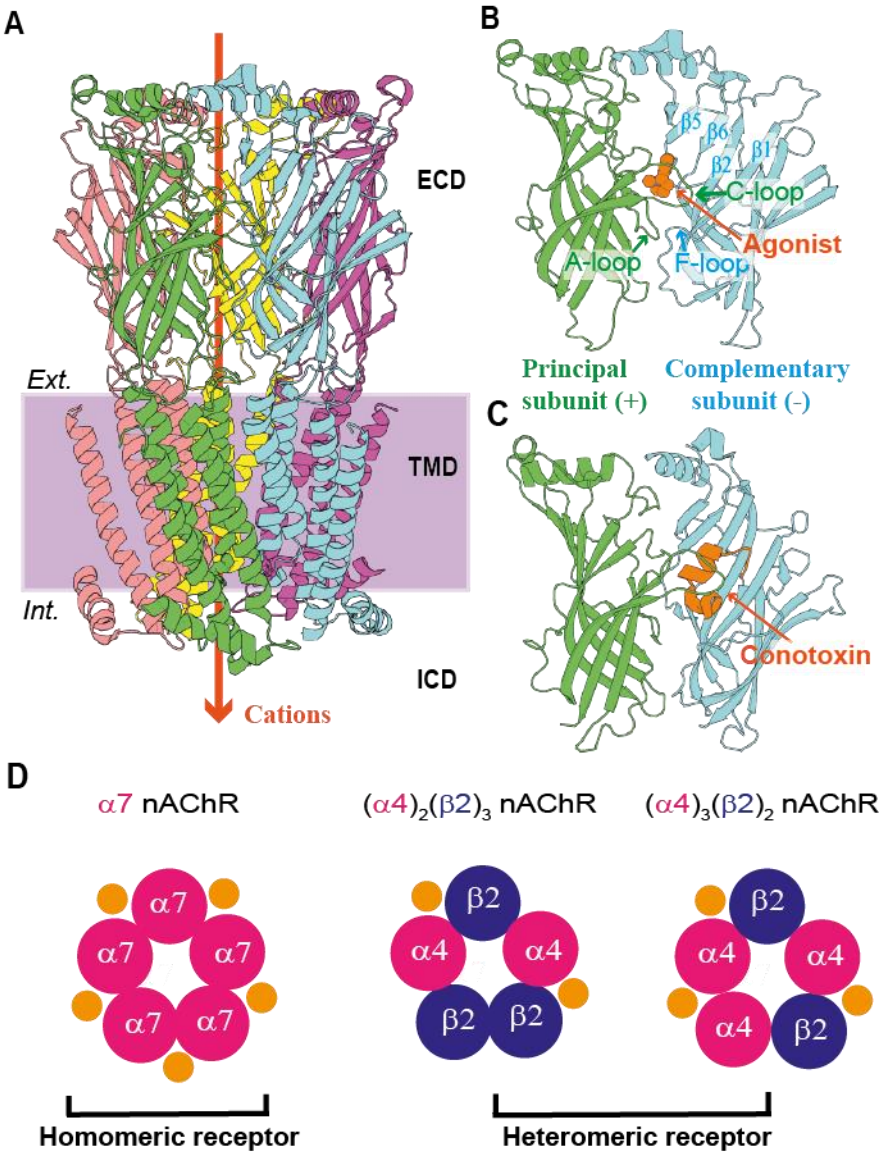

Figure 1.1 Basic structure of neuronal nAChRs. A: The structure of nAChRs comprises three domains: an extracellular domain (ECD), a transmembrane domain (TMD), and an intracellular domain (ICD; ICD has not been resolved in the crystal structure). The ribbon representation of the nAChR used the coordinates from the X-ray crystallography structure of the α4β2 nAChR (PDB ID: 5KXI). The membrane is represented by a purple rectangle, the extracellular (*Ext.*) and intracellular (*Int.*) sides of the membrane are indicated. B: Structure of the agonist binding site in the ECD. C: Crystal structure of α-conotoxin PnIA (orange) binding to *Aplysia californica* AChBP. D: Simplified diagram of the subunit arrangement of homomeric α7 nAChR and heteromeric α4β2 nAChRs. The ACh binding sites are identified by orange discs. The nAChRs are shown as seen from the extracellular side, parallel to the membrane with the pore in the centre of the pentamer. The C-loop of each subunit is indicated by a curved line. The α7(+)α7(-), α4(+)β2(-) and α4(+)α4(-) agonist binding sites are indicated by orange discs.

neuronal nAChR subtypes is differently contributed by two subunits: the principle (+) subunit is typically an α subunit (α2, α3, α4, α6, α7 or α9) (13,32) and contacts the agonist with the A-

, B- and C-loops; and the complementary (–) subunit (which could be an α or a β subunit) contributes to the binding site through the β-strands 2, 5 and 6 (Figure 1.1B) (13,33-36).

Although there is no available experimental structure of nAChRs in complex with α-conotoxins, the acetylcholine binding proteins (AChBPs) are homologous to ECDs of the nAChRs, which can be relatively easily crystallised and studied using X-ray crystallography. Despite low sequence identity with nAChRs, the AChBPs have a similar three-dimensional structure to nAChRs and can bind ACh as well as other ligands, such as α-conotoxins. AChBPs are therefore considered as structural surrogates of nAChR ECDs (37). A large number of X-ray structures of AChBP bound to various ligands have been determined, and seven α-conotoxins have been crystallised in complex with AChBP (38-43), namely the α-conotoxins PnIA (PDB:2BR8), ImI (PDB:2BYP and 2C9T), TxIA (PDB:2UZ6) and more recently LvIA (PDB:5XGL), GIC (PDB:5CO5), LsIA (PDB:5T90) and PeIA (PDB:5JME).

Figure 1.1C illustrates how conotoxin PnIA occupies the ACh binding site of AChBP. All seven crystal structures of conotoxin/AChBP display a very similar binding mode. Homomeric nAChRs have five identical binding sites (*e.g.* α7 nAChR; Figure 1.1D). In contrast, the ACh binding sites of heteromeric nAChRs can be different and can vary with different stoichiometries, *i.e.* the number of subunits of a given type. For example, α4β2 nAChR exists *in vivo* as two main stoichiometries: the $(\alpha4)_3(\beta2)_2$ nAChR and the $(\alpha4)_2(\beta2)_3$ nAChR (44). The $(\alpha4)_2(\beta2)_3$ has two binding sites but the other stoichiometry displays an additional binding site between two α4 subunits (noted α4(+)/α4(-) binding site; "+" and "-" means the principle and complementary subunits, respectively) (33), as illustrated in Figure 1.1D.

1.2.2 nAChR stoichiometries

Different subunit stoichiometries with distinct functional properties have been identified in heteromeric nAChR subtypes (34-36,44). The $(\alpha4)_2(\beta2)_3$ and $(\alpha4)_3(\beta2)_2$ differ in their sensitivities to agonists, antagonists and allosteric modulators, and have distinct single-channel conductance, mean open lifetime, activation and deactivation kinetics. These differences arise from an additional agonist binding site located at the α4(+)α4(-) interface for the $(\alpha4)_3(\beta2)_2$ nAChR (33,45,46). Interestingly, the two α4(+)β2(-) binding sites, which are surrounded by different neighbouring subunits, contribute differently to the activation within and between the $(\alpha4)_2(\beta2)_3$ and $(\alpha4)_3(\beta2)_2$ isoforms (47). Subunit stoichiometries of other nAChR subtypes such as the α3β4, α7β2 and α9α10 nAChR have been reported (34-36). In these receptors, an

additional binding site was predicted to exist at the α3(+)α3(-), α7(+)α7(-) and α9(+)α9(-), affecting the function of the α3β4, α7β2 and α9α10 nAChR subtypes, respectively (34-36). Although the subunit stoichiometries of nAChR subtypes were shown to have different functions, the connection between these different functions and pathophysiology states is still unknown, mostly because the identification of nAChR subtype stoichiometries is challenging.

1.3 Toxins from cone snails

Marine snails of the genus *Conus* produce a vast array of bioactive peptides used primarily for prey capture and defence against predators (48-50). Most of these peptides, namely conopeptides, bind to a range of mammalian ion channels and receptors that have been implicated as targets in some diseases, including pain, Alzheimer's disease, Parkinson's disease, schizophrenia, epilepsy, cancer, and tobacco addiction. Conopeptides are divided into two main classes, those that contain one or no disulfide bond and those that contain two or more disulfide bonds; with the latter referred to as conotoxins (48).

Each cone snail species can produce up to thousands of conopeptides (51,52), and it is estimated that more than 100,000 different conopeptides exist (53). They are typically 10 to 30 residues in size and are often post-translationally modified. ConoServer (www.conoserver.org), a database of conopeptides, catalogues more than 2,000 such peptides (54,55). In addition to the broad classification in disulfide-rich and disulfide-poor peptides, conopeptides are classified according to three other criteria: their evolutionary relationships (gene superfamily classification), the cysteine residue patterns along their primary sequence (cysteine framework classification; Table 1.1), and their activity at pharmacological targets (pharmacological family classification; Table 1.2) (56).

Table 1.1 Cysteine frameworks of conotoxins[a]

Framework	Cysteine pattern	No. of cysteines	No. of conotoxins[b]
I*	CC-C-C	4	366
II	CCC-C-C-C	6	3
III	CC-C-C-CC	6	334
IV	CC-C-C-C-C	6	57
V	CC-CC	4	206
VI/VII*	C-C-CC-C-C	6	705
VIII	C-C-C-C-C-CC-C-C-C	10	23
IX*	C-C-C-C-C-C	6	39
X	CC-C.(PO)[c]C	4	10
XI	C-C-CC-CC-C-C	8	109
XII	C-C-C-C-CC-C-C	8	49
XIII	C-C-C-CC-C-C-C	8	4
XIV	C-C-C-C	4	93
XV	C-C-CC-C-C-C-C	8	29
XVI	C-C-CC	4	12
XVII	C-C-CC-C-CC-C	8	1
XVIII	C-C-CC-CC	6	2
XIX	C-C-C-CCC-C-C-C-C	10	2
XX	C-CC-C-CC-C-C-C-C	10	43
XXI	CC-C-C-C-CC-C-C-C	10	6
XXII	C-C-C-C-C-C-C-C	8	22
XXIII	C-C-C-CC-C	6	6
XXIV	C-CC-C	4	6
XXV	C-C-C-C-CC	6	1
XXVI	C-C-C-C-CC-CC	8	1

[a] Frameworks with an asterisk are those that have been cyclised. [b] Data from ConoServer (54,55). [c] Any amino acid residue followed by either a proline (P) or hydroxyproline (O) residue.

Table 1.2 Pharmacological classes of conotoxins[a]

Class	Target	Representative conotoxin(s)	Cysteine framework	Refs
α (alpha)	Nicotinic acetylcholine receptors (nAChR)	Vc1.1*	I, II, III, IV, V, VIII, XIV, XX, XXIV	(57)
γ (gamma)	Neuronal pacemaker cation currents (inward cation current)	PnVIIA, TxVIIA	VI/VII	(58)
δ (delta)	Voltage-gated Na channels (agonist, delay inactivation)	EVIA*	VI/ VII, XXVII	(59)
ε (epsilon)	Presynaptic calcium channels or G protein-coupled presynaptic receptors	TxVA	V	(60)
ι (iota)	Voltage-gated Na channels (agonist, no delayed inactivation)	RXIA	III, XI	(61)
κ (kappa)	Voltage-gated K channels (blocker)	PVIIA*	III, IV, VI/ VII, XI, XIV, XXVII	(62)
μ (mu)	Voltage-gated Na channels (antagonist, blocker)	SIIIA*, MrVIB*	III, IV, V, VI/VII	(63,64)
ρ (rho)	α1-Adrenoceptors (GPCR)	TIA*	I	(65)
σ (sigma)	Serotonin-gated ion channels (GPCR)	GVIIIA*	VIII	(66)
τ (tau)	Somatostatin receptor	CnVA	V	(67)
χ (chi)	Neuronal noradrenaline transporter	MrIA*	X	(65)
ω (omega)	Voltage-gated calcium channels (blocker)	MVIIA*	VI/VII, XVI, XXVI	(68)

[a] Conotoxins labelled with an asterisk were reported to have clinical potential in pain and cardiac reperfusion.

Conotoxins have attracted considerable attention as drug leads due to their high selectivity for ion channels, transporters and receptors (48). The pharmacological properties of representative conotoxins are listed in Table 1.2, with some reported to have clinical potential in the treatment of neuropathic pain (50,56,69-73). Presently, there is only one conotoxin-based drug to have reached the clinic: MVIIA (ziconotide/Prialt), a peptide derived from *Conus magus*, which has been approved since 2004 as a drug for the treatment of neuropathic pain (7,8). Its applications

are primarily directed at late stage cancer or AIDS patients who are intolerant or non-responsive to morphine therapy as it requires intrathecal injection.

1.4 Conotoxins as drug leads

1.4.1 Interactions between ω-conotoxins and calcium channels

Voltage-dependent calcium channels (Ca_v) are complexes of several subunits, including a pore-forming α1 subunit, and several associated subunits (α2δ, β1–4 and γ subunits). There are 10 human Ca_v α1 isoforms, which can be classified into five types: Ca_v1.1–1.4 (long-lasting L-type), Ca_v2.1 (P/Q-type), Ca_v2.2 (neural non-L N-type), Ca_v2.3 (residual R-type), and Ca_v3.1–3.3 (transient T-type). These isoforms are associated with a range of diseases, including neuropathic pain and neurological disorders (74-76). ω-Conotoxins act at mammalian Ca_v channels and especially as inhibitors of neuronal Ca_v2.1 and Ca_v2.2 (77-79). Ca_v2.2 is expressed by nociceptive primary afferent neurons and has been reported to play a crucial role in pain signalling (80). ω-Conotoxin MVIIA antagonises N-type Ca_v2.2 channels with 100-fold greater potency than morphine and is used in the clinic to treat chronic pain (81). Positions Lys2, Arg10, Leu11, Tyr13 and Arg21 of MVIIA have been reported to be important for its affinity to Ca_v2.2 (77,82-84).

1.4.2 Interactions between conotoxins and voltage-gated sodium channels

Human voltage-gated sodium channels (Na_v) comprise nine isoforms (Na_v1.1–1.9) (85-88). Each isoform is made up of four homologous domains, comprising a voltage-sensing unit formed by four α-helices and a central pore contributed by two α-helices from each of the four domains. Na_v isoforms are expressed in the central nervous system, cardiac myocytes and skeletal muscle, and they are associated with some diseases (85-88).

Cone snails produce several families of Na_v modulators, including μ-, δ- and ι-conotoxins (61,89-91), which have various activity on Na_v channels. Here we focus on μ-conotoxins because some members of this family have been reported to be promising drug candidates. Framework III μ-conotoxins target the Na_v channel pore (92) and are selective inhibitors of Na_v1.4 and/or Na_v1.2 (93). For example, μ-SIIIA is an irreversible blocker of Na_v1.2, which has clinical potential in the treatment of pain (94). Structure-activity relationship (SAR) studies show that Lys11, Trp12, Arg14, Asp15, His16 and Arg18 of SIIIA are key residues modulating its activity (95). Framework IV/VII μ-conotoxins often referred to as μO-conotoxins, act on

the voltage sensor of Na_v domain II (96). μO-MrVIA and MrVIB selectively target $Na_v1.8$, which is associated with neuropathic and inflammatory pain, and show analgesic effects in animal models (64,97,98). There are currently no detailed SAR studies reported on these peptides.

1.4.3 Interactions between κ-conotoxins and voltage-gated potassium channels

Voltage-gated potassium channels (K_v) are tetramers of four identical α subunits, each having a voltage-sensor unit and contributing to the central pore, similarly to the individual domains of Na_v. The human genome has 40 K_v α-subunit genes, which are classified into 12 functional classes, including outward-rectifying, inwardly-rectifying or slowly inactivating, as described in the IUPHAR database (99).

Eleven κ-conotoxins that block K_v channels, have been discovered so far, and they display a range of cysteine frameworks, including Frameworks III, IV, VI/VII, XI, and XVI. Two κ-conotoxins are disulfide-poor conopeptides. Most of these conotoxins have μM to high nM activity, and the most active κ-conotoxin, PVIIA, blocks the *shaker* K_v channel with an half-maximal inhibitory concentration (IC_{50}) of 57 nM (100). This 27-residue conotoxin exhibits cardio-protective properties in animal models and has clinical potential associated with cardiac reperfusion (101). SAR studies of PVIIA show that Arg2, Lys7, Phe9, Phe23, Asn24 and Lys25 are important for blocking the pore of the *shaker* K_v channel (100,102,103).

1.4.4 Interactions between conotoxins and G protein-coupled receptors

G protein-coupled receptors (GPCRs) are renowned for being the class of receptor that is the most targeted by current drugs. These receptors are highly diverse and account for about 400 human coding genes (104). The GPCRs targeted by conopeptides are the α1-adreno receptors, which are associated with the central nervous system and are pharmaceutical targets implicated in cardiovascular diseases. There are three homologous α1-adrenoceptor subtypes: α_{1A}, α_{1B} and α_{1D} (105). ρ-Conotoxin TIA, isolated from *Conus tulipa*, is a selective inhibitor of the α_{1B}-adrenoceptor with an IC_{50} of 2 nM (65,106). SAR studies showed that residues Asn2, Trp3, Arg4, Leu7, Ile8 and Arg12 are important for the activity of TIA at the α_{1B} subtype (107).

1.4.5 Interactions between conotoxins and the norepinephrine transporter

χ-Conotoxins are inhibitors of the norepinephrine transporter (NET). Many neurological conditions, such as neuropathic pain, depression and anxiety, are related to NET function (108). χ-MrIA specifically acts on NET and a slightly modified analogue, Xen2174, progressed to clinical trial (phase II) as an analgesic; although, ultimately it was withdrawn due to safety concerns (109). The native disulfide connectivity of MrIA is a ribbon isomer (Cys I–Cys IV, Cys II–Cys III) and displays a Framework X (65). The 3D structure of MrIA revealed that it adopts a hairpin structure and that the Cys I–Cys IV and the Cys II–Cys III disulfide bonds are located on opposite sides of the β-sheet (110). Gly6, Tyr7, Lys8 and Leu9, which are in the γ-turn, as well as His11 in Loop 2, are thought to interact with the NET (111).

1.4.6 Interactions between conotoxins and ligand-gated ion channels

The two pharmacological families of conotoxins acting on LGICs are the α- and σ-conotoxins, which act on nAChRs and serotonin-gated ion channels, respectively (72). The best studied of the two pharmacological families, the α-conotoxins, block nAChRs by competing with acetylcholine (72,112). The general background of the α-conotoxins and the studies about isomers of the α-conotoxins are introduced below.

1.4.6.1 α-Conotoxins are potent and specific inhibitors of nAChR subtypes

α-Conotoxin is the largest class of conotoxins (113). Most of them have a size between 12 and 19 amino acid residues (56). Because of their small size, they can be chemically synthesised relatively easily, and their selectivity and potency for important molecular targets make them interesting candidate drug leads. Most α-conotoxins share a conserved cysteine pattern (CC-C-C, Figure 1.2). The length of the two loops existing between Cys II and Cys III (loop m) and between Cys III and Cys IV (loop n) is used to classify them into different classes noted m/n (Figure 1.2). The most common α-conotoxin classes are the 3/5, 3/6, 4/2, 4/3, 4/4, 4/5, 4/6, 4/7, 4/8, 5/2, 5/5 and 5/8 (114,115). The four cysteine residues can theoretically form three disulfide connectivities (Figure 1.2), which are designated as the globular isomer (Cys I-III, Cys II-IV), ribbon isomer (Cys I-IV, Cys II-III) or bead isomer (Cys I-II, Cys III-IV). These disulfide connectivities play an important role in determining the activity of α-conotoxin against specific nAChR isoforms (112,116). The globular isomer is displayed by wild-type α-conotoxins, but the ribbon connectivity has been shown to also be active in some cases and to have interesting properties.

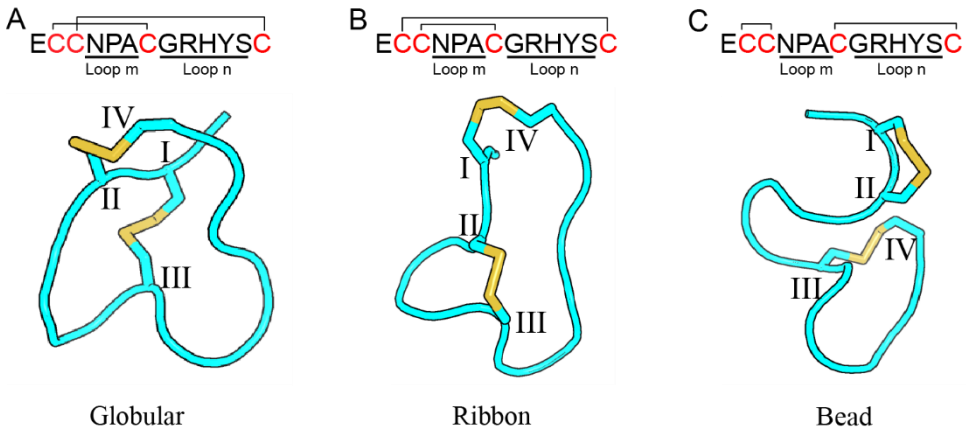

Figure 1.2 Three-dimensional nuclear magnetic resonance (NMR) solution structure of the three disulfide isomers of α-conotoxin GI. Cysteines are numbered with Roman numerals, and the disulfide bonds are shown as yellow sticks. A: the globular isomer (PDB: 1XGA); B: the ribbon isomer (PDB: 1XGB); C: the bead isomer (PDB: 1XGC). The structure shown for each isomer is the lowest energy conformer from an ensemble of the 35 (globular), 24 (ribbon) and 25 (bead) NMR models.

1.4.6.2 Studies on some representative globular α-conotoxins

A number of comprehensive reviews have described the structure-activity relationship (SAR) of globular α-conotoxins (72,112). Several globular α-conotoxins, including LvIA, TxID, TxIB, BuIA, ImI, Vc1.1 and RgIA, have therapeutic potential arising from their high selectivity and potency for certain nAChR subtypes. Here, I give a brief overview of these α-conotoxins in their SAR studies.

LvIA selectively and potently inhibits both human and rat α3β2 nAChR with IC_{50}s of 17.5 nM and 8.67 nM, respectively (117). The Val111 of β2 subunit contributes to the binding of LvIA on α3β2 nAChR (118) and the crystal structure of Ac-AChBP in complex with LvIA suggested that Asn9 and Asp11 of LvIA were important for the selectivity on α3β2 nAChR (41). TxID selectively targets the rat α3β4 nAChR and alanine scanning results suggested that Gly1, His5, Pro6, Val7, Met11 and Pro13 are important for the biological activity of TxID, and the [S9K]TxID only targets α3β4 with IC_{50} of 6.9 nM (119-121). TxIB and [T5A; P6O]BuIA selectively blocks the α6/α3β2β3 and α6/α3β4 nAChR, respectively (122,123). ImI inhibits the rat α7 and α9 nAChRs (124) as well as the human α3β2 nAChR (125). SAR studies have shown that Asp5, Pro6, Arg7 and Trp10 of ImI are important for targeting the α7 nAChR (126,127). Vc1.1 and RgIA inhibit the α9α10 nAChR with IC_{50} values of 19 nM and 4.5 nM, respectively (27,128). SAR studies show that Ser4, Asp5, Pro6, Arg7, Asn9, Asp11, His12, Pro13, Glu14

and Ile15 of Vc1.1 are important for its activity and Asp5, Pro6, Arg7 and Arg9 are key residues for RgIA activity (129,130).

1.4.6.3 Studies of ribbon and bead α-conotoxins

Research on the ribbon and/or bead α-conotoxins is summarised below (Table 1.3):

GI

α-Conotoxin GI belongs to the 3/5 class and targets the muscle-type nAChR. The native globular isomer was shown to have 10-fold greater potency than the other two isomers in mice (131). Another study concluded that globular GI has an IC_{50} of 20 nM at rat α1β1δγ/ε nAChR expressed in *Xenopus* oocytes (Ach = 500 nM) (124). Gehrmann *et al.* studied the structures of the three isomers of GI, showing that the globular isomer has a well-defined and rigid structure, whereas the two non-native isomers have multiple conformers in solution (Figure 1.2) (132).

ImII

α-Conotoxin ImII belongs to the 4/3 class and inhibits the rat and human α7 nAChRs as well as the human muscle-type nAChR. Ellison *et al.* suggested that ImII inhibits the α7 nAChR subtype using a novel binding site differing from the binding site on the α7 nAChR targeted by ImI (125,133). It was demonstrated that both globular and ribbon isomers of ImII can target the human α7 nAChR , with IC_{50} = 1.5 μM and IC_{50} = 3 μM, respectively, and the muscle type nAChRs with IC_{50} = 9.5 ± 3.8 μM; IC_{50} = 2.6 ± 0.4 μM, respectively (134).

BuIA

α-Conotoxin BuIA belongs to the 4/4 class, and its globular isomer inhibits the rat α6/α3β2 and α6/α3β4 nAChR with IC_{50} = 258 pM and 1.54 nM, respectively (135). Interestingly, the 3D structure of the globular isomer showed that it has three conformations in solution, whereas the ribbon isomer only has a single well-defined structure (136). Globular BuIA also blocks α3β2 and α3β4 nAChR, with IC_{50} of 4.8 ± 0.4 nM and 59.1 ± 2.3 nM, respectively, but the ribbon isomer does not have any activity at these subtypes (136). One potential explanation for this difference in potency is that Pro6 and Pro7 adopt a *trans/trans* conformation in conformer A of globular BuIA but are in a *trans/cis* conformation in the ribbon isomer (136). This different isomerisation of the Pro residues results in a different backbone conformation and therefore side chain presentation at the receptor (136). Additionally, the structure of globular BuIA

contains a two-turn helical motif associated with binding to α3-subunit of neuronal nAChRs (136).

AuIB

α-Conotoxin AuIB belongs to the 4/6 class and selectively inhibits α3β4 nAChR. Dutton *et al.* reported that the ribbon isomer of AuIB (IC_{50} = 0.1 nM) has 10-fold higher potency than the globular isomer (IC_{50} = 1.2 nM) in rat parasympathetic neurons (137). By contrast, another study showed that globular AuIB has more potency than the ribbon AuIB on α3β4 nAChR expressed in Xenopus oocytes (138). Grishin *et al.* suggested that these apparently conflicting results could be explained if the two isomers of AuIB have differential sensitivity to the two main stoichiometries of the α3β4 nAChR, *i.e.* if they have different activity at $(\alpha3)_3(\beta4)_2$ and the $(\alpha3)_2(\beta4)_3$ (139). A mutational study of globular AuIB was carried out, and Phe9 was shown to be the most critical residue for the activity (140). The mutational study of ribbon AuIB is reported in Chapter 3.

TxIA

α-Conotoxin TxIA belongs to the 4/7 class and selectively blocks α3β2 nAChR. The globular TxIA potently inhibited rat α3β2 nAChRs with an IC_{50} of 5.4 nM, whereas the ribbon TxIA has an IC_{50} of 430 nM (141). The bead isomer has little activity at the α3β2 nAChR at 5 μM. Globular TxIA was shown using circular dichroism to have an α-helical structure because the CD spectrum displayed two minima around 208 nm and 222 nm. The bead TxIA exhibited a minimum at around 200 nm, suggesting a random coil conformation and no α-helical or β-sheet structure. Interestingly, the CD spectrum of the ribbon isomer was between those of the globular and bead isomers (141).

AusIA

α-Conotoxin AusIA was isolated from *Conus australis,* and it was the first member of 5/5 α-conotoxin class to be identified. Both globular and ribbon isomers of AusIA are antagonists of α7 nAChR with IC_{50} values of 11.68 ± 1.53 μM and 9.67 ± 0.01 μM, respectively (142). An NMR spectroscopy analysis of the two isomers concluded that they do not have a folded structure (142).

GeXIVA

αO-Conotoxin GeXIVA was predicted to exist from transcriptome analysis of *Conus generalis* venom duct (143). The synthesised peptide inhibits both human and rat α9α10 nAChR and has potential in treating neuropathic pain in an animal model (143-145). Surprisingly, the three isomers of GeXIVA have similar activity, with the bead and ribbon being slightly more potent than the globular isomer (IC_{50}: bead = 4.6 nM (rat), 20.3 nM (human); ribbon = 7 nM (rat), 47.3 nM (human); globular = 22.7 nM (rat), 116 nM (human)) (143,145).

α-Conotoxin isomers targeting calcium channels via $GABA_B$ receptor activation

Recently, α-conotoxins Pn1.2 (4/6 class), Pu1.2 (4/7 class) and Vc1.1 (4/7 class) were reported to act on high voltage-activated calcium channels via $GABA_B$ receptor activation, and the non-native isomers can be as potent as the globular peptides at this target. The 3D structures of three isomers of Pu1.2 were determined which showed that the globular and ribbon Pu1.2 had a well-defined structure compared to that of the bead Pu1.2. The RMSD from Cys3-Pro8 of Pu1.2 isomers was less than 1 Å which helped Carstens *et al.* to identify a simplified biologically active peptide motif (116). Likewise, globular α-conotoxin Lt1.3 (4/7 class) acts on the α3β2 nAChR whereas the ribbon Lt1.3 inhibits $GABA_B$ receptor-coupled Cav2.2. The circular dichroism spectra results indicated the globular Lt1.3 has a helical structure whilst ribbon Lt1.3 does not (146).

Table 1.3 The sequence and cysteine framework folding class of ribbon or bead α-conotoxins

Peptide	Sequence	Cysteine framework folding class
GI	ECCNPACGRHYSC-NH2	framework I 3/5 class
ImII	ACCSDRRCRWRC-NH2	framework I 4/3 class
BuIA	GCCSTPPCAVLYC-NH2	framework I 4/4 class
AuIB	GCCSYPPCFATNPDC-NH2	framework I 4/6 class
Pu1.2	GGCCSYPPCIANNPLC-NH2	framework I 4/6 class
TxIA	GCCSRPPCIANNPDLC-NH2	framework I 4/7 class
PnI.2	GCCSHPPCFLNNPDYC-NH2	framework I 4/7 class
Vc1.1	GCCSDPRCNYDHPEIC-NH2	framework I 4/7 class
Lt1.3	GCCSHPACSGNNPYFC-NH2	framework I 4/7 class
AusIA	SCCARNPACRHNHPCV	framework I 5/5 class
GeXIVA	TCRSSGRYCRSPYDRRRRYCRRITDACV	framework XIV

1.5 Aims and scope of this thesis

So far, most studies on α-conotoxins have focused on the globular isomer, also called the "native isomer", because it is typically displayed by the wild-type conotoxins. Nevertheless, it has been shown in one instance that the venom of a cone snail can contain the ribbon isomer of an α-conotoxin, albeit in much smaller quantity than the corresponding globular isomer (147). As noted already, recent studies have shown that ribbon and/or bead isomer of α-conotoxins can be used in drug design application and can have potencies equal to or greater than the native isomer (116,137,143,146). This thesis focuses on investigating the SAR of the ribbon isomer of a range of α-conotoxins, providing the basis for using the α-conotoxin ribbon isomer as a scaffold in drug design to target nAChRs. The specific aims of this thesis are:
Aim 1: To design analogues of the ribbon GeXIVA with the aim of improving its folding yield.
Aim 2: To underdstand the interactions of ribbon α-conotoxin AuIB (rAuIB) to the α3β4 nAChR.
Aim 3: To identify the best energy calculation method that can be used in the design of α-conotoxin analogues.
Aim 4: To design stoichiometry-specific inhibitors of the nAChR stoichiometry based on a ribbon α-conotoxin scaffold.

This thesis comprises six chapters, including four chapters containing new experimental data as well as an introduction chapter (Chapter 1) and a conclusion chapter (Chapter 6). The experimental chapters (2-5) are each focused on one of the specific aims.

Aim 1 focused on the improvement of the oxidation yield of αO-conotoxin ribbon GeXIVA (Chapter 2). In Chapter 2, backbone cyclisation of αO-conotoxin GeXIVA facilitated direct folding of the ribbon isomer. This improved the folding yield by 17-fold higher than the uncyclised ribbon GeXIVA obtained by two-step oxidation. This study showed that ribbon α-conotoxins can be engineered to have favourable properties to inhibt nAChRs. Therefore, it is necessary to investigate the binding mode of the ribbon α-conotoxin at nAChRs, which can be used to design ribbon α-conotoxins.

Aim 2 explored the binding mode of the ribbon isomer at nAChRs (Chapter 3). In Chapter 3, the binding mode of rAuIB at α3β4 nAChR was built. Similar to globular α-conotoxins, the molecular model indicates that the first loop of rAuIB binds in the "aromatic box" of the

acetylcholine orthosteric binding site. In contrast, the second loop and the termini of the ribbon isomer have different orientations and interactions in the binding sites to those of the globular α-conotoxins.

Aim 3 identified the best energy prediction method (Chapter 4). In Chapter 4, four energy prediction methods were benchmarked. Foldx was the most reliable method. It successfully predicted which mutants would have increased and decreased affinities with the receptor. Therefore, it is a valuable computational tool to design ribbon α-conotoxin mutants.

The findings from Aims 2 and 3 were applied in Aim 4 to design selective and potent α4β2 nAChR inhibitors (Chapter 5). In Chapter 5, the binding mode of ribbon [Gla4E]GID with $(\alpha4)_3(\beta2)_2$ nAChR was built using information on the binding mode of rAuIB studied in Aim 2. Foldx predicted mutational energies of ribbon [Gla4E]GID at $(\alpha4)_3(\beta2)_2$ nAChR, and S7L, S7M, S7P, H17P and V18F mutants of ribbon [Gla4E]GID were suggested to have desirable properties to inhibit $(\alpha3)_3(\beta4)_2$ nAChR.

Overall, the design of ribbon α-conotoxins is an alternative strategy to develop specific nAChR inhibitors.

1.6 References

1. de Vries, D. J., and Beart, P. M. (1995) Fishing for drugs from the sea: status and strategies. *Trends Pharmacol. Sci.* **16**, 275-279
2. Aneiros, A., and Garateix, A. (2004) Bioactive peptides from marine sources: pharmacological properties and isolation procedures. *J. Chromatogr. B* **803**, 41-53
3. Blunt, J. W., Copp, B. R., Keyzers, R. A., Munro, M. H. G., and Prinsep, M. R. (2017) Marine natural products. *Nat. Prod. Rep.* **34**, 235-294
4. Blunt, J. W., Carroll, A. R., Copp, B. R., Davis, R. A., Keyzers, R. A., and Prinsep, M. R. (2018) Marine natural products. *Nat. Prod. Rep.* **35**, 8-53
5. Newman, D. J., and Cragg, G. M. (2016) Drugs and drug candidates from marine sources: an assessment of the current "state of play". *Planta Med.* **82**, 775-789
6. Gogineni, V., and Hamann, M. T. (2018) Marine natural product peptides with therapeutic potential: Chemistry, biosynthesis, and pharmacology. *Biochim. Biophys. Acta.* **1862**, 81-196
7. Miljanich, G. (2004) Ziconotide: neuronal calcium channel blocker for treating severe chronic pain. *Curr. Med. Chem.* **11**, 3029-3040
8. Jain, K. K. (2000) An evaluation of intrathecal ziconotide for the treatment of chronic pain. *Expert. Opin. Inv. Drug.* **9**, 2403-2410
9. Lee, J.-Y., Orlikova, B., and Diederich, M. (2015) Signal transducers and activators of transcription (STAT) regulatory networks in marine organisms: from physiological observations towards marine drug discovery. *Mar. Drugs.* **13**, 4967
10. D'Incalci, M., and Galmarini, C. M. (2010) A review of trabectedin (ET-743): a unique mechanism of action. *Mol. Cancer Ther.* **9**, 2157-2163
11. Gorson, J., and Holford, M. (2016) Small packages, big returns: uncovering the venom diversity of small invertebrate conoidean snails. *Integr. Comp. Biol.* **56**, 962-972
12. Millar, N. S., and Gotti, C. (2009) Diversity of vertebrate nicotinic acetylcholine receptors. *Neuropharmacology* **56**, 237-246
13. Albuquerque, E. X., Pereira, E. F., Alkondon, M., and Rogers, S. W. (2009) Mammalian nicotinic acetylcholine receptors: from structure to function. *Physiol. Rev.* **89**, 73-120
14. Cecchini, M., and Changeux, J. P. (2015) The nicotinic acetylcholine receptor and its prokaryotic homologues: Structure, conformational transitions & allosteric modulation. *Neuropharmacology* **96**, 137-149

15. Zoli, M., Pistillo, F., and Gotti, C. (2015) Diversity of native nicotinic receptor subtypes in mammalian brain. *Neuropharmacology* **96, Part B**, 302-311
16. Palma, E., Reyes-Ruiz, J. M., Lopergolo, D., Roseti, C., Bertollini, C., Ruffolo, G., Cifelli, P., Onesti, E., Limatola, C., Miledi, R., and Inghilleri, M. (2016) Acetylcholine receptors from human muscle as pharmacological targets for ALS therapy. *Proc. Natl. Acad.Sci. U. S. A.* **113**, 3060-3065
17. Cuny, H., Yu, R., Tae, H. S., Kompella, S. N., and Adams, D. J. (2017) Alpha-conotoxins active at alpha3-containing nicotinic acetylcholine receptors and their molecular determinants for selective inhibition. *Br. J. Pharmacol.* **175**, 1855-1868
18. Rueter, L. E., Donnelly-Roberts, D. L., Curzon, P., Briggs, C. A., Anderson, D. J., and Bitner, R. S. (2006) A-85380: A pharmacological probe for the preclinical and clinical investigation of the alpha4beta2 neuronal nicotinic acetylcholine receptor. *CNS. Drug. Rev.* **12**, 100-112
19. Ebbert, J. O. (2009) Emerging drugs for the treatment of tobacco dependence. *Expert. Opin. Emerg. Drugs.* **14**, 23-32
20. Taly, A., Corringer, P. J., Guedin, D., Lestage, P., and Changeux, J. P. (2009) Nicotinic receptors: allosteric transitions and therapeutic targets in the nervous system. *Nat. Rev. Drug. Discov.* **8**, 733-750
21. Wieskopf, J. S., Mathur, J., Limapichat, W., Post, M. R., Al-Qazzaz, M., Sorge, R. E., Martin, L. J., Zaykin, D. V., Smith, S. B., and Freitas, K. (2015) The nicotinic alpha6 subunit gene determines variability in chronic pain sensitivity via cross-inhibition of P2X2/3 receptors. *Sci. Transl. Med.* **7**, 287ra272
22. Engle, S. E., McIntosh, J. M., and Drenan, R. M. (2015) Nicotine and ethanol cooperate to enhance ventral tegmental area AMPA receptor function via alpha6-containing nicotinic receptors. *Neuropharmacology* **91**, 13-22
23. Elgoyhen, A. B., Vetter, D. E., Katz, E., Rothlin, C. V., Heinemann, S. F., and Boulter, J. (2001) Alpha10: a determinant of nicotinic cholinergic receptor function in mammalian vestibular and cochlear mechanosensory hair cells. *Proc. Natl. Acad. Sci. U. S. A.* **98**, 3501-3506
24. Koval, L., Lykhmus, O., Zhmak, M., Khruschov, A., Tsetlin, V., Magrini, E., Viola, A., Chernyavsky, A., Qian, J., Grando, S., Komisarenko, S., and Skok, M. (2011) Differential involvement of alpha4beta2, alpha7 and alpha9alpha10 nicotinic acetylcholine receptors in B lymphocyte activation in vitro. *Int. J. Biochem. Cell Biol.* **43**, 516-524

25. Peng, H., Ferris, R. L., Matthews, T., Hiel, H., Lopez-Albaitero, A., and Lustig, L. R. (2004) Characterization of the human nicotinic acetylcholine receptor subunit alpha9 (CHRNA9) and alpha10 (CHRNA10) in lymphocytes. *Life. Sci.* **76**, 263-280

26. Romero, H. K., Christensen, S. B., Di Cesare Mannelli, L., Gajewiak, J., Ramachandra, R., Elmslie, K. S., Vetter, D. E., Ghelardini, C., Iadonato, S. P., Mercado, J. L., Olivera, B. M., and McIntosh, J. M. (2017) Inhibition of alpha9alpha10 nicotinic acetylcholine receptors prevents chemotherapy-induced neuropathic pain. *Proc. Natl. Acad. Sci. U. S. A.* **114**, E1825-E1832

27. Vincler, M., Wittenauer, S., Parker, R., Ellison, M., Olivera, B. M., and McIntosh, J. M. (2006) Molecular mechanism for analgesia involving specific antagonism of alpha9alpha10 nicotinic acetylcholine receptors. *Proc. Natl. Acad. Sci. U. S. A.* **103**, 17880-17884

28. Unwin, N. (2005) Refined structure of the nicotinic acetylcholine receptor at 4A resolution. *J. Mol. Biol.* **346**, 967-989

29. Kouvatsos, N., Giastas, P., Chroni-Tzartou, D., Poulopoulou, C., and Tzartos, S. J. (2016) Crystal structure of a human neuronal nAChR extracellular domain in pentameric assembly: Ligand-bound alpha2 homopentamer. *Proc. Natl. Acad. Sci. U. S. A.* **113**, 9635-9640

30. Morales-Perez, C. L., Noviello, C. M., and Hibbs, R. E. (2016) X-ray structure of the human alpha4beta2 nicotinic receptor. *Nature* **538**, 411-415

31. Walsh, R. M., Jr., Roh, S. H., Gharpure, A., Morales-Perez, C. L., Teng, J., and Hibbs, R. E. (2018) Structural principles of distinct assemblies of the human alpha4beta2 nicotinic receptor. *Nature* **557**, 261-265

32. Gotti, C., Clementi, F., Fornari, A., Gaimarri, A., Guiducci, S., Manfredi, I., Moretti, M., Pedrazzi, P., Pucci, L., and Zoli, M. (2009) Structural and functional diversity of native brain neuronal nicotinic receptors. *Biochem. Pharmacol.* **78**, 703-711

33. Moroni, M., Zwart, R., Sher, E., Cassels, B. K., and Bermudez, I. (2006) Alpha4beta2 nicotinic receptors with high and low acetylcholine sensitivity: pharmacology, stoichiometry, and sensitivity to long-term exposure to nicotine. *Mol. Pharmacol.* **70**, 755-768

34. Krashia, P., Moroni, M., Broadbent, S., Hofmann, G., Kracun, S., Beato, M., Groot-Kormelink, P. J., and Sivilotti, L. G. (2010) Human alpha3beta4 neuronal nicotinic receptors show different stoichiometry if they are expressed in Xenopus oocytes or mammalian HEK293 cells. *PLoS. One.* **5**, e13611

35. Murray, T. A., Bertrand, D., Papke, R. L., George, A. A., Pantoja, R., Srinivasan, R., Liu, Q., Wu, J., Whiteaker, P., and Lester, H. A. (2012) Alpha7beta2 nicotinic acetylcholine receptors assemble, function, and are activated primarily via their alpha7-alpha7 interfaces. *Mol. Pharmacol.* **81**, 175-188

36. Indurthi, D. C., Pera, E., Kim, H.-L., Chu, C., McLeod, M. D., McIntosh, J. M., Absalom, N. L., and Chebib, M. (2014) Presence of multiple binding sites on alpha9alpha10 nAChR receptors alludes to stoichiometric-dependent action of the alpha-conotoxin, Vc1. 1. *Biochem. Pharmacol.* **89**, 131-140

37. Smit, A. B., Syed, N. I., Schaap, D., van Minnen, J., Klumperman, J., Kits, K. S., Lodder, H., van der Schors, R. C., van Elk, R., and Sorgedrager, B. (2001) A glia-derived acetylcholine-binding protein that modulates synaptic transmission. *Nature* **411**, 261-268

38. Celie, P. H., Kasheverov, I. E., Mordvintsev, D. Y., Hogg, R. C., van Nierop, P., van Elk, R., van Rossum-Fikkert, S. E., Zhmak, M. N., Bertrand, D., and Tsetlin, V. (2005) Crystal structure of nicotinic acetylcholine receptor homolog AChBP in complex with an alpha-conotoxin PnIA variant. *Nat. Struct. Mol. Biol.* **12**, 582-588

39. Ulens, C., Hogg, R. C., Celie, P. H., Bertrand, D., Tsetlin, V., Smit, A. B., and Sixma, T. K. (2006) Structural determinants of selective α-conotoxin binding to a nicotinic acetylcholine receptor homolog AChBP. *Proc. Natl. Acad. Sci. U. S. A.* **103**, 3615-3620

40. Dutertre, S., Ulens, C., Büttner, R., Fish, A., van Elk, R., Kendel, Y., Hopping, G., Alewood, P. F., Schroeder, C., and Nicke, A. (2007) AChBP-targeted alpha-conotoxin correlates distinct binding orientations with nAChR subtype selectivity. *EMBO J.* **26**, 3858-3867

41. Xu, M., Zhu, X., Yu, J., Yu, J., Luo, S., and Wang, X. (2017) The crystal structure of Ac-AChBP in complex with alpha-conotoxin LvIA reveals the mechanism of its selectivity towards different nAChR subtypes. *Protein Cell.* **8**, 1-11

42. Lin, B., Xu, M., Zhu, X., Wu, Y., Liu, X., Zhangsun, D., Hu, Y., Xiang, S. H., Kasheverov, I. E., Tsetlin, V. I., Wang, X., and Luo, S. (2016) From crystal structure of alpha-conotoxin GIC in complex with Ac-AChBP to molecular determinants of its high selectivity for alpha3beta2 nAChR. *Sci. Rep.* **6**, 22349

43. Abraham, N., Healy, M., Ragnarsson, L., Brust, A., Alewood, P. F., and Lewis, R. J. (2017) Structural mechanisms for alpha-conotoxin activity at the human alpha3beta4 nicotinic acetylcholine receptor. *Sci. Rep.* **7**, 45466

44. Nelson, M. E., Kuryatov, A., Choi, C. H., Zhou, Y., and Lindstrom, J. (2003) Alternate stoichiometries of alpha4beta2 nicotinic acetylcholine receptors. *Mol. Pharmacol.* **63**, 332-341

45. Mazzaferro, S., Bermudez, I., and Sine, S. M. (2017) Alpha4beta2 nicotinic acetylcholine receptors: relationship between subunit stoichiometry and function at the single channel level. *J. Biol. Chem.* **292**, 2729-2740

46. Moroni, M., Vijayan, R., Carbone, A., Zwart, R., Biggin, P. C., and Bermudez, I. (2008) Non-agonist-binding subunit interfaces confer distinct functional signatures to the alternate stoichiometries of the alpha4beta2 nicotinic receptor: an alpha4-alpha4 interface is required for Zn2+ potentiation. *J. Neurosci.* **28**, 6884-6894

47. Lucero, L. M., Weltzin, M. M., Eaton, J. B., Cooper, J. F., Lindstrom, J. M., Lukas, R. J., and Whiteaker, P. (2016) Differential alpha4(+)/(-)beta2 agonist-binding site contributions to alpha4beta2 nicotinic acetylcholine receptor function within and between isoforms. *J. Biol. Chem.* **291**, 2444-2459

48. Terlau, H., and Olivera, B. M. (2004) *Conus* venoms: a rich source of novel ion channel-targeted peptides. *Physiol. Rev.* **84**, 41-68

49. Dutertre, S., Jin, A. H., Vetter, I., Hamilton, B., Sunagar, K., Lavergne, V., Dutertre, V., Fry, B. G., Antunes, A., Venter, D. J., Alewood, P. F., and Lewis, R. J. (2014) Evolution of separate predation- and defence-evoked venoms in carnivorous cone snails. *Nat. Commun.* **5**, 3521

50. Halai, R., and Craik, D. J. (2009) Conotoxins: natural product drug leads. *Nat. Prod. Rep.* **26**, 526-536

51. Davis, J., Jones, A., and Lewis, R. J. (2009) Remarkable inter- and intra-species complexity of conotoxins revealed by LC/MS. *Peptides* **30**, 1222-1227

52. Olivera, B. M. (2002) "*Conus*" venom peptides: Reflections from the biology of clades and species. *Annual. Rev. Ecol. Syst.* **33**, 25-47

53. Han, T. S., Teichert, R. W., Olivera, B. M., and Bulaj, G. (2008) *Conus* venoms-a rich source of peptide-based therapeutics. *Curr. Pharm. Des.* **14**, 2462-2479

54. Kaas, Q., Yu, R., Jin, A. H., Dutertre, S., and Craik, D. J. (2012) ConoServer: updated content, knowledge, and discovery tools in the conopeptide database. *Nucleic. Acids. Res.* **40**, D325-330

55. Kaas, Q., Westermann, J. C., Halai, R., Wang, C. K., and Craik, D. J. (2008) ConoServer, a database for conopeptide sequences and structures. *Bioinformatics (Oxford, England)* **24**, 445-446

56. Kaas, Q., Westermann, J. C., and Craik, D. J. (2010) Conopeptide characterization and classifications: an analysis using ConoServer. *Toxicon* **55**, 1491-1509

57. Clark, R. J., Fischer, H., Nevin, S. T., Adams, D. J., and Craik, D. J. (2006) The synthesis, structural characterization, and receptor specificity of the alpha-conotoxin Vc1. 1. *J. Biol. Chem.* **281**, 23254-23263

58. Fainzilber, M., Nakamura, T., Lodder, J. C., Zlotkin, E., Kits, K. S., and Burlingame, A. L. (1998) Gamma-conotoxin PnVIIA, a gamma-carboxyglutamate-containing peptide agonist of neuronal pacemaker cation currents. *Biochemistry* **37**, 1470-1477

59. Barbier, J., Lamthanh, H., Le Gall, F., Favreau, P., Benoit, E., Chen, H., Gilles, N., Ilan, N., Heinemann, S. H., and Gordon, D. (2004) A delta-conotoxin from *Conus ermineus* venom inhibits inactivation in vertebrate neuronal Na+ channels but not in skeletal and cardiac muscles. *J. Biol. Chem.* **279**, 4680-4685

60. Rigby, A. C., Lucas-Meunier, E., Kalume, D. E., Czerwiec, E., Hambe, B., Dahlqvist, I., Fossier, P., Baux, G., Roepstorff, P., Baleja, J. D., Furie, B. C., Furie, B., and Stenflo, J. (1999) A conotoxin from *Conus textile* with unusual posttranslational modifications reduces presynaptic Ca2+ influx. *Proc. Natl. Acad. Sci. U. S. A.* **96**, 5758-5763

61. Buczek, O., Wei, D., Babon, J. J., Yang, X., Fiedler, B., Chen, P., Yoshikami, D., Olivera, B. M., Bulaj, G., and Norton, R. S. (2007) Structure and sodium channel activity of an excitatory I1-superfamily conotoxin. *Biochemistry* **46**, 9929-9940

62. Terlau, H., Shon, K. J., Grilley, M., Stocker, M., Stuhmer, W., and Olivera, B. M. (1996) Strategy for rapid immobilization of prey by a fish-hunting marine snail. *Nature* **381**, 148-151

63. Wang, C. Z., Zhang, H., Jiang, H., Lu, W., Zhao, Z. Q., and Chi, C. W. (2006) A novel conotoxin from *Conus striatus*, mu-SIIIA, selectively blocking rat tetrodotoxin-resistant sodium channels. *Toxicon* **47**, 122-132

64. Ekberg, J., Jayamanne, A., Vaughan, C., Aslan, S., Thomas, L., Mould, J., Drinkwater, R., Baker, M., Abrahamsen, B., and Wood, J. (2006) MuO-conotoxin MrVIB selectively blocks Nav1. 8 sensory neuron specific sodium channels and chronic pain behavior without motor deficits. *Proc. Natl. Acad. Sci. U. S. A.* **103**, 17030-17035

65. Sharpe, I. A., Gehrmann, J., Loughnan, M. L., Thomas, L., Adams, D. A., Atkins, A., Palant, E., Craik, D. J., Adams, D. J., Alewood, P. F., and Lewis, R. J. (2001) Two new classes of conopeptides inhibit the alpha1-adrenoceptor and noradrenaline transporter. *Nat. Neurosci.* **4**, 902-907

66. England, L. J., Imperial, J., Jacobsen, R., Craig, A. G., Gulyas, J., Akhtar, M., Rivier, J., Julius, D., and Olivera, B. M. (1998) Inactivation of a serotonin-gated ion channel by a polypeptide toxin from marine snails. *Science* **281**, 575-578

67. Petrel, C., Hocking, H. G., Reynaud, M., Upert, G., Favreau, P., Biass, D., Paolini-Bertrand, M., Peigneur, S., Tytgat, J., Gilles, N., Hartley, O., Boelens, R., Stocklin, R., and Servent, D. (2013) Identification, structural and pharmacological characterization of tau-CnVA, a conopeptide that selectively interacts with somatostatin sst3 receptor. *Biochem. Pharmacol.* **85**, 1663-1671

68. Olivera, B. M., Cruz, L. J., de Santos, V., LeCheminant, G. W., Griffin, D., Zeikus, R., McIntosh, J. M., Galyean, R., Varga, J., Gray, W. R., and et al. (1987) Neuronal calcium channel antagonists. Discrimination between calcium channel subtypes using omega-conotoxin from *Conus magus* venom. *Biochemistry* **26**, 2086-2090

69. Olivera, B. M., and Cruz, L. J. (2001) Conotoxins, in retrospect. *Toxicon* **39**, 7-14

70. Olivera, B. M. (2006) *Conus* peptides: biodiversity-based discovery and exogenomics. *J. Biol. Chem.* **281**, 31173-31177

71. McIntosh, J. M., Santos, A. D., and Olivera, B. M. (1999) *Conus* peptides targeted to specific nicotinic acetylcholine receptor subtypes. *Annu. Rev. Biochem.* **68**, 59-88

72. Akondi, K. B., Muttenthaler, M., Dutertre, S., Kaas, Q., Craik, D. J., Lewis, R. J., and Alewood, P. F. (2014) Discovery, synthesis, and structure-activity relationships of conotoxins. *Chem. Rev.* **114**, 5815-5847

73. Lewis, R. J., Dutertre, S., Vetter, I., and Christie, M. J. (2012) *Conus* venom peptide pharmacology. *Pharmacol. Rev.* **64**, 259-298

74. Miller, R. J. (1987) Multiple calcium channels and neuronal function. *Science* **235**, 46-52

75. Catterall, W. A., Perez-Reyes, E., Snutch, T. P., and Striessnig, J. (2005) International union of pharmacology. xlviii. Nomenclature and structure-function relationships of voltage-gated calcium channels. *Pharmacol. Rev.* **57**, 411-425

76. Triggle, D. J. (2007) Calcium channel antagonists: clinical uses—past, present and future. *Biochem. Pharmacol.* **74**, 1-9

77. Nadasdi, L., Yamashiro, D., Chung, D., Tarczy-Hornoch, K., Adriaenssens, P., and Ramachandran, J. (1995) Structure-activity analysis of a *Conus* peptide blocker of N-type neuronal calcium channels. *Biochemistry* **34**, 8076-8081

78. Nielsen, K. J., Thomas, L., Lewis, R. J., Alewood, P. F., and Craik, D. J. (1996) A consensus structure for omega-conotoxins with different selectivities for voltage-

sensitive calcium channel subtypes: comparison of MVIIA, SVIB and SNX-202. *J. Mol. Biol.* **263**, 297-310

79. Berecki, G., Motin, L., Haythornthwaite, A., Vink, S., Bansal, P., Drinkwater, R., Wang, C. I., Moretta, M., Lewis, R. J., and Alewood, P. F. (2010) Analgesic omega-conotoxins CVIE and CVIF selectively and voltage-dependently block recombinant and native N-type calcium channels. *Mol. Pharmacol.* **77**, 139-148
80. Bauer, C. S., Rahman, W., Tran-Van-Minh, A., Lujan, R., Dickenson, A. H., and Dolphin, A. C. (2010) The anti-allodynic alpha (2) delta ligand pregabalin inhibits the trafficking of the calcium channel alpha (2) delta-1 subunit to presynaptic terminals in vivo. *Biochem. Soc. Trans.* **38**, 525-528
81. Olivera, B. M., Miljanich, G., Ramachandran, J., and Adams, M. E. (1994) Calcium channel diversity and neurotransmitter release: the omega-conotoxins and omega-agatoxins. *Annu. Rev. Biochem.* **63**, 823-867
82. Kim, J. I., Takahashi, M., Ogura, A., Kohno, T., Kudo, Y., and Sato, K. (1994) Hydroxyl group of Tyr13 is essential for the activity of omega-conotoxin GVIA, a peptide toxin for N-type calcium channel. *J. Biol. Chem.* **269**, 23876-23878
83. Flinn, J. P., Pallaghy, P. K., Lew, M. J., Murphy, R., Angus, J. A., and Norton, R. S. (1999) Roles of key functional groups in omega-conotoxin GVIA. *Eur. J. Biochem.* **262**, 447-455
84. Nielsen, K. J., Adams, D., Thomas, L., Bond, T., Alewood, P. F., Craik, D. J., and Lewis, R. J. (1999) Structure-activity relationships of omega-conotoxins MVIIA, MVIIC and 14 loop splice hybrids at n and p/q-type calcium channels. *J. Mol. Biol.* **289**, 1405-1421
85. Goldin, A. L. (2001) Resurgence of sodium channel research. *Annu. Rev. Physiol.* **63**, 871-894
86. Catterall, W. A. (2000) From ionic currents to molecular mechanisms: the structure and function of voltage-gated sodium channels. *Neuron* **26**, 13-25
87. Eijkelkamp, N., Linley, J. E., Baker, M. D., Minett, M. S., Cregg, R., Werdehausen, R., Rugiero, F., and Wood, J. N. (2012) Neurological perspectives on voltage-gated sodium channels. *Brain* **135**, 2585-2612
88. WCatterall, G. A., and Waxman, S. (2005) International union of pharmacology. xlvii. Nomenclature and structure–function relationships of voltage-gated sodium channels. *Pharmacol. Rev.* **57**, 397-409

89. Fainzilber, M., Gordon, D., Hasson, A., Spira, M. E., and Zlotkin, E. (1991) Mollusc-specific toxins from the venom of *Conus textile* neovicarius. *Eur. J. Biochem.* **202**, 589-595

90. Cruz, L., Gray, W., Olivera, B., Zeikus, R., Kerr, L., Yoshikami, D., and Moczydlowski, E. (1985) *Conus geographus* toxins that discriminate between neuronal and muscle sodium channels. *J. Biol. Chem.* **260**, 9280-9288

91. McIntosh, J. M., Hasson, A., Spira, M. E., Gray, W. R., Li, W., Marsh, M., Hillyard, D. R., and Olivera, B. M. (1995) A new family of conotoxins that blocks voltage-gated sodium channels. *J. Biol. Chem.* **270**, 16796-16802

92. Al-Sabi, A., McArthur, J., Ostroumov, V., and French, R. J. (2006) Marine toxins that target voltage-gated sodium channels. *Mar. Drugs.* **4**, 157-192

93. Wilson, M. J., Yoshikami, D., Azam, L., Gajewiak, J., Olivera, B. M., Bulaj, G., and Zhang, M.-M. (2011) Mu-conotoxins that differentially block sodium channels NaV1. 1 through 1.8 identify those responsible for action potentials in sciatic nerve. *Proc. Natl. Acad. Sci. U. S. A.* **108**, 10302-10307

94. Yao, S., Zhang, M.-M., Yoshikami, D., Azam, L., Olivera, B. M., Bulaj, G., and Norton, R. S. (2008) Structure, dynamics, and selectivity of the sodium channel blocker mu-conotoxin SIIIA. *Biochemistry* **47**, 10940-10949

95. Schroeder, C. I., Ekberg, J., Nielsen, K. J., Adams, D., Loughnan, M. L., Thomas, L., Adams, D. J., Alewood, P. F., and Lewis, R. J. (2008) Neuronally selective mu-conotoxins from *Conus striatus* utilize an alpha-helical motif to target mammalian sodium channels. *J. Biol. Chem.* **283**, 21621-21628

96. Leipold, E., DeBie, H., Zorn, S., Adolfo, B., Olivera, B. M., Terlau, H., and Heinemann, S. H. (2007) MuO-conotoxins inhibit Nav channels by interfering with their voltage sensors in domain-2. *Channels* **1**, 253-262

97. Daly, N. L., Ekberg, J. A., Thomas, L., Adams, D. J., Lewis, R. J., and Craik, D. J. (2004) Structures of muO-conotoxins from *Conus marmoreus* inhibitors of tetrodotoxin (TTX)-sensitive and TTX-resistant sodium channels in mammalian sensory neurons. *J. Biol. Chem.* **279**, 25774-25782

98. Bulaj, G., Zhang, M.-M., Green, B. R., Fiedler, B., Layer, R. T., Wei, S., Nielsen, J. S., Low, S. J., Klein, B. D., and Wagstaff, J. D. (2006) Synthetic muO-conotoxin MrVIB blocks TTX-resistant sodium channel $Na_V1.8$ and has a long-lasting analgesic activity. *Biochemistry* **45**, 7404-7414

99. Southan, C., Sharman, J. L., Benson, H. E., Faccenda, E., Pawson, A. J., Alexander, S. P., Buneman, O. P., Davenport, A. P., McGrath, J. C., Peters, J. A., Spedding, M., Catterall, W. A., Fabbro, D., and Davies, J. A. (2016) The IUPHAR/BPS guide to pharmacology in 2016: towards curated quantitative interactions between 1300 protein targets and 6000 ligands. *Nucleic. Acids. Res.* **44**, D1054-1068

100. Jacobsen, R. B., Koch, E. D., Lange-Malecki, B., Stocker, M., Verhey, J., Van Wagoner, R. M., Vyazovkina, A., Olivera, B. M., and Terlau, H. (2000) Single amino acid substitutions in kappa-conotoxin PVIIA disrupt interaction with the shaker K+ channel. *J. Biol .Chem.* **275**, 24639-24644

101. Lubbers, N. L., Campbell, T. J., Polakowski, J. S., Bulaj, G., Layer, R. T., Moore, J., Gross, G. J., and Cox, B. F. (2005) Postischemic administration of CGX-1051, a peptide from cone snail venom, reduces infarct size in both rat and dog models of myocardial ischemia and reperfusion. *J. Cardiovasc. Pharmacol.* **46**, 141-146

102. Scanlon, M. J., Naranjo, D., Thomas, L., Alewood, P. F., Lewis, R. J., and Craik, D. J. (1997) Solution structure and proposed binding mechanism of a novel potassium channel toxin kappa-conotoxin PVIIA. *Structure* **5**, 1585-1597

103. Savarin, P., Guenneugues, M., Gilquin, B., Lamthanh, H., Gasparini, S., Zinn-Justin, S., and Menez, A. (1998) Three-dimensional structure of kappa-conotoxin PVIIA, a novel potassium channel-blocking toxin from cone snails. *Biochemistry* **37**, 5407-5416

104. Bjarnadóttir, T. K., Gloriam, D. E., Hellstrand, S. H., Kristiansson, H., Fredriksson, R., and Schiöth, H. B. (2006) Comprehensive repertoire and phylogenetic analysis of the G protein-coupled receptors in human and mouse. *Genomics* **88**, 263-273

105. Bylund, D. B., Eikenberg, D. C., Hieble, J. P., Langer, S. Z., Lefkowitz, R. J., Minneman, K. P., Molinoff, P. B., Ruffolo, R. R., and Trendelenburg, U. (1994) International union of pharmacology nomenclature of adrenoceptors. *Pharmacol. Rev.* **46**, 121-136

106. Chen, Z., Rogge, G., Hague, C., Alewood, D., Colless, B., Lewis, R. J., and Minneman, K. P. (2004) Subtype-selective noncompetitive or competitive inhibition of human alpha1-adrenergic receptors by rho-TIA. *J. Biol. Chem.* **279**, 35326-35333

107. Sharpe, I. A., Thomas, L., Loughnan, M., Motin, L., Palant, E., Croker, D. E., Alewood, D., Chen, S., Graham, R. M., and Alewood, P. F. (2003) Allosteric alpha1-adrenoreceptor antagonism by the conopeptide rho-TIA. *J. Biol. Chem.* **278**, 34451-34457

108. Goddard, A. W., Ball, S. G., Martinez, J., Robinson, M. J., Yang, C. R., Russell, J. M., and Shekhar, A. (2010) Current perspectives of the roles of the central norepinephrine system in anxiety and depression. *Depress. Anxiety.* **27**, 339-350

109. Brust, A., Palant, E., Croker, D. E., Colless, B., Drinkwater, R., Patterson, B., Schroeder, C. I., Wilson, D., Nielsen, C. K., and Smith, M. T. (2009) Chi-conopeptide pharmacophore development: toward a novel class of norepinephrine transporter inhibitor (Xen2174) for Pain. *J. Med. Chem.* **52**, 6991-7002

110. Nilsson, K. P. R., Lovelace, E. S., Caesar, C. E., Tynngård, N., Alewood, P. F., Johansson, H. M., Sharpe, I. A., Lewis, R. J., Daly, N. L., and Craik, D. J. (2005) Solution structure of chi-conopeptide MrIA, a modulator of the human norepinephrine transporter. *Biopolymers* **80**, 815-823

111. Sharpe, I. A., Palant, E., Schroeder, C. I., Kaye, D. M., Adams, D. J., Alewood, P. F., and Lewis, R. J. (2003) Inhibition of the norepinephrine transporter by the venom peptide chi-MrIA site of action, Na+ dependence, and structure-activity relationship. *J. Biol. Chem.* **278**, 40317-40323

112. Lebbe, E. K., Peigneur, S., Wijesekara, I., and Tytgat, J. (2014) Conotoxins targeting nicotinic acetylcholine receptors: an overview. *Mar. Drugs.* **12**, 2970-3004

113. Chang, D., and Duda, T. F. (2012) Extensive and continuous duplication facilitates rapid evolution and diversification of gene families. *Mol. Biol. Evol.* **29**, 2019-2029

114. Azam, L., and McIntosh, J. M. (2009) Alpha-conotoxins as pharmacological probes of nicotinic acetylcholine receptors. *Acta. Pharmacol. Sin.* **30**, 771-783

115. Janes, R. W. (2005) Alpha-conotoxins as selective probes for nicotinic acetylcholine receptor subclasses. *Curr. Opin. Pharmacol.* **5**, 280-292

116. Carstens, B. B., Berecki, G., Daniel, J. T., Lee, H. S., Jackson, K. A., Tae, H. S., Sadeghi, M., Castro, J., O'Donnell, T., Deiteren, A., Brierley, S. M., Craik, D. J., Adams, D. J., and Clark, R. J. (2016) Structure-activity studies of cysteine-rich alpha-conotoxins that inhibit high-voltage-activated calcium channels via GABAB receptor activation reveal a minimal functional motif. *Angew. Chem. Int. Ed. Engl.* **55**, 4692-4696

117. Luo, S., Zhangsun, D., Schroeder, C. I., Zhu, X., Hu, Y., Wu, Y., Weltzin, M. M., Eberhard, S., Kaas, Q., and Craik, D. J. (2014) A novel alpha4/7-conotoxin LvIA from *Conus lividus* that selectively blocks alpha3beta2 vs. alpha6/alpha3beta2beta3 nicotinic acetylcholine receptors. *FASEB J.* **28**, 1842-1853

118. Zhangsun, D., Zhu, X., Wu, Y., Hu, Y., Kaas, Q., Craik, D. J., McIntosh, J. M., and Luo, S. (2015) Key residues in the nicotinic acetylcholine receptor beta2 subunit contribute to alpha-conotoxin LvIA binding. *J. Biol. Chem.* **290**, 9855-9862

119. Luo, S., Zhangsun, D., Zhu, X., Wu, Y., Hu, Y., Christensen, S., Harvey, P. J., Akcan, M., Craik, D. J., and McIntosh, J. M. (2013) Characterization of a novel alpha-conotoxin TxID from *Conus textile* that potently blocks rat alpha3beta4 nicotinic acetylcholine receptors. *J. Med. Chem.* **56**, 9655-9663

120. Wu, Y., Zhangsun, D., Zhu, X., Kaas, Q., Zhangsun, M., Harvey, P. J., Craik, D. J., McIntosh, J. M., and Luo, S. (2017) Alpha-conotoxin [S9A]TxID potently discriminates between alpha3beta4 and alpha6/alpha3beta4 nicotinic acetylcholine receptors. *J. Med. Chem.* **60**, 5826-5833

121. Yu, J., Zhu, X., Harvey, P. J., Kaas, Q., Zhangsun, D., Craik, D. J., and Luo, S. (2018) Single amino acid substitution in alpha-conotoxin TxID reveals a specific alpha3beta4 nicotinic acetylcholine receptor antagonist. *J. Med. Chem.* **61**, 9256-9265

122. Luo, S., Zhangsun, D., Wu, Y., Zhu, X., Hu, Y., McIntyre, M., Christensen, S., Akcan, M., Craik, D. J., and McIntosh, J. M. (2013) Characterization of a novel alpha-conotoxin from *Conus textile* that selectively targets α6/α3β2β3 nicotinic acetylcholine receptors. *J. Biol. Chem.* **288**, 894-902

123. Azam, L., Maskos, U., Changeux, J. P., Dowell, C. D., Christensen, S., De Biasi, M., and McIntosh, J. M. (2010) Alpha-conotoxin BuIA[T5A;P6O]: a novel ligand that discriminates between alpha6beta4 and alpha6beta2 nicotinic acetylcholine receptors and blocks nicotine-stimulated norepinephrine release. *FASEB J.* **24**, 5113-5123

124. Johnson, D. S., Martinez, J., Elgoyhen, A. B., Heinemann, S. F., and McIntosh, J. M. (1995) Alpha-Conotoxin ImI exhibits subtype-specific nicotinic acetylcholine receptor blockade: preferential inhibition of homomeric alpha 7 and alpha 9 receptors. *Mol. Pharmacol.* **48**, 194-199

125. Ellison, M., Gao, F., Wang, H. L., Sine, S. M., McIntosh, J. M., and Olivera, B. M. (2004) Alpha-conotoxins ImI and ImII target distinct regions of the human alpha7 nicotinic acetylcholine receptor and distinguish human nicotinic receptor subtypes. *Biochemistry* **43**, 16019-16026

126. Quiram, P. A., and Sine, S. M. (1998) Structural elements in α-conotoxin ImI essential for binding to neuronal alpha7 receptors. *J. Biol. Chem.* **273**, 11007-11011

127. Servent, D., Thanh, H. L., Antil, S., Bertrand, D., Corringer, P.-J., Changeux, J.-P., and Ménez, A. (1998) Functional determinants by which snake and cone snail toxins block the alpha7 neuronal nicotinic acetylcholine receptors. *J. Physiol.(Paris)* **92**, 107-111

128. Ellison, M., Haberlandt, C., Gomez-Casati, M. E., Watkins, M., Elgoyhen, A. B., McIntosh, J. M., and Olivera, B. M. (2006) α-RgIA: a novel conotoxin that specifically and potently blocks the α9α10 nAChR. *Biochemistry* **45**, 1511-1517

129. Halai, R., Clark, R. J., Nevin, S. T., Jensen, J. E., Adams, D. J., and Craik, D. J. (2009) Scanning mutagenesis of alpha-conotoxin Vc1.1 reveals residues crucial for activity at the alpha9alpha10 nicotinic acetylcholine receptor. *J. Biol. Chem.* **284**, 20275-20284

130. Ellison, M., Feng, Z. P., Park, A. J., Zhang, X., Olivera, B. M., McIntosh, J. M., and Norton, R. S. (2008) Alpha-RgIA, a novel conotoxin that blocks the alpha9alpha10 nAChR: structure and identification of key receptor-binding residues. *J. Mol. Biol.* **377**, 1216-1227

131. Nishiuchi, Y., and Sakakibara, S. (1982) Primary and secondary structure of conotoxin GI, a neurotoxic tridecapeptide from a marine snail. *FEBS Lett.* **148**, 260-262

132. Gehrmann, J., Alewood, P. F., and Craik, D. J. (1998) Structure determination of the three disulfide bond isomers of alpha-conotoxin GI: a model for the role of disulfide bonds in structural stability. *J. Mol. Biol.* **278**, 401-415

133. Ellison, M., McIntosh, J. M., and Olivera, B. M. (2003) Alpha-conotoxins ImI and ImII similar alpha7 nicotinic receptor antagonists act at different sites. *J. Biol. Chem.* **278**, 757-764

134. Kasheverov, I. E., Zhmak, M. N., Fish, A., Rucktooa, P., Khruschov, A. Y., Osipov, A. V., Ziganshin, R. H., D'hoedt, D., Bertrand, D., Sixma, T. K., Smit, A. B., and Tsetlin, V. I. (2009) Interaction of alpha-conotoxin ImII and its analogs with nicotinic receptors and acetylcholine-binding proteins: additional binding sites on Torpedo receptor. *J. Neurochem.* **111**, 934-944

135. Azam, L., Dowell, C., Watkins, M., Stitzel, J. A., Olivera, B. M., and McIntosh, J. M. (2005) Alpha-conotoxin BuIA, a novel peptide from *Conus bullatus*, distinguishes among neuronal nicotinic acetylcholine receptors. *J. Biol. Chem.* **280**, 80-87

136. Jin, A. H., Brandstaetter, H., Nevin, S. T., Tan, C. C., Clark, R. J., Adams, D. J., Alewood, P. F., Craik, D. J., and Daly, N. L. (2007) Structure of alpha-conotoxin BuIA: influences of disulfide connectivity on structural dynamics. *BMC Struct. Biol.* **7**, 28

137. Dutton, J. L., Bansal, P. S., Hogg, R. C., Adams, D. J., Alewood, P. F., and Craik, D. J. (2002) A new level of conotoxin diversity, a non-native disulfide bond connectivity in

alpha-conotoxin AuIB reduces structural definition but increases biological activity. *J. Biol. Chem.* **277**, 48849-48857

138. Nicke, A., Samochocki, M., Loughnan, M. L., Bansal, P. S., Maelicke, A., and Lewis, R. J. (2003) Alpha-conotoxins EpI and AuIB switch subtype selectivity and activity in native versus recombinant nicotinic acetylcholine receptors. *FEBS. Lett.* **554**, 219-223
139. Grishin, A. A., Wang, C. I., Muttenthaler, M., Alewood, P. F., Lewis, R. J., and Adams, D. J. (2010) Alpha-conotoxin AuIB isomers exhibit distinct inhibitory mechanisms and differential sensitivity to stoichiometry of alpha3beta4 nicotinic acetylcholine receptors. *J. Biol. Chem.* **285**, 22254-22263
140. Grishin, A. A., Cuny, H., Hung, A., Clark, R. J., Brust, A., Akondi, K., Alewood, P. F., Craik, D. J., and Adams, D. J. (2013) Identifying key amino acid residues that affect alpha-conotoxin AuIB inhibition of alpha3beta4 nicotinic acetylcholine receptors. *J. Biol. Chem.* **288**, 34428-34442
141. Wu, Y., Wu, X., Yu, J., Zhu, X., Zhangsun, D., and Luo, S. (2014) Influence of disulfide connectivity on structure and bioactivity of alpha-conotoxin TxIA. *Molecules* **19**, 966-979
142. Lebbe, E. K., Peigneur, S., Maiti, M., Mille, B. G., Devi, P., Ravichandran, S., Lescrinier, E., Waelkens, E., D'Souza, L., Herdewijn, P., and Tytgat, J. (2014) Discovery of a new subclass of alpha-conotoxins in the venom of *Conus australis*. *Toxicon* **91**, 145-154
143. Luo, S., Zhangsun, D., Harvey, P. J., Kaas, Q., Wu, Y., Zhu, X., Hu, Y., Li, X., Tsetlin, V. I., Christensen, S., Romero, H. K., McIntyre, M., Dowell, C., Baxter, J. C., Elmslie, K. S., Craik, D. J., and McIntosh, J. M. (2015) Cloning, synthesis, and characterization of alphaO-conotoxin GeXIVA, a potent alpha9alpha10 nicotinic acetylcholine receptor antagonist *Proc. Natl. Acad. Sci. U. S. A.* **112**, E4026-4035
144. Li, X., Hu, Y., Wu, Y., Huang, Y., Yu, S., Ding, Q., Zhangsun, D., and Luo, S. (2015) Anti-hypersensitive effect of intramuscular administration of alphaO-conotoxin GeXIVA[1,2] and GeXIVA[1,4] in rats of neuropathic pain. *Prog. Neuropsychopharmacol. Biol. Psychiatry.* **66**, 112-119
145. Zhangsun, D., Zhu, X., Kaas, Q., Wu, Y., Craik, D. J., McIntosh, J. M., and Luo, S. (2017) AlphaO-Conotoxin GeXIVA disulfide bond isomers exhibit differential sensitivity for various nicotinic acetylcholine receptors but retain potency and selectivity for the human alpha9alpha10 subtype. *Neuropharmacology* **127**, 243-252

146. Chen, J., Liang, L., Ning, H., Cai, F., Liu, Z., Zhang, L., Zhou, L., and Dai, Q. (2018) Cloning, synthesis and functional characterization of a novel alpha-conotoxin Lt1.3. *Mar. Drugs.* **16**, 112

147. Safavi-Hemami, H., Gorasia, D. G., Steiner, A. M., Williamson, N. A., Karas, J. A., Gajewiak, J., Olivera, B. M., Bulaj, G., and Purcell, A. W. (2012) Modulation of conotoxin structure and function is achieved through a multienzyme complex in the venom glands of cone snails. *J. Biol. Chem.* **287**, 34288-34303

Chapter 2: Backbone cyclisation of analgesic ribbon conotoxin GeXIVA helps direct oxidative folding

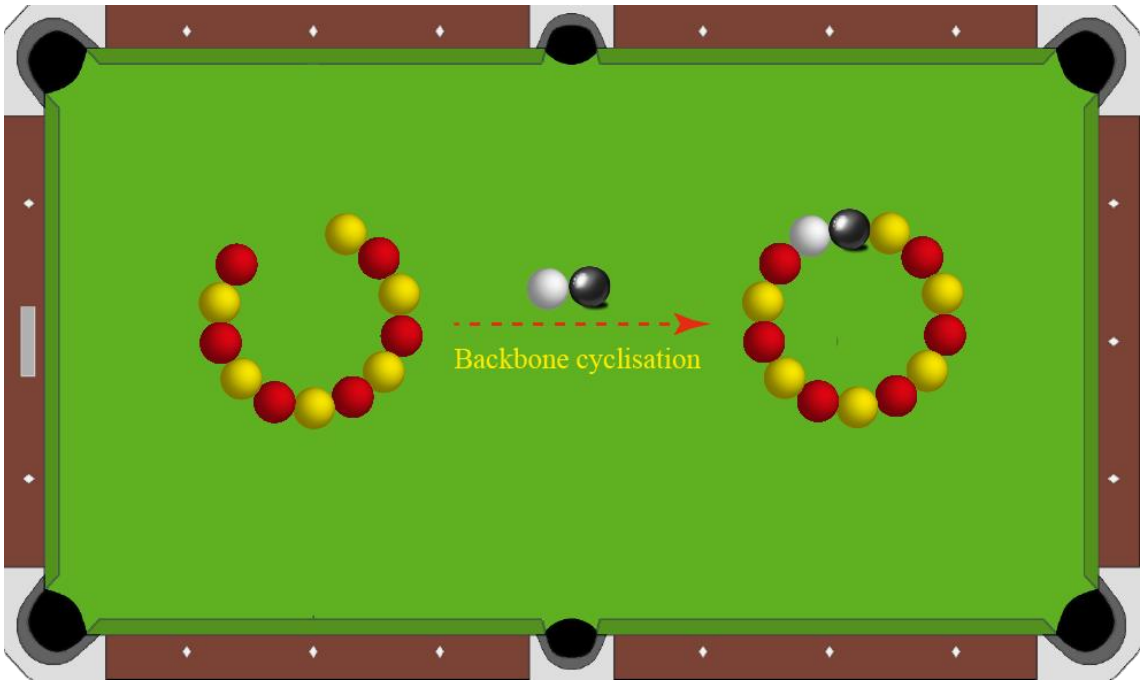

Publications included in this chapter

1. **Wu, X.**, Huang, Y. H., Kaas, Q., and Craik, D. J. (2016) Cyclisation of disulfide-rich conotoxins in drug design applications. *Eur. J. Org. Chem.* **2016**, 3462-3472

Contributions

Xiaosa Wu was responsible for the following work:

- 60% of conception and design
- 100% of data collection
- 70% analysis of data
- 90% drafting and writing

2. **Wu, X.**, Huang, Y. H., Kaas, Q., Harvey, P. J., Wang, C. K., Tae, H. S., Adams, D. J., and Craik, D. J. (2017) Backbone cyclization of analgesic conotoxin GeXIVA facilitates direct folding of the ribbon isomer. *J. Biol. Chem.* **292**, 17101-17112

Contributions

Xiaosa Wu was responsible for the following work:

- 50% of conception and design
- 100% of peptide cleavage, cyclisation and purification
- 100% of one-pot oxidative folding
- 50% of structural characterisation
- 100% of serum stability assays
- 60% of analysis of data
- 70% drafting and writing

2.1 An overview of cyclisation of conotoxins

In this Chapter, some general principles for the cyclisation of conotoxins are described and then the cyclisation of individual conotoxins is discussed in more detail. Knowledge of the 3D structure of a conotoxin can help in the design of a linker to cyclise its backbone, and thereby potentially improve its biopharmaceutical properties. Factors that influence successful cyclisation include the distance between the N- and C- termini, their flexibility, and the positions in the sequence of cysteine and other residues essential for activity. Too short a linker can strain the structure and too long a linker can result in difficult folding, increase degradation by endoproteases and reduce biological activity. In principle, any amino acid can be used to constitute a linker sequence (1) but Gly and Ala residues are often employed because they are small and their side chains cannot form hydrogen bonds, which could potentially disrupt the active fold. No more than two consecutive amino acid residues of the same type are used in the linker to avoid overlap in the NMR spectra (2,3).

The primary method for cyclisation of peptides assembled using solid-phase peptide synthesis (SPPS) is native chemical ligation (NCL) (4). The NCL approach involves a reaction whereby an N-terminal cysteine residue and a C-terminal thioester undergo a thioester exchange followed by an intermolecular rearrangement to create a new amide bond. Any conotoxin containing both a N-terminal cysteine residue and a C-terminal thioester can potentially be cyclised using the NCL method. NCL has been successfully applied to cyclise a number of conotoxins, as illustrated in Figure 2.1 A, as well as other peptides (5-7). Recently, a straightforward in-solution cyclisation method has been developed to cyclise peptides ranging in size from 26 to 34 residues (Figure 2.1 B) (8). The NCL approach has also been complemented by semi biological approaches (Figure 2.1C and D). In particular, several enzymes have been reported to have the function of cyclisation (9-11). Enzyme-mediated cyclisation of synthetic linear peptides is fast and efficient, and so far has been applied to cyclise the backbone of three exemplary conotoxins, Vc1.1, MrIA and PVIIA.

Overall, 10 conotoxins have been cyclised to date, using chemical or enzymatic approaches. Six of these conotoxins are globular or ribbon Framework I, and the other four toxins have a knottin fold and a Frameworks VI/VII or IX (Table 2.1; Figure 2.2).

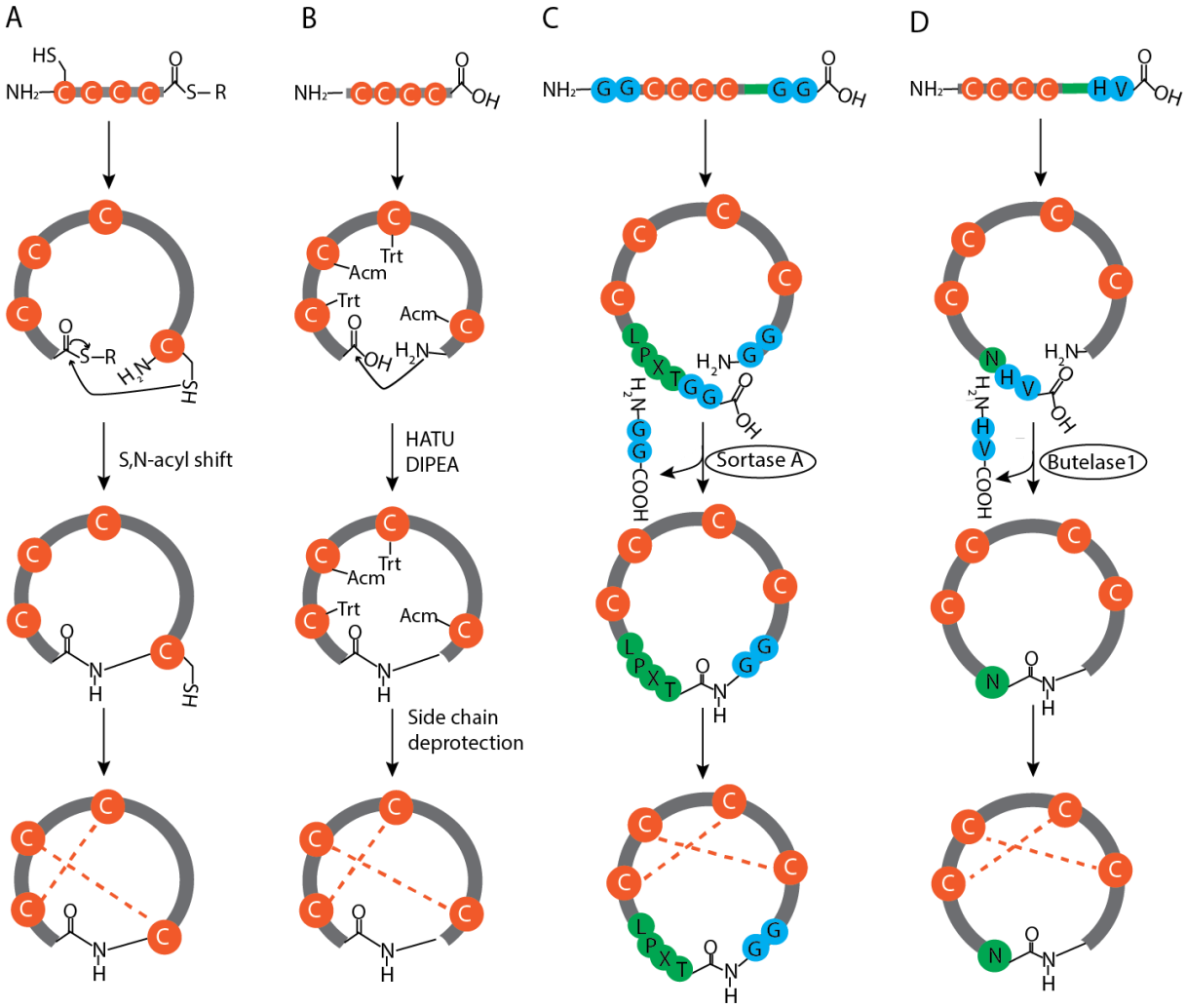

Figure 2.1. Cyclisation of conotoxins. A: cyclisation using native chemical ligation; B: cyclisation using chemical amide coupling; C and D: cyclisation using enzymes. The use of Sortase A requires the incorporation of sortase recognition sequence (green) at the C-terminus and GG (blue) at the N-terminus. By contrast, only an Asn recognition residue (green) is needed for butelase-mediated cyclisation.

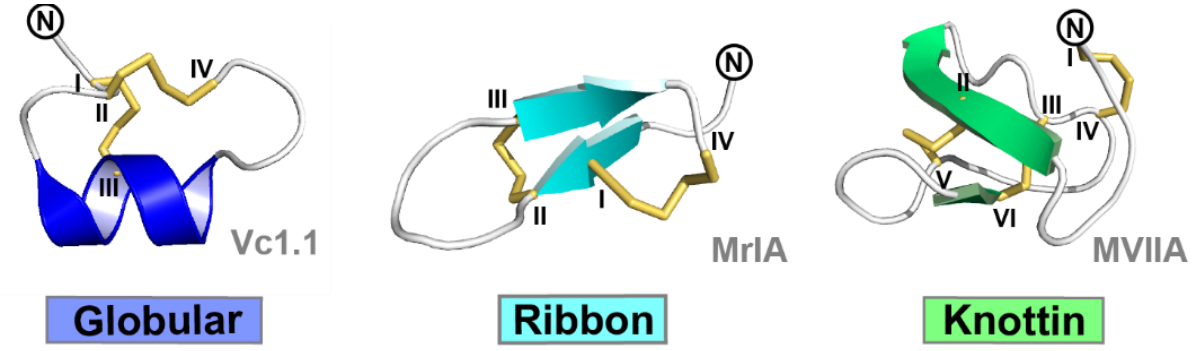

Figure 2.2 The 3D solution structures of representative globular (Vc1.1; PDB: 2H8S), ribbon (MrIA; 2EW4) and knottin conotoxins (MVIIA; 1TTK).

Table 2.1 Summary of cyclic variants of conotoxins

Name	Target(s)	Linker(s)	Activity Cyclic vs. Linear		% Improvement in stability of the cyclic variants		Stability assays
			Globular	Ribbon	Globular	Ribbon	
MII(2)	α6* nAChR[a]	GAGGAAG[b]	NC[c]	ND[d]	~40%; ~20%	ND	EndogluC (10 h) and human serum
ImI(12)	α3β2, α7 and α9 nAChRs	A/βA[e]	ND	ND	~75%	NC	Trypsin (5 h)
Vc1.1(9,13)	α9α10 nAChR & Ca_V via $GABA_B$ receptor	GGAAGG	Reduced	ND	~15%; ~30%; ~25%	ND	Simulated gastric fluid, simulated intestinal fluid and human serum
			Improved	ND			
		GLPETG[f]	ND	ND	ND	ND	ND
RgIA(3)	α9α10 nAChR	GGAAGAG	NC	ND	~ 15%	ND	Human serum
	GABAB receptor	GGAAGG	NC	ND	~ 10%	ND	
AuIB(14,15)	α3β4 nAChR	AG	Reduced	NA[g]	~ 30%	~ 50%	Chymotrypsin (48 h)
		AGGG	Reduced	NA	ND	> 75%	
		GGAA	Reduced	Reduced	NC	NC	Human serum
MrIA(6,11,16)	Norepinephrine transporter 1	AG	ND	NC	ND	~ 40%	Trypsin
		RGD	ND	NC	ND	~ 50%	Rat plasma
		LPX[h]TG[f]	ND	ND	ND	ND	ND
MVIIA(17)	N-type Cav2.2	GGPG	ND		ND		ND
PVIIA(18)	*Shaker* Kv	LPETGG[f]	Reduced		Reduced by ~ 50%		Human serum
Gm9a(19)	ND	GLP	ND		NC[i]		Human serum
Bru9a(19)	ND	GLP	ND		NC[i]		Human serum

[a] Nicotinic acetylcholine receptor. [b] There is a conflict between the linker sequence reported in the article and that reported in the supporting information and the NMR solution structure of cMII-7; the latter sequence shown here was confirmed by the authors (personal communication) [c] No changed. [d] Not determined. [e] Ala and βAla gave better yield for the ribbon and globular isomers, respectively. [f] Enzyme-mediated cyclisation. [g] No activity (IC_{50} > 300 μM). [h] Any amino acids. [i] Linear Gm9a and Bru9a are naturally highly stable. The incubation time of stability assay is specified in the brackets following the biological fluids or enzymes if different from 24 h.

2.1.1 Framework I conotoxins (two disulfide bonds)

As illustrated in Table 1.1 in Chapter 1, the primary sequences of Framework I conotoxins display the cysteine pattern CC-C-C, which has been found in more than 300 conotoxins to date.

2.1.1.1 Globular isomers

Most native Framework I α-conotoxins have the globular disulfide connectivity (Cys I-Cys III, Cys II-Cys IV). These conotoxins have been the most extensively studied substrate for cyclisation approaches.

α-Conotoxin MII

The first report on the cyclisation of a conotoxin was that of the 16-residue 4/7 α-conotoxin MII (2), which derives from *Conus magus* and is highly potent and specific at the α6* nAChR

subtype (20). The short distance between its N- and C- termini made MII an ideal conotoxin to be backbone cyclised (21). Three linkers, GGAAG, GGAAGG and GAGGAAG, were designed, and three corresponding cyclic MII variants, cMII-5, cMII-6 and cMII-7, were successfully synthesised using SPPS and cyclised using NCL. The yield of cMII-5 was <10%, whereas cMII-6 and cMII-7 folded with yields of around 50% and 90%, respectively. An analysis of Hα NMR secondary chemical shifts suggested that cMII-6 and cMII-7 had a similar structure to linear MII but cMII-5 did not. The solution NMR structures of cMII-6 and cMII-7 are well defined with their backbone RMSD from the average structure is 0.41 and 0.43 Å, respectively. The structures were consistent with that of native MII, with a backbone RMSD of 0.5 Å from residues Gly1 to Cys16.

Native MII and cyclic variants were tested for their ability to inhibit nicotinic-evoked currents in bovine chromaffin cells. cMII-7 had similar activity to native MII and cMII-6 was slightly less potent than native MII, whereas cMII-5 had no activity. This study demonstrates that the length of the cyclising linker can have a major influence on biological activity. The stability of MII and its analogues were tested for degradation by endoproteinase GluC (EndoGluC) and proteases in human serum. After 24 hours, cMII-6 and cMII-7 had 15-20% more peptide remaining than linear MII in human serum, indicating that cyclisation is indeed an effective strategy to improve the stability of MII with no loss of potency.

α-Conotoxin ImI

ImI selectively inhibits the α7 neuronal nAChR among all rat nAChR subtypes. But for human nAChR subtypes, it blocks the human α3β2 nAChR with 10-fold more potency than at the human α7 nAChR (22,23). The NMR solution structure shows that the distance between the N- and C- termini is ~9.5 Å (24), suggesting that only a short linker would be required for cyclisation.

Armishaw *et al.*(12) designed four linkers (A, βA, AG and AGG) and used a one-pot oxidation method to form the disulfide bonds. For all cyclic variants, all three possible disulfide bond connectivities (globular, ribbon and bead) were observed. Wild-type ImI preferentially formed the globular isomer (96%), whereas the cyclic variants mainly folded into the ribbon isomer, with the exception of cImI-βA. The length of the cyclisation linker was found to impact the yield of ribbon isomer, with the yield of ribbon varying with the different lengths of linkers.

Interestingly, the yield of bead isomer was higher than that of the globular isomer for cImI-AG. These results suggest that the length of the linker plays a crucial role in directing the disulfide bond connectivity. Overall, it can be concluded that the structure of the globular isomer of ImI with short linkers is highly constrained and disfavoured under normal folding conditions, as compared to the ribbon isomer.

Stability assays were performed to test proteolytic susceptibility to trypsin. Overall, the results demonstrated that backbone cyclisation could make the native isomer of ImI more resistant to trypsin degradation. The globular isomers of cyclic ImI were the most resistant to proteolytic degradation, especially the globular of cImI-A, for which almost 95% peptide remained after a 5-hour incubation with trypsin, whereas wild-type ImI only had 20% peptide remained. The stability of the cyclic variants of the ribbon isomers was not significantly improved compared to the wild-type ImI, indicating that cyclisation is not the only factor that leads to peptide stability for non-native disulfide isomers. For examples, the disulfide bonds can be reduced by glutathione.

α-Conotoxin Vc1.1

Conotoxin Vc1.1 targets the α9α10 nAChR and the N-type calcium channel via the $GABA_B$ receptor (25-27). In several animal models, this peptide has been shown to have potential as a treatment for neuropathic pain (28). However, Vc1.1 is susceptible to disulfide shuffling and degradation by proteases, and backbone cyclisation of this peptide was successfully applied to stabilise it against enzymatic proteolysis (13).

Based on Vc1.1 NMR solution structure, the distance between the N- and C- termini is ~12 Å, which is similar to that of MII. Two linkers with five and six residues, respectively, were designed: GGAAG and GGAAGG. Under thermodynamic conditions, both globular and ribbon isomers formed in the proportions of 72:28 for cVc1.1-6 and 50:50 for cVc1.1-5. NMR chemical shift analysis suggested that the globular isomers of both cVc1.1-5 and -6 were similar to wild-type Vc1.1. The solution structure of cVc1.1-6 evidenced that the side chains and backbone had similar conformations to those of linear Vc1.1. Cartstens *et al.* investigated the effects of the composition of linker sequence of Vc1.1 on the structure, activity and stability, the results showed that non-neutral amino acids in the cyclising linker sequence can have a negative effect on biological activity but not for structure and stability (29).

cVc1.1-5 showed a substantial loss of activity in inhibiting the nAChR in adrenal chromaffin cells, whereas cVc1.1-6 retained the activity of linear Vc1.1. cVc1.1-6 was tested for inhibition of both rat α9α10 nAChR and high voltage-activated (HVA) calcium channels in rat DRG neurons. cVc1.1-6 was more potent at inhibiting the HVA calcium channels with full biological activity via the $GABA_B$ receptor than linear Vc1.1, with IC_{50} values of 0.3 and 1.7 nM, respectively. By contrast, the activity at the rat α9α10 nAChR dropped 10-fold, from IC_{50}= 64 nM (Vc1.1) to IC_{50}= 765 nM (cVc1.1-6). The solution structure of cVc1.1-6 suggests that the linker might interfere with binding of Ser4 and Asp5, which have both been shown to be important for activity at nAChR. This same region of the sequence was recently reported to be crucial for activity on HVA calcium channels (30).

Using the chronic constriction injury model of neuropathic pain in rats, cVc1.1-6 delivered orally was 120-fold more potent than gabapentin, which is in clinical use. By contrast, linear Vc1.1 had no effect in a similar assay, suggesting that cyclisation was responsible for introducing the oral activity. In a more recent study, cVc1.1-6 and its analogous, [C2H,C8F]cVc1.1 and [N9W]cVc1.1, showed to have the ability to inhibit colonic nociceptors and to reduce chronic abdominal pain in a mouse model (31). The stability of linear Vc1.1 and cVc1.1-6 in three different fluids was measured. Compared to Vc1.1, stability was only slightly improved in simulated gastric fluid, but remarkably improved in both simulated intestinal fluid and human serum. cVc1.1-6 was significantly more stable than Vc1.1, judged by increased amounts remaining after 24 hours in all three assays. Cyclisation also prevented the shuffling of disulfide bonds, which was suggested to occur for Vc1.1 in simulated intestinal fluid and human serum.

Jia *et al.* (9) showed that Vc1.1 could be cyclised enzymatically using sortase A, a bacterial enzyme with transpeptidase activity. Sortase A recognises the "LPXTG" motif at the C-terminus of a peptide, cleaving the amide bond between the Thr and Gly residues to form a thioacyl-linked intermediate, which in turn reacts with a N-terminal Gly residue to form a peptide bond. The linear substrate [G]Vc1.1[GLPETGGS] was synthesised and successfully cyclised by sortase A to yield cyclo-[G]Vc1.1[GLPET]. NMR Hα secondary chemical shift analysis suggested that there was no significant structural difference between cyclo-[G]Vc1.1[GLPET] and cVc1.1-6. The biological activity and stability of cyclo-[G]Vc1.1[GLPET] were not investigated.

α-Conotoxin RgIA

RgIA inhibits the α9α10 nAChR and also blocks N-type calcium channels via activation of the $GABA_B$ receptor. Five linkers were designed to cyclise RgIA (3), with the longer ones (GAAGG, GGAAGG and GGAAGAG) resulting in similar structures to the parent globular isomer according to NMR Hα secondary chemical shifts. The shorter linkers (GAA and GAAG) resulted in peptides adopting a different conformation from RgIA, according to NMR chemical shifts, and were not further investigated. The NMR solution structure of cRgIA-6 (with linker GGAAGG) was solved and revealed a well-defined structure, which is similar to RgIA. From an analysis of the NMR models, Loop 2 was suggested to be slightly more disordered than in RgIA. This difference in the resulting NMR models probably arose from broader NMR peaks and fewer NOEs near Tyr10 in cRgIA-6.

cRgIA-7 was as potent as the parent peptide at inhibiting the hα9/rα10 nAChR expressed in *Xenopus oocytes* but the other four variants displayed reduced activity. Interestingly, the selectivity of cRgIA-6 for the calcium channel via the $GABA_B$ receptor was increased, as it has more than 10-fold higher inhibition of this pathway compared to its activity at hα9/rα10 nAChR whereas RgIA was equipotent at both target (3). Positions important for the activity of RgIA are not at the proximity of the termini in the sequence and therefore were *a priori* expected not to be affected by cyclisation. The unexpected higher flexibility of Loop 2 in cRgIA-6 could have affected the interaction of Arg9, which is important for binding to α9α10 nAChR, providing a possible explanation with the decreased activity at this receptor.

The stability of linear RgIA and of all cyclic analogues was assayed in human serum. About 8% of linear RgIA remained after 5 hours, whereas 57% and 46% of cRgIA-6 and cRgIA-7 remained at the same time-point, respectively, showing the significantly improved stability brought about by backbone cyclisation.

α-Conotoxin AuIB

α-Conotoxin AuIB selectively inhibits the α3β4 nAChR (32, 33), which is implicated in the mediation of signalling in various physiological systems, including ganglionic transmission peripherally and nicotine-evoked neurotransmitter release centrally (34).

Armishaw *et al*.(14) designed seven linkers, varying in length from one to seven residues (A, AG, AGG, AGGG, GGAAG, GAGAAG and GGAGGAG), to cyclise AuIB. The cyclic peptides were folded using a one-pot oxidation procedure. Cyclic peptides using the short linkers A, AGG or AGGG preferentially formed the ribbon isomer, whereas other cyclic variants, ie using two-, five-, six- or seven-residue linkers, folded into both globular and ribbon isomers. All cyclic AuIB analogues lost their activity at the rat α3β4 nAChR except cAuIB-2 globular isomer, which had only slightly reduced activity (three-fold) compared to AuIB. In a stability assay carried out in the same study, the parent peptide was >90% degraded after a 48-hour incubation with chymotrypsin but ~40% of cAuIB-2 globular isomer remained and >90% of cAuIB-3, -4, -5, -6 and -7 ribbon isomers remained.

In an independent study, Lovelace *et al*. (15) cyclised AuIB using four different linkers (GGAA, AGAGA, GGAAGG and GGAAAGG). A one-pot oxidation method was also used to form the disulfide bonds. Similarly to Armishaw *et al*., the four-residue linker cyclic peptide folded into a ribbon isomer, whereas cyclic peptides using longer linkers of five, six or seven residues resulted in a mixture of ribbon and globular isomers. In contrast to Armishaw *et al*., the preponderant isomer of five and six residue linker cyclic peptides was the globular isomer, indicating that the nature of the linker and its size affect disulfide connectivities. The NMR solution structures of globular cAuIB-4, -5 and -6 were solved, showing that these three globular isomers had a similar structure to their parent peptide. The structures of the ribbon isomers could not be determined because their NMR spectra contained few NOEs, suggesting that their structures were not well defined.

All cyclic peptides showed decreased or no activity at the α3β4 nAChR expressed in oocytes compared to AuIB. The most active analogue active was globular cAuIB-4, which reduced 65% of the current at 3 μM, compared to 50% reduction at the same concentration for globular AuIB. Ribbon cAuIB-4 was the most active cyclic ribbon isomer, with 65% current reduction at 10 μM compared to 50% for ribbon AuIB. A possible explanation for the decrease of activity of the cyclic variants is that the N-terminal Gly1 was shown to be important for activity, and the cyclisation linker might affect its interaction with nAChR.

Overall, cyclisation of AuIB can improve, to some extent, its stability as less than 5% of the linear ribbon isomer remained after a 24-hour incubation in human serum, whereas >70% of the linear globular and all cyclic variants (both the globular and ribbon isomers) remained.

2.1.1.2 Ribbon isomers

As noted earlier, ribbon isomers are much less common than globular isomers amongst native conotoxins but some interesting conotoxins adopt this fold. For example, MrIA, has been extensively studied and has been the subject of both chemical and chemo-enzymatic cyclisation approaches.

χ-Conotoxin MrIA

This 13-residue conotoxin was the first ribbon conotoxin to be cyclised. The analogue of MrIA that progressed to clinical trials as an inhibitor of the NET, Xen2174, has a modified N-terminus, i.e. a pyroglutamic acid, which led to an increase in plasma stability. After a 6-hour incubation in plasma, ~70% of Xen2174 remained compared to ~50% for the parent peptide, ie the improvement in stability was of 20% (35).

Chemical cyclisation rather than just N-terminal modification has been used as an alternative approach to further improve the stability of MrIA (6,16). MrIA has a β-hairpin structure, and the two termini are in spatial proximity. As a result, a short peptide linker of only two amino acid residues (AG) could be used to cyclise MrIA, resulting in a compound, cMrIA-AG, with a similar structure and activity to the parent peptide (16). The cyclic peptide was substantially more resistant to trypsin digestion than the parent peptide, with 97% of cMrIA-AG remaining compared to ~55% of linear MrIA after 24 hours of incubation with trypsin. Amide exchange rates monitored by NMR spectroscopy evidenced that cMrIA-AG was more rigid than the native peptide. The improved resistance toward endoproteases such as trypsin, of cMrIA-AG was suggested to originate from this backbone increased rigidity (16).

In a recent study, cMrIA-AG was used as a scaffold to stabilise the RGD motif, which targets the integrin receptor $\alpha_{IIb}\beta_3$ and prevents platelet aggregation (6). This study aimed at incorporating two pharmacophores in the same peptide, which could then interact with two different targets. Because Gly6, Tyr7, Lys8, Leu9 and His11 of MrIA are important for binding to the NET, Asn1 and Ala14 of cMrIA-AG were replaced by Asp1 and Arg14, respectively, to form the RGD motif in the cyclisation linker. The NET inhibitory activity of cMrIA-RGD was similar to that of MrIA, and the grafted RGD peptide also prevented platelet aggregation. Interestingly, cMrIA-RGD displayed better plasma stability than cMrIA-AG, with >50% and ~30% remaining after 24 hours of digestion, respectively. From mass spectrometry data, the

authors propose that Asn1 of cMrIA-AG can be deamidated in rat plasma but Asp1 of cMrIA-RGD cannot, providing an explanation for the difference of stability (6).

MrIA has also been recently cyclised enzymatically using butelase 1(11), a naturally occurring asparaginyl endopeptidase (AEP) from the butterfly pea plant (*Clitoria ternatea*) that is involved in the biosynthetic production of cyclotides (11). The enzyme requires an Asn or Asp residue followed by the dipeptide His-Val at the C-terminus of the linear substrate peptide to be cyclised (Figure 2.1 C). The dipeptide is ultimately cleaved off during the ligation reaction (11). The two residues His and Val were added to the C-terminus of synthetic linear MrIA-AG to create a substrate for butelase. The enzymatic reaction was very rapid (12 minutes) and the yield of cyclisation was >95% (11), demonstrating the value of chemoenzymatic cyclisation. However, biological assays and structure and stability assays were not performed, and further studies are required to confirm whether cyclic MrIA generated by butelase 1 can retain the native biological activity and improved stability. At the time of writing, butelase 1 had not been able to be produced recombinantly, but Harris *et al*.(36) recently reported recombinant production of an AEP from *Oldenlandia affinis* – a very efficient cyclising agent for a range of peptides. We anticipate that chemoenzymatic cyclisation of conotoxins and a variety of other peptides will be facilitated by this development.

2.1.2 Framework VI/VII conotoxins (three disulfide bonds)

As illustrated in Chapter Table 1.1, Framework VI/VII conotoxins contain the cysteine pattern C-C-CC-C-C, a very common pattern, found in more than 600 conotoxins to date. This is the pattern of MVIIA, a 25-residue conotoxin that has attracted significant attention for its therapeutic applications.

ω-Conotoxin MVIIA

MVIIA blocks N-type calcium channels and was the first conotoxin-based drug approved to treat neuropathic pain (37,38). It contains three disulfide bonds that are connected to form an inhibitor cystine knot (ICK) motif, which is a particular class of knottin (in practice, the term knottin and cystine knot are used interchangeably). MVIIA is administered to patients intrathecally, a route of administration that has limited the market of this drug to severe or intractable pain cases (39). Backbone cyclisation of MVIIA was reported in the early patent literature and more recently by Hemu *et al*. (17).

Tert-butoxycarbonyl (Boc) solid phase peptide synthesis is typically used to synthesise cyclic peptides because the thioesters used in NCL are not compatible with the repetitive piperidine deprotection steps and base solutions in fluorenymethoxycarbony (Fmoc) chemistry. HF acid treatment is required to deprotect side chains in Boc chemistry, but using such strong acid is inconvenient because it requires specialised equipment and is potentially hazardous. Thus, it is of interest that Hemu *et al.* succeeded in using Fmoc chemistry to synthesise cyclic conotoxins. Specifically, they developed an N-methyl Cys (MeCys) thioester surrogate, which they used to synthesise cyclic MVIIA with a four-residue linker (GGPG). The disulfide bonds with native connectivity (Cys I-Cys IV, Cys II-Cys V and Cys III-Cys VI) were formed after the cyclisation reaction.

k-Conotoxin PVIIA

PVIIA blocks the *shaker* K_v channel with an IC_{50} of 57 nM (40). This conotoxin exhibits cardio-protective properties in animal models and has clinical potential associated with cardiac reperfusion (41). As for MVIIA, it contains three disulfide bonds which form an ICK motif.

Kwon *et al.* showed that the ICK PVIIA could also be cyclised enzymatically using sortase A, which was successfully applied to cyclise Vc1.1, as noted in the last section. The linear [GGG]PVIIA[LPETGG] was cyclised to cyclic PVIIA with the yield of 57 % after 8 h incubation in sortase A. Interestingly, the cyclic PVIIA reduced activity on *shaker* K_v channel with IC_{50} value of 824 ± 60 nM which was 10-folds higher than that of native PVIIA (IC_{50}: 80 ± 5 nM), although the 3D structures and overall backbone conformations of the cyclic and acyclic PVIIA are high similar. Molecular modelling results indicated that the N-terminus of PVIIA was required for an interaction between PVIIA and the *shaker* K_v channel, which possibly resulted in the drop of the potency of cyclic PVIIA. The N-terminus acetylated PVIIA was synthesised and the activity decreased by 20-fold compared to PVIIA, which confirmed the hypothesis. Surprisingly, the PVIIA remained intact after 12 h incubation in human serum whereas only ~ 50 % of cyclic PVIIA was detected. But there is no accurate interpretation for this finding (18).

2.1.3 Framework IX conotoxins (three disulfide bonds)

Framework IX conotoxins have the cysteine pattern C-C-C-C-C-C and are relatively limited in number (Table 1.1 in Chapter 1) but two examples from this family have been cyclised recently, as described below.

Conotoxin gm9a and bru9a

The conotoxins gm9a and bru9a have three disulfide bonds that form an ICK, similarly to other toxins displaying a Framework VI/VII. A cystine knot embedded within a cyclic backbone is referred to as a cyclic cystine knot framework, which is a structural motif that has been widely used in developing new treatments for a range of diseases, including pain, cancer, cardiovascular disease and multiple sclerosis (42). Thus, the cyclisation of Framework IX conotoxins provides a strong link to grafting studies of cyclotide, which share the same framework. As an illustration of this, a recent study reported the cyclisation of gm9a and bru9a, thereby transforming their ICK motif into a cyclic cystine knot motif (19). It should be noted that the biological target of these peptides is still unknown, but cyclisation was attempted as a proof-of-concept that conotoxins displaying an ICK motif could be cyclised.

The primary purpose of cyclisation is typically to improve the stability of peptides, while maintaining their biological activity. The ICK motif is already highly stable and the aim in cyclising. Framework IX conotoxins were to prove that cyclisation can be applied to conotoxins with an ICK motif. Using a 3-residue Gly-Leu-Pro linker, which is present in the cyclisation loop of cyclotides, both gm9a and bru9a were successfully cyclised. The NMR solution structures of the two cyclic peptides were well-defined with mean backbone RMSD to the average structure of 0.16 Å for cyclic gm9a and 0.46 Å for cyclic bru9a. Both cyclic peptides had similar structures to their parent peptide.

The linear and cyclic peptides were both very stable in human serum with ~90% peptide remaining after 24 hours(19). This result is consistent with a previous study that reported the cystine knot being more important than the cyclic backbone for stabilizing peptides against endo-proteases (43).

2.2 Introduction

The sequence of conotoxin GeXIVA was identified recently in a transcriptome analysis of the venom duct of *Conus generalis* (44). This 28-amino acid peptide has four cysteines (Cys I–IV) which can theoretically form three isomers depending on the disulfide connections: globular (Cys I-Cys III; Cys II-Cys IV); ribbon (Cys I-Cys IV; Cys II-Cys III) or bead (Cys I-Cys II; Cys III-Cys IV) as shown in Figure 2.3. The bead and ribbon isomers are slightly more potent than the globular on both human and rat α9α10 nAChR (44). NMR structure calculations have

shown that ribbon GeXIVA is flexible, while still having a more defined structure than the other two isomers (44). These isomers exhibit higher or similar potency at rat α9α10 nAChR compared with Vc1.1 (45) or RgIA (46). In addition, the ribbon and bead isomers of GeXIVA showed promise in relieving neuropathic pain in a chronic constriction injury model and also in a tail flick model of acute pain (47).

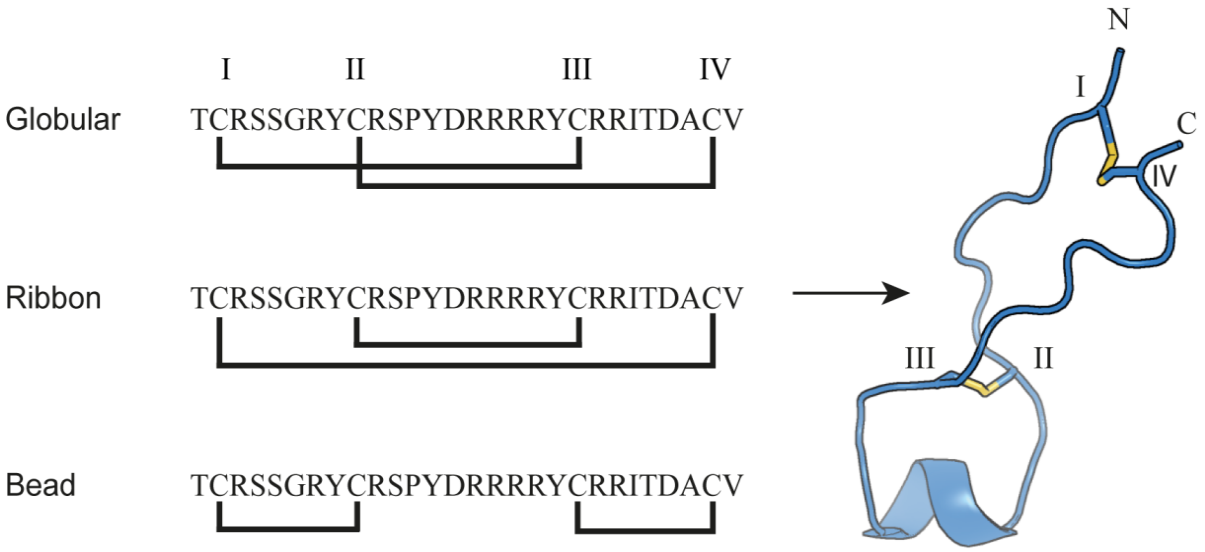

Figure 2.3 The three isomers of αO-conotoxin GeXIVA and the 3D NMR solution structure of ribbon GeXIVA (44). Cys residues are numbered with Roman numerals (I–IV) and the disulfide bonds are shown as yellow sticks; the structure shown for the ribbon GeXIVA is the lowest energy conformer from an ensemble of 10 NMR models.

Despite significant therapeutic properties of α-conotoxins, one major challenge is that the delivery of the conotoxin-based drugs to their receptors is potentially hindered by their susceptibility to proteolytic degradation in a biological fluid (48-50). Backbone cyclisation of conotoxins is a robust and effective method to improve the stability of conotoxins and also can improve the activity of conotoxins (13,51). In this Chapter, we investigated whether a similar strategy could be used for αO-conotoxin GeXIVA. We used backbone cyclisation to control the selective formation of the ribbon isomer and investigated the effects of cyclisation on structure, activity and stability. The ribbon isomer is formed by the oxidation of two cysteine residues located near the N- and C-termini of the peptide, suggesting that backbone cyclisation could be used to direct the selective formation of the resultant disulfide bond. The three isomers of linear GeXIVA and a suite of cyclic ribbon GeXIVA analogs were synthesised, and their stabilities in human serum and biological activities at the human α9α10 (hα9α10) nAChR were tested.

2.3 Methods and materials

2.3.1 Design of linkers

Linkers were designed using molecular modelling. The structure of the ribbon isomer cyclised with linkers from one to five amino acid residues was modelled. Fifty models of the backbone cyclised ribbon GeXIVA were generated for each of the linkers using Modeller 6v13 (52), and the conservation of ribbon GeXIVA native conformation was measured by computing the mean Cα RMSD between the models and the 20 lowest-energy NMR structures (44).

2.3.2 Peptide synthesis, cyclisation, oxidation and purification of peptides

The three isomers of GeXIVA and the three cyclic analogs (cGeXIVA_G, cGeXIVA_GG and cGeXIVA_GAG) were synthesised using Fmoc-based solid phase peptide synthesis on an acid-sensitive resin 2-chlorotrityl chloride. Side chains of Cys residues were protected in pairs with orthogonal protective groups that can be removed selectively under different oxidation conditions. The acid-labile trityl group was used to protect the side chains of Cys^{2} and Cys^{27}, and acetamidomethyl group to protect Cys^{9} and Cys^{20} for the ribbon GeXIVA and its cyclic variants. The backbone cyclisation of cyclic variants was achieved using the protocol described recently (8). Briefly, a solution of 1% TFA in dichloromethane (v/v) was used to cleave the linear precursor peptides of the cyclic variants off the resin. The side chain protected precursor peptides were dried, cyclised in O-(7-azabenzotriazol-1-yl)-*N*,*N*,*N'*,*N'*-tetramethyluronium hexafluorophosphate (5 mM) and *N*,*N'*-diisopropylethylamine (10 mM) in *N*,*N* -dimethylformamide for 3 h and lyophilized. The protecting group on side chains was removed in TFA with 2% triisopropylsilane and 2% water (v/v) for 2 h.

A two-step oxidative folding was used to form disulfide bonds: the first disulfide bond was formed in 0.1 M ammonium bicarbonate (NH_4HCO_3; pH 8.3) at room temperature (21-24°C) for 24 h and the second disulfide bond was formed in 0.1 M iodine solution for 1 h. All peptides were purified by reversed-phase high-performance liquid chromatography (RP-HPLC) using Phenomenex C_{18} columns (Gemini®: 5µM, 110Å, 250 × 10mm; Jupiter®: 5µM, 300Å, 250 × 4.6mm) and the purification method is 15-25% buffer B within 40 minutes (increasing 1% buffer B per 4 minutes). Buffer A is 0.05 % TFA in water and buffer B is 0.045% TFA in 90% acetonitrile.

2.3.3 NMR spectroscopy

Samples of peptide 2 and its cyclic analogs were prepared by dissolving peptide (~1mg) in 90% H_2O/10% D_2O at a pH of ~3. Spectra were recorded on a Bruker Avance III 600 MHz NMR spectrometer at 298K and included TOCSY (mixing times of 80ms), NOESY (mixing times of 200ms), H-N HSQC and H-C HSQC. Chemical shifts were referenced to internal 2, 2-dimethyl-2-silapentane-5-sulfonate (DSS) at 0 ppm. Spectra were processed with Topspin (Bruker Biospin) and analysed with CcpNMR analysis (version 2.4.1) (53). Secondary αH chemical shifts were calculated as the difference between the observed αH chemical shifts and that of the corresponding residues in a random coil peptide (54). Structure calculations were based upon distance restraints as derived from NOESY spectra, and on backbone φ and ψ dihedral angle restraints generated using TALOS+ (55). A family of structures consistent with the experimental restraints was calculated using CYANA (56).

2.3.4 Relaxation measurements

NMR relaxation measurements were carried out as described previously (57). Briefly, ^{13}C T_1 (spin-lattice) relaxation times were measured using the Bruker pulse program hsqct1etgpsi3d.2. Spectra were acquired with a spectral width of 10 ppm over 2048 complex points in the ^{1}H dimension and 22 ppm over 60 complex points in the ^{13}C dimension. To determine T_1 values, nine relaxation delays in the range of 0.01 to 1.0 s were used. A recycle delay of 3 s was used. ^{13}C NOEs were measured using the pulse program hsqcnoegpsi.2. Peak volumes were measured in CCPNMR. A recycle delay of 5 s was used. All experiments were carried out in triplicate. Order parameters were calculated by a model-free analysis using the same protocol and target function as described previously (57), but here the goodness-of-fit for the NOE values were given a 25% weighting compared to the T_1 values to allow for the higher uncertainty in the experimental NOE measurements.

2.3.5 Folding assays

Ribbon GeXIVA and cGeXIVA_GG were reduced with 10 mM dithiothreitol and isolated using RP-HPLC**.** Reduced peptides were dissolved in 0.1 M NH_4HCO_3 buffer (pH 8.3) at 20 µM and stirred at room temperature. An aliquot of peptide solution was removed after 0, 1, 4, 8, 12, 16, 20 and 24 h and quenched with 2% TFA. All samples were analysed with ultra-performance liquid chromatography using a gradient 11–18% buffer B within 28 min (increasing 1% buffer B per 4 min) in an analytical Vydac C_{18} column (201TP5415: 5µM, 300Å, 150 × 4.6mm).

2.3.6 In vitro cRNA synthesis

Plasmid pT7TS constructs of human α9 and α10 nAChR subunits were linearised with *XbaI* restriction enzymes (NEB, Ipswich, MA) for *in vitro* cRNA transcription using T7 mMessage mMachine® transcription kits (AMBION, Foster City, CA).

2.3.7 Oocyte preparation and microinjection

Stage V-VI oocytes were obtained from *X. laevis*, defolliculated with 1.5 mg/ml collagenase Type II (Worthington Biochemical Corp., Lakewood, NJ) at room temperature (21−23 °C) for 1−2 h in OR-2 solution containing (in mM) 82.5 NaCl, 2 KCl, 1 $MgCl_2$ and 5 HEPES at pH 7.4. Oocytes were injected with 35 ng cRNA for hα9α10 nAChR (concentration confirmed spectrophotometrically and by gel electrophoresis) using glass pipettes pulled from glass capillaries (3-000-203 GX, Drummond Scientific Co., Broomall, PA). Oocytes were incubated at 18 ºC in sterile ND96 solution composed of (in mM) 96 NaCl, 2 KCl, 1 $CaCl_2$, 1 $MgCl_2$ and 5 HEPES at pH 7.4, supplemented with 5% fetal bovine serum, 50 mg/L gentamicin (GIBCO, Grand Island, NY) and 10000 U/mL penicillin-streptomycin (GIBCO, Grand Island, NY).

2.3.8 Oocyte two-electrode voltage clamp recording and data analysis

Electrophysiological recordings were carried out 2–5 days post cRNA microinjection. Oocytes expressing hα9α10 nAChRs were incubated in 100 μM BAPTA-AM ~3 h before recording. Two-electrode voltage clamp recordings were performed at room temperature using a GeneClamp 500B amplifier and pClamp9 software interface (Molecular Devices, Sunnyvale, CA) at a holding potential −80 mV. Voltage-recording and current-injecting electrodes were pulled from GC150T-7.5 borosilicate glass (Harvard Apparatus, Holliston, MA) and filled with 3 M KCl, giving resistances of 0.3–1 MΩ. Oocytes were perfused with ND115 solution containing (in mM): 115 NaCl, 2.5 KCl, 1.8 CaCl2, and 10 HEPES at pH 7.4, using a continuous Legato 270 push/pull syringe pump perfusion system (KD Scientific, Holliston, MA) at a rate of 2 mL/min.

Initially, oocytes were briefly washed with ND115 solution followed by 3 applications of acetylcholine (ACh) at a half-maximal effective concentration (EC_{50}) of 6 μM ACh for hα9α10 nAChR. Washout with bath solution was done for 3 min between ACh applications. Oocytes were incubated with peptides for 5 min with the perfusion system turned off, followed by co-application of ACh and peptide with flowing bath solution. All peptide solutions were prepared

in ND115 + 0.1% bovine serum albumin. Peak current amplitudes before (ACh alone) and after (ACh + peptide) peptide incubation were measured using Clampfit 10.7 software (Molecular Devices, Sunnyvale, CA), where the ratio of ACh + peptide-evoked current amplitude to ACh alone-evoked current amplitude was used to assess the activity of the peptides at human nAChRs.

All electrophysiological data were pooled (n = 4 to 12) and represent means ± standard error of the mean (SEM). Concentration-response curves were obtained using GraphPad Prism 7 nonlinear regression analysis (GraphPad Software, La Jolla, CA, USA). The IC_{50} was determined from the concentration-response curve and reported with an error of the fit.

2.3.9 Stability assays

Serum stability of peptides was carried out in 25% human serum (human male AB plasma, Sigma-Aldrich) over 4 h using a 20 μM final peptide concentration. Serum was prepared by centrifugation at 17,000 g for 15 min to remove the lipid component, and the supernatant was diluted 1 in 4 in phosphate buffered saline and incubated at 37°C for 15 min before the assay. Each peptide was incubated in 25% human serum at 37°C and aliquots were taken out at time points 0, 1, 2, 3 and 4 h, respectively. Serum proteins were denatured with 2 M urea and precipitated with 20% TFA. All samples were centrifuged at 17,000 g for 10 min, and the supernatant was analysed by analytical RP-HPLC. Remaining peptides were quantified using peak height with absorption at 214 nm.

2.4 Results

2.4.1 Cyclic GeXIVA ribbon isomer retains native structure

NMR structure calculations for ribbon GeXIVA (44) showed that its N- and C- termini are maintained in close proximity (~6.4 Å) by a disulfide bridge between the first and last Cys residues (Figure 2.3). Five linkers (Figure 2.4) were designed using molecular modelling to bridge the termini, and all were geometrically compatible with the linear peptide structure, with the cyclic backbones maintained within 1 Å RMSD of the linear peptide. The data suggested that even a one-residue linker is sufficient to cyclise the backbone of ribbon GeXIVA without perturbing structure. Models of cyclic GeXIVA with minimum perturbation of the parent peptide backbone are shown in Figure 2.4. For experimental validation, we focused on three short linkers (G, GG and GAG) and the three corresponding cyclic variants: ribbon

cGeXIVA_G, ribbon cGeXIVA_GG and ribbon cGeXIVA_GAG. The three isomers of linear GeXIVA and the three cyclic ribbon analogs were synthesised using orthogonal protection of the cysteine side chains to orient the folding toward a unique disulfide isomer. The yields of three isomers of linear GeXIVA and cyclic ribbon GeXIVA were low (<1%) using a two-step oxidation method. Although we optimised the purification procedure, globular GeXIVA could not be completely purified. We therefore explored an alternative one-spot synthetic approach.

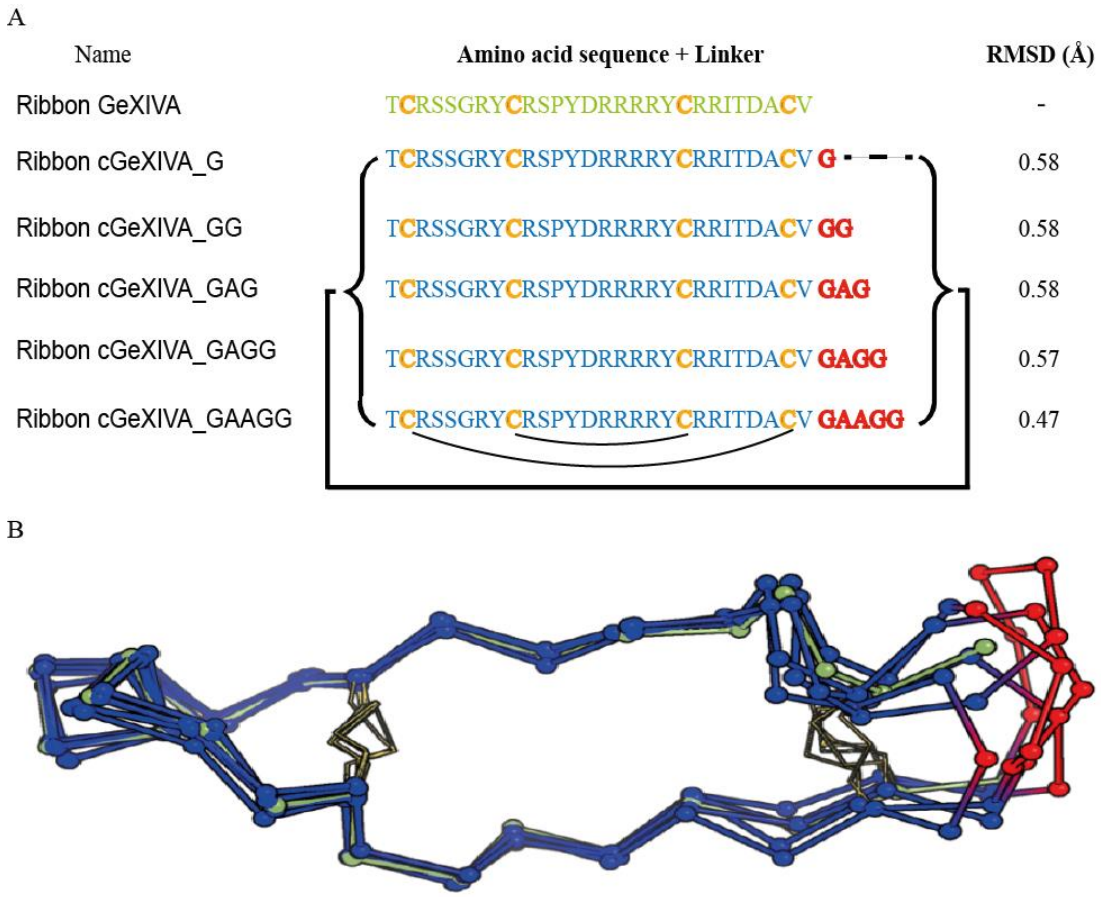

Figure 2.4 Amino acid sequences and NMR structure of ribbon GeXIVA and cyclic ribbon isomers of GeXIVA. **A**: Amino acid sequences of ribbon GeXIVA and cyclic analogs. The backbone cyclisation of ribbon GeXIVA was carried out using differently sized linkers (highlighted in red) spanning its N- and C-termini (indicated by the black bracket and line). The black curved lines below the sequence show the ribbon disulfide connectivity. The α-carbon (Cα) RMSD of the backbone for the parent peptide and molecular models of the cyclic peptides are shown in the last column. **B**: NMR solution structure of ribbon GeXIVA (green) and models of cyclic variants (backbones in blue and linkers in red). The disulfide bonds are represented by yellow sticks and the Cα are shown as balls.

2.4.2 One-pot oxidative folding

Fristly, linear peptides GeXIVA and cGeXIVA_GG were folded under thermodynamic oxidation conditions (NH_4HCO_3 (pH 8.3), room temperature) (Figure 2.5A). For the GeXIVA, three major products were formed within 20 h. The three major peaks were observed in the

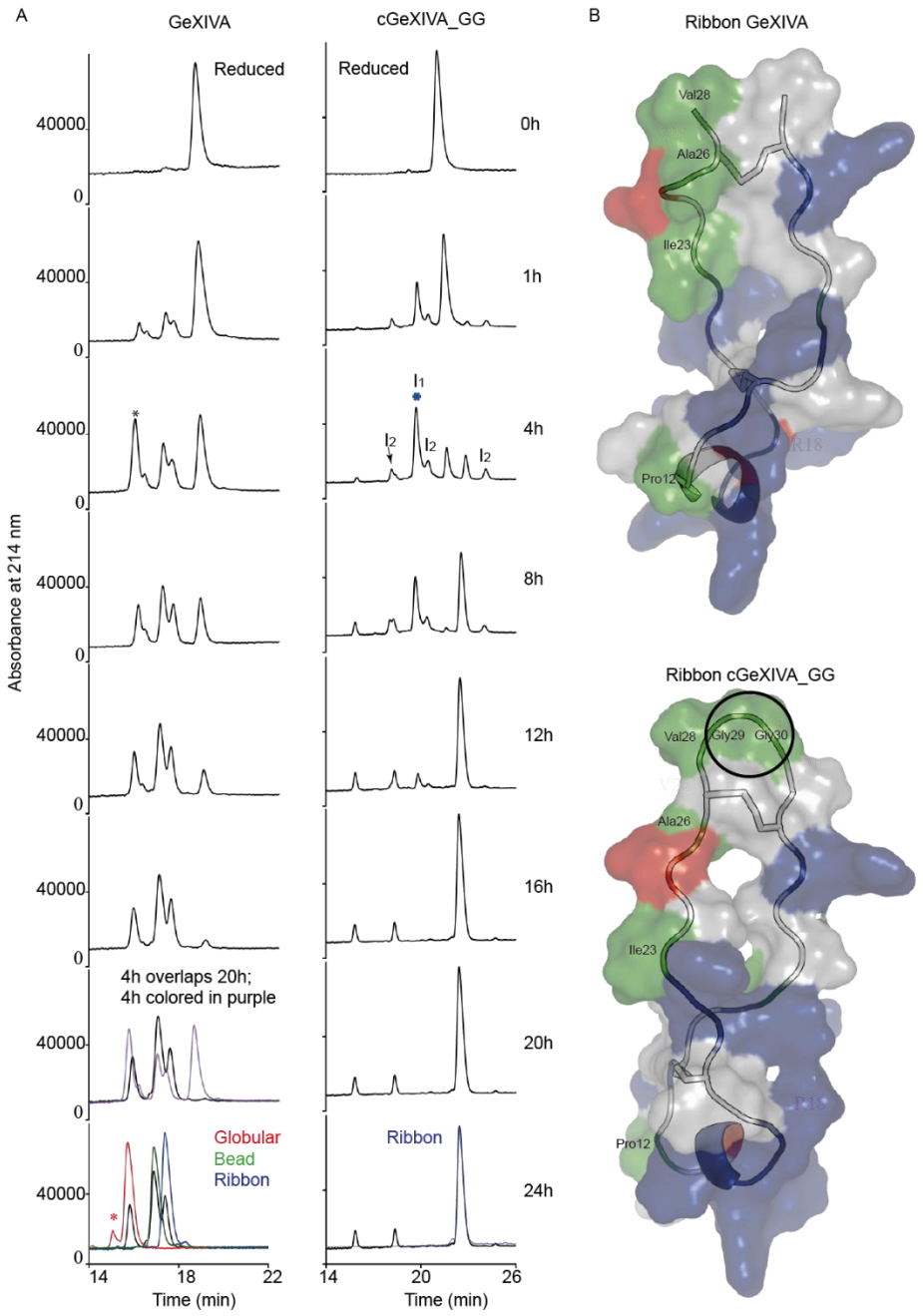

Figure 2.5 Time course of the oxidative folding of GeXIVA and cGeXIVA_GG. **A**: HPLC traces of samples taken at various times during the random folding process. For GeXIVA, the black asterisk indicates that the peak occurring in the folding process of GeXIVA comprises intermediate forms with similar retention time to the globular isomer and the red asterisk indicates an impurity. The globular, bead and ribbon GeXIVA from two-step oxidations are shown as red, green and blue traces, respectively. For cGeXIVA_GG, the blue asterisk indicates the major intermediate occurring in the folding process of cGeXIVA_GG. The ribbon cGeXIVA_GG from two-step oxidation is shown as a blue trace. I_1 represents the intermediate with one disulfide bond and I_2 represents the intermediates with two disulfide bonds. **B**: Surface representations of ribbon GeXIVA and ribbon cGeXIVA_GG. Positively charged residues are shown in blue, negative residues are red, polar residues are white, and hydrophobic residues are green. Surface representations were created using program PYMOL. Cyclisation of ribbon GeXIVA resulted in an additional hydrophobic patch (circle) in cGeXIVA_GG.

ultra-performance liquid chromatography trace, accounting for ~25%, 45% and 30% of the total peptide, respectively. Analysis of each peak using a TripleTOF 5600 mass spectrometer (AB SCIEX, Ontario, Canada) with a nanoelectrospray ionization source revealed masses of 3450.62, 3450.62 and 3450.63 Da, respectively, each corresponding to fully oxidised GeXIVA. The three peaks were unambiguously identified by co-elution with the globular GeXIVA, bead GeXIVA and ribbon GeXIVA isomers. The HPLC peaks of ribbon and bead GeXIVA partly overlapped and were difficult to separate (Figure 2.5A, 24 h). Interestingly, a single peak representing the majority of the oxidised forms transiently appeared from 1 to 4 h, and then disappeared from 4 to 8 h (Figure 2.5A; indicated by a black asterisk). This transient peak partly overlaps with the major final product (Figure 2.5A, 20 h), which was identified as globular GeXIVA. We hypothesized that the globular isomer might form within 4 h and then gradually convert into other isomers. We incubated globular GeXIVA in NH_4HCO_3 (pH 8.3) at room temperature at a final concentration of 20 μM and the globular GeXIVA was found to be very stable in the folding buffer for 24 h (data not shown), suggesting that the first major peak at 4 h mainly comprises intermediate forms with similar retention time to the globular isomer.

The one-step oxidation of reduced cGeXIVA_GG was complete at 16 h, whereas some intermediates could still be seen at that time for the linear GeXIVA. Only three products were formed, all of mass 3546.66 Da, corresponding to that of the fully oxidised cGeXIVA_GG. The third major peak, accounted for 86% of the total peptide content, and was confirmed as being the ribbon isomer by co-elution. The two other peaks are presumably the globular and bead isomers. In contrast to linear GeXIVA, the retention time of globular, bead and ribbon isomers of the cGeXIVA_GG separate well (Figure 2.5A) as the linker engenders ribbon cGeXIVA_GG with a larger hydrophobic patch than ribbon GeXIVA (Figure 2.5B; shown in green), which could explain its later retention time. Four intermediate forms were identified over the time course. The major intermediate (Figure 2.5A; indicated by a blue asterisk and named I_1) was the most abundant of the oxidised forms from 1 to 4 h. The major intermediate I_1 of cGeXIVA_GG was isolated and its mass was 3548.66 Da, indicating that it has only one disulfide bond. The masses of the three minor intermediates were each 3546.65 Da, suggesting that they have two disulfide bonds (all designated as I_2 in Figure 2.5A).

2.4.3 NMR analyses of ribbon GeXIVA and oxidatively folded and cyclised ribbon cGeXIVA_GG

A comparison of the secondary αH chemical shifts of ribbon GeXIVA with those of ribbon cGeXIVA_GG suggested very little difference in structure between the linear and cyclic analogs (Figure 2.6A). The different chemical environment created by the presence of the cyclising linker can easily explain the minimal shift differences near the termini. Overlapping peaks in the 2D NMR spectra prevented the unambiguous assignment of the cGeXIVA_G and cGeXIVA_GAG spin systems.

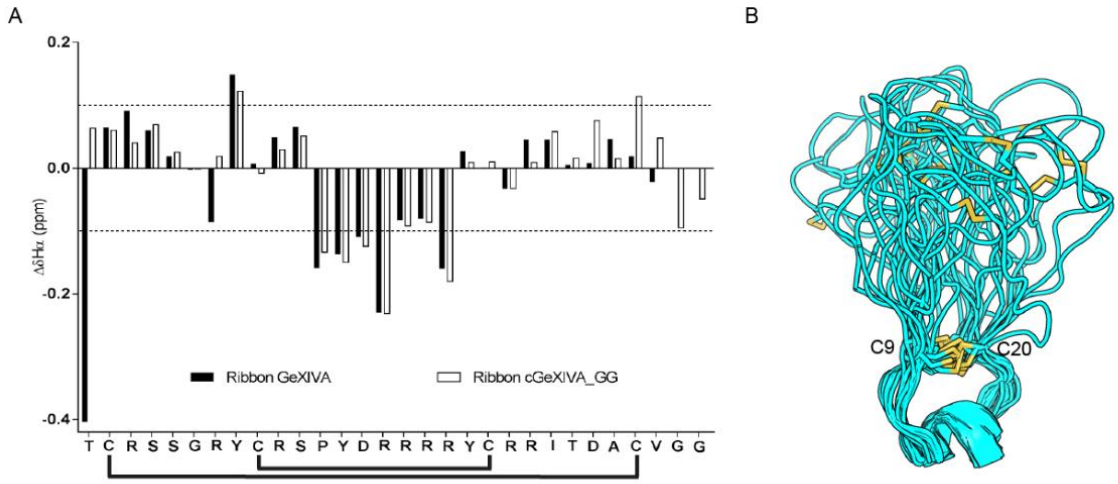

Figure 2.6 Structural characterisation of cGeXIVA_GG. **A:** Secondary αH chemical shifts of ribbon GeXIVA and ribbon cGeXIVA_GG (ΔδHα). The overall secondary structures of ribbon GeXIVA and ribbon cGeXIVA_GG are similar and both peptides display a 3_{10}-helix from Pro12 to Arg16. The black lines below the sequence show the ribbon disulfide connectivity. **B:** Ribbon diagram of the NMR solution structure of cGeXIVA_GG. Models were overlaid over the C9–C20 segment. Disulfide bonds are shown in yellow.

The 3D structure of cGeXIVA_GG was calculated with a total of 171 distance restraints and found to contain a short 3_{10}-helix (from P12–R16; Figure 2.6B). The S11-P12 peptide bond was determined to adopt a *trans* configuration, similar to the configuration of this bond in the ribbon and bead isomers of linear GeXIVA (44). As shown for ribbon GeXIVA (44), the loop formed between C9 and C20 overlays reasonably well between NMR models (RMSD of 1.38 ± 0.56 Å across backbone atoms of residues 9–20, Table 2.2); although the remainder of the peptide is somewhat disordered, suggesting a degree of flexibility. We thus used NMR spin relaxation measurements to characterise the backbone dynamics of cGeXIVA_GG (Figure 2.7, Table 2.3). Heteronuclear T_1 and NOEs were measured and used to derive order parameters reflective of motion of the Cα-Hα bonds. Due to spectral overlap, only 18 of the 22 residues could be analysed. Nevertheless, the order parameters (0.53–0.81; mean of 0.63) suggest that

cGeXIVA_GG is moderately flexible, which agrees with the geometric analysis of the lowest energy structures. The least flexible region is at the C-terminal end of the C9 to C20 loop.

Table 2.2 Statistical analysis of cGeXIVA_GG structures[a]

cGeXIVA_GG	Value
Experimental restraints	
total no. distance restraints	171
intraresidue	90
sequential	73
medium range, i-j<5	8
long range, i-j≥5	0
hydrogen bond restraints	2
dihedral angle restraints	32
NOE violations exceeding 0.3 Å	0
Dihedral violations exceeding 2.0 Å	0
Rms deviation from mean structure, Å	
backbone atoms (residues 9-20)	1.38 ± 0.56
all heavy atoms (residues 9-20)	3.33 ± 0.98
Stereochemical quality[b]	
Residues in most favoured Ramachandran region, %	77.9 ± 8.9
Ramachandran outliers, %	1.4 ± 1.8
Unfavourable sidechain rotamers, %	3.7 ± 2.6
Clashscore, all atoms	0.1 ± 0.4
Overall MolProbity score	1.6 ± 0.3

[a]All statistics are given as mean ± SD.
[b]According to MolProbity (58).

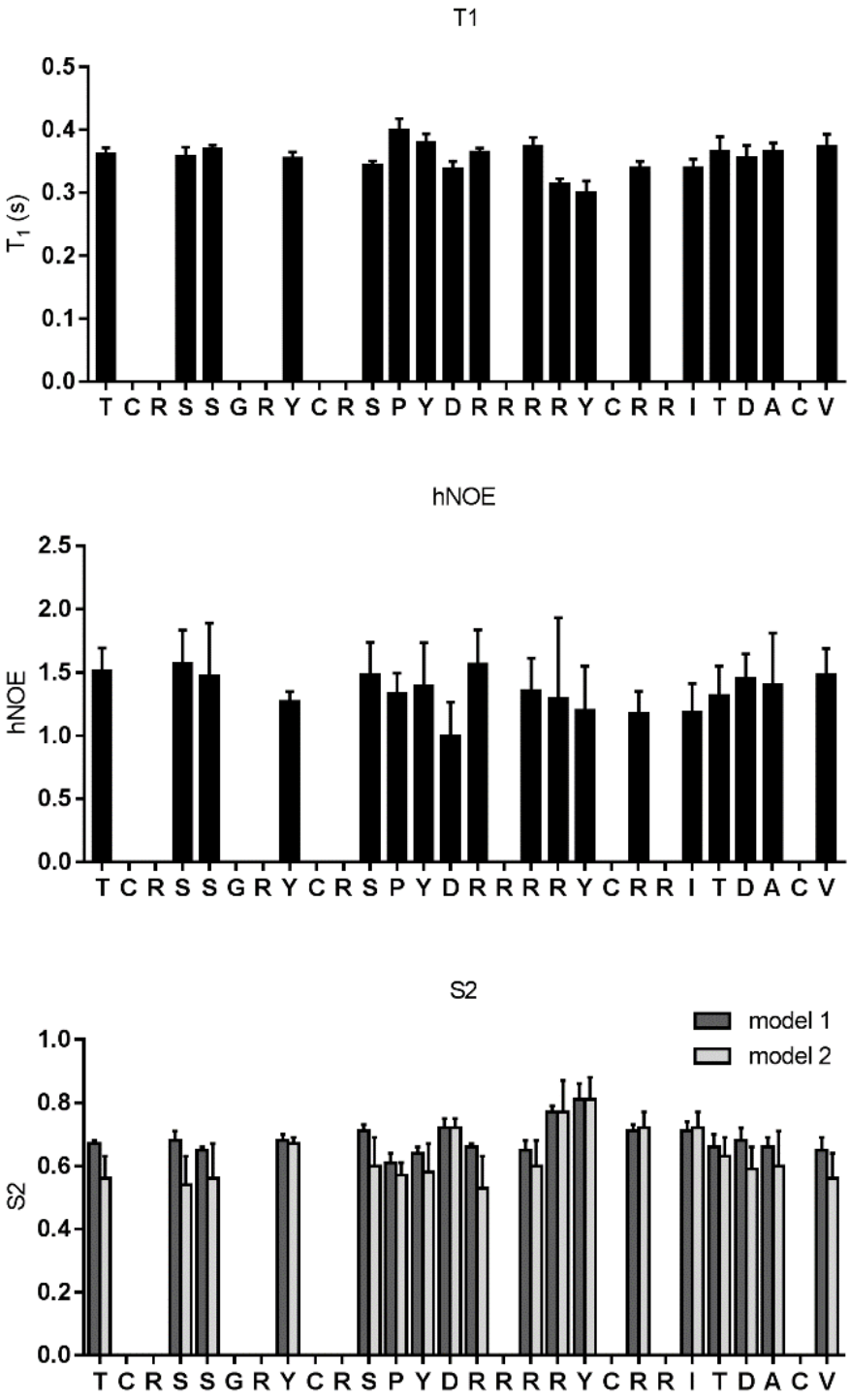

Figure 2.7 Experimental relaxation data and derived order parameters for cGeXIVA_GG. T1 (panel a) and heteronuclear NOE (panel b) values for the Cα nuclei were measured at 600 MHz. Errors are shown as the standard deviation of triplicate measurements. Only 18 of the residues could be analysed. A model-free analysis was used to derive order parameters (panel c). Models 1 and 2 of model-free were used in the analysis. Errors, shown as standard deviation, were estimated using a Monte Carlo algorithm.

Table 2.3 Relaxation data, fitted parameters, and error estimates for cGeXIVA_GG

Res[a]	Data[b]	T_1 (s)[c]	NOE[c]	τ_o	err[d]	τ_i	err[d]	S^2	err[d]	RMSD[e]
T1	***Exp***[f]	***0.36***	***1.51***							
	m1	0.36	1.23	1.38	0.08			0.67	0.01	
	m2	1.51	1.39	1.39	0.02	49.17	27.53	0.56	0.07	
C2	***Exp***	*NA*[g]	*NA*							
R3	***Exp***	*NA*	*NA*							
S4	***Exp***	0.36	1.57							
	m1	0.36	1.23	1.38	0.08			0.68	0.03	0.64
	m2	0.36	1.57	1.39	0.02	58.79	31.61	0.54	0.09	0.00
S5	***Exp***	0.37	1.47							
	m1	0.37	1.23	1.38	0.08			0.65	0.01	0.29
	m2	0.37	1.47	1.39	0.02	40.48	41.41	0.56	0.11	0.00
G6	***Exp***	*NA*	*NA*							
R7	***Exp***	*NA*	*NA*							
Y8	***Exp***	0.35	1.27							
	m1	0.35	1.23	1.38	0.08			0.68	0.02	0.24
	m2	0.35	1.27	1.39	0.02	8.30	12.68	0.67	0.02	0.00
C9	***Exp***	*NA*	*NA*							
R10	***Exp***	*NA*	*NA*							
S11	***Exp***	0.34	1.48							
	m1	0.34	1.23	1.38	0.08			0.71	0.02	0.48
	m2	0.34	1.48	1.39	0.02	50.50	36.54	0.60	0.09	0.00
P12	***Exp***	0.40	1.33							
	m1	0.40	1.23	1.38	0.08			0.61	0.03	0.30
	m2	0.40	1.33	1.39	0.02	15.00	16.53	0.57	0.04	0.00
Y13	***Exp***	0.38	1.39							
	m1	0.38	1.23	1.38	0.08			0.64	0.02	0.23
	m2	0.38	1.39	1.39	0.02	26.05	32.83	0.58	0.09	0.00
D14	***Exp***	0.34	1.00							
	m1	0.34	1.23	1.38	0.08			0.72	0.03	0.43
	m2	0.34	1.23	1.39	0.02	0.00	7.88	0.72	0.03	0.43
R15	***Exp***	0.36	1.57							
	m1	0.36	1.23	1.38	0.08			0.66	0.01	0.62
	m2	0.36	1.57	1.39	0.02	55.40	34.31	0.53	0.10	0.00
R16	***Exp***	*NA*	*NA*							
R17	***Exp***	0.37	1.35							
	m1	0.37	1.23	1.38	0.08			0.65	0.03	0.24
	m2	0.37	1.35	1.39	0.02	21.78	32.78	0.60	0.08	0.00
R18	***Exp***	0.31	1.29							
	m1	0.31	1.23	1.38	0.08			0.77	0.02	0.06
	m2	0.31	1.23	1.39	0.02	0.00	51.04	0.77	0.10	0.05
Y19	***Exp***	0.30	1.20							
	m1	0.30	1.23	1.38	0.08			0.81	0.05	0.05
	m2	0.30	1.23	1.39	0.02	0.00	44.45	0.81	0.07	0.05
C20	***Exp***	*NA*	*NA*							
R21	***Exp***	0.34	1.17							
	m1	0.34	1.23	1.38	0.08			0.71	0.02	0.17
	m2	0.34	1.23	1.39	0.02	0.00	21.77	0.72	0.05	0.16
R22	***Exp***	*NA*	*NA*							

I23	***Exp***	0.34	1.19							
	m1	0.34	1.23	1.38	0.08			0.71	0.03	0.10
	m2	0.34	1.23	1.39	0.02	0.00	25.60	0.72	0.05	0.10
T24	***Exp***	0.37	1.31							
	m1	0.36	1.23	1.38	0.08			0.66	0.04	0.18
	m2	0.37	1.31	1.39	0.02	16.23	28.58	0.63	0.06	0.00
D25	***Exp***	0.36	1.45							
	m1	0.36	1.23	1.38	0.08			0.68	0.04	0.58
	m2	0.36	1.45	1.39	0.02	41.87	27.89	0.59	0.07	0.00
A26	***Exp***	0.37	1.40							
	m1	0.37	1.23	1.38	0.08			0.66	0.03	0.21
	m2	0.37	1.40	1.39	0.02	31.06	39.01	0.60	0.11	0.00
C27	***Exp***	*NA*	*NA*							
	m1	0.37	1.23	1.38	0.08			0.65	0.04	0.58
	m2	0.37	1.48	1.39	0.02	40.22	23.05	0.56	0.08	0.00
G29	***Exp***	*NA*	*NA*							
G30	***Exp***	*NA*	*NA*							

[a] Relaxation data shown
[b] Two model-free models were analysed – m1 and m2
[c] Relaxation data measured at 600.13 MHz
[d] Errors obtained from 20 Monte Carlo simulations
[e] RMSD is the root-mean-squared deviation between experimental and fitted T_1 and NOE values. The NOE deviations were down-weighted to account for their intrinsically higher errors $RMSD = \sqrt{\sum \frac{\left(T_1^{exp} - T_1^{calc}\right)^2}{{\sigma_{T_1}}^2} + 0.25 \sum \frac{\left(NOE^{exp} - NOE^{calc}\right)^2}{{\sigma_{NOE}}^2}}$
[f] Exp, refers to the experimentally determined T1 and NOE values
[g] NA, not assigned due to spectral overlap.

2.4.4 Ribbon cGeXIVA_GG and ribbon GeXIVA are equipotent inhibitors of the human α9α10 nAChR subtype

Linear GeXIVA isomers have been shown to selectively and potently inhibit the rat α9α10 nAChR subtype (44). Here, globular, bead and ribbon isomers of linear GeXIVA, and cyclic constructs of ribbon GeXIVA (cGeXIVA_G, cGeXIVA_GG and ribbon cGeXIVA_GAG) were tested for their functional activity at the hα9α10 nAChR subtype heterologously expressed in *Xenopus laevis* oocytes. All three cyclic ribbon constructs tested at 100 nM, inhibited ACh-evoked currents mediated by hα9α10 nAChRs by ~60–70% (n = 4–6). Similarly, the bead (n = 5) and ribbon isomers (n = 8) of GeXIVA inhibited the hα9α10 ACh-evoked current amplitude by ~60–70%. In contrast, the globular GeXIVA was less potent, inhibiting hα9α10 ACh-evoked currents by ~40% (n = 12) (Figure 2.8A).

The concentration-dependent activity of globular and ribbon GeXIVA and ribbon cGeXIVA_GG at hα9α10 nAChRs were determined (Figure 2.8B). All peptides reversibly

inhibited ACh-evoked currents in a concentration-dependent manner, giving IC_{50} values of 198.6 ± 18.9 nM (n = 4–12) for globular GeXIVA, 35.1 ± 2.7 nM (n = 4–8) for ribbon GeXIVA and 37.6 ± 4.9 nM (n = 4–11) for ribbon cGeXIVA_GG. Consistent with the previously reported potency of globular and ribbon GeXIVA at rat α9α10 nAChRs, the globular isomer of GeXIVA had lower potency at hα9α10 nAChRs than the ribbon analog. Ribbon GeXIVA and ribbon cGeXIVA_GG had similar IC_{50}s, suggesting that backbone cyclisation had no impact on the potency of inhibition at hα9α10 nAChRs.

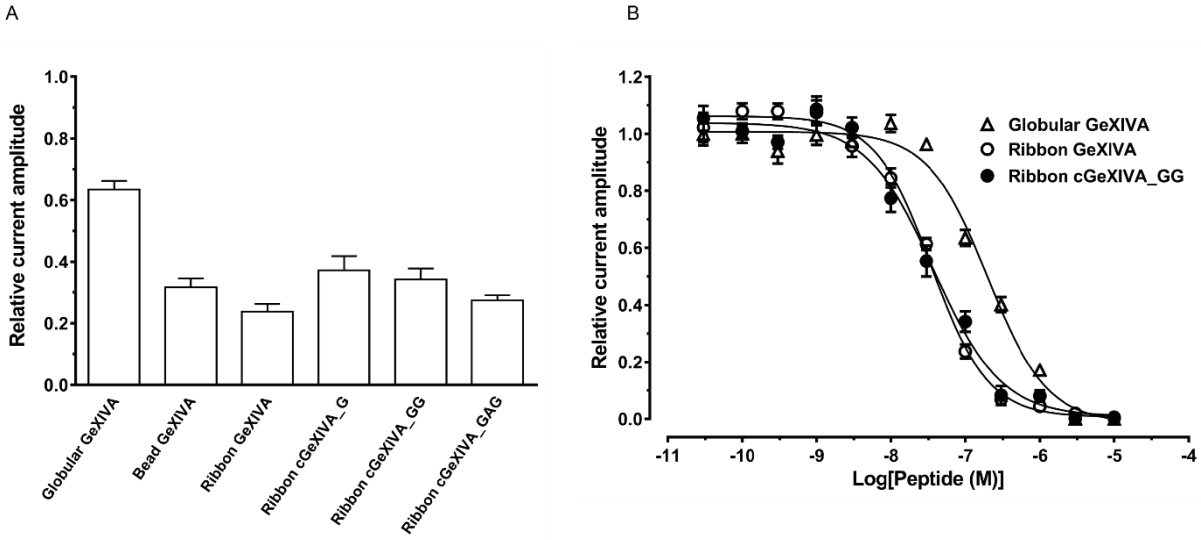

Figure 2.8 Inhibition of human α9α10 nAChR by linear GeXIVA and ribbon cGeXIVA isomers. **A:** Bar graph of globular GeXIVA, bead GeXIVA, ribbon GeXIVA, and ribbon cGeXIVA_G, ribbon cGeXIVA_GG and ribbon cGeXIVA_GAG (100 nM) inhibition of ACh-evoked peak current amplitude mediated by hα9α10 nAChRs. Whole-cell hα9α10 nAChR-mediated currents were activated by 6 μM ACh. **B:** Concentration-response curves of globular and ribbon GeXIVA, and ribbon cGeXIVA_GG inhibition of ACh-evoked currents mediated by hα9α10 nAChRs (mean ± SEM, n = 4-12).

2.4.5 Serum stability of linear GeXIVA and ribbon cGeXIVA isomers

Stability assays for the ribbon isomer of GeXIVA and its three cyclic analogs were carried out in human serum. All four peptides degraded within 2 h but the ribbon cGeXIVA_GG was slightly more stable than the other peptides (data for cGeXIVA_G and GeXIVA_GAG not shown). Subsequently, the stability of the three isomers of linear GeXIVA and of ribbon cGeXIVA_GG was compared to that of α-conotoxin cVc1.1 (13) in 25% human serum. The positive control, cVc1.1, was highly stable, whereas only ~20% of the three isomers of GeXIVA remained after 4 h incubation. Ribbon cGeXIVA_GG was more stable than the three linear isomers of GeXIVA ($p < 0.001$) at 4 h time point, with 38% of cGeXIVA_GG remaining (Figure 2.9).

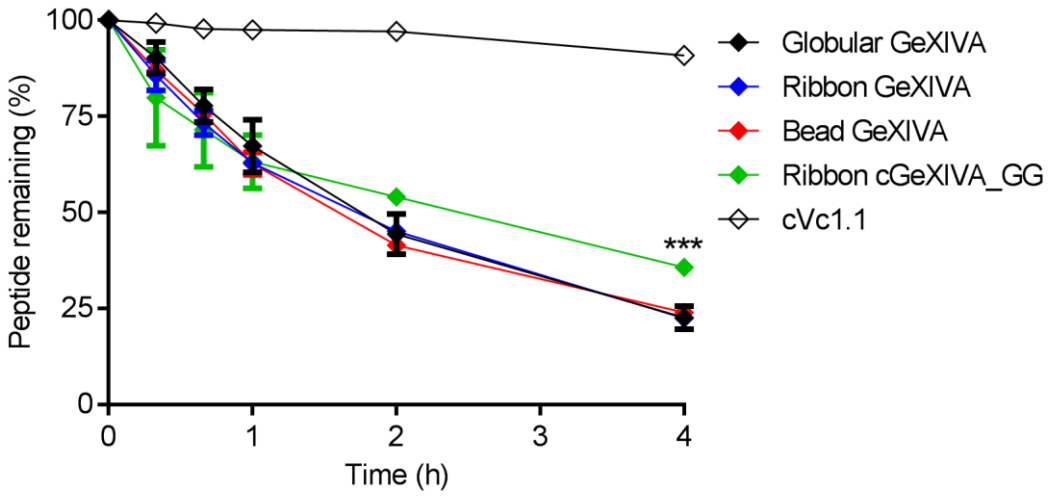

Figure 2.9 The stability of GeXIVA isomers, ribbon cGeXIVA_GG and cVc1.1 (positive control) in 25% human serum. The one-way ANOVA/Tukey test was used for comparing the remaining peptides at 4 h time point, and data were expressed as the mean ± SEM (*** $p < 0.001$); all values (except cVc1.1) were compared with that of ribbon GeXIVA.

2.5 Discussion

The α9α10 nAChR mediates efferent olivocochlear innervations in outer hair cells and modulates immune responses in lymphocytes (59-61). It is also reported to be implicated in pain and cancer (62,63). Only a handful of α-conotoxins is currently known to selectively inhibit the α9α10 nAChR (44,64-66), so studies of new examples, such as GeXIVA are important for defining receptor specificity. Furthermore, previous studies have highlighted the value of backbone cyclisation to enhance the biopharmaceutical properties of α-conotoxins (3,13) and so here we attempted to apply this approach to GeXIVA.

Molecular modelling was used to design linkers comprising only a small number of amino acids that would introduce minimal constraints into the peptide fold. A recent study highlighted the importance of the distance between the N- and C- termini in designing cyclizing linkers (1), but considering distances alone will not address limitations due to accessible conformations of backbones nor the orientation of the termini. Structural perturbations may be introduced unintentionally into a cyclic peptide when a linker is designed on the basis of distance only, ultimately decreasing biological activity (2,3). In the case of ribbon GeXIVA, modelling showed that the proximity of the termini would allow cyclisation with a single residue linker without affecting the structure. Since non-neutral amino acids in the cyclizing linker sequence can have a negative effect on biological activity (29), only Gly and Ala amino acids were used in the linkers in the current study. These residues are small, flexible and non-charged, and likely

to have minimal interference with biological activity. No more than two sequential Gly or Ala were used in any individual linker to avoid overlapping peaks in NMR spectra and thus avoid spectral assignment difficulties. Linkers composed of Gly and Ala residues have been successfully used to cyclise the α-conotoxins MII, RgIA and Vc1.1, without adversely affecting biological activity or structure (2,3,13).

The linkers used in this study did not affect the activity and structure of ribbon GeXIVA. Indeed, all cyclic ribbon variants, i.e. cGeXIVA_G, cGeXIVA_GG and cGeXIVA_GAG, had similar activity to the linear ribbon form at the hα9α10 nAChR. Although no structural data from peptides cyclised with a G or GAG linker was obtained due to NMR spectral overlap, the GG linker did yield a cyclised peptide with a very similar conformation to the linear ribbon GeXIVA. Alignment of the lowest energy model generated from NMR data and an analysis of the backbone relaxation measurements suggests that the cyclic variant is most rigid in the C9-C20 loop region but slightly more flexible in the remainder of the molecule. It has recently been shown that backbone cyclisation can enhance or retain backbone rigidity for three different classes of peptides, including for the conotoxin Vc1.1 (57). Cyclisation appears to have less of a rigidifying effect in GeXIVA.

The non-directed oxidation of GeXIVA resulted in the preferential formation of the bead isomer, followed by the ribbon and globular forms, which interestingly parallels their biological activity (44). By contrast, two previous studies employing the one-step oxidation of α-conotoxins showed the preferential formation of the globular isomer under similar conditions (0.1 M NH_4HCO_3; pH 8; room temperature) (67,68). A possible explanation for this difference in isomer formation is that GeXIVA displays a Cys framework XIV (C-C-C-C) with 6, 10 and 6 residues within the Cys I-Cys II, Cys II-Cys III and Cys III-Cys IV backbone segments, respectively, rather than the Cys framework I (CC-C-C) of most α-conotoxins with 0, 4 and 3–7 residues between the cysteines.

The one-step oxidation of cGeXIVA_GG was notably different from that of the linear parent peptide as it resulted in the preferential formation of the ribbon isomer. The use of short cyclising linkers has also been reported to drive oxidative folding towards the ribbon connectivity for three other conotoxins: α-conotoxins ImI and AuIB, and χ-conotoxin MrIA. Like GeXIVA, these peptides have four Cys residues, with Cys I and Cys IV being no more than three residues from the N- and C-termini, respectively. A short cyclising linker should

maintain these two Cys residues in spatial proximity in the reduced form and favour their cross-linking by a disulfide bond during oxidation.

During the oxidative folding of ribbon GeXIVA and ribbon cGeXIVA_GG, a major intermediate was identified. For GeXIVA, the amount of ribbon and globular isomers plateaued after 8 and 12 h incubation, respectively, whereas the bead form plateaued after 20 h. According to Wedemeyer *et al*., the rate of formation of disulfide bonds in an unstructured chain decreases with the number of residues between the two cysteines (69). Since 6, 10 and 6 residues exist between successive cysteines in GeXIVA we speculate that the major intermediate might involve a disulfide bond between Cys I and Cys II or between Cys III and Cys IV and that this intermediate subsequently translates into the bead isomer. For cGeXIVA_GG, there are only four residues between Cys I and Cys IV after backbone cyclisation, which may favour the formation of either a Cys I-Cys IV or Cys II-Cys III disulfide bond in the intermediate, thus leading to the ribbon isomer. Interestingly, three intermediates with two disulfide connectivities appeared during the course of folding of cGeXIVA_GG. The retention times of these three intermediates were different from the three stable isomers, suggesting that the intermediates have native-like connectivities but have meta-stable conformations.

We hypothesize that the preferential formation of the ribbon isomer probably results from the destabilisation of the alternative connectivities rather than through stabilisation of the ribbon form (Figure 2.10). Backbone cyclisation of ribbon GeXIVA is likely to affect folding energy

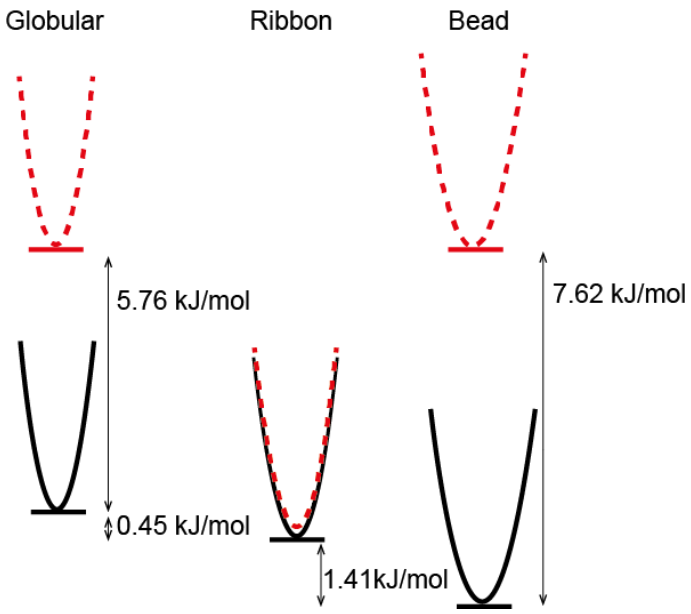

Figure 2.10 Schematic representation of the relative energy of the three linear isomers of GeXIVA (black) and their cGeXIVA_GG (dotted red) analogous. The energy difference between isomers of the same peptide was computed using a Boltzmann distribution of the isomers at equilibrium.

through an entropic effect, mainly impacting the unfolded state. Indeed, the linker has little interaction with the rest of the peptide in molecular models, suggesting that the termini are already maintained in proximity in the linear form and cyclisation does not result in structural perturbation to the core of the peptide. By contrast, the bead and globular isomers probably adopt a different set of conformations after being backbone cyclised because NMR characterisation of these isomers indicates that the globular form is disordered and the N- and C-termini of the bead isomer are uncoupled (44).

A two-step oxidation strategy is often used to oxidise conotoxins containing two disulfide bonds because the yields are typically improved compared to undirected folding (70). However, the oxidation of GeXIVA using this strategy only produced small amounts of products, hindering high-throughput structure-activity relationship studies and therapeutic studies. The yield of folded ribbon GeXIVA calculated from the final weight of oxidised peptide divided by the weight of reduced peptide was 0.5%. Using the results of Cheneval *et al*., to extrapolate the yield for the synthesis of an unprotected peptide (8), the yield of cyclic ribbon cGeXIVA_GG through a one-step folding method should be 8.6% using Fmoc-based solid-phase peptide synthesis and considerably higher for a Boc-based approach. Additionally, the HPLC elution peaks of ribbon and bead isomers of GeXIVA overlapped, whereas the ribbon isomer of cGeXIVA_GG is distinct, and ribbon cGeXIVA_GG therefore can be produced in greater purity using one-step oxidation than the ribbon GeXIVA using the same strategy.

An alternative strategy to increase the oxidative folding yield has been used in other cases of disulfide-rich peptides, including the widely used model system bovine pancreatic trypsin inhibitor (BPTI). Undirected folding of this protein results in the formation of two main species, one being native BPTI and the other a native-like two-disulfide intermediate (71). The addition of the N-terminal pro-region increased substantially the native BPTI formation, and it was identified that a cysteine residue in this region was responsible for this increased yield (72). Tethering a cysteine residue to the C-terminus with a flexible linker resulted in a similar effect, indicating that this residue acts as an internal catalyst.

Backbone cyclisation typically improves the stability of disulfide-rich peptides against enzymatic degradation, as demonstrated for several conotoxins, chlorotoxin, and a spider toxin (6,14-16,73-75). However, it was recently reported that cyclisation of κ-conotoxin PVIIA

decreased its stability in human serum (76), without significantly perturbing the structure relative to the native form (77). Here, we show that the IC_{50} for cGeXIVA_GG inhibition of hα9α10 nAChR (37.7 ± 5.0 nM) is comparable to that for ribbon GeXIVA (35.1 ± 2.7 nM). The stability in human serum of ribbon cGeXIVA_GG is only slightly improved compared to linear GeXIVA, suggesting that the main routes of degradation of GeXIVA are by endoproteases or side chain denaturation, which are typically less affected by backbone cyclisation. A possible target for such endoproteases are the nine arginine residues in the sequence of GeXIVA (78).

Using short linkers to enhance oxidative folding and other biopharmaceutical properties of bioactive peptides have broader applications than just for toxins, with perhaps a most striking example being for insulin. Insulin is an extremely important hormone but is difficult to synthesise owing to its two chains unique structure (79). In one study, the two peptide chains of human insulin were fused, increasing the production yield compared to native human proinsulin (80) while maintaining a native-like structure (81) but with an attendant loss of biological activity (82). In a later study, Hua *et al*. used a 6-residue linker, and the resulting insulin variant maintained biological activity and structure, and also had improved folding yield and stability (83). More recently, the nature of the linker region between the two insulin chains was further investigated, resulting in the identification of an insulin variant with the highest folding-efficiency to-date (79). In that study, it was shown that the linker region had a direct effect on folding yield by enhancing the formation of the native disulfide bond connectivity. The peptides in the current study have a direct analogy to single-chain insulin analogs: a suitable linker for cGeXIVA_GG, led to the preferential formation of the ribbon isomer, and significantly improved the product yield and stability whilst retaining the native-like structure and biological activity. The enhanced pharmaceutical properties deriving from a suitable linker provide an opportunity to develop GeXIVA as a potential therapeutic for the treatment of neuropathic pain, a condition with a huge unmet medical need (84). Treatment of neuropathic pain is challenging and alternative therapeutics are needed as currently available drugs such as morphine, gabapentin or antidepressants, are subject either to the development of tolerance or to significant side-effects (85,86).

In summary, the head-to-tail backbone cyclisation via a short linker of ribbon GeXIVA had no impact on the potency of inhibition at hα9α10 nAChR and a rationally designed linker favoured the formation of the ribbon disulfide connectivity and improved stability in human serum.

2.6 References

1. Clark, R. J., and Craik, D. J. (2012) Engineering cyclic peptide toxins. *Methods. Enzymol.* **503**, 57-74
2. Clark, R. J., Fischer, H., Dempster, L., Daly, N. L., Rosengren, K. J., Nevin, S. T., Meunier, F. A., Adams, D. J., and Craik, D. J. (2005) Engineering stable peptide toxins by means of backbone cyclization: stabilization of the alpha-conotoxin MII. *Proc. Natl. Acad. Sci. U. S. A.* **102**, 13767-13772
3. Halai, R., Callaghan, B., Daly, N. L., Clark, R. J., Adams, D. J., and Craik, D. J. (2011) Effects of cyclization on stability, structure, and activity of alpha-conotoxin RgIA at the alpha9alpha10 nicotinic acetylcholine receptor and GABA(B) receptor. *J. Med. Chem.* **54**, 6984-6992
4. Dawson, P. E., Muir, T. W., Clark-Lewis, I., and Kent, S. (1994) Synthesis of proteins by native chemical ligation. *Science* **266**, 776-779
5. Akcan, M., and Craik, D. J. (2015) Chapter 11. Engineering venom peptides to improve their stability and bioavailability. in *Venoms to drugs : venom as a source for the development of human therapeutics*. pp 275-289
6. Dekan, Z., Wang, C.-I. A., Andrews, R. K., Lewis, R. J., and Alewood, P. F. (2012) Conotoxin engineering: dual pharmacophoric noradrenaline transport inhibitor/integrin binding peptide with improved stability. *Org. Biomol. Chem.* **10**, 5791-5794
7. Clark, R. J., and Craik, D. J. (2010) Native chemical ligation applied to the synthesis and bioengineering of circular peptides and proteins. *Biopolymers* **94**, 414-422
8. Cheneval, O., Schroeder, C. I., Durek, T., Walsh, P., Huang, Y. H., Liras, S., Price, D. A., and Craik, D. J. (2014) Fmoc-based synthesis of disulfide-rich cyclic peptides. *J. Org. Chem.* **79**, 5538-5544
9. Jia, X., Kwon, S., Wang, C. I., Huang, Y. H., Chan, L. Y., Tan, C. C., Rosengren, K. J., Mulvenna, J. P., Schroeder, C. I., and Craik, D. J. (2014) Semienzymatic cyclization of disulfide-rich peptides using Sortase A. *J. Biol. Chem.* **289**, 6627-6638
10. Heinis, C. (2014) Drug discovery: tools and rules for macrocycles. *Nat. Chem. Biol.* **10**, 696-698
11. Nguyen, G. K., Wang, S., Qiu, Y., Hemu, X., Lian, Y., and Tam, J. P. (2014) Butelase 1 is an Asx-specific ligase enabling peptide macrocyclization and synthesis. *Nat. Chem. Biol.* **10**, 732-738

12. Armishaw, C. J., Dutton, J. L., Craik, D. J., and Alewood, P. F. (2010) Establishing regiocontrol of disulfide bond isomers of alpha-conotoxin ImI via the synthesis of N-to-C cyclic analogs. *Biopolymers* **94**, 307-313

13. Clark, R. J., Jensen, J., Nevin, S. T., Callaghan, B. P., Adams, D. J., and Craik, D. J. (2010) The Engineering of an orally active conotoxin for the treatment of neuropathic pain. *Angew. Chem. Int. Ed. Engl.* **49**, 6545-6548

14. Armishaw, C. J., Jensen, A. A., Balle, L. D., Scott, K. C. M., Sorensen, L., and Stromgaard, K. (2011) Improving the stability of alpha-conotoxin AuIB through N-to-C cyclization: the effect of linker length on stability and activity at nicotinic acetylcholine receptors. *Antioxid. Redox. Signal.* **14**, 65-76

15. Lovelace, E. S., Gunasekera, S., Alvarmo, C., Clark, R. J., Nevin, S. T., Grishin, A. A., Adams, D. J., Craik, D. J., and Daly, N. L. (2011) Stabilization of alpha-conotoxin AuIB: influences of disulfide connectivity and backbone cyclization. *Antioxid. Redox. Signal.* **14**, 87-95

16. Lovelace, E. S., Armishaw, C. J., Colgrave, M. L., Wahlstrom, M. E., Alewood, P. F., Daly, N. L., and Craik, D. J. (2006) Cyclic MrIA: a stable and potent cyclic conotoxin with a novel topological fold that targets the norepinephrine transporter. *J. Med. Chem.* **49**, 6561-6568

17. Hemu, X., Taichi, M., Qiu, Y., Liu, D. X., and Tam, J. P. (2013) Biomimetic synthesis of cyclic peptides using novel thioester surrogates. *Biopolymers* **100**, 492-501

18. Kwon, S., Bosmans, F., Kaas, Q., Cheneval, O., Conibear, A. C., Rosengren, K. J., Wang, C. K., Schroeder, C. I., and Craik, D. J. (2016) Efficient enzymatic cyclization of an inhibitory cystine knot-containing peptide. *Biotechnol. Bioeng.* **113**, 2202-2212

19. Akcan, M., Clark, R. J., Daly, N. L., Conibear, A. C., de Faoite, A., Heghinian, M. D., Sahil, T., Adams, D. J., Marí, F., and Craik, D. J. (2015) Transforming conotoxins into cyclotides: Backbone cyclization of P-superfamily conotoxins. *Biopolymers* **104**, 682-692

20. McIntosh, J. M., Azam, L., Staheli, S., Dowell, C., Lindstrom, J. M., Kuryatov, A., Garrett, J. E., Marks, M. J., and Whiteaker, P. (2004) Analogs of alpha-conotoxin MII are selective for alpha6-containing nicotinic acetylcholine receptors. *Mol. Pharmacol.* **65**, 944-952

21. Hill, J. M., Oomen, C. J., Miranda, L. P., Bingham, J.-P., Alewood, P. F., and Craik, D. J. (1998) Three-dimensional solution structure of alpha-conotoxin MII by NMR

spectroscopy: effects of solution environment on helicity. *Biochemistry* **37**, 15621-15630

22. Johnson, D. S., Martinez, J., Elgoyhen, A. B., Heinemann, S. F., and McIntosh, J. M. (1995) Alpha-Conotoxin ImI exhibits subtype-specific nicotinic acetylcholine receptor blockade: preferential inhibition of homomeric alpha 7 and alpha 9 receptors. *Mol. Pharmacol.* **48**, 194-199
23. Ellison, M., Gao, F., Wang, H. L., Sine, S. M., McIntosh, J. M., and Olivera, B. M. (2004) Alpha-conotoxins ImI and ImII target distinct regions of the human alpha7 nicotinic acetylcholine receptor and distinguish human nicotinic receptor subtypes. *Biochemistry* **43**, 16019-16026
24. Gehrmann, J., Daly, N. L., Alewood, P. F., and Craik, D. J. (1999) Solution structure of alpha-conotoxin ImI by ^{1}H nuclear magnetic resonance. *J. Med. Chem.* **42**, 2364-2372
25. Clark, R. J., Fischer, H., Nevin, S. T., Adams, D. J., and Craik, D. J. (2006) The synthesis, structural characterization, and receptor specificity of the alpha-conotoxin Vc1. 1. *J. Biol. Chem.* **281**, 23254-23263
26. Callaghan, B., Haythornthwaite, A., Berecki, G., Clark, R. J., Craik, D. J., and Adams, D. J. (2008) Analgesic alpha-conotoxins Vc1.1 and Rg1A inhibit N-type calcium channels in rat sensory neurons via GABAB receptor activation. *J. Neurosci.* **28**, 10943-10951
27. Azam, L., and McIntosh, J. M. (2009) Alpha-conotoxins as pharmacological probes of nicotinic acetylcholine receptors. *Acta. Pharmacol. Sin.* **30**, 771-783
28. Klimis, H., Adams, D., Callaghan, B., Nevin, S., Alewood, P., Vaughan, C., Mozar, C., and Christie, M. (2011) A novel mechanism of inhibition of high-voltage activated calcium channels by alpha-conotoxins contributes to relief of nerve injury-induced neuropathic pain. *Pain* **152**, 259-266
29. Carstens, B. B., Swedberg, J., Berecki, G., Adams, D. J., Craik, D. J., and Clark, R. J. (2016) Effects of linker sequence modifications on the structure, stability and biological activity of a cyclic alpha-conotoxin. *Biopolymers* **106**, 864-875
30. Carstens, B. B., Berecki, G., Daniel, J. T., Lee, H. S., Jackson, K. A., Tae, H. S., Sadeghi, M., Castro, J., O'Donnell, T., Deiteren, A., Brierley, S. M., Craik, D. J., Adams, D. J., and Clark, R. J. (2016) Structure-activity studies of cysteine-rich alpha-conotoxins that inhibit high-voltage-activated calcium channels via GABAB receptor activation reveal a minimal functional motif. *Angew. Chem. Int. Ed. Engl.* **55**, 4692-4696

31. Castro, J., Grundy, L., Deiteren, A., Harrington, A. M., O'Donnell, T., Maddern, J., Moore, J., Garcia-Caraballo, S., Rychkov, G. Y., Yu, R., Kaas, Q., Craik, D. J., Adams, D. J., and Brierley, S. M. (2017) Cyclic analogues of alpha-conotoxin Vc1.1 inhibit colonic nociceptors and provide analgesia in a mouse model of chronic abdominal pain. *Br. J. Pharmacol.* **175**, 2384-2398

32. Luo, S., Kulak, J. M., Cartier, G. E., Jacobsen, R. B., Yoshikami, D., Olivera, B. M., and McIntosh, J. M. (1998) Alpha-conotoxin AuIB selectively blocks alpha3beta4 nicotinic acetylcholine receptors and nicotine-evoked norepinephrine release. *J. Neurosci.* **18**, 8571-8579

33. Grishin, A. A., Wang, C. I., Muttenthaler, M., Alewood, P. F., Lewis, R. J., and Adams, D. J. (2010) Alpha-conotoxin AuIB isomers exhibit distinct inhibitory mechanisms and differential sensitivity to stoichiometry of alpha3beta4 nicotinic acetylcholine receptors. *J. Biol. Chem.* **285**, 22254-22263

34. Gotti, C., Clementi, F., Fornari, A., Gaimarri, A., Guiducci, S., Manfredi, I., Moretti, M., Pedrazzi, P., Pucci, L., and Zoli, M. (2009) Structural and functional diversity of native brain neuronal nicotinic receptors. *Biochem. Pharmacol.* **78**, 703-711

35. Brust, A., Palant, E., Croker, D. E., Colless, B., Drinkwater, R., Patterson, B., Schroeder, C. I., Wilson, D., Nielsen, C. K., and Smith, M. T. (2009) Chi-conopeptide pharmacophore development: toward a novel class of norepinephrine transporter inhibitor (Xen2174) for Pain. *J. Med. Chem.* **52**, 6991-7002

36. Harris, K. S., Durek, T., Kaas, Q., Poth, A. G., Gilding, E. K., Conlan, B. F., Saska, I., Daly, N. L., Van Der Weerden, N. L., and Craik, D. J. (2015) Efficient backbone cyclization of linear peptides by a recombinant asparaginyl endopeptidase. *Nat. Commun.* **6**, 10199

37. Miljanich, G. (2004) Ziconotide: neuronal calcium channel blocker for treating severe chronic pain. *Curr. Med. Chem.* **11**, 3029-3040

38. Jain, K. K. (2000) An evaluation of intrathecal ziconotide for the treatment of chronic pain. *Expert. Opin. Inv. Drug.* **9**, 2403-2410

39. Pope, J. E., and Deer, T. R. (2013) Ziconotide: a clinical update and pharmacologic review. *Expert. Opin. Pharmacother.* **14**, 957-966

40. Jacobsen, R. B., Koch, E. D., Lange-Malecki, B., Stocker, M., Verhey, J., Van Wagoner, R. M., Vyazovkina, A., Olivera, B. M., and Terlau, H. (2000) Single amino acid substitutions in kappa-conotoxin PVIIA disrupt interaction with the shaker K+ channel. *J. Biol .Chem.* **275**, 24639-24644

41. Lubbers, N. L., Campbell, T. J., Polakowski, J. S., Bulaj, G., Layer, R. T., Moore, J., Gross, G. J., and Cox, B. F. (2005) Postischemic administration of CGX-1051, a peptide from cone snail venom, reduces infarct size in both rat and dog models of myocardial ischemia and reperfusion. *J. Cardiovasc. Pharmacol.* **46**, 141-146

42. Craik, D. J., Swedberg, J. E., Mylne, J. S., and Cemazar, M. (2012) Cyclotides as a basis for drug design. *Expert. Opin. Drug. Discov.* **7**, 179-194

43. Colgrave, M. L., and Craik, D. J. (2004) Thermal, chemical, and enzymatic stability of the cyclotide kalata B1: the importance of the cyclic cystine knot. *Biochemistry* **43**, 5965-5975

44. Luo, S., Zhangsun, D., Harvey, P. J., Kaas, Q., Wu, Y., Zhu, X., Hu, Y., Li, X., Tsetlin, V. I., Christensen, S., Romero, H. K., McIntyre, M., Dowell, C., Baxter, J. C., Elmslie, K. S., Craik, D. J., and McIntosh, J. M. (2015) Cloning, synthesis, and characterization of alphaO-conotoxin GeXIVA, a potent alpha9alpha10 nicotinic acetylcholine receptor antagonist *Proc. Natl. Acad. Sci. U. S. A.* **112**, E4026-4035

45. Yu, R., Kompella, S. N., Adams, D. J., Craik, D. J., and Kaas, Q. (2013) Determination of the alpha-conotoxin Vc1.1 binding site on the alpha9alpha10 nicotinic acetylcholine receptor. *J. Med. Chem.* **56**, 3557-3567

46. Ellison, M., Haberlandt, C., Gomez-Casati, M. E., Watkins, M., Elgoyhen, A. B., McIntosh, J. M., and Olivera, B. M. (2006) Alpha-RgIA: a novel conotoxin that specifically and potently blocks the alpha9alpha10 nAChR. *Biochemistry* **45**, 1511-1517

47. Li, X., Hu, Y., Wu, Y., Huang, Y., Yu, S., Ding, Q., Zhangsun, D., and Luo, S. (2016) Anti-hypersensitive effect of intramuscular administration of alphaO-conotoxin GeXIVA [1, 2] and GeXIVA [1, 4] in rats of neuropathic pain. *Prog. Neuropsychopharmacol. Biol. Psychiatry.* **66**, 112-119

48. Craik, D. J., Fairlie, D. P., Liras, S., and Price, D. (2013) The future of peptide-based drugs. *Chem. Biol. Drug. Des.* **81**, 136-147

49. King, G. F. (2011) Venoms as a platform for human drugs: translating toxins into therapeutics. *Expert. Opin. Biol. Th.* **11**, 1469-1484

50. Frokjaer, S., and Otzen, D. E. (2005) Protein drug stability: a formulation challenge. *Nat. Rev. Drug. Discov.* **4**, 298-306

51. Clark, R. J., Akcan, M., Kaas, Q., Daly, N. L., and Craik, D. J. (2012) Cyclization of conotoxins to improve their biopharmaceutical properties. *Toxicon* **59**, 446-455

52. Šali, A., and Blundell, T. L. (1993) Comparative protein modelling by satisfaction of spatial restraints. *J. Mol. Biol.* **234**, 779-815

53. Skinner, S. P., Fogh, R. H., Boucher, W., Ragan, T. J., Mureddu, L. G., and Vuister, G. W. (2016) CcpNmr AnalysisAssign: a flexible platform for integrated NMR analysis. *J. Biomol. NMR.* **66**, 111-124

54. Wishart, D., Sykes, B., and Richards, F. (1992) The chemical shift index: a fast and simple method for the assignment of protein secondary structure through NMR spectroscopy. *Biochemistry* **31**, 1647-1651

55. Shen, Y., Delaglio, F., Cornilescu, G., and Bax, A. (2009) TALOS+: a hybrid method for predicting protein backbone torsion angles from NMR chemical shifts. *J. Biomol. NMR.* **44**, 213-223

56. Ikeya, T., Terauchi, T., Guntert, P., and Kainosho, M. (2006) Evaluation of stereo-array isotope labeling (SAIL) patterns for automated structural analysis of proteins with CYANA. *Magn. Reson. Chem.* **44**, S152-S157

57. Wang, C. K., Swedberg, J. E., Northfield, S. E., and Craik, D. J. (2015) Effects of cyclization on peptide backbone dynamics. *J. Phys. Chem. B.* **119**, 15821-15830

58. Chen, V. B., Arendall III, W. B., Headd, J. J., Keedy, D. A., Immormino, R. M., Kapral, G. J., Murray, L. W., Richardson, J. S., and Richardson, D. C. (2010) MolProbity: all-atom structure validation for macromolecular crystallography. *Acta. Crystallogr. D. Biol. Crystallogr.* **D66**, 12-21

59. Elgoyhen, A. B., Vetter, D. E., Katz, E., Rothlin, C. V., Heinemann, S. F., and Boulter, J. (2001) Alpha10: a determinant of nicotinic cholinergic receptor function in mammalian vestibular and cochlear mechanosensory hair cells. *Proc. Natl. Acad. Sci. U. S. A.* **98**, 3501-3506

60. Koval, L., Lykhmus, O., Zhmak, M., Khruschov, A., Tsetlin, V., Magrini, E., Viola, A., Chernyavsky, A., Qian, J., Grando, S., Komisarenko, S., and Skok, M. (2011) Differential involvement of alpha4beta2, alpha7 and alpha9alpha10 nicotinic acetylcholine receptors in B lymphocyte activation in vitro. *Int. J. Biochem. Cell Biol.* **43**, 516-524

61. Peng, H., Ferris, R. L., Matthews, T., Hiel, H., Lopez-Albaitero, A., and Lustig, L. R. (2004) Characterization of the human nicotinic acetylcholine receptor subunit alpha9 (CHRNA9) and alpha10 (CHRNA10) in lymphocytes. *Life. Sci.* **76**, 263-280

62. Satkunanathan, N., Livett, B., Gayler, K., Sandall, D., Down, J., and Khalil, Z. (2005) Alpha-conotoxin Vc1.1 alleviates neuropathic pain and accelerates functional recovery of injured neurones. *Brain. Res.* **1059**, 149-158

63. Wu, C. H., Lee, C. H., and Ho, Y. S. (2011) Nicotinic acetylcholine receptor-based blockade: applications of molecular targets for cancer therapy. *Clin. Cancer. Res.* **17**, 3533-3541

64. Wu, R. J., Wang, L., and Xiang, H. (2015) The structural features of alpha-conotoxin specifically target different isoforms of nicotinic acetylcholine receptors. *Curr. Top. Med. Chem.* **16**, 156-169

65. Xu, S., Zhang, T., Kompella, S. N., Yan, M., Lu, A., Wang, Y., Shao, X., Chi, C., Adams, D. J., Ding, J., and Wang, C. (2015) Conotoxin alphaD-GeXXA utilizes a novel strategy to antagonize nicotinic acetylcholine receptors. *Sci. Rep.* **5**, 14261

66. Luo, S., Christensen, S., Zhangsun, D., Wu, Y., Hu, Y., Zhu, X., Chhabra, S., Norton, R. S., and McIntosh, J. M. (2013) A novel inhibitor of alpha9alpha10 nicotinic acetylcholine receptors from *Conus vexillum* delineates a new conotoxin superfamily. *PLoS. One.* **8**, e54648

67. Wu, X., Wu, Y., Zhu, F., Yang, Q., Wu, Q., Zhangsun, D., and Luo, S. (2013) Optimal cleavage and oxidative folding of alpha-conotoxin TxIB as a therapeutic candidate peptide. *Mar. Drugs.* **11**, 3537-3553

68. Gyanda, R., Banerjee, J., Chang, Y.-P., Phillips, A. M., Toll, L., and Armishaw, C. J. (2013) Oxidative folding and preparation of alpha-conotoxins for use in high-throughput structure–activity relationship studies. *J. Pept. Sci.* **19**, 16-24

69. Wedemeyer, W. J., Xu, X., Welker, E., and Scheraga, H. A. (2002) Conformational propensities of protein folding intermediates: distribution of species in the 1S, 2S, and 3S ensembles of the [C40A,C95A] mutant of bovine pancreatic ribonuclease A. *Biochemistry* **41**, 1483-1491

70. Bulaj, G., and Olivera, B. M. (2008) Folding of conotoxins: formation of the native disulfide bridges during chemical synthesis and biosynthesis of *Conus* peptides. *Antioxid. Redox. Signal.* **10**, 141-155

71. States, D., Dobson, C., Karplus, M., and Creighton, T. (1984) A new two-disulphide intermediate in the refolding of reduced bovine pancreatic trypsin inhibitor. *J. Mol. Biol.* **174**, 411-418

72. Weissman, J. S., and Kim, P. S. (1992) The pro region of BPTI facilitates folding. *Cell* **71**, 841-851

73. Akcan, M., Stroud, M. R., Hansen, S. J., Clark, R. J., Daly, N. L., Craik, D. J., and Olson, J. M. (2011) Chemical re-engineering of chlorotoxin improves bioconjugation properties for tumor imaging and targeted therapy. *J. Med. Chem.* **54**, 782-787

74. Jensen, J. E., Mobli, M., Brust, A., Alewood, P. F., King, G. F., and Rash, L. D. (2012) Cyclisation increases the stability of the sea anemone peptide APETx2 but decreases its activity at acid-sensing ion channel 3. *Mar. Drugs.* **10**, 1511-1527

75. Wu, X., Huang, Y. H., Kaas, Q., and Craik, D. J. (2016) Cyclisation of disulfide-rich conotoxins in drug design applications. *Eur. J. Org. Chem.* **2016**, 3462-3472

76. Kwon, S., Bosmans, F., Kaas, Q., Cheneval, O., Conibear, A. C., Rosengren, K. J., Wang, C. K., Schroeder, C. I., and Craik, D. J. (2016) Efficient enzymatic cyclization of an inhibitory cystine knot-containing peptide. *Biotechnol. Bioeng.* **113**, 2202-2212

77. Scanlon, M. J., Naranjo, D., Thomas, L., Alewood, P. F., Lewis, R. J., and Craik, D. J. (1997) Solution structure and proposed binding mechanism of a novel potassium channel toxin kappa-conotoxin PVIIA. *Structure* **5**, 1585-1597

78. Thomas, G. (2002) Furin at the cutting edge: from protein traffic to embryogenesis and disease. *Nat. Rev. Mol. Cell. Biol.* **3**, 753-766

79. Zaykov, A. N., Mayer, J. P., Gelfanov, V. M., and DiMarchi, R. D. (2014) Chemical synthesis of insulin analogs through a novel precursor. *ACS. Chem. Biol.* **9**, 683-691

80. Markussen, J. (1985) Comparative reduction/oxidation studies with single chain des-(B30) insulin and porcine proinsulin. *Chem. Biol. Drug. Des.* **25**, 431-434

81. Derewenda, U., Derewenda, Z., Dodson, E., Dodson, G., Bing, X., and Markussen, J. (1991) X-ray analysis of the single chain B29-A1 peptide-linked insulin molecule: A completely inactive analogue. *J. Mol. Biol.* **220**, 425-433

82. Markussen, J., Jørgensen, K., Sørensen, A., and Thim, L. (1985) Single chain des-(B30) insulin. Intramolecular crosslinking of insulin by trypsin catalyzed transpeptidation. *Int. J. Pept. Protein. Res.* **26**, 70-77

83. Hua, Q. X., Nakagawa, S. H., Jia, W., Huang, K., Phillips, N. B., Hu, S. Q., and Weiss, M. A. (2008) Design of an active ultrastable single-chain insulin analog: synthesis, structure, and therapeutic implications. *J. Biol. Chem.* **283**, 14703-14716

84. Colloca, L., Ludman, T., Bouhassira, D., Baron, R., Dickenson, A. H., Yarnitsky, D., Freeman, R., Truini, A., Attal, N., Finnerup, N. B., Eccleston, C., Kalso, E., Bennett, D. L., Dworkin, R. H., and Raja, S. N. (2017) Neuropathic pain. *Nat. Rev. Dis. Primers.* **3**, 17002

85. Dworkin, R. H., O'connor, A. B., Backonja, M., Farrar, J. T., Finnerup, N. B., Jensen, T. S., Kalso, E. A., Loeser, J. D., Miaskowski, C., and Nurmikko, T. J. (2007) Pharmacologic management of neuropathic pain: evidence-based recommendations. *Pain* **132**, 237-251

86. Cruccu, G. (2007) Treatment of painful neuropathy. *Curr. Opin. Neurol.* **20**, 531-535

Chapter 3: Stoichiometry specific inhibition of rat α3β4 nAChR by ribbon α-conotoxin AuIB

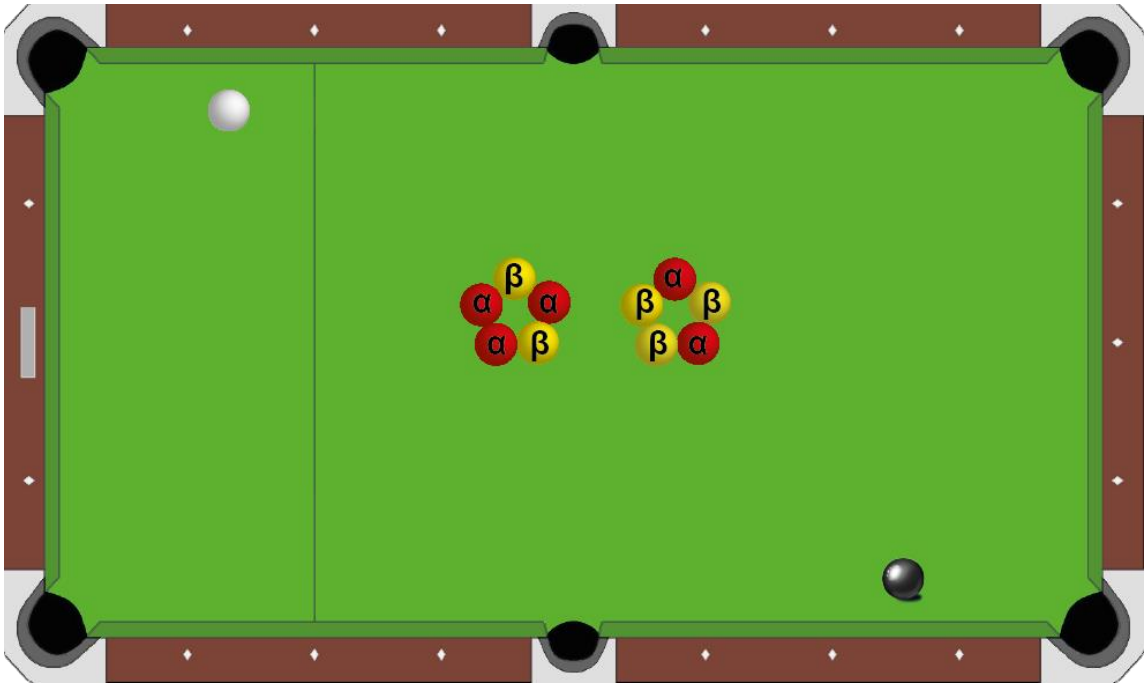

Publications included in this chapter

1. **Wu, X**., Tae, H.-S., Huang, Y.H., Adams, D. J., Craik, D. J., and Kaas, Q. (2018) Stoichiometry dependent inhibition of rat α3β4 nicotinic acetylcholine receptor by the ribbon isomer of α-conotoxin AuIB. *Biochem. Pharmacol.* **155**, 288-297

Contributions

Xiaosa Wu was responsible for the following work:

- 50% of conception and design
- 100% of peptide cleavage, oxidation and purification
- 100% of structural characterisation
- 100% of homology modelling
- 100% of molecular dynamics simulations
- 60% of analysis of data
- 80% of drafting and writing

3.1 Introduction

The combinatorial nature of nAChR subtypes requires molecular probes to study their physiology. The existence of different stoichiometries adds another layer of complexity to the identification of nAChR subtypes but designing specific probes of a certain stoichiometry is exceptionally challenging. The α3β4 nAChR has two main stoichiometries:$(\alpha3)_2(\beta4)_3$ and $(\alpha3)_3(\beta4)_2$. The $(\alpha3)_2(\beta4)_3$ nAChR subtype has α3(+)β4(-) functional binding sites (Figure 3.1 A), and the $(\alpha3)_3(\beta4)_2$ subtype has additional functional binding site(s) between two α3 subunits, i.e. α3(+)α3(-) (1). In the current study, we focused on engineered α3-containing nAChRs of these compositions, but in native tissue, the ganglionic nAChRs are more complex and could include accessory subunits of α3, α5, α6, β2 or β4 (2). As the α3β4 nAChR subtype is involved in a range of drug addictions, (e.g. for morphine (3), methamphetamine (4) and nicotine (5-7)), and the β4 subunit is linked to anxiety behaviour (8), these receptors are of considerable pharmaceutical interest. Thus, high-affinity molecular probes are required to tease apart the neurological functions of the two α3β4 nAChR stoichiometries.

α-Conotoxin AuIB (Figure 3.1 B) belongs to the 4/6 class of conotoxins (9), and the globular form (gAuIB) inhibits the rat α3β4 nAChR with an IC_{50} of 1-3 μM (10). rAuIB was the first ribbon isomer reported to have a higher potency than the globular isomer, with rAuIB displaying a 10-fold improved inhibition of Ach-evoked current in rat parasympathetic neurons compared to gAuIB, with IC_{50}s of 0.1 nM and 1.2 nM, respectively (11). However, another study reported that gAuIB was more potent than rAuIB at inhibiting rat α3β4 nAChR expressed in *Xenopus laevis* oocytes (12). These apparently conflicting results were explained by a switch in the major stoichiometry of the α3β4 nAChR when expressed in mammalian cells compared to *X. laevis* oocytes (1). AuIB isomers were shown to have differential sensitivity to the two stoichiometries of the α3β4 nAChR: gAuIB inhibited the $(\alpha3)_3(\beta4)_2$ nAChR (transfected at 10:1 ratio) and $(\alpha3)_2(\beta4)_3$ nAChR (1:10 ratio) with IC_{50}s of 1.1 μM and 3.0 μM, respectively; whereas rAuIB inhibited the $(\alpha3)_3(\beta4)_2$ nAChR with an IC_{50} of 0.86 μM and was inactive at the other stoichiometry (10). Therefore, rAuIB only inhibited the stoichiometry displaying an α3(+)α3(-) binding site, indicating that it binds at the interface between two α3 subunits. Conotoxin rAuIB can therefore potentially be used to identify a single subtype and stoichiometry among all α3β4 subtypes expressed *in vivo*. Here, we investigated the SAR and binding mode of rAuIB on the rat α3β4 nAChR putatively expressed as $(\alpha3)_3(\beta4)_2$

stoichiometry from the injection of 10:1 α3:β4 RNA ratio. This is the first detailed SAR study of the binding mode of a ribbon α-conotoxin.

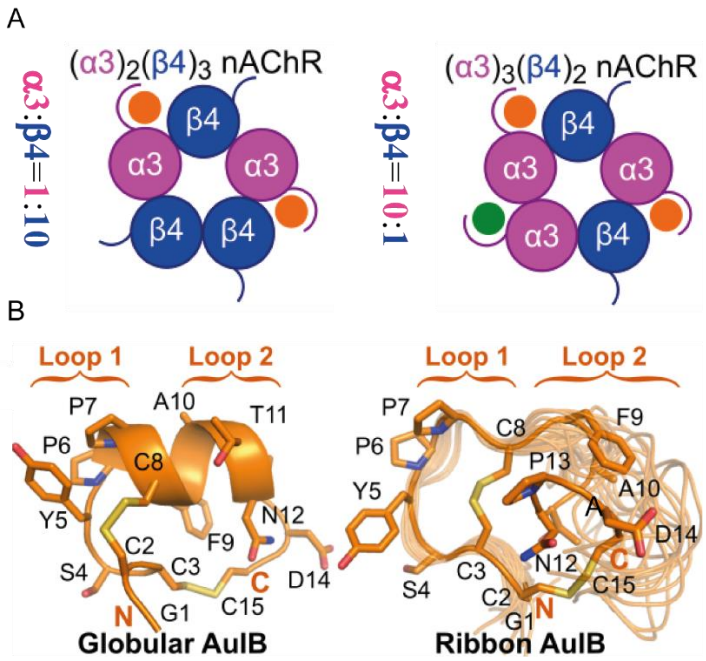

Figure 3.1 Overview of the two possible stoichiometries of α3β4 nAChRs and the NMR spectroscopy solution structures of rAuIB and gAuIB. A: Illustration of the two possible stoichiometries of homopentameric α3β4 nAChRs and identification of the functional binding sites. The illustration represents the nAChR as seen from the extracellular side and parallel to the membrane; the pore is in the centre of the pentamer. The C-loop of each subunit is indicated by a curved line. The α3(+)β4(-) and α3(+)α3(-) agonist binding sites are indicated by orange and green discs, respectively. B: Three-dimensional NMR solution structures of gAuIB (PDB: 1MXN) and rAuIB (PDB: 1MXP).

3.2 Materials and methods

3.2.1 Peptide synthesis and cleavage

A suite of 13 AuIB peptides (gAuIB, rAuIB, 10 Ala variants of rAuIB and [P7A]gAuIB) was synthesised using Fmoc SPPS on a rink amide resin (Novabiochem®, Merck, Kenilworth, NJ, USA), with the side chains of Cys residues protected in pairs using orthogonal protective groups, which were then selectively removed in different oxidation solutions. For this purpose, we used the acid labile trityl (Trt) group to protect Cys II and Cys III, and the S-acetamidomethyl (Acm) group to protect Cys I and Cys IV for rAuIB and its mutants. Likewise for gAuIB, the Trt group was used to protect Cys II and Cys IV, and the Acm group was used to protect Cys I and Cys III. All crude linear peptides were cleaved and deprotected in a cleavage cocktail comprising 96% trifluoroacetic acid (TFA, Auspep, VIC, Australia), 2% H_2O and 2% triisopropylsilane (v/v) for 2 h. The crude peptides were purified by HPLC using a

gradient of 0−50% buffer B (0.045% TFA in 90% acetonitrile [Merck]) over 50 min and monitoring at 214/280 nm. The same method was also used in subsequent purifications. A two-step oxidative folding was used to form the disulfide bonds; the first disulfide bond was formed by adding peptides (80 mg crude peptide dissolved in 100 mL water) into an equal volume of 20 mM potassium ferricyanide, 0.1 M Tris, pH 7.5 for 1 h. The reaction mixture was frozen and lyophilized overnight, and the second disulfide bond was formed by adding 50 mL of 0.1 M iodine solution for 1 h. All Fmoc-amino acids were from Chem-Impex International (Wood Dale, IL, USA). All organic reagents and solvents, unless stated otherwise, were purchased from Sigma-Aldrich (St Louis, MO, USA).

3.2.2 NMR spectroscopy

With a few exceptions, where crystallization has been possible (13), NMR is the preferred technique for conotoxin structural characterization. Two-dimensional total correlation TOCSY and NOESY spectra of rAuIB, gAuIB and the variants were acquired using an Avance-600 MHz NMR spectrometer (Bruker) with mixing times of 80 ms and 200–300 ms, respectively. The α-proton (Hα) chemical shifts of synthetic peptides were assigned using CcpNmr analysis (version 2.4.1). Subsequently, the differences between the observed Hα chemical shifts and those of the corresponding residues in a random coil peptide (14), referred to as secondary Hα chemical shifts, were calculated to provide information on folding and secondary structure, as has been widely applied for other conotoxins (15).

3.2.3 Electrophysiological assay of peptides

RNA preparation, oocyte preparation, and expression of nAChR subunits in *Xenopus* were performed as described previously (10). Breifly, Plasmid constructs of rat α3 (pT7TS) and β4 (pNKS2) nAChR subunits were linearised with the XbaI restriction enzyme (NEB, Ipswich, MA, USA) for *in vitro* cRNA transcription using the T7/SP6 mMessage mMachine® transcription kits (AMBION, Forster City, CA, USA). Oocytes were injected with 5 ng cRNA of rat α3β4 nAChR (α3:β4 = 10:1; concentration confirmed spectrophotometrically and by gel electrophoresis), and they were incubated at 18 °C in sterile ND96 solution (96 mM NaCl, 2 mM KCl, 1 mM $CaCl_2$, 1 mM $MgCl_2$ and 5 mM HEPES at pH 7.4), supplemented with 5% fetal bovine serum, 0.1 mg/mL gentamicin (Gibco, Grand Island, NY, USA) and 100 U/mL penicillin-streptomycin (Gibco, Grand Island, NY, USA) 2-5 days before recording. Two-electrode voltage clamp recordings were performed at room temperature using a GeneClamp

500B amplifier and pClamp9 software interface (Molecular Devices, Sunnyvale, CA, USA) at a holding potential of −80 mV. Voltage-recording and current-injecting electrodes were pulled from GC150T-7.5 borosilicate glass (Harvard Apparatus, Holliston, MA, USA) and filled with 3 M KCl, giving resistances of 0.3–1 MΩ. Initially, oocytes were briefly washed with ND96 solution followed by three applications of 50 μM ACh for rat α3β4 nAChR (α3:β4 = 10:1) (10). Washout with bath solution was done for 3 min between ACh applications. Oocytes were incubated with peptides for 5 min with the perfusion system turned off, followed by co-application of ACh and peptide with flowing bath solution. All peptide solutions were prepared in ND96 solution containing 0.1% bovine serum albumin. Peak current amplitudes before (ACh alone) and after (ACh + peptide) peptide incubation were measured using AxoGraph X software (Axograph Scientific, Berkeley, CA, USA), where the ratio of ACh + peptide-evoked current amplitude to ACh alone-evoked current amplitude was used to assess the activity of the peptides at the rat α3β4 nAChR.

3.2.4 Molecular modelling

Molecular models of the interaction between AuIB and the ECD of rat α3β4 nAChR were built by homology with Modeller 9v18 (16) using the following crystal structures as templates: [1] the complex between *Aplysia californica* AChBP and conotoxin PnIA variant (PDB: 2BR8), and [2] the human α4β2 nAChR (PDB: 5KXI). The complex between rAuIB and the ECD of $(\alpha3)_3(\beta4)_2$ nAChR was modelled by assuming an interaction in the α3(+)α3(-) orthosteric binding site whereas the complex between gAuIB and the ECD of $(\alpha3)_2(\beta4)_3$ nAChR was built by assuming an interaction in the α3(+)β4(-) orthosteric binding site. Similar to most other α-conotoxins rAuIB is a competitive inhibitor of the α3β4 nAChR, suggesting that it binds in the orthosteric binding site (10). In contrast, α-conotoxin gAuIB inhibits non-competitively the α3β4 nAChR (10), but it was shown to nevertheless bind to the orthosteric binding site (17). This latter study unequivocally identified that gAuIB binds at the α3(+)β4(-) interface using the electrophysiological recording of nAChRs expressing β4 subunit mutants. As an explanation to the non-competitive nature of the inhibition, gAuIB was proposed to stabilise the desensitized state of α3β4 nAChR (17). It was previously demonstrated using single channel recording that another antagonist, DHβE, stabilised the desensitized state of a nAChR (18), despite binding in the orthosteric binding site (19).

The molecular models were refined by a 50 ns molecular dynamics simulation in explicit water using the GROMACS 5.1.4 package (20) and the Amber99SB-ILDN protein force field (21), as described previously (22,23). Briefly, the systems were gradually heated from 50 to 300 K at constant volume and then simulated with constant pressure while removing progressively the restraints imposed on the protein and peptide atoms. All bonds involving hydrogen atoms were constrained with the LINCS algorithm, allowing the use of a 2 fs time step. The particle-mesh Ewald method was used to compute long-range electrostatic interactions. The models of complexes involving two rAuIB mutants, [S4A]rAuIB and [F9A]rAuIB, were initially generated by substituting residue side chains using Modeller 9v18 and then carrying out molecular dynamics simulations as described above. The backbone root-mean-square deviation from the starting conformation was stable over the last 20 ns of the simulations and this period was used for analysis. The solvent accessible surface area was calculated using the GROMACS package with a probe radius of 1.4 Å. Additional 200 ns molecular dynamics simulations were also carried out using a similar set-up for rAuIB and [P7A]rAuIB in the absence of the receptor. Secondary structure analyses of these simulations were computed using the DSSP program (24) and the GROMACS package.

3.3 Results

3.3.1 Peptide synthesis and oxidative folding

We designed a suite of mutants in which all non-Cys residues of rAuIB were separately substituted by Ala to identify the positions that are crucial for the inhibition of the α3β4 nAChR (Table 3.1). All the Ala mutants of rAuIB as well as rAuIB, gAuIB and [P7A]gAuIB were successfully synthesised with orthogonal protection of the cysteine side chains to orient the folding toward a unique disulfide isomer.

Table 3.1 Amino acid sequences, yield and purity of gAuIB, rAuIB and variants in this study.

Peptide	Sequence	Theoretical mass[a]	Observed mass[a]	Yield	Purity
gAuIB	GCCSYPPCFATNPDC*	1572.8	1572.2	17.7%	> 95%
rAuIB	GCCSYPPCFATNPDC*	1572.8	1572.4	15.1%	> 95%
[G1A]rAuIB	ACCSYPPCFATNPDC*	1586.8	1586.6	12%	> 95%
[S4A]rAuIB	GCCAYPPCFATNPDC*	1556.8	1556.6	12.6%	> 95%
[Y5A]rAuIB	GCCSAPPCFATNPDC*	1480.7	1480.3	18.3%	> 95%
[P6A]rAuIB	GCCSYAPCFATNPDC*	1546.7	1546.4	22%	> 95%
[P7A]rAuIB	GCCSYPACFATNPDC*	1546.7	1546.4	26%	> 95%
[F9A]rAuIB	GCCSYPPCAATNPDC*	1496.7	1496.3	23.3%	> 95%
[T11A]rAuIB	GCCSYPPCFAANPDC*	1542.8	1542.4	6%	> 95%
[N12A]rAuIB	GCCSYPPCFATAPDC*	1529.8	1529.4	19.3%	> 95%
[P13A]rAuIB	GCCSYPPCFATNADC*	1546.8	1546.4	22%	> 95%
[D14A]rAuIB	GCCSYPPCFATNPAC*	1528.8	1528.4	21.6%	> 95%
[P7A]gAuIB	GCCSYPACFATNPDC*	1546.7	1546.2	21.6%	> 95%

[a] Average mass in Dalton; * C-terminal amidation

3.3.2 [P7A]rAuIB has more similar secondary Hα chemical shifts to gAuIB

Secondary Hα chemical shifts analysis, which is useful for deducing secondary structure elements, was conducted for gAuIB, rAuIB and all mutants (Figure 3.2). The Hα secondary chemical shifts of rAuIB synthesised in this study were in agreement with previously reported values (11), indicating that the fold of rAuIB is the same as in previous studies. Apart from some local changes in the chemical shift at the substitution site, all mutants displayed a similar pattern of shifts to the parent peptide except [P7A]rAuIB (Figure 3.2 C). Interestingly, residues from Pro6 to Phe9 of [P7A]rAuIB had negative secondary Hα chemical shifts (Figure 3.2 C), indicating that this segment adopts an α-helical structure, a motif that exists in the globular isomer but not in the ribbon isomer. The P7A substitution therefore seems to have improved the definition of the structure of rAuIB, with the parent peptide being devoid of stable regular secondary structure. The retention time and secondary Hα chemical shifts between [P7A]rAuIB and [P7A]gAuIB were different, excluding the possibility that [P7A]rAuIB converted into [P7A]gAuIB during the folding process (Figure 3.2D). To further substantiate this difference of conformation, we carried out two 200 ns molecular dynamics simulations: one simulation

starting from the NMR solution structure of rAuIB, and the second from a model of the P7A variant, which was created by simple side chain swaps in the NMR structure of rAuIB. Consistent with the NMR measurements, the simulation of [P7A]rAuIB suggested the existence of a stable α-helix from Pro6 to Phe9 (Figure 3.2 E). Interestingly, the P7A variant was more rigid than the parent peptide, as measured using the root-mean-square fluctuation (Figure 3.2 F).

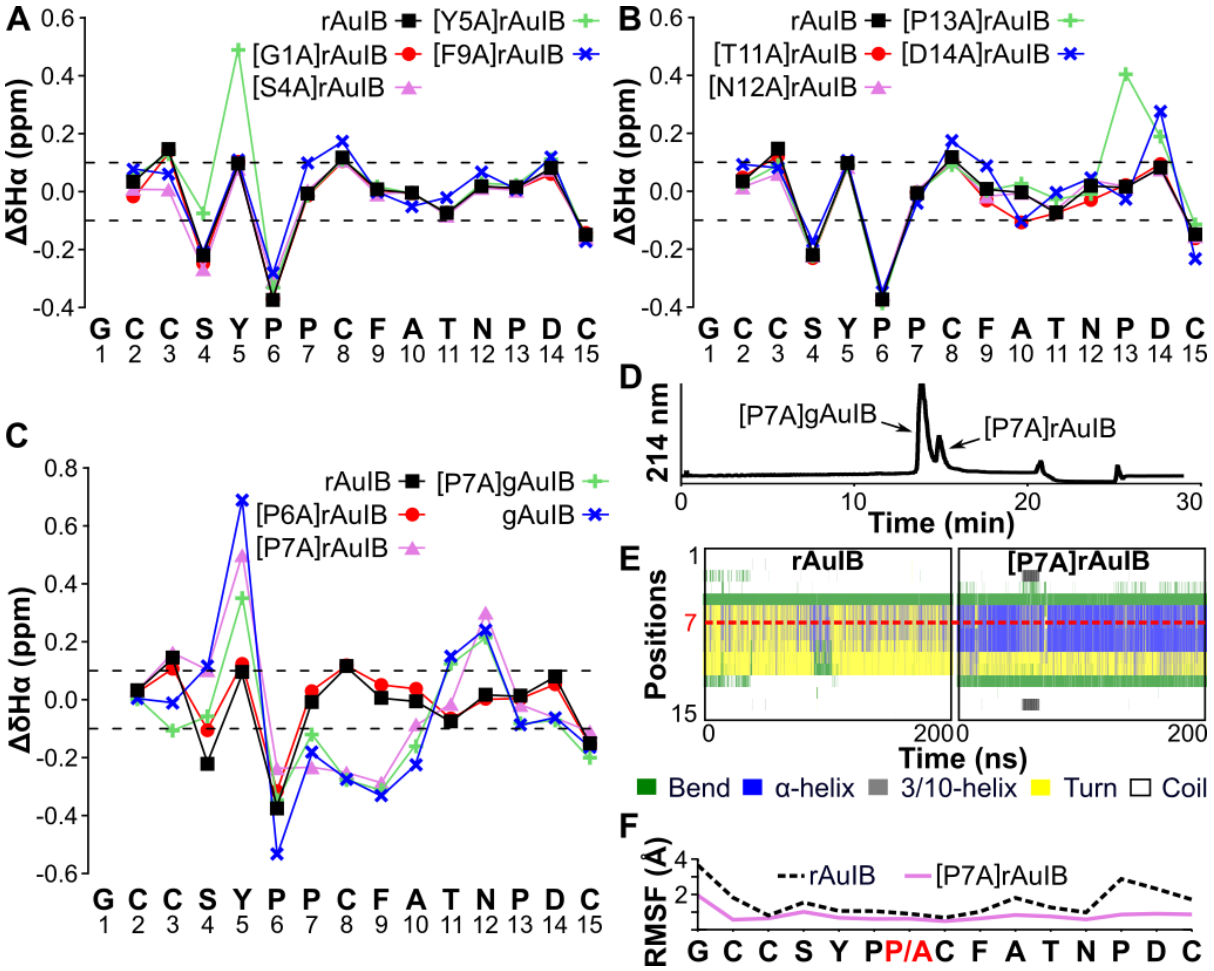

Figure 3.2 Secondary Hα chemical shifts (ΔδHα) of gAuIB, rAuIB and their variants (panels A, B and C) and analysis of the conformation of [P7A]rAuIB (panels D, E and F). A, B and C: Secondary Hα chemical shifts of gAuIB, [P7A]gAuIB, rAuIB, and the rAuIB variants. The sequence of AuIB is indicated at the bottom. The dashed lines at 0.1 ppm and -0.1 ppm indicate the cut-off considered for assessing regular secondary structure content (above 0.1 ppm is β-strand and under -0.1 ppm is α-helix). D: Co-elution profile by reversed-phase HPLC of [P7A]rAuIB and [P7A]gAuIB monitored by absorbance at 214 nm. E: Secondary structure content of rAuIB and [P7A]rAuIB monitored over 200 ns molecular dynamics simulations. The positions in the sequence are on the y-axis. The secondary structure around position 7 is highlighted using a red dashed line. F: Root-mean-square fluctuation (RMSF) of the Cα of each position of rAuIB and [P7A]rAuIB over 200 ns molecular dynamics simulations. The RMSF was computed by fitting the Cα of the molecules to the first frame of each simulation.

3.3.3 Several rAuIB analogues have decreased potency at rat α3β4 nAChR

All peptides were tested for inhibition of the rat α3β4 nAChR subtype heterologously expressed in *X. laevis* oocytes. In the first round of electrophysiological experiments, all rAuIB Ala mutants were tested at 1 µM (corresponding to the reported IC_{50} of rAuIB (10)) and gAuIB was tested at 3 µM, resulting in 30–40% inhibition of ACh-evoked currents of rat α3β4 (α3:β4 = 10:1) nAChR (Figure 3.3 A). The rAuIB Ala mutants exhibited comparable activity

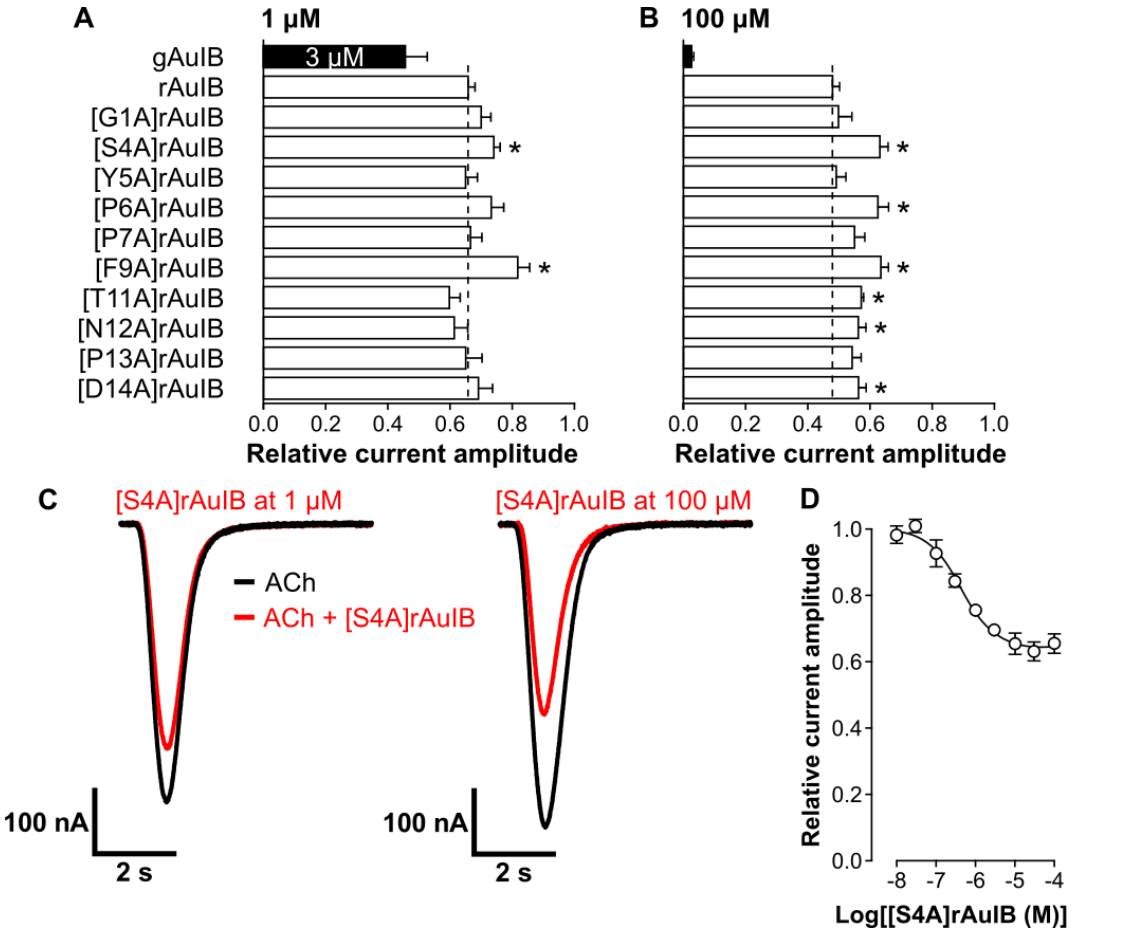

Figure 3.3 Activity of gAuIB, rAuIB and alanine mutants of rAuIB at the rat α3β4 nAChR. A and B: Bar graphs showing relative ACh-evoked peak current inhibition of rat α3β4 nAChR (α3:β4 = 10:1) by rAuIB analogues and gAuIB compared with rAuIB. In A, the peptides were tested at 1 µM, except gAuIB (3 µM). In B, the peptides were tested at 100 µM. The dashed lines indicate relative current amplitude in the presence of rAuIB. C: Superimposed representative traces of ACh-evoked currents mediated by rat α3β4 nAChR in the absence (black) and presence (red) of 1 µM (left) or 100 µM (right) [S4A]rAuIB. D: Concentration-response relationship of relative ACh-evoked current amplitude mediated by rat α3β4 nAChR (α3:β4 = 10:1) in the presence of [S4A]rAuIB (10 nM−100 µM) giving an IC_{50} of 441.8 ± 98.5 nM. Whole-cell currents at rat α3β4 were activated by 50 µM ACh. Relative current amplitude values are mean ± standard error of the mean; n = 5-9. The difference between the relative current amplitude of rAuIB and each variant was evaluated using the unpaired Student's t-test; * indicates a $p < 0.05$.

to the parent peptide except for [S4A] and [F9A]rAuIB, which caused 25% and 20% inhibition, respectively (Figure 3.3 A). Comparison of the rat α3β4 nAChR inhibition by [S4A] and [F9A]rAuIB indicates that the difference was not statistically significant. In the second round, all peptides were tested at 100 μM, inhibiting 35–55% of ACh-evoked currents of rat α3β4 (α3:β4 = 10:1) nAChR (Figure 3.3 A). Mutation at S4, P6, F9, T11, N12 and D14 caused a decrease in activity, *ca.* 40% inhibition, whereas other peptides had higher activity, with 45–55% inhibition (Figure 3.3 B and C). The efficacy (maximum inhibition of ACh-evoked currents) of rAuIB was ~55%, which is ~15% lower than reported previously (10). This difference may arise from variations in the relative levels of expression of α3 and β4 subunits in different batches of oocytes.

In summary, none of the single position variants displayed a dramatic loss of activity compared to the parent peptide. The Ala substitution of six positions in rAuIB led to a decreased activity at high concentration, but only two substitutions, S4A and F9A, significantly impacted activity at a concentration similar to the IC_{50} of rAuIB, suggesting they are more critical for antagonizing the activity of rat α3β4 nAChR. To better quantify the loss of activity, we calculated the IC_{50} of [S4A]rAuIB at the α3β4 nAChR (α3:β4 = 10:1) to be 442 ± 99 nM (Figure 3.3 D); the IC_{50} of rAuIB was previously reported to be 860 nM at the same receptor stoichiometry (10). Considering the variability between different electrophysiological set-ups, we believe that inhibition by rAuIB and [S4A] rAuIB are of the same order of magnitude, i.e., the S4A substitution caused a less than 10-fold drop decrease in inhibition.

3.3.4 rAuIB adopts a binding mode similar to that of globular α-conotoxins

Since the functional data indicated that rAuIB inhibits the α3(+)α3(-) interface of the $(\alpha3)_3(\beta4)_2$ nAChR (10) we built molecular models of the interaction between the α3(+)α3(-) binding site and rAuIB. This model was refined using molecular dynamics simulations and used to propose explanations for the SAR data. A molecular model of the interaction between gAuIB and the α3(+)β4(-) binding site was built similarly to that of rAuIB for comparison purposes. The molecular interactions between the peptides and the receptors were monitored over the last 20 ns of each 50 ns simulation. This period of 20 ns, during which the system reached equilibrium, is referred to as the "simulation time".

3.3.4.1 Binding mode of gAuIB at the rat α3β4 nAChR

The G1A, P6A and F9A mutants of gAuIB are reported to display decreased inhibitory activity at rat α3β4 nAChR compared to gAuIB (17). The molecular model of the complex between gAuIB and the α3(+)β4(-) binding site (Figure 3.4 A), which is very similar to a reported molecular model of the same system (17), can be used to suggest rational explanations to the consequence of these substitutions. The positively charged N-terminus (Gly1) is in the proximity of the negatively charged side chain oxygen atoms of D168 and D169 in the simulation, with an average distance of 3.9 Å and 2.8 Å. A stable salt bridge was established between D169 and the N-terminus during the simulation time and a similar interaction was transiently formed between D169 and the N-terminus. Therefore, substitution of this first residue of the toxin by Ala could change the peptide backbone conformation and prevent the establishment of these salt bridges.

Pro6 is a highly conserved residue among α-conotoxins because it anchors the conotoxins into an aromatic pocket on the nAChR that is important for the interaction between nAChR and agonists (25). It is therefore not surprising that the substitution of Pro6 by Ala caused a decrease in activity. The side chain of Phe9 is embedded in a hydrophobic pocket formed by K57, E59, Q117 and L119 of the β4 subunit, and the backbone oxygen of Phe9 formed a hydrogen bond with the receptor Q117 during 85% of the simulation time. The substitution of the bulky Phe9 by an Ala, which has a smaller side chain, would cause a change in shape complementarity at the interface, possibly resulting in a reorientation of the peptide in the binding pocket (similar to [F9A]rAuIB described below).

3.3.4.2 Binding mode of rAuIB at the rat α3β4 nAChR

Our molecular models suggest that the conformation adopted by rAuIB when bound to the rat α3β4 nAChR is similar to that of gAuIB except for the N- and C- termini (Figure 3.4 B). The interactions established by the first loop of AuIB are similar for the two isomers, and this loop sits deeply in the orthosteric binding site of the α3β4 nAChR. The first disulfide bond (i.e., Cys I-Cys III for gAuIB and Cys I-Cys IV for rAuIB) packs similarly against the vicinal disulfide bond of the C-loop, and this interaction is a conserved feature in the crystal structures of α-conotoxins/AChBP. Because of this interaction, the different disulfide connectivities of the two isomers resulted in different peptide conformation and a different location of their N- and C-termini within the nAChR binding site. The charged N-terminus, (Gly1) interacts with the

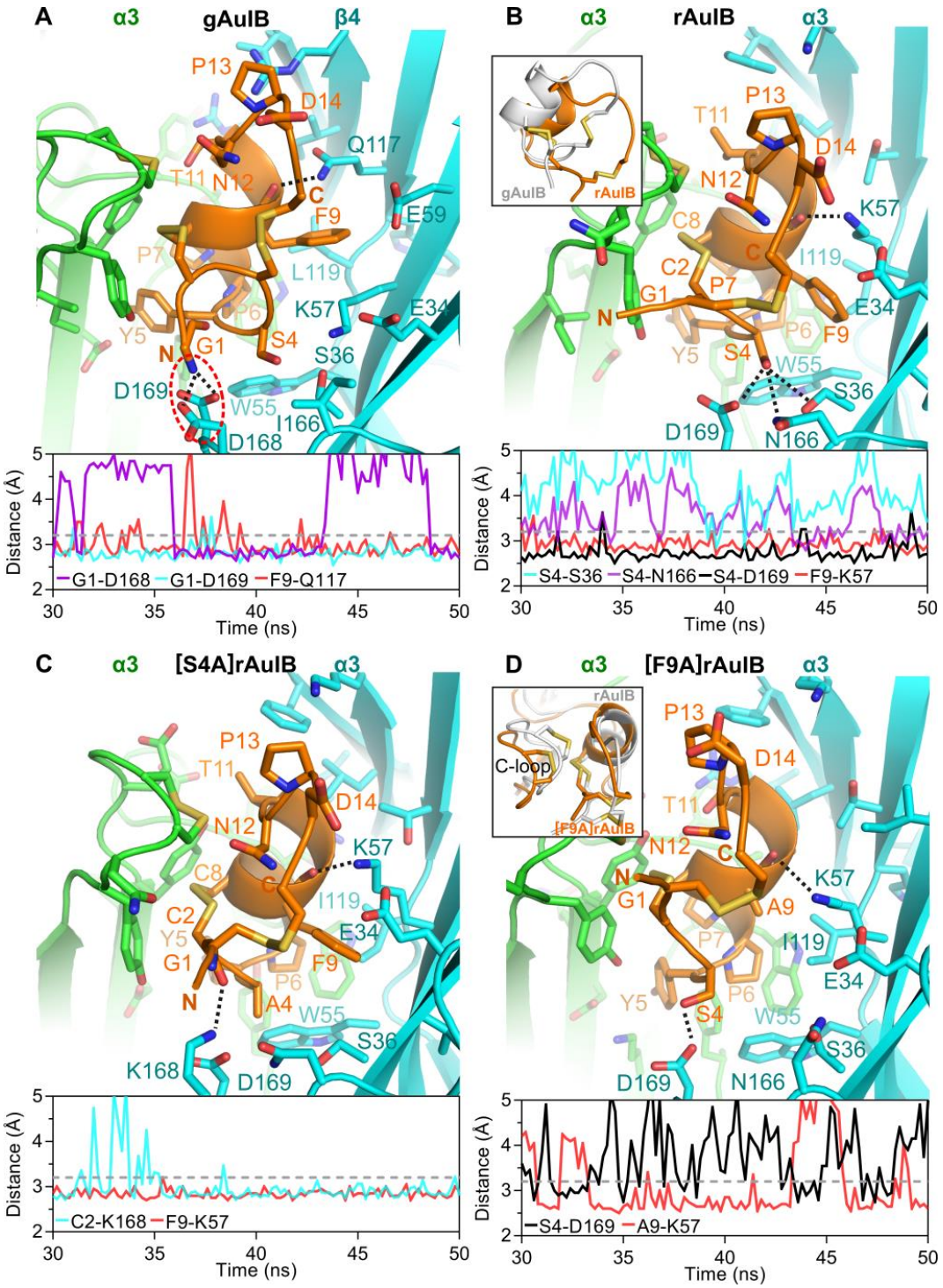

Figure 3.4 Molecular models of complexes between α3β4 nAChR and gAuIB (A), rAuIB (B), [S4A]rAuIB (C), or [F9A]rAuIB (D). The evolution of a selection of distances indicative of hydrogen bonds between pairs of residues at the interface is shown at the bottom for each model. Hydrogen bonds monitored in the bottom panel are displayed as dotted black lines on the structure. Interactions between charged side chains are circled with a dotted red line. The label for each distance comprises the residue of the toxin followed by the residue of the receptor. A dashed line at 3.2 Å indicates the upper-limit between the donor and acceptor atoms involved in a hydrogen bond. Panel B inset shows an overlay of the binding modes of rAuIB (orange) and gAuIB (white). Panel D inset shows that the C-loop in the [F9A]rAuIB molecular model (orange) moves outward compared to the C-loop in the model of the rAuIB/α3β4 nAChR complex (white).

acidic residues of the F-loop of α3β4 nAChR in the gAuIB model (Figure 3.4 A) but not in the model of rAuIB (Figure 3.4 B). The location of the amidated C-terminus in the nAChR binding site is also different between the two isomers; this difference results from the different conformation of the second loop.

We have shown the side chains of Ser4 and Phe9 in rAuIB are the most important for activity at the rat α3β4 nAChR. As shown in Figure 3.4B, Ser4 of rAuIB establishes a stable side chain-side chain hydrogen bond with D169 (98% of the simulation time). Additionally, Ser4 forms transient hydrogen bonds with S36 and N166 (40% of the simulation time). Phe9 of rAuIB interacts with the α3(-) subunit: it creates a hydrogen bond with K57 through its backbone oxygen during 93% of the simulation and its side chain contacts the residues E34, S36, W55, K57 and I119. The distance between the heavy atoms of Phe9 and of the aforementioned residues of the α3(-) subunit was below 5.0 Å, the distance considered to define a contact.

Positions 11, 12 and 14 of rAuIB caused a small drop of inhibition when mutated to Ala. These three residues are located at the interface with the receptor in the binding model but their side chains are also solvated, suggesting that their contribution to the electrostatic component of the binding energy is at best weak. Indeed, their involvement was only detected experimentally at the highest concentration (100 μM). By contrast, the impact of the substitutions S4A and F9A were detected at the lower concentration of 1 μM. We further studied the impact of these two substitutions on the binding mode by carrying out further molecular dynamics simulations.

3.3.4.3 Binding mode of [S4A]rAuIB at the rat α3β4 nAChR

The binding mode resulting from the 50 ns molecular dynamics simulation of [S4A]rAuIB displayed subtle variations from that of the parent peptide, with differences mainly located in the proximity of the modified position 4 (Figure 3.4 C). Besides position 4, all positions at the interface with the β4 subunit, such as Phe9, established similar molecular interactions in the S4A mutated model. The simulation suggests that the loss of the hydrogen bond between Ser4 and D169 is compensated by the establishment of a hydrogen bond between the side chain of α3(-) K168 and the backbone oxygen of the toxin Cys2, which was stable for 89% of the simulation time. The conformation of the side chain of K168 of the receptor seems to be also stabilised by electrostatic interactions with the D169 side chain. This electrostatic interaction was not possible in the rAuIB model because D169 was engaged in a hydrogen bond with Ser4

and consequently maintained away from K168 (Figure 3.4 B and C). The transient hydrogen bonds between Ser4 and α3(-) S36/N166 established in the model of rAuIB were not compensated in the mutated model of [S4A]rAuIB. Therefore, we suggest that [S4A]rAuIB displays overall fewer hydrogen bonds with the receptor than the parent peptide. Based on electrophysiological measurements, we proposed that the decrease in activity was lower than 10-fold, corresponding to a loss of less than 1.4 kcal/mol. This energy is typical of a weak hydrogen bond interaction, which is consistent with the 40% occurrence of the hydrogen bonds between Ser4 and S36/N166 during the molecular dynamics simulations.

3.3.4.4 Binding mode of [F9A]rAuIB at the rat α3β4 nAChR

According to the molecular model of rAuIB bound to the α3(+)α3(-) binding site, Phe9 is buried at the interface with the receptor. Its substitution by Ala creates a gap between the α3(-) subunit and the peptide in the initial step of the simulation. During this simulation, the peptide reoriented slightly in the binding site, resulting in several changes of pairwise interactions and a slight outward reorientation of the C-loop (Figure 3.4 D). Globally, the F9A variant had fewer contacts with the receptor than the parent peptide, as evidenced by a decrease in buried surface area from 1646 $Å^2$ to 1452 $Å^2$. As a result of the slight shift in orientation, the backbone oxygen of Ala9 only forms a transient hydrogen bond (42% of the simulation time) with the side chain of K57, whereas this interaction was present during 93% of the simulation time for the parent peptide. Similarly, the hydrogen bond between Ser4 (rAuIB) and D169 (α3 subunit) of the receptor was only observed during 75% of the simulation time compared to 98% for the parent peptide. We therefore propose that the F9A substitution caused a slight shift in the binding mode, resulting in fewer contacts and hydrogen bonds at the interface.

3.4 Discussion

The surprising discovery that the ribbon isomer of an α-conotoxin displays higher potency than the corresponding globular isomer (11) contrasts with the previously held assumption that native (globular) disulfide isomers have optimal activity. We carried out a complete Ala-scan of rAuIB, discovering the side chains of two positions, Ser4 and Phe9, were the most important for activity against the rat α3β4 nAChR. We have rationalized these data by proposing a binding mode between rAuIB and α3β4 nAChR. Molecular dynamics simulation suggested that rAuIB adopts a well-defined conformation when bound to its molecular target and that the binding mode is highly stable. A number of other SAR studies have been conducted on globular α-

conotoxins (26), and we compared our results to these studies to further evaluate the molecular model of rAuIB binding mode.

Position 1 was identified to be important for gAuIB activity at the α3β4 nAChR (17) but this was not the case for rAuIB (this study), paralleling the contrasting role of this position observed in several other studies on α-conotoxins. As for rAuIB, the G1A substitution had no impact on the inhibition of α7 nAChR by α-conotoxin ImI (27), and a minor impact on the affinity of α-conotoxin MII for the α3β2 nAChR (< 5-fold difference) (28). A molecular model of the interaction between ImI and the α7 nAChR indeed suggested that ImI Gly1 does not interact with the receptor (23), similar to our model of the rAuIB/α3β4 nAChR complex. In contrast, the G1A mutation of α-conotoxin TxID resulted in a ~20-fold decreased activity at the α3β4 nAChR (29), and the same substitution caused a significant decrease in activity for α-conotoxin gAuIB at the α3β4 nAChR (17). The molecular models of the corresponding complexes suggested that the N-terminus of these peptides potentially forms a salt bridge with negatively charged residues located in the F-loop of the receptor (17,29), as in our model of the gAuIB/α3β4 nAChR complex.

The S4A substitution impacted the activity of rAuIB at the α3β4 nAChR, but it was reported not to affect that of gAuIB (17). As for gAuIB, this substitution had no effect on the activity or affinity of α-conotoxin RgIA at α9α10 (30), ImI at α7 (27,31), PeIA at α3β2 and α6/α3β2β3 (32), BuIA at α6/α3β2β3 (33) and TxID at α3β4 nAChRs (29). Only a small decrease of inhibition of five- to eight-fold was reported after a substitution equivalent to S4A in GID* (S7A for GID*) and MII at the α4β2 and α3β2 nAChRs, respectively (28,34,35). TxID Ser4 was suggested to have no interaction with the receptor using molecular modelling, explaining that its substitution to Ala was innocuous (29). In contrast, a molecular model of the complexes involving GID* and the α4β2 nAChR suggested that the Ser side chain potentially forms a hydrogen bond with an Asp residue in the F-loop of the receptor (36), similar to our model of the rAuIB/α3β4 nAChR complex.

Pro6 is highly conserved among all α-conotoxins and typically interacts with the aromatic box, which is a conserved ACh interaction site in the nAChR and AChBP orthosteric binding sites (37-39). Pro6 is also essential for stabilizing the structure of globular α-conotoxins: replacing this Pro with Ala typically results in a change of conformation linked to a decrease or loss of activity. For example, the P6A substitution of α-conotoxin PeIA caused a 20-fold decrease of

inhibition of the α6/α3β2β3 nAChR compared to the parent peptide (32). The P6A substitution of α-conotoxins ImI and MI resulted in a 50–70 fold decrease in affinity for the α7 and muscle type nAChRs, respectively (27,31,40), whereas this substitution caused a >700-fold decrease in activity for α-conotoxin MII at the α3β2 nAChR (27,34). The same substitution resulted in a loss of helical content for globular Vc1.1 and a marked decrease in inhibitory activity of α-conotoxin Vc1.1 (41). Similarly, the P6A substitution of gAuIB resulted in a decrease in secondary structure content as well as a complete loss of inhibitory activity (17). In contrast, [P6A]rAuIB showed only a small decrease in activity compared to the parent peptide. Our molecular models suggest that Pro6 of rAuIB and gAuIB should make similar interactions with the receptor and we propose that the different impact that P6A substitution had on the activity of the two peptides arises from its differential effect on the peptide structures. Indeed, P6A substitution destabilises the small α-helical motif required for the activity of gAuIB. In contrast, as rAuIB already lacks regular secondary structure, P6A does not further impact its propensity to adopt the α-helical content required for binding to the receptor. The substantial decrease in inhibitory activity of gAuIB resulting from P6A substitution appears therefore to result primarily from the change of conformation of the peptide rather than decreased interactions of the position 6 side chain at the interface.

The only rAuIB variant that displayed different Hα secondary chemical shifts from the parent peptide was [P7A]rAuIB, indicating that this variant adopts a different fold in solution. NMR spectroscopy data suggest that [P7A]rAuIB adopts a helical structure, whereas rAuIB lacked regular secondary structure and was globally less structured. A possible explanation for this change of conformation is that Ala residues promote the formation of α-helices, whereas Pro residues typically destabilise regular secondary structure elements. BuIA is the only other α-conotoxin that has a similar cysteine scaffold to AuIB and had its ribbon isomer studied by NMR spectroscopy (42). As for ribbon AuIB, ribbon BuIA displays Pro residues at positions 6 and 7. The ribbon isomer of BuIA also has a more flexible backbone than the globular isomer and does not form the α-helix that is a conserved feature of α-conotoxin globular isomers. It would be interesting to study the influence of the P7A substitution on the structure of ribbon BuIA because this substitution could increase the helical content similarly to rAuIB. In our molecular models, rAuIB interacts with the receptor using a conformation that is stabilised by the P7A substitution, suggesting that the binding energy of the variant would benefit from a more favourable entropy term than the parent peptide. Nevertheless, the activity of the mutant

was not experimentally different from the parent peptide, which could be interpreted by the loss of a number of contacts between the Pro side chain and the receptor.

The substitution of position 9 with Ala caused a decrease in affinity for both gAuIB (17) and rAuIB (this work). Position 9 of globular α-conotoxins is buried at the interface with the complementary subunit and has been identified as important for modulating the activity of a range of globular α-conotoxins (17,29,30,33,35,41). For example, Ala mutation at this position caused a 50-fold decrease in activity of α-conotoxin GI at the muscle-type nAChR (43), a 20–30 fold decrease in affinity of α-conotoxin MII at α3β2 nAChR (28,34), and a >17-fold decrease in activity of α-conotoxin GID* at α4β2 nAChR (35). In addition, the R9A substitution resulted in a 1500-fold decrease in activity of RgIA at α9α10 nAChR (30). Substitution of position 9 can also enhance activity, with the [S9A]PeIA displaying three-fold lower IC_{50} than the parent peptide at the α3β2 nAChR (32) and the [N9W]Vc1.1 and [N9A]Vc1.1 increasing activity by 20- and 30-fold at the human α9α10 nAChR compared to Vc1.1, respectively (22,42). Several molecular models have been built to explain the ability of α-conotoxin position 9 to modulate nAChR inhibition, which suggests this residue interacts with various positions of the complementary subunit depending on the conotoxin and nAChR subtype (22,36,44). In the proposed binding mode of rAuIB, Phe9 mainly interacts with β4 K57, whereas GID* Arg12 was proposed to interact with β2 position 59 (36), [N9W]Vc1.1 Trp9 with α10 W118 (22) and RgIA Arg9 with α10 W81 (44).

In summary, we have identified a number of positions crucial for the activity of the ribbon isomer of AuIB that are also important for the activity of gAuIB and/or other globular α-conotoxins, indicating rAuIB has a globally similar binding mode to the globular isomers of α-conotoxins. According to our models, the main difference between the ribbon and globular AuIB at the interface with α3β4 nAChR is at their N- and C- termini. Changing the disulfide connectivity of α-conotoxins from a globular to ribbon isomer therefore does not introduce a dramatic change of binding mode at the interface with the receptor but it does create some different interactions that can have a substantial impact on the selectivity, as is the case for AuIB. Ribbon isomers should therefore be more systematically considered in the design of molecular probes and specific inhibitors of nAChR subtypes based on α-conotoxins.

3.5 References

1. Krashia, P., Moroni, M., Broadbent, S., Hofmann, G., Kracun, S., Beato, M., Groot-Kormelink, P. J., and Sivilotti, L. G. (2010) Human alpha3beta4 neuronal nicotinic receptors show different stoichiometry if they are expressed in Xenopus oocytes or mammalian HEK293 cells. *PLoS. One.* **5**, e13611
2. Cuny, H., Yu, R., Tae, H. S., Kompella, S. N., and Adams, D. J. (2017) Alpha-Conotoxins active at alpha3-containing nicotinic acetylcholine receptors and their molecular determinants for selective inhibition. *Br. J. Pharmacol.* **175**, 1855-1868
3. Taraschenko, O. D., Shulan, J. M., Maisonneuve, I. M., and Glick, S. D. (2007) 18-MC acts in the medial habenula and interpeduncular nucleus to attenuate dopamine sensitization to morphine in the nucleus accumbens. *Synapse* **61**, 547-560
4. Glick, S. D., Maisonneuve, I. M., Kitchen, B. A., and Fleck, M. W. (2002) Antagonism of alpha3beta4 nicotinic receptors as a strategy to reduce opioid and stimulant self-administration. *Eur. J. Pharmacol.* **438**, 99-105
5. Berrettini, W., Yuan, X., Tozzi, F., Song, K., Francks, C., Chilcoat, H., Waterworth, D., Muglia, P., and Mooser, V. (2008) Alpha-5/alpha-3 nicotinic receptor subunit alleles increase risk for heavy smoking. *Mol. Psychiatry* **13**, 368-373
6. Glick, S. D., Maisonneuve, I. M., and Kitchen, B. A. (2002) Modulation of nicotine self-administration in rats by combination therapy with agents blocking alpha3beta4 nicotinic receptors. *Eur. J. Pharmacol.* **448**, 185-191
7. Maisonneuve, I. M., and Glick, S. D. (2003) Anti-addictive actions of an iboga alkaloid congener: a novel mechanism for a novel treatment. *Pharmacol. Biochem. Behav.* **75**, 607-618
8. Salas, R., Pieri, F., Fung, B., Dani, J. A., and De Biasi, M. (2003) Altered anxiety-related responses in mutant mice lacking the beta4 subunit of the nicotinic receptor. *J. Neurosci.* **23**, 6255-6263
9. Luo, S., Kulak, J. M., Cartier, G. E., Jacobsen, R. B., Yoshikami, D., Olivera, B. M., and McIntosh, J. M. (1998) Alpha-conotoxin AuIB selectively blocks alpha3beta4 nicotinic acetylcholine receptors and nicotine-evoked norepinephrine release. *J. Neurosci.* **18**, 8571-8579
10. Grishin, A. A., Wang, C. I., Muttenthaler, M., Alewood, P. F., Lewis, R. J., and Adams, D. J. (2010) Alpha-conotoxin AuIB isomers exhibit distinct inhibitory mechanisms and

differential sensitivity to stoichiometry of alpha3beta4 nicotinic acetylcholine receptors. *J. Biol. Chem.* **285**, 22254-22263

11. Dutton, J. L., Bansal, P. S., Hogg, R. C., Adams, D. J., Alewood, P. F., and Craik, D. J. (2002) A new level of conotoxin diversity, a non-native disulfide bond connectivity in alpha-conotoxin AuIB reduces structural definition but increases biological activity. *J. Biol. Chem.* **277**, 48849-48857
12. Nicke, A., Samochocki, M., Loughnan, M. L., Bansal, P. S., Maelicke, A., and Lewis, R. J. (2003) Alpha-conotoxins EpI and AuIB switch subtype selectivity and activity in native versus recombinant nicotinic acetylcholine receptors. *FEBS. Lett.* **554**, 219-223
13. Hu, S. H., Gehrmann, J., Alewood, P. F., Craik, D. J., and Martin, J. L. (1997) Crystal structure at 1.1 A resolution of alpha-conotoxin PnIB: comparison with alpha-conotoxins PnIA and GI. *Biochemistry* **36**, 11323-11330
14. Wishart, D. S., and Sykes, B. D. (1994) The ^{13}C chemical-shift index: a simple method for the identification of protein secondary structure using ^{13}C chemical-shift data. *J. Biomol. NMR.* **4**, 171-180
15. Nielsen, K. J., Thomas, L., Lewis, R. J., Alewood, P. F., and Craik, D. J. (1996) A consensus structure for omega-conotoxins with different selectivities for voltage-sensitive calcium channel subtypes: comparison of MVIIA, SVIB and SNX-202. *J. Mol. Biol.* **263**, 297-310
16. Šali, A., and Blundell, T. L. (1993) Comparative protein modelling by satisfaction of spatial restraints. *J. Mol. Biol.* **234**, 779-815
17. Grishin, A. A., Cuny, H., Hung, A., Clark, R. J., Brust, A., Akondi, K., Alewood, P. F., Craik, D. J., and Adams, D. J. (2013) Identifying key amino acid residues that affect alpha-conotoxin AuIB inhibition of alpha3beta4 nicotinic acetylcholine receptors. *J. Biol. Chem.* **288**, 34428-34442
18. Bertrand, D., Devillers-Thiery, A., Revah, F., Galzi, J. L., Hussy, N., Mulle, C., Bertrand, S., Ballivet, M., and Changeux, J. P. (1992) Unconventional pharmacology of a neuronal nicotinic receptor mutated in the channel domain. *Proc. Natl. Acad. Sci. U. S. A.* **89**, 1261-1265
19. Shahsavar, A., Kastrup, J. S., Nielsen, E. O., Kristensen, J. L., Gajhede, M., and Balle, T. (2012) Crystal structure of Lymnaea stagnalis AChBP complexed with the potent nAChR antagonist DHbetaE suggests a unique mode of antagonism. *PLoS. One.* **7**, e40757

20. Abraham, M. J., Murtola, T., Schulz, R., Páll, S., Smith, J. C., Hess, B., and Lindahl, E. (2015) GROMACS: High performance molecular simulations through multi-level parallelism from laptops to supercomputers. *SoftwareX* **1-2**, 19-25
21. Lindorff-Larsen, K., Piana, S., Palmo, K., Maragakis, P., Klepeis, J. L., Dror, R. O., and Shaw, D. E. (2010) Improved side-chain torsion potentials for the Amber ff99SB protein force field. *Proteins* **78**, 1950-1958
22. Yu, R., Kompella, S. N., Adams, D. J., Craik, D. J., and Kaas, Q. (2013) Determination of the alpha-conotoxin Vc1.1 binding site on the alpha9alpha10 nicotinic acetylcholine receptor. *J. Med. Chem.* **56**, 3557-3567
23. Yu, R., Craik, D. J., and Kaas, Q. (2011) Blockade of neuronal alpha7-nAChR by alpha-conotoxin ImI explained by computational scanning and energy calculations. *PLoS. Comput. Biol.* **7**, e1002011
24. Kabsch, W., and Sander, C. (1983) Dictionary of protein secondary structure: pattern recognition of hydrogen-bonded and geometrical features. *Biopolymers* **22**, 2577-2637
25. Clark, R. J., Fischer, H., Nevin, S. T., Adams, D. J., and Craik, D. J. (2006) The synthesis, structural characterization, and receptor specificity of the alpha-conotoxin Vc1. 1. *J. Biol. Chem.* **281**, 23254-23263
26. Akondi, K. B., Muttenthaler, M., Dutertre, S., Kaas, Q., Craik, D. J., Lewis, R. J., and Alewood, P. F. (2014) Discovery, synthesis, and structure-activity relationships of conotoxins. *Chem. Rev.* **114**, 5815-5847
27. Servent, D., Thanh, H. L., Antil, S., Bertrand, D., Corringer, P.-J., Changeux, J.-P., and Ménez, A. (1998) Functional determinants by which snake and cone snail toxins block the alpha7 neuronal nicotinic acetylcholine receptors. *J. Physiol-Paris.* **92**, 107-111
28. Everhart, D., Cartier, G. E., Malhotra, A., Gomes, A. V., McIntosh, J. M., and Luetje, C. W. (2004) Determinants of potency on alpha-conotoxin MII, a peptide antagonist of neuronal nicotinic receptors. *Biochemistry* **43**, 2732-2737
29. Wu, Y., Zhangsun, D., Zhu, X., Kaas, Q., Zhangsun, M., Harvey, P. J., Craik, D. J., McIntosh, J. M., and Luo, S. (2017) Alpha-conotoxin [S9A]TxID potently discriminates between alpha3beta4 and alpha6/alpha3beta4 nicotinic acetylcholine receptors. *J. Med. Chem.* **60**, 5826-5833
30. Ellison, M., Feng, Z. P., Park, A. J., Zhang, X., Olivera, B. M., McIntosh, J. M., and Norton, R. S. (2008) Alpha-RgIA, a novel conotoxin that blocks the alpha9alpha10 nAChR: structure and identification of key receptor-binding residues. *J. Mol. Biol.* **377**, 1216-1227

31. Quiram, P. A., and Sine, S. M. (1998) Structural elements in alpha-conotoxin ImI essential for binding to neuronal alpha7 receptors. *J. Biol. Chem.* **273**, 11007-11011

32. Hone, A. J., Ruiz, M., Scadden, M., Christensen, S., Gajewiak, J., Azam, L., and McIntosh, J. M. (2013) Positional scanning mutagenesis of alpha-conotoxin PeIA identifies critical residues that confer potency and selectivity for alpha6/alpha3beta2beta3 and alpha3beta2 nicotinic acetylcholine receptors. *J. Biol. Chem.* **288**, 25428-25439

33. Azam, L., Maskos, U., Changeux, J. P., Dowell, C. D., Christensen, S., De Biasi, M., and McIntosh, J. M. (2010) Alpha-conotoxin BuIA[T5A;P6O]: a novel ligand that discriminates between alpha6beta4 and alpha6beta2 nicotinic acetylcholine receptors and blocks nicotine-stimulated norepinephrine release. *FASEB J.* **24**, 5113-5123

34. McIntosh, J. M., Azam, L., Staheli, S., Dowell, C., Lindstrom, J. M., Kuryatov, A., Garrett, J. E., Marks, M. J., and Whiteaker, P. (2004) Analogs of alpha-conotoxin MII are selective for alpha6-containing nicotinic acetylcholine receptors. *Mol. Pharmacol.* **65**, 944-952

35. Millard, E. L., Nevin, S. T., Loughnan, M. L., Nicke, A., Clark, R. J., Alewood, P. F., Lewis, R. J., Adams, D. J., Craik, D. J., and Daly, N. L. (2009) Inhibition of neuronal nicotinic acetylcholine receptor subtypes by alpha-conotoxin GID and analogues. *J. Biol. Chem.* **284**, 4944-4951

36. Banerjee, J., Yongye, A. B., Chang, Y. P., Gyanda, R., Medina-Franco, J. L., and Armishaw, C. J. (2014) Design and synthesis of alpha-conotoxin GID analogues as selective alpha4beta2 nicotinic acetylcholine receptor antagonists. *Biopolymers* **102**, 78-87

37. Celie, P. H., Kasheverov, I. E., Mordvintsev, D. Y., Hogg, R. C., van Nierop, P., van Elk, R., van Rossum-Fikkert, S. E., Zhmak, M. N., Bertrand, D., and Tsetlin, V. (2005) Crystal structure of nicotinic acetylcholine receptor homolog AChBP in complex with an alpha-conotoxin PnIA variant. *Nat. Struct. Mol. Biol.* **12**, 582-588

38. Dutertre, S., Ulens, C., Büttner, R., Fish, A., van Elk, R., Kendel, Y., Hopping, G., Alewood, P. F., Schroeder, C., and Nicke, A. (2007) AChBP-targeted alpha-conotoxin correlates distinct binding orientations with nAChR subtype selectivity. *EMBO J.* **26**, 3858-3867

39. Hansen, S. B., Sulzenbacher, G., Huxford, T., Marchot, P., Taylor, P., and Bourne, Y. (2005) Structures of Aplysia AChBP complexes with nicotinic agonists and antagonists reveal distinctive binding interfaces and conformations. *EMBO J.* **24**, 3635-3646

40. Jacobsen, R. B., DelaCruz, R. G., Grose, J. H., McIntosh, J. M., Yoshikami, D., and Olivera, B. M. (1999) Critical residues influence the affinity and selectivity of alpha-conotoxin MI for nicotinic acetylcholine receptors. *Biochemistry* **38**, 13310-13315

41. Halai, R., Clark, R. J., Nevin, S. T., Jensen, J. E., Adams, D. J., and Craik, D. J. (2009) Scanning mutagenesis of alpha-conotoxin Vc1.1 reveals residues crucial for activity at the alpha9alpha10 nicotinic acetylcholine receptor. *J. Biol. Chem.* **284**, 20275-20284

42. Jin, A. H., Brandstaetter, H., Nevin, S. T., Tan, C. C., Clark, R. J., Adams, D. J., Alewood, P. F., Craik, D. J., and Daly, N. L. (2007) Structure of alpha-conotoxin BuIA: influences of disulfide connectivity on structural dynamics. *BMC Struct. Biol.* **7**, 28

43. Groebe, D. R., Gray, W. R., and Abramson, S. N. (1997) Determinants involved in the affinity of alpha-conotoxins GI and SI for the muscle subtype of nicotinic acetylcholine receptors. *Biochemistry* **36**, 6469-6474

44. Chhabra, S., Belgi, A., Bartels, P., van Lierop, B. J., Robinson, S. D., Kompella, S. N., Hung, A., Callaghan, B. P., Adams, D. J., Robinson, A. J., and Norton, R. S. (2014) Dicarba analogues of alpha-conotoxin RgIA. Structure, stability, and activity at potential pain targets. *J. Med. Chem.* **57**, 9933-9944

Chapter 4: Evaluation of structure-based computational methods for predicting the mutational free energy changes of α-conotoxins

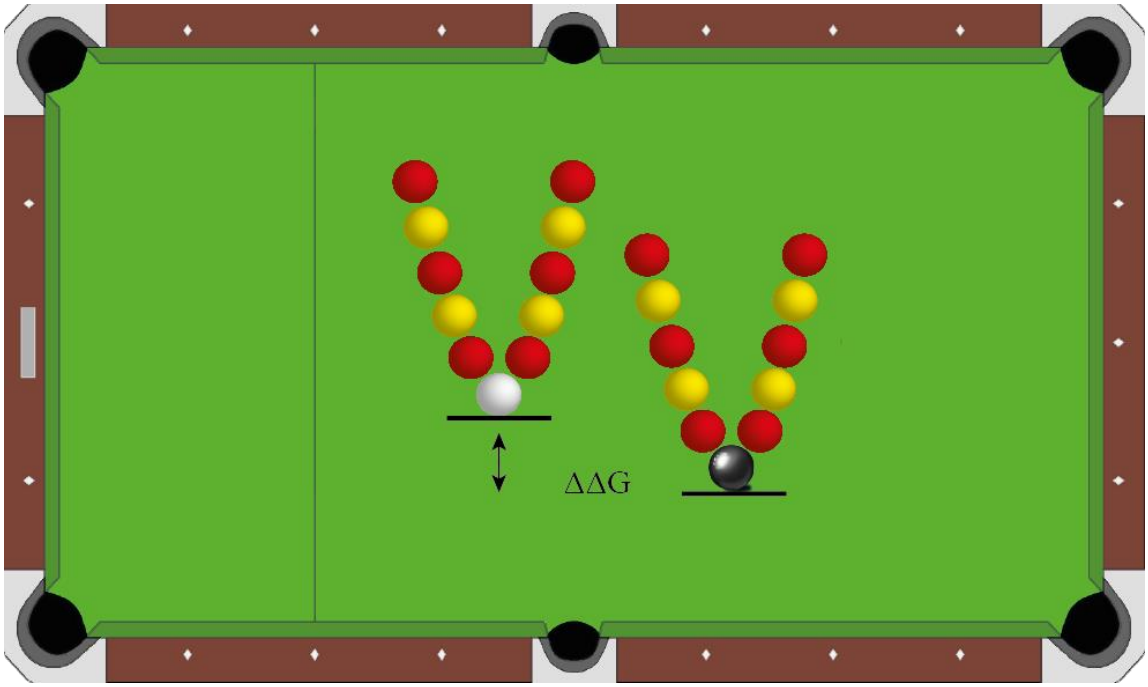

4.1 Introduction

As mentioned in Chapter 1, α-conotoxins have potential in the development of novel drugs to treat diseases such as neuropathic pain, nicotine addiction, and Alzheimer's disease (1-5). However, two main challenges currently limit their translational application. The first challenge is that some α-conotoxins have less potency at human compared to rat nAChR subtypes (6-10). Species-level differences in the amino acid sequences of target nAChRs can have substantial effects on ligand activity. For example, the α-conotoxin Vc1.1 can potently inhibit α9α10 nAChR, which is involved in chronic pain (11). Vc1.1 was discontinued in clinical trial phase II for the treatment of pain because it was discovered that this peptide's behaviour at the human receptor was different from the rat receptor (12). A recent study suggested that a single amino acid difference between human and rat α9 nAChR subunits causes globular α-conotoxin Vc1.1 to inhibit rat α9α10 nAChR two orders of magnitude more potently than human α9α10 nAChR (7). More broadly, designing α-conotoxins to be selective for a particular nAChR subtype is challenging (13-16). For example, α-conotoxin RegIIA inhibits the α3β2, α3β4 and α7 nAChRs with an IC_{50} of 33, 97 and 103 nM, respectively (16). Since it is relatively unselective, designing RegIIA as a selective and potent probe of one subtype has been challenging (17).

The design of α-conotoxins selective and potent for human nAChR subtypes has been carried out by synthesising large libraries of α-conotoxin mutants (18,19). For example, Romero *et al.* discovered a globular RgIA mutant that inhibits the human and rat α9α10 nAChR with the same order of magnitude, improving the activity from > 10,000 nM to 1.5 nM at human α9α10 nAChR (18). A globular PeIA mutant was shown to be > 15,000-fold more potent at blocking α6β2* over α3β2 nAChRs, whereas the parent peptides had IC_{50}s of 17.2 nM and 19.2 nM at these two receptors, respectively (19). However, large SAR studies are costly and time-consuming, and computational methods could be used to focus these studies on the most interesting variants (7). Recently, our laboratory has designed two Vc1.1 mutants informed by a combination of molecular modelling and energy calculation methods. One of these variants, [N9W]Vc1.1, has improved activity by ~30-fold on human α9α10 nAChR compared to the parent peptide with the IC_{50} value of 33 nM (7). This suggests computational methods have potential to guide design of selective nAChR subtypes inhibitors based on α-conotoxins. This variant was shown to be an effective analgesic in a mouse model of chronic abdominal pain (20).

Binding free energy computations are potentially important tools for designing selective inhibitors based on α-conotoxins. Nevertheless, these methods need to be benchmarked to assess their accuracy in the context of nAChR/α-conotoxin systems because they are especially sensitive to the accuracy of the structural models. Ideally, these methods should be employed with high-resolution experimental structures. Unfortunately, there is so far no crystal structure of any nAChR in complex with α-conotoxin. The acetylcholine binding proteins (AChBPs), which are structurally homologous to the extracellular domains (ECDs) of the nAChRs, can be relatively easily crystallised and studied using X-ray crystallography. AChBPs have been co-crystallised in complex with several α-conotoxins (21-26), providing relatively accurate information on the binding mode of α-conotoxins. In this study, we benchmarked four mutational energy prediction methods using the recently published crystal structures of the AChBP/α-conotoxin LsIA (PDB: 5T90) and AChBP/α-conotoxin LvIA complexes (PDB: 5XGL). In addition, we used the associated experimental affinity of LsIA mutants for AChBP with results from a competitive radioligand binding assay with ^{3}H-epibatidine and LvIA mutants for AChBP measured using surface plasmon resonance (24,26).

4.2 Materials and Methods

4.2.1 Binding free energy predictors

We have compared four methods: BeAtMuSic (27), Foldx (28,29), coarse-grained umbrella-sampling (CG_US) (30,31), and MMGBSA/MMPBSA (32). BeAtMuSiC predicts the change in binding affinity upon mutation. It relies on a set of statistical potentials derived from coarse-grained representation of protein structures. It is used to predict the effect of the mutations on the overall stability of a complex and the strength of interactions at the interface (27). Foldx uses an empirical energy function that was optimised using experimental data to predict unfolding free energy upon mutations (28,29). The umbrella sampling (US) method predicts the binding free energy by computing the potential of mean force (PMF) derived from a series of simulations of unbinding of the ligand from the receptor (30). This method is considered too computationally intensive to be applied systematically to study a large number of mutations of α-conotoxin/nAChR systems (33-35), but we will benchmark a recent method that applies US to a coarse-grained simplified representation of the system, dramatically speeding the computations (31). Finally, MM/PBSA computes free energies by combining three energies: 1) internal energy of the solute using a molecular mechanics force field (MM), 2) electrostatic component of solute/solvent interaction using the Poisson-Boltzmann equation (PB) and 3)

non-polar component of solute/solvent interaction using an equation depending on the surface area (SA) (32). The MM/GBSA variant employs the Generalized Born approximation instead of PB, which is faster and in some instance more accurate than PB when the accuracy of the system is low.

4.2.2 Experimental data

Experimental data from two recently published papers was used to guide the computations in this study (24,26). Specifically, Abraham *et al.* (26) calculated the crystal structure of the Ls-AChBP/LsIA complex, synthesised 10 LsIA variants, and measured their competitive affinity at AChBP. The IC_{50} values were calculated for only six of the LsIA variants. For the remaining four mutants, the IC_{50} values were reported as greater than 10 µM (26). Xu *et al.* (24) calculated the crystal structure of the Ac-AChBP/LvIA complex, and the competitive binding of seven LvIA variants were measured at AChBP. Another four variants were reported to lose their binding capacity for Ac-AChBP, but the maximal concentration of the peptide used to test for these four variants were not provided (24). Because of these missing values, we used the confusion matrix to analyse the performance of energy prediction methods (described below). Some regions of the flexible loops were not resolved in the 5T90 structure, and these loops were modelled using Modeller 9v18.

4.2.3 Molecular dynamics simulation

Refinement. The two crystal structures were refined by a 10 ns molecular dynamics simulation in explicit water using the AMBER 16 package and the ff14SB protein force field. Briefly, the receptor complexes were solvated in a truncated octahedral TIP3P water box simulation. Sodium ions were added to neutralise the systems. 2,000 steps of steepest descent minimisation and then 10,000 steps of conjugate gradient minimisation were performed to ensure that the systems have no steric clashes or inappropriate geometry. The systems were then gradually heated up from 50 to 300 K in the NVT ensemble over 100 ps with the solute restrained to their position by a harmonic force of 100 kcal/mol·$Å^2$. MD simulations were then carried out in the NPT ensemble, and the position restraints were gradually removed over 100 ps. All bonds involving hydrogen atoms were constrained with the SHAKE algorithm, allowing the use of a 2 fs time step and the Particle-mesh Ewald method was used to compute long-range electrostatic interactions. The systems were mutated by substituting residue side chains using Modeller 9v18 and then molecular dynamics simulations were carried out as above.

Coarse-grained simulations. All coarse-grained molecular dynamics simulations (500 ns) in explicit water were performed using the GROMACS 5.2 package (36) and the SIRAH force field (http://www.sirahff.com/) (37). Protonation state of each residue was assigned at pH 7 using PROPKA (38) and the PDB2PQR server (http://nbcr-222.ucsd.edu/pdb2pqr_2.0.0/) with the output naming scheme set to AMBER. The protein complexes were placed in a box of 8 nm × 20 nm × 8 nm, which is large enough to have the conotoxin and the receptor at a distance along the Y-axis during unbinding. Each system was firstly minimised with 10,000 steps using the steepest descent. Each system was then gradually heated up from 50 to 300 K in the NVT ensemble over 2 ns. Position restraints were gradually removed from 1,000 kJ mol^{-1} nm^{-2} to 0 kJ mol^{-1} nm^{-2} over 1 ns, followed by an unrestrained 500 ns simulation. The Particle-mesh Ewald method (39) was used to compute long-range electrostatic interactions with a cutoff of 1.2 nm and a grid spacing of 0.33 nm. A 1.2 nm cutoff was used for van der Waals interactions. The models of complexes involving mutant peptides were initially generated by substituting residue side chains using Modeller 9v18 and then coarse-grained umbrella simulations were carried out as described above. The backbone RMSD from the starting conformation was stable over the last 100 ns of the 500 ns simulations and this period was used for analysis. After this initial simulation, the α-conotoxin was pulled away from the receptor using an umbrella pulling force with a harmonic force constant of 2,000 kJ/mol/nm^2 over 500 ps of MD simulation along the Y-axis. 500 frames were extracted from the pulling trajectory, and the center of mass (COM) distance of each frame from the starting position was measured between the ligand and receptor. A total of 30 frames with a COM spaced by 0.15 nm were chosen and used to carry out US. The selected 30 frames from each system were run in the independent US. The PMF was calculated with the weighted histogram analysis method (WHAM) (30), which is implemented in the wham module of GROMACS. PMF value of each peptide was an average value calculated from last 30 ns using the WHAM. Each system was simulated until the PMF converges. The PMF values were used to compute the relative binding free energies.

4.2.4 Analysis of energy prediction data using confusion matrix

The experimental data and predicted ΔΔGs were divided into three classes as below: For experimental data, 1) decreased in activity (IC_{50} of mutant is at least 8-fold higher than the IC_{50} of wild type); 2) similar activity (IC_{50}s value of wild type and mutant are within 8-fold); 3) increased in activity (IC_{50} of mutant is at least 8-fold lower than the IC_{50} of the wild type). The predicted ΔΔG were binned into three classes: 1) decreased in affinity (ΔΔG ≥ 1 kcal/mol for

BeAtMuSiC, Foldx and CG_US; ΔΔG ≥ 13 kcal/mol for MMPBSA/MMGBSA); 2) similar affinity (-1 kcal/mol < ΔΔG < 1 kcal/mol for BeAtMuSiC, Foldx and CG_US; -13 kcal/mol < ΔΔG < 13 kcal/mol for MMPBSA/MMGBSA); increased in affinity (ΔΔG ≤ -1 kcal/mol for BeAtMuSiC, Foldx and CG_US; ΔΔG ≤ -13 kcal/mol for MMPBSA/MMGBSA).

The confusion matrix was used to analyse for energy prediction data. The terms of Positive (P), Negative (N), True (T) and False (F) were defined as follow: 1) Positive: IC_{50} decreased or no change in experimental data; 2) Negative: IC_{50} increased in experimental data; 3) True: predicted ΔΔG class is consistent with experimental data; 4) False: predicted ΔΔG class is not consistent with experimental data. The ΔΔG results were classified as true positives (TP), false positives (FP), true negatives (TN) and false positives (FP). On the basis of these four values, the accuracy and Matthews Correlation Coefficient (MCC) were calculated using the equations as below:

$$\text{Accuracy} = \frac{\mathbf{TP + TN}}{\mathbf{TP + TN + FP + FN}} \times 100\%$$

$$\text{MCC} = \frac{\mathbf{TP \times TN - FP \times FN}}{\sqrt{(\boldsymbol{TP+FP})(\boldsymbol{TP+FN})(\boldsymbol{TN+FP})(\boldsymbol{TN+FN})}}$$

4.3 Results

4.3.1 BeAtMuSic

The crystal structures of AChBP/LvIA and AChBP/LsIA were firstly used to predict the mutational energies for all site-directed mutants. Then refinements were put on these structures using either the energy minimisation (EM) or the molecular dynamics simulation (MD), and the refined structures were used as inputs to calculate ΔΔGs (Table 4.1). The accuracies and MCCs of the predicted ΔΔGs based on published IC_{50}s were calculated using the confusion matrix, and the results are shown in Table 4.1.

According to our tests, BeAtMuSic can make accurate ΔΔG predictions for mutants displaying a decreased in IC_{50} (Table 4.1). Interestingly, the EM and MD refinement approaches were unable to improve the performance of BeAtMuSic in mutational energy calculation. The predicted ΔΔGs of [S4A]LvIA, [N12L]LsIA and LsIA-[Q55K]AChBP do not agree with the experimental affinity data (highlighted in red in Table 4.1) and were the main data points lowering the accuracy and MCC values.

Table 4.1 Fold change in IC_{50} of mutants *versus* wild type for the LvIA/AChBP and LsIA/AChBP systems, and ΔΔGs computed using BeAtMuSic. IC_{50}s were taken from Xu *et al.* (24) and Abraham *et al.*(26). TP: True Positive; TN: True Negative; FP: False Positive; FN: False Negative.

Position	Experimental fold change	Crystal structure		Energy minimisation		Molecular simulation[a]	
		BeAtMuSic		BeAtMuSic		BeAtMuSic	
[S4A]LvIA	0.18	1.3	FN	1.2	FN	1.1	FN
[H5A]LvIA	No activity	2.1	TN	2.2	TN	2.2	TN
[P6A]LvIA	No activity	2.4	TN	2.3	TN	2.2	TN
[A7G]LvIA	No activity	1	TN	1.1	TN	1	TN
[N9A]LvIA	0.63	0.4	TP	0.7	TP	1	FN
[D11A]LvIA	0.13	0.8	TP	0.7	TP	0.8	TP
[H12A]LvIA	No activity	1.7	TN	1.5	TN	1.3	TN
[R10M]LsIA	2.4	0.3	TP	0.3	TP	0.3	TP
[R10D]LsIA	> 47.6	2.1	TN	1.9	TN	2	TN
[R10F]LsIA	0.52	-0.1	TP	0	TP	0	TP
[N12Q]LsIA	11.62	1.1	TN	1.3	TN	0.9	FP
[N12D]LsIA	> 47.6	1.6	TN	1.7	TN	1.4	TN
[N12L]LsIA	> 47.6	0.5	FP	0.4	FP	0.6	FP
LsIA-[Q55K]AChBP	82.86	0.7	FP	0.9	FP	0.8	FP
[R10M]LsIA - [Q55K]AChBP	0.41	0.1	TP	0.1	TP	0.2	TP
[R10F]LsIA - [Q55K]AChBP	0.05	-0.1	TP	-0.2	TP	-0.1	TP
Accuracy		81.3%		81.3%		68.8%	
MCC		0.63		0.63		0.38	

[a] the ΔΔGs values were averaged on five frames (2ns, 4ns, 6ns, 8ns, and 10ns) extracted from the MD simulation.

4.3.2 Foldx

In our hands, Foldx had 75% accuracy and an MCC score of 0.52 when performed using the crystal structure. The predictions were improved to 87.5% accuracy and 0.75 MCC when using EM structures, mainly because the effects of mutations were better accounted for the [N12L]LsIA and [Q55K]AChBP variants (highlighted in blue, Table 4.2). MD refinement did

Table 4.2 Fold change in IC_{50} of mutants *versus* wild type for the LvIA/AChBP and LsIA/AChBP systems, and ΔΔGs computed using Foldx. IC_{50}s were taken from Xu *et al.*(24) and Abraham *et al.*(26). TP: True Positive; TN: True Negative; FP: False Positive; FN: False Negative.

Position	Experimental fold change	Crystal structure		Energy minimisation		Molecular simulation[a]	
		Foldx		Foldx		Foldx	
[S4A]LvIA	0.18	-0.3	TP	0	TP	0.3	TP
[H5A]LvIA	No activity	1.2	TN	1.9	TN	1.3	TN
[P6A]LvIA	No activity	1.7	TN	1.8	TN	1.4	TN
[A7G]LvIA	No activity	0.7	FP	0.9	FP	0.9	FP
[N9A]LvIA	0.63	-0.1	TP	0.2	TP	0.1	TP
[D11A]LvIA	0.13	-1.6	TP	-1.7	TP	-0.9	TP
[H12A]LvIA	No activity	1.9	TN	2.5	TN	0.9	FP
[R10M]LsIA	2.4	0.6	TP	-0.2	TP	1.1	FN
[R10D]LsIA	> 47.6	3.1	TN	2.3	TN	3.6	TN
[R10F]LsIA	0.52	2.5	FN	2	FN	3	FN
[N12Q]LsIA	11.62	1.9	TN	1.5	TN	2.9	TN
[N12D]LsIA	> 47.6	2.1	TN	3.5	TN	2.9	TN
[N12L]LsIA	> 47.6	0.5	FP	1.4	TN	2.8	TN
LsIA-[Q55K]AChBP	82.86	0.9	FP	1.2	TN	2.2	TN
[R10M]LsIA - [Q55K]AChBP	0.41	-2.2	TP	-1.1	TP	-1.4	TP
[R10F]LsIA - [Q55K]AChBP	0.05	-1	TP	-1	TP	-0.1	TP
Accuracy		75%		87.5%		75%	
MCC		0.52		0.75		0.49	

[a] the ΔΔGs values were averaged on five frames (2ns, 4ns, 6ns, 8ns, and 10ns) extracted from the MD simulation.

not improve performance, probably because this type of refinement requires longer sampling times and increased number of data points along the trajectory (40). Interestingly, Foldx failed to achieve accurate predictions for the [A7G]LvIA and [R10F]LsIA mutants, regardless of refinement procedure.

4.3.3 Coarse-grained umbrella-sampling (CG_US)

All LvIA and LsIA mutants reached PMF convergence using the last 30 ns period of each US simulation (Figure 4.1 and 4.2). Nevertheless, the calculated ΔΔG values of LvIA and LsIA mutants were all < -1 kcal/mol with the exception of [N9A]LvIA, indicating all mutated peptides had an improved affinity compared to parent peptide (Table 4.3). This was not in agreement with experimental affinity data. For LvIA, the computed ΔΔGs of H5A, A7G and H12A are -22.5 kcal/mol, -26.8 kcal/mol and -35.7 kcal/mol, respectively, but these mutants had no affinity for AChBP experimentally. The R10D, N12Q, N12D, and N12L substitutions of LsIA caused a significant decrease in affinity (> 8-fold) according to the simulations. In contrast, experimentally the IC_{50} of LsIA decreased from 0.21 µM to 17.4 µM when AChBP Gln55 was substituted by a Lys residue. The accuracy and MCC of the calculated ΔΔGs are 47% and 0 respectively, demonstrating this energy prediction method is not suitable for α-conotoxin/AChBP complexes.

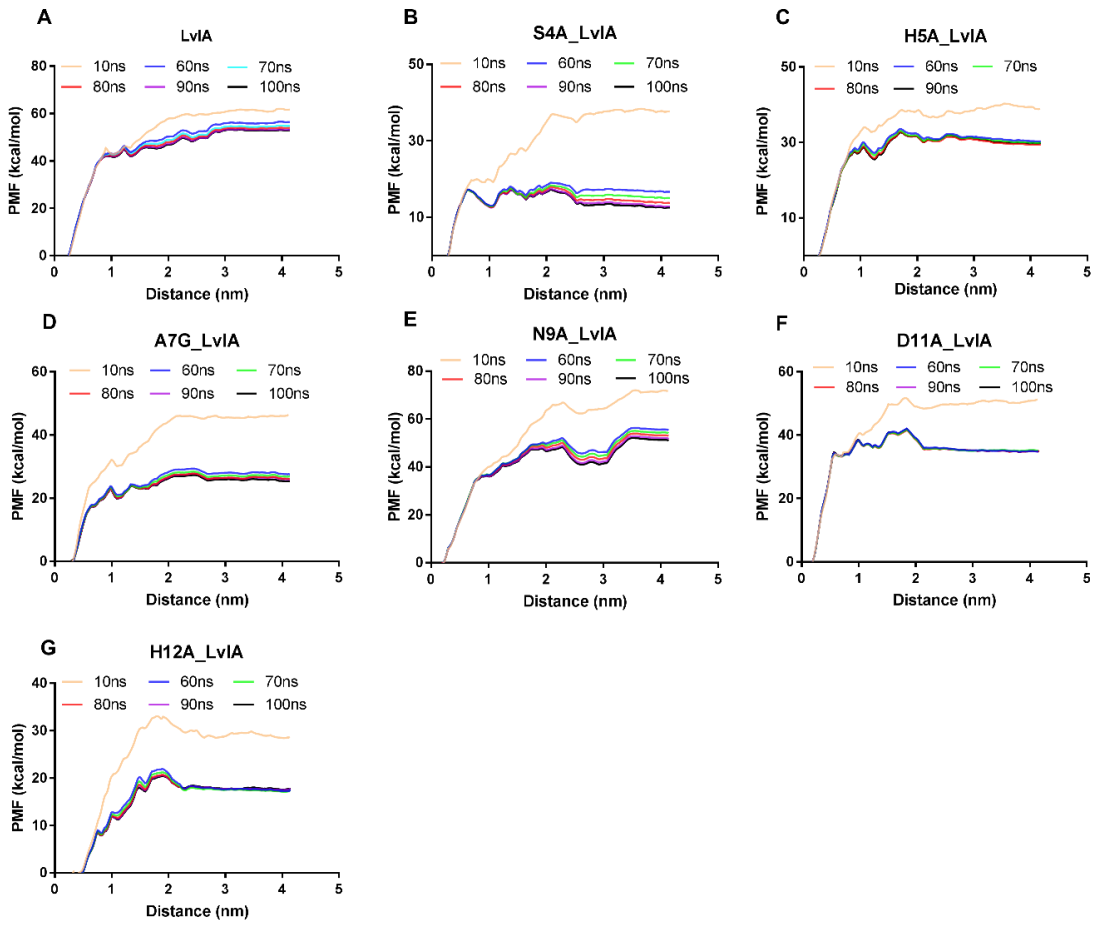

Figure 4.1 PMF profiles (kcal/mol) for AChBP in complex with LvIA and its mutants as a function of separation distance (nm).

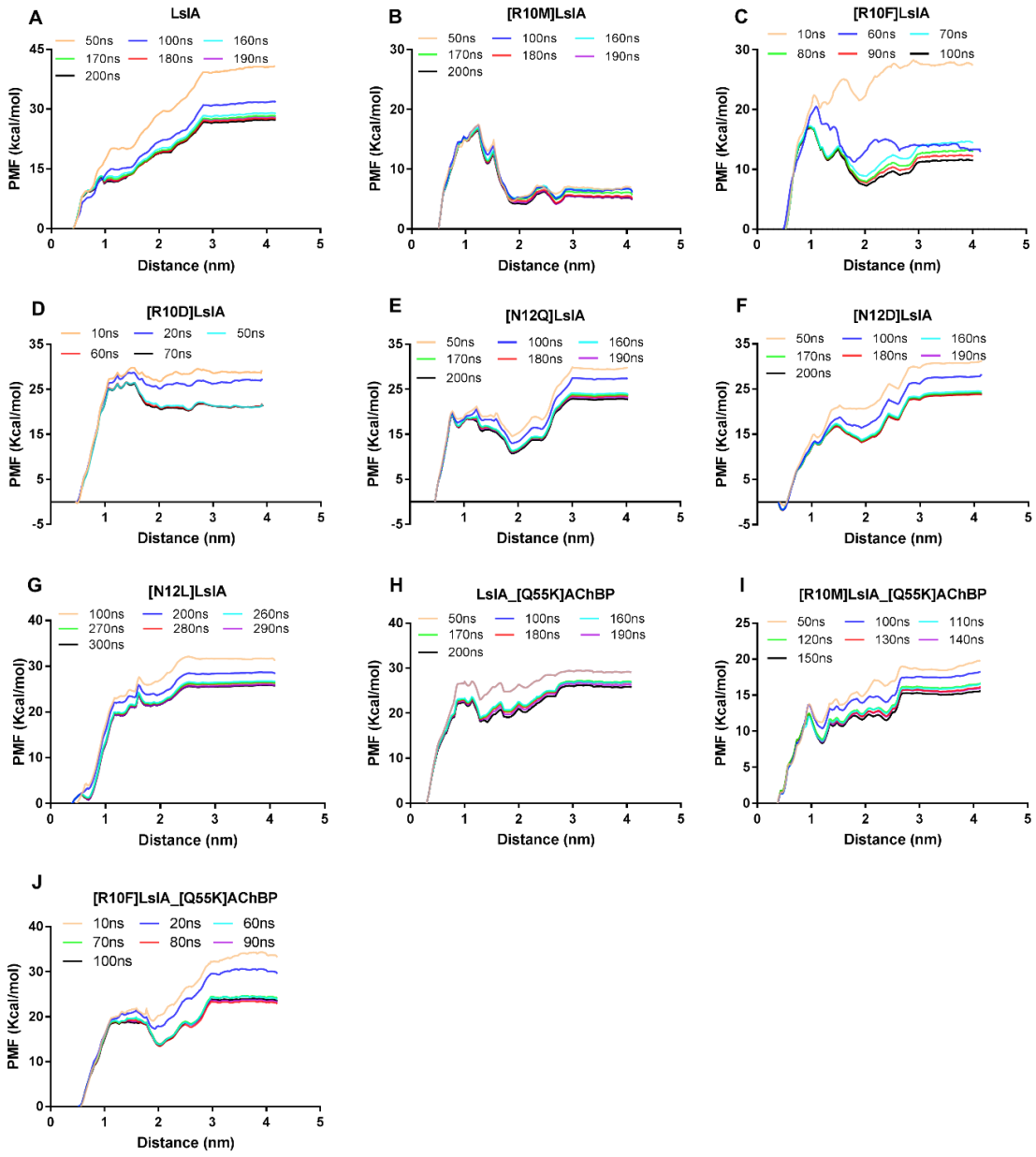

Figure 4.2 PMF profiles (kcal/mol) for AChBP in complex with LsIA and its mutants as a function of separation distance (nm).

Table 4.3 Fold change in IC_{50} of mutants *versus* wild type for the LvIA/AChBP and LsIA/AChBP systems, and ΔΔGs computed using CG_US, MMGBSA and MMPBSA. IC_{50}s were taken from Xu *et al*. (24) and Abraham *et al*.(26). TP: True Positive; TN: True Negative; FP: False Positive; FN: False Negative.

position	Experimental fold change	CG_US		MMGBSA		MMPBSA	
[S4A]LvIA	0.18	-39.7	TP	10.1	TP	-1.4	TP
[H5A]LvIA	No activity	-22.5	FP	15.7	TN	-3.3	FP
[P6A]LvIA	No activity	–	–	19.6	TN	8.6	FP
[A7G]LvIA	No activity	-26.8	FP	5	FP	-3.9	FP
[N9A]LvIA	0.63	-0.9	TP	4.6	TN	4	TP
[D11A]LvIA	0.13	-16.8	TP	17.4	FN	-6.2	TP
[H12A]LvIA	No activity	-35.7	FP	20.4	TN	6.6	FP
[R10M]LsIA	2.4	-22.2	TP	8.9	TP	7.9	TP
[R10D]LsIA	> 47.6	-6.3	FP	6.7	FP	21.1	TN
[R10F]LsIA	0.52	-4	TP	10.8	TP	12.3	TP
[N12Q]LsIA	11.62	-4.5	FP	7.6	FP	6.4	FP
[N12D]LsIA	> 47.6	-3.8	FP	11.1	FP	19.2	TN
[N12L]LsIA	> 47.6	-1.6	FP	8.7	FP	8.2	FP
LsIA-[Q55K]AChBP	82.86	-1.2	FP	15.6	TN	12.6	FP
[R10M]LsIA -[Q55K]AChBP	0.41	-10.9	TP	14	FN	8.1	TP
[R10F]LsIA -[Q55K]AChBP	0.05	-2.9	TP	6.5	TP	7	TP
Accuracy		47%		56.3%		56.3%	
MCC		0		0.16		0.33	

[a] The [P6A]_LvIA moved away from the binding site of the AChBP after 500 ns molecular dynamics simulation. Therefore the ΔΔG of [P6A]LvIA was not calculated.

4.3.4 MMGBSA and MMPBSA

Each model was refined using 10 ns molecular dynamics simulations in triplicate with all atoms of the receptor located more than 5 Å from α-conotoxins restrained to their starting position. The mutational energies of peptides were calculated using MMGBSA and MMPBSA (Table 4.3). The predictions had an Accuracy and MCC results of 56.3% and 0.16 for MMGBSA, respectively, and 56.3% and 0.33 of MMPBSA, respectively, suggesting that these two energy methods are not highly accurate. Interestingly, incorrect predictions of MMGBSA and

MMPBSA were made for mutants with decreased IC_{50}s (five mutants for MMGBSA and seven mutants for MMPBSA).

4.4 Discussion

Computational protein design method could be potentially used for increasing the selectivity of α-conotoxins on human nAChRs. Binding free energy prediction has been successfully applied in peptide design (7). We here benchmarked four binding free energy computation methods using experimental structures of complexes between α-conotoxins and AChBP.

Most predicted mutational energies made by BeAtMuSiC were consistent with experimental data. Incorrect predictions were made for three LvIA mutants: [S4A]LvIA, [N12L]LsIA and LsIA/[Q55K]AChBP. The [S4A]LvIA, has comparable affinity to the parent peptide according to experimental data, but our models predicted decreased affinity compared to the parent peptide (Table 4.1). In the crystal structure of the AChBP/LvIA complex, the S4 of LvIA forms a hydrogen bond with Ser166 of the complementary subunit (Figure 4.3A) (24). In the molecular model of [S4A]LvIA/AChBP complex after MD refinement (Figure 4.3B), the substitution of S4 to Ala resulted in a small change of conformation of the second loop, resulting in the creation of a hydrogen bond between LvIA Asn9 and AChBP Gln55 (complementary subunit). BeAtMuSic likely cannot provide an accurate prediction for [S4A]LvIA because it does not account for change of backbone conformation (27). The experimental data showed reduced activity for [N12L]LsIA and LsIA/[Q55K]AChBP, but predicted ΔΔGs suggested these two mutants had comparable affinity compared to parent peptide. In the molecular models of AChBP/[N12L]LsIA and [Q55K]AChBP/LsIA complexes after MD refinement (data not shown here), these two peptides also have a small conformation change in the second loop at the binding site. Thus, BeAtMuSic made incorrect predictions for these two mutants. A previous study showed that BeAtMuSic only performs well in predicting large decrease in affinity (41). Our results confirm this, noting that BeAtMuSic was not able to correctly predict any increase in affinity. The EM and MD refinements had no impact on the performance of BeAtMuSic, probably because the coarse-grained treatment of side chains of BeAtMuSiC is insensitive to the quality of the structure (27,42). BeAtMusic could be used to predict mutants that would have decreased activity using a low resolution molecular model of α-conotxin/nAChR.

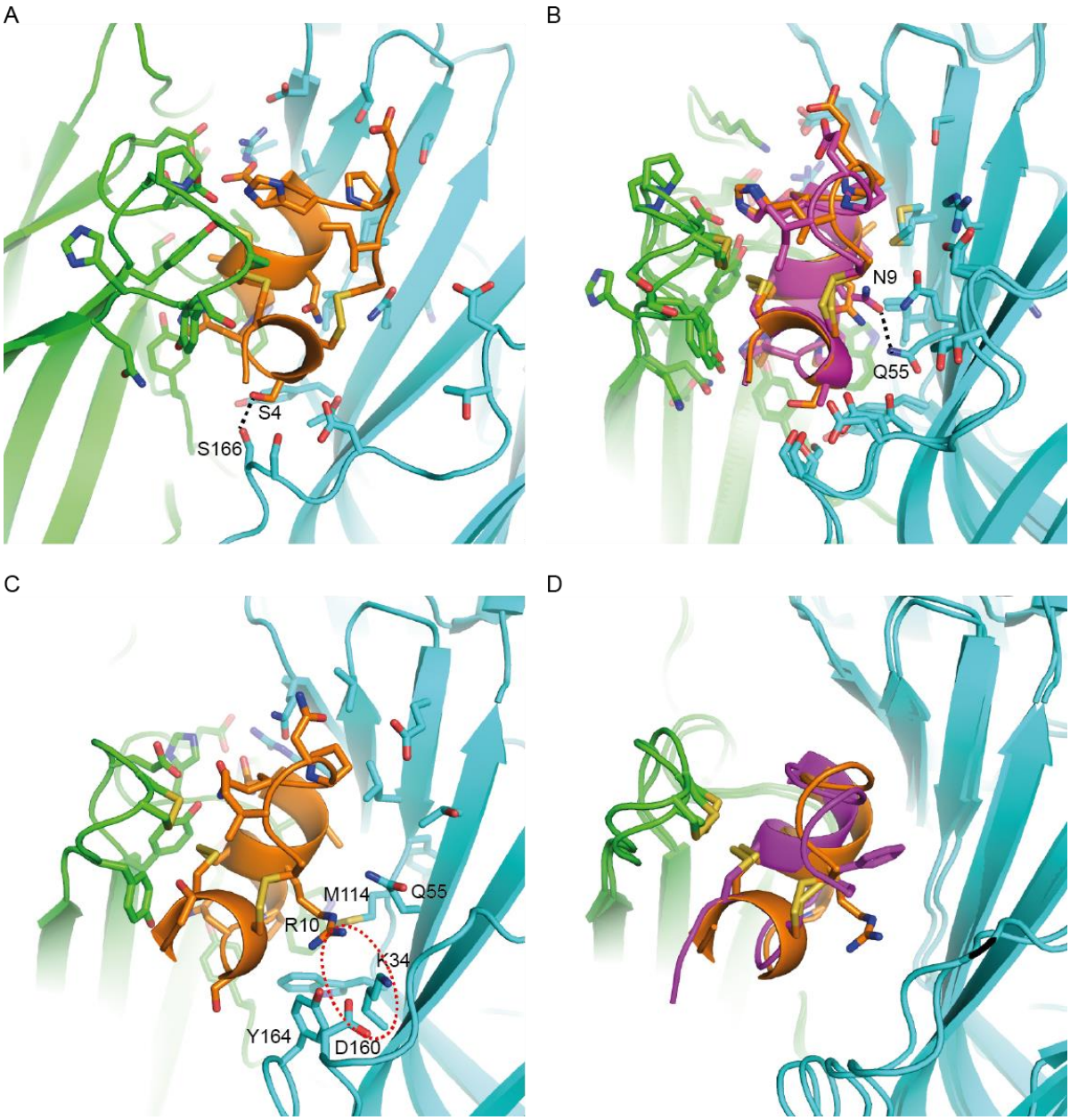

Figure 4.3 Interactions between AChBP and LvIA, [S4A]LvIA, LsIA or [R10F]LsIA. A: Crystal structure of the AChBP/LvIA complex **(**PDB: 5XGL**)**; B: Overlay of the crystal structure of the AChBP/LvIA (orange) complex and MD structure of the AChBP/[S4A]LvIA (magenta) complex; C: The crystal structure of the AChBP/LsIA complex **(**PDB: 5T90); D: Overlay of the crystal structure of the AChBP/LsIA (orange) complex and MD structure of the AChBP/[R10F]LsIA (magenta) complex. The hydrogen bonds are displayed as dotted black lines and interactions between charged side chains are circled with a dotted red line.

The performance of Foldx was significantly improved on EM structures, increasing the accuracy and MCC values from 75% and 0.52 to 87.5% and 0.75, respectively. The MCC of 0.75 is the best recorded among all methods tested here, suggesting that Foldx is the best method for predicting the mutational effect if the model is refined by EM. Because Foldx is highly sensitive to the quality of the structure (43,44), EM is likely to improve the quality of

the structure. EM refinement allowed the program to have accurate ΔΔG predictions for [N12L]LsIA and LsIA-[Q55K]AChBP but still not enough for a correct prediction for [A7G]LvIA. In contrast, MD did not improve the performance of Foldx in ΔΔG prediction, possibly because 10 ns simulation time is insufficient for the α-conotoxin/AChBP systems to reach equilibrium. [R10F]LsIA was inaccurately predicted by Foldx using the crystal structure, EM structure and MD structure. LvIA Arg10 is buried at the interface with the complementary subunit in the crystal structure (PDB: 5XGL). It forms a salt bridge with Asp160 and has a repulsive force with Lys34 (Figure 4.3C), and its side chain makes contact with Lys34, Gln55, Met114 and Tyr164 of AChBP (26). The substitution of the charged residue (equivalent to position 9 of other α-conotoxins) to a hydrophobic Phe could cause the change of binding mode of LsIA at the binding site, discussed in Chapter 3. However, Foldx does not consider change of binding mode upon mutations as it only computes change in the conformation of side chains (45). During the MD simulation of the complex between [R10F]LsIA and AChBP (Figure 4.3D), the backbone of [R10F]LsIA shifted, suggesting that the [R10F] mutation indeed resulted in a small change of binding mode. A previous study showed that the correlation (R^2) value between the Foldx calculated ΔΔGs and the experimentally derived ΔΔGs was 0.7 for the α-conotoxin ImI/human α7 nAChR system (35), suggesting that Foldx is a reliable energy prediction tool for α-conotoxin/nAChR systems. A recent review summarised the use of Foldx in protein engineering applications and concluded that Foldx is better than random and is useful for protein design applications (46). Accordingly, we here suggest that Foldx could be used to design α-conotoxins with improved selectivity and potency for nAChR subtypes.

The mutational energies obtained from CG_US were all negative, which does not correlate with the experimental affinity data. In contrast, the CG_US was successfully applied to calculate ΔΔGs in three different protein-protein complexes from the SKEMPI database. The R^2 with experimental values reached 0.88, 0.92 and 0.5 for the three complexes, and it clearly outperformed Foldx (47). Additionally, the umbrella sampling has accurately calculated PMFs of disassociation for a range of conotoxins complexed with different ion channels and receptors. For example, the PMFs of α-conotoxins [A10L,D14K]PnIA and ImI from AChBP were -24.2 kcal/mol and -20.3 kcal/mol, in agreement with experimental values (33). The PMFs of [γ4E]GID from α7 and α4β2 nAChR were also in accordance with their experimental data (35). Similarly, the PMFs of μ-conotoxin PIIIA from Nav1.1 to Nav1.9 were calculated, and the R^2 between PMFs and experimentally derived energies was 0.68 (48). The PMFs of ω-

conotoxin GVIA from Cav2.2 were calculated, and the IC_{50}s obtained from PMFs were similar to the experimental IC_{50} of ω-conotoxin GVIA (~1 nM) (49). These successful examples show that US could predict mutational energies for the α-conotoxin/nAChR systems with reasonable accuracy. However, in our study, we found that CG_US method did not result in correct predictions. Therefore we suggest that the SIRAH force field is not suitable for simulating the α-conotoxin/AChBP systems.

Surprisingly, the mutational energies calculated using MMGBSA and MMPBSA did not perform as expected in this study. Our results contrast with previous report in which MMGBSA was shown to correctly predict ΔΔG (40). Initially, the MMGBSA performed well, predicting mutational energies of α-conotoxin ImI correlating with experimental data ($R^2 = 0.74$) (40). In a subsequent study, this method was used to pinpoint the binding site of α-conotoxin Vc1.1 on the α9α10 nAChR. The mutational energy prediction by MMGBSA successfully helped design an α-conotoxin Vc1.1 mutant, [N9W]Vc1.1, with improved activity on human α9α10 nAChR α10(+)α9(-) binding pocket (7). Recently, α9α10 nAChR has been reported to have two stoichiometries: $(\alpha9)_2(\alpha10)_3$ and $(\alpha9)_3(\alpha10)_2$ (50). The MMGBSA method assisted in the elucidation of structural characterisitcs which affect Vc1.1 binding to the α10(+)α9(-) binding pocket of the $(\alpha9)_2(\alpha10)_3$ stoichiometry and the α9(+)α9(-) binding pocket of the $(\alpha9)_3(\alpha10)_2$ stoichiometry (51). Two main approaches are likely to improve the performance of MMGBSA or MMPBSA in our study: 1) predicting the mutational energy using energy minimisation structures, which has been reported by Yu *et al.*(40); 2) prolonging the simulation time, because the α-conotoxin/AChBP systems might not reach equilibrium by 10 ns.

In summary, we have benchmarked a series of mutational energy prediction methods and identified that Foldx is the most reliable method. Notably, this method successfully predicted which mutated peptides would exhibit increased and decreased affinities with the receptor. Foldx therefore is useful for designing selective inhibitors of nAChR subtypes based on α-conotoxins.

4.5 References

1. Lebbe, E. K., Peigneur, S., Wijesekara, I., and Tytgat, J. (2014) Conotoxins targeting nicotinic acetylcholine receptors: an overview. *Mar. Drugs.* **12**, 2970-3004
2. Dutton, J. L., Bansal, P. S., Hogg, R. C., Adams, D. J., Alewood, P. F., and Craik, D. J. (2002) A new level of conotoxin diversity, a non-native disulfide bond connectivity in alpha-conotoxin AuIB reduces structural definition but increases biological activity. *J. Biol. Chem.* **277**, 48849-48857
3. Wu, Y., Wu, X., Yu, J., Zhu, X., Zhangsun, D., and Luo, S. (2014) Influence of disulfide connectivity on structure and bioactivity of alpha-conotoxin TxIA. *Molecules* **19**, 966-979
4. Kasheverov, I. E., Zhmak, M. N., Fish, A., Rucktooa, P., Khruschov, A. Y., Osipov, A. V., Ziganshin, R. H., D'hoedt, D., Bertrand, D., Sixma, T. K., Smit, A. B., and Tsetlin, V. I. (2009) Interaction of alpha-conotoxin ImII and its analogs with nicotinic receptors and acetylcholine-binding proteins: additional binding sites on Torpedo receptor. *J. Neurochem.* **111**, 934-944
5. Lebbe, E. K., Peigneur, S., Maiti, M., Mille, B. G., Devi, P., Ravichandran, S., Lescrinier, E., Waelkens, E., D'Souza, L., Herdewijn, P., and Tytgat, J. (2014) Discovery of a new subclass of alpha-conotoxins in the venom of *Conus australis*. *Toxicon* **91**, 145-154
6. Halai, R., Clark, R. J., Nevin, S. T., Jensen, J. E., Adams, D. J., and Craik, D. J. (2009) Scanning mutagenesis of alpha-conotoxin Vc1.1 reveals residues crucial for activity at the alpha9alpha10 nicotinic acetylcholine receptor. *J. Biol. Chem.* **284**, 20275-20284
7. Yu, R., Kompella, S. N., Adams, D. J., Craik, D. J., and Kaas, Q. (2013) Determination of the alpha-conotoxin Vc1.1 binding site on the alpha9alpha10 nicotinic acetylcholine receptor. *J. Med. Chem.* **56**, 3557-3567
8. Azam, L., and McIntosh, J. M. (2012) Molecular basis for the differential sensitivity of rat and human alpha9alpha10 nAChRs to alpha-conotoxin RgIA. *J. Neurochem.* **122**, 1137-1144
9. Grishin, A. A., Wang, C. I., Muttenthaler, M., Alewood, P. F., Lewis, R. J., and Adams, D. J. (2010) Alpha-conotoxin AuIB isomers exhibit distinct inhibitory mechanisms and differential sensitivity to stoichiometry of alpha3beta4 nicotinic acetylcholine receptors. *J. Biol. Chem.* **285**, 22254-22263

10. Cuny, H., Kompella, S. N., Tae, H. S., Yu, R., and Adams, D. J. (2016) Key structural determinants in the agonist binding loops of human beta2 and beta4 nicotinic acetylcholine receptor subunits contribute to alpha3beta4 subtype selectivity of alpha-conotoxins. *J. Biol. Chem.* **291**, 23779-23792
11. Vincler, M., Wittenauer, S., Parker, R., Ellison, M., Olivera, B. M., and McIntosh, J. M. (2006) Molecular mechanism for analgesia involving specific antagonism of alpha9alpha10 nicotinic acetylcholine receptors. *Proc. Natl. Acad. Sci. U. S. A.* **103**, 17880-17884
12. Akondi, K. B., Muttenthaler, M., Dutertre, S., Kaas, Q., Craik, D. J., Lewis, R. J., and Alewood, P. F. (2014) Discovery, synthesis, and structure-activity relationships of conotoxins. *Chem. Rev.* **114**, 5815-5847
13. Inserra, M. C., Kompella, S. N., Vetter, I., Brust, A., Daly, N. L., Cuny, H., Craik, D. J., Alewood, P. F., Adams, D. J., and Lewis, R. J. (2013) Isolation and characterization of alpha-conotoxin LsIA with potent activity at nicotinic acetylcholine receptors. *Biochem. Pharmacol.* **86**, 791-799
14. Luo, S., Zhangsun, D., Zhu, X., Wu, Y., Hu, Y., Christensen, S., Harvey, P. J., Akcan, M., Craik, D. J., and McIntosh, J. M. (2013) Characterization of a novel alpha-conotoxin TxID from *Conus textile* that potently blocks rat alpha3beta4 nicotinic acetylcholine receptors. *J. Med. Chem.* **56**, 9655-9663
15. Nicke, A., Loughnan, M. L., Millard, E. L., Alewood, P. F., Adams, D. J., Daly, N. L., Craik, D. J., and Lewis, R. J. (2003) Isolation, structure, and activity of GID, a novel alpha 4/7-conotoxin with an extended N-terminal sequence. *J. Biol. Chem.* **278**, 3137-3144
16. Franco, A., Kompella, S. N., Akondi, K. B., Melaun, C., Daly, N. L., Luetje, C. W., Alewood, P. F., Craik, D. J., Adams, D. J., and Mari, F. (2012) RegIIA: an alpha4/7-conotoxin from the venom of *Conus regius* that potently blocks alpha3beta4 nAChRs. *Biochem. Pharmacol.* **83**, 419-426
17. Cuny, H., Yu, R., Tae, H. S., Kompella, S. N., and Adams, D. J. (2017) Alpha-Conotoxins active at alpha3-containing nicotinic acetylcholine receptors and their molecular determinants for selective inhibition. *Br. J. Pharmacol.* **175**, 1855-1868
18. Romero, H. K., Christensen, S. B., Di Cesare Mannelli, L., Gajewiak, J., Ramachandra, R., Elmslie, K. S., Vetter, D. E., Ghelardini, C., Iadonato, S. P., Mercado, J. L., Olivera, B. M., and McIntosh, J. M. (2017) Inhibition of alpha9alpha10 nicotinic acetylcholine

receptors prevents chemotherapy-induced neuropathic pain. *Proc. Natl. Acad. Sci. U. S. A.* **114**, E1825-E1832

19. Hone, A. J., Ruiz, M., Scadden, M., Christensen, S., Gajewiak, J., Azam, L., and McIntosh, J. M. (2013) Positional scanning mutagenesis of alpha-conotoxin PeIA identifies critical residues that confer potency and selectivity for alpha6/alpha3beta2beta3 and alpha3beta2 nicotinic acetylcholine receptors. *J. Biol. Chem.* **288**, 25428-25439
20. Castro, J., Grundy, L., Deiteren, A., Harrington, A. M., O'Donnell, T., Maddern, J., Moore, J., Garcia-Caraballo, S., Rychkov, G. Y., Yu, R., Kaas, Q., Craik, D. J., Adams, D. J., and Brierley, S. M. (2017) Cyclic analogues of alpha-conotoxin Vc1.1 inhibit colonic nociceptors and provide analgesia in a mouse model of chronic abdominal pain. *Br. J. Pharmacol.* **175**, 2384-2398
21. Celie, P. H., Kasheverov, I. E., Mordvintsev, D. Y., Hogg, R. C., van Nierop, P., van Elk, R., van Rossum-Fikkert, S. E., Zhmak, M. N., Bertrand, D., and Tsetlin, V. (2005) Crystal structure of nicotinic acetylcholine receptor homolog AChBP in complex with an alpha-conotoxin PnIA variant. *Nat. Struct. Mol. Biol.* **12**, 582-588
22. Ulens, C., Hogg, R. C., Celie, P. H., Bertrand, D., Tsetlin, V., Smit, A. B., and Sixma, T. K. (2006) Structural determinants of selective α-conotoxin binding to a nicotinic acetylcholine receptor homolog AChBP. *Proc. Natl. Acad. Sci. U. S. A.* **103**, 3615-3620
23. Dutertre, S., Ulens, C., Büttner, R., Fish, A., van Elk, R., Kendel, Y., Hopping, G., Alewood, P. F., Schroeder, C., and Nicke, A. (2007) AChBP-targeted alpha-conotoxin correlates distinct binding orientations with nAChR subtype selectivity. *EMBO J.* **26**, 3858-3867
24. Xu, M., Zhu, X., Yu, J., Yu, J., Luo, S., and Wang, X. (2017) The crystal structure of Ac-AChBP in complex with alpha-conotoxin LvIA reveals the mechanism of its selectivity towards different nAChR subtypes. *Protein Cell.* **8**, 1-11
25. Lin, B., Xu, M., Zhu, X., Wu, Y., Liu, X., Zhangsun, D., Hu, Y., Xiang, S. H., Kasheverov, I. E., Tsetlin, V. I., Wang, X., and Luo, S. (2016) From crystal structure of alpha-conotoxin GIC in complex with Ac-AChBP to molecular determinants of its high selectivity for alpha3beta2 nAChR. *Sci. Rep.* **6**, 22349
26. Abraham, N., Healy, M., Ragnarsson, L., Brust, A., Alewood, P. F., and Lewis, R. J. (2017) Structural mechanisms for alpha-conotoxin activity at the human alpha3beta4 nicotinic acetylcholine receptor. *Sci. Rep.* **7**, 45466

27. Dehouck, Y., Kwasigroch, J. M., Rooman, M., and Gilis, D. (2013) BeAtMuSiC: Prediction of changes in protein-protein binding affinity on mutations. *Nucleic Acids Res.* **41**, W333-339

28. Guerois, R., Nielsen, J. E., and Serrano, L. (2002) Predicting changes in the stability of poteins and protein complexes: A study of more than 1000 mutations. *J. Mol. Biol.* **320**, 369-387

29. Schymkowitz, J., Borg, J., Stricher, F., Nys, R., Rousseau, F., and Serrano, L. (2005) The Foldx web server: an online force field. *Nucleic. Acids. Res.* **33**, W382-W388

30. Kumar, S., Rosenberg, J. M., Bouzida, D., Swendsen, R. H., and Kollman, P. A. (1992) The weighted histogram analysis method for free energy calculations on biomolecules. I. The method. *J. Comput. Chem.* **13**, 1011-1021

31. Kmiecik, S., Gront, D., Kolinski, M., Wieteska, L., Dawid, A. E., and Kolinski, A. (2016) Coarse-grained protein models and their applications. *Chem. Rev.* **116**, 7898-7936

32. Genheden, S., and Ryde, U. (2015) The MM/PBSA and MM/GBSA methods to estimate ligand-binding affinities. *Expert Opin. Drug Discov.* **10**, 449-461

33. Yu, R., Tabassum, N., and Jiang, T. (2016) Investigation of alpha-conotoxin unbinding using umbrella sampling. *Bioorg. Med. Chem. Lett.* **26**, 1296-1300

34. Yu, R., Kaas, Q., and Craik, D. J. (2012) Delineation of the unbinding pathway of alpha-conotoxin ImI from the alpha7 nicotinic acetylcholine receptor. *J. Phys. Chem. B* **116**, 6097-6105

35. Suresh, A., and Hung, A. (2016) Molecular simulation study of the unbinding of alpha-conotoxin [Ƴ4E]GID at the alpha7 and alpha4beta2 neuronal nicotinic acetylcholine receptors. *J. Mol. Graph. Model.* **70**, 109-121

36. Abraham, M. J., Murtola, T., Schulz, R., Páll, S., Smith, J. C., Hess, B., and Lindahl, E. (2015) GROMACS: High performance molecular simulations through multi-level parallelism from laptops to supercomputers. *SoftwareX* **1-2**, 19-25

37. Darré, L., Machado, M. R., Brandner, A. F., González, H. C., Ferreira, S. n., and Pantano, S. (2015) SIRAH: a structurally unbiased coarse-grained force field for proteins with aqueous solvation and long-range electrostatics. *J. Chem. Theory Comput.* **11**, 723-739

38. Li, H., Robertson, A. D., and Jensen, J. H. (2005) Very fast empirical prediction and rationalization of protein pKa values. *Proteins* **61**, 704-721

39. Darden, T., York, D., and Pedersen, L. (1993) Particle mesh Ewald: An N· log (N) method for Ewald sums in large systems. *J. Chem. Phys* **98**, 10089-10092
40. Yu, R., Craik, D. J., and Kaas, Q. (2011) Blockade of neuronal alpha7-nAChR by alpha-conotoxin ImI explained by computational scanning and energy calculations. *PLoS. Comput. Biol.* **7**, e1002011
41. Adamski, C. J., and Palzkill, T. (2017) Systematic substitutions at BLIP position 50 result in changes in binding specificity for class A beta-lactamases. *BMC Biochem.* **18**, 2
42. Kumar, V., Rahman, S., Choudhry, H., Zamzami, M. A., Sarwar Jamal, M., Islam, A., Ahmad, F., and Hassan, M. I. (2017) Computing disease-linked SOD1 mutations: deciphering protein stability and patient-phenotype relations. *Sci. Rep.* **7**, 4678
43. Christensen, N. J., and Kepp, K. P. (2012) Accurate stabilities of laccase mutants predicted with a modified Foldx protocol. *J. Chem. Inf. Model.* **52**, 3028-3042
44. Kepp, K. P. (2015) Towards a "Golden Standard" for computing globin stability: Stability and structure sensitivity of myoglobin mutants. *Biochim. Biophys. Acta. Proteins. Proteom.* **1854**, 1239-1248
45. Dourado, D. F. A. R., and Flores, S. C. (2014) A multiscale approach to predicting affinity changes in protein–protein interfaces. *Proteins* **82**, 2681-2690
46. Buss, O., Rudat, J., and Ochsenreither, K. (2018) Foldx as protein engineering tool: better than random based approaches? *Comput. Struct. Biotechnol. J.* **16**, 25-33
47. Patel, J. S., and Ytreberg, F. M. (2018) Fast calculation of protein-protein binding free energies using umbrella sampling with a coarse-grained model. *J. Chem. Theory. Comput.* **14**, 991-997
48. Chen, F., Huang, W., Jiang, T., and Yu, R. (2018) Determination of the μ-Conotoxin PIIIA specificity against voltage-gated sodium channels from binding energy calculations. *Mar. Drugs* **16**, 153
49. Chen, R., and Chung, S. H. (2013) Complex structures between the N-type calcium channel (Cav2.2) and omega-conotoxin GVIA predicted via molecular dynamics. *Biochemistry* **52**, 3765-3772
50. Indurthi, D. C., Pera, E., Kim, H.-L., Chu, C., McLeod, M. D., McIntosh, J. M., Absalom, N. L., and Chebib, M. (2014) Presence of multiple binding sites on alpha9alpha10 nAChR receptors alludes to stoichiometric-dependent action of the alpha-conotoxin, Vc1. 1. *Biochem. Pharmacol.* **89**, 131-140

51. Yu, R., Tae, H. S., Tabassum, N., Shi, J., Jiang, T., and Adams, D. J. (2018) Molecular determinants conferring the stoichiometric-dependent activity of alpha-conotoxins at the human alpha9alpha10 nicotinic acetylcholine receptor subtype. *J. Med. Chem.* **61**, 4628-4634

Chapter 5: Engineering globular and ribbon α-conotoxin GID to selectively target α4β2 nAChR

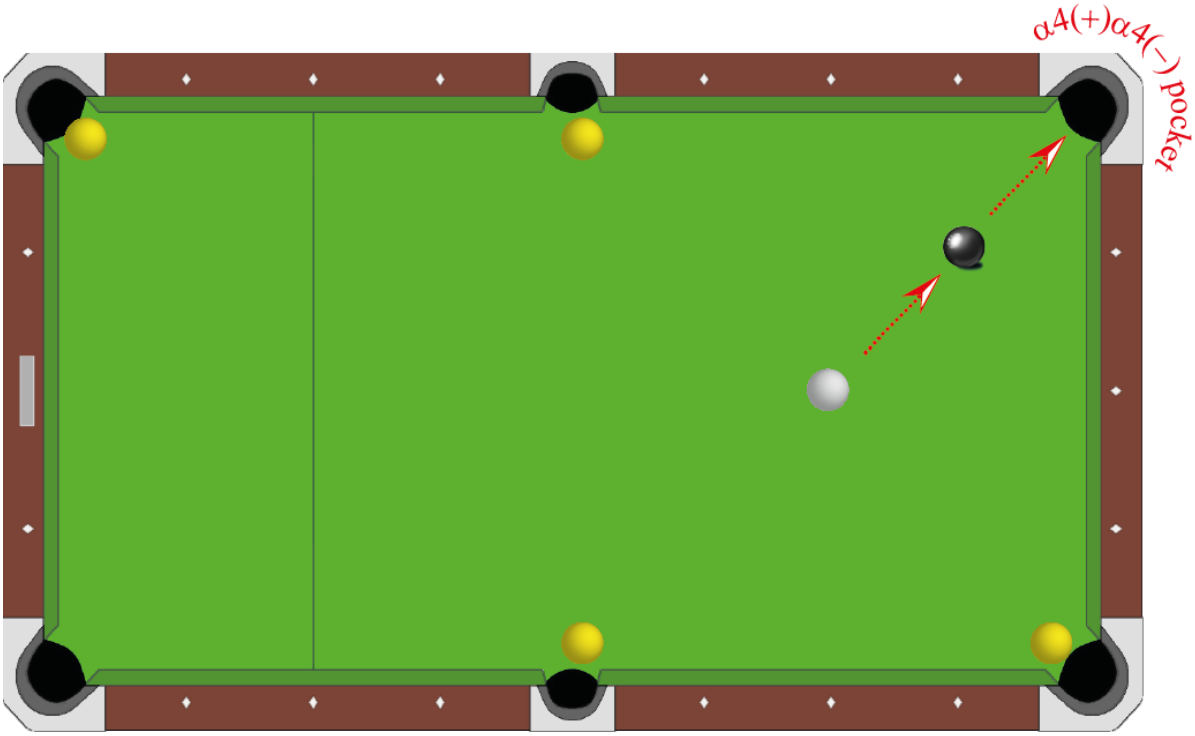

5.1 Introduction

The α4β2 nAChR is the most abundant and widely distributed neuronal nAChR, and is a potential target for a range of neurological conditions and disorders, such as nicotine addiction (1,2), epilepsy (3), Parkinson's, and Alzheimer's disease (4). The heteromeric α4β2 nAChR has two major stoichiometries with distinct functional properties: $(\alpha4)_2(\beta2)_3$ (a pentamer with two α4 subunits and three β2 subunits) and $(\alpha4)_3(\beta2)_2$ nAChR (5,6). The two subtypes differ in sensitivity to agonists, antagonists and allosteric modulators. Each subtype also has distinct single-channel conductance, mean open lifetime, and activation-deactivation kinetics (7). Interestingly, both stoichiometries are associated with nicotine addiction and congenital epilepsy (8,9). Previous studies showed that chronic inactivation of α4β2 nAChR could result in a significant impairment in spatial memory (10), indicating that understanding α4β2 nAChR antagonists could assist in designing drugs to treat memory impairment.

To date, no conotoxin that can selectively and potently block the α4β2 subtypes has been discovered (11). Some globular α-conotoxins have shown low inhibition of the α4β2 receptor, suggesting that it is possible to target it with a peptide (12-15). These conotoxins are nevertheless more active at other nAChR subtypes, and they need modification to generate selective compounds for the α4β2 nAChR. α-Conotoxin GID was discovered from *C. geographus*. It has a four-residue N-terminal tail and residues with post-translational modifications in positions 4 and 16 (Figure 5.1) (13). Globular α-conotoxin GID (gGID) inhibits the rat α3β2, α4β2 and α7 nAChRs with IC_{50}s of 3.4 nM, 128.6 nM and 5.1 nM, respectively (16). An alanine scan of non-cysteine residues showed that most of the gGID Ala mutants had at least a 10-fold decrease in activity at the α4β2 nAChR (Table 5.1) (16).

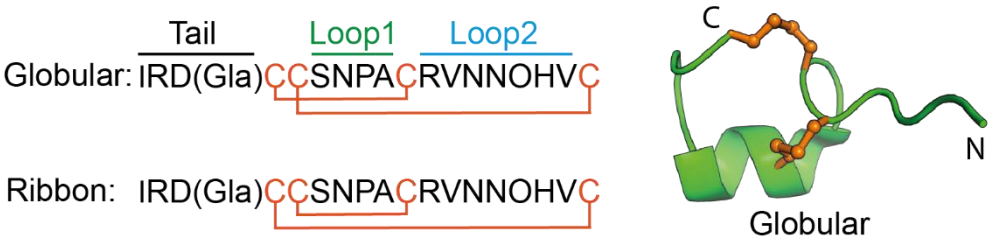

Figure 5.1 Amino acid sequence of globular and ribbon GID and the 3D NMR solution structure of gGID (PDB: 1MTQ). Gla:γ-carboxyglutamate acid, O: hydroxyproline; The connectivities of disulfide bonds are shown as orange lines and the disulfide bonds are shown as orange sticks in the 3D structure; "C" and "N" stand for the C-terminus and N-terminus, respectively.

Table 5.1 Electrophysiology results for gGID and its analogues (16).

Peptide name	IC_{50} values (mean_S.E.) (nM)		
	α4β2 nAChR	α3β2 nAChR	α7 nAChR
gGID	128.6 ± 13.1	3.4 ± 0.5	5.1 ± 1.3
[Gla4E]gGID	56.8 ± 13.2	2.9 ± 0.6	5.9 ± 0.6
[Gla4E,I1A]gGID	255.9 ± 57.2	15.5 ± 2.2	5.9 ± 1.6
[Gla4E,R2A]gGID	NA	97.6 ± 28.4	12.5 ± 4.4
[Gla4E,D3A]gGID	NA	69.8 ± 16.5	42.1 ± 10.9
[Gla4A]gGID	52 ± 16.5	3.0 ± 0.6	6.1 ± 2.8
[Gla4E,S7A]gGID	429.9 ± 82.6	2.5 ± 0.3	12.8 ± 1.5
[Gla4E,N8A]gGID	NA	4.1 ± 1.6	>30[a]
[Gla4E,P9A]gGID	NA	172.6 ± 50.1	90.5 ± 22.6
[Gla4E,R12A]gGID	NA	10.4 ± 0.7	48.8 ± 4.2
[Gla4E,V13A]gGID	112.5 ± 32.1	0.6 ± 0.1	11.2 ± 4.0
[Gla4E,N14A]gGID	NA	1.3 ± 0.5	51.4 ± 6.8
[Gla4E,N15A]gGID	NA	3.3 ± 0.2	6.0 ± 1.0
[Gla4E,O16A]gGID	NA	13.5 ± 2.1	13.0 ± 4.4
[Gla4E,H17A]gGID	571.7 ± 59.6	2.7 ± 0.2	5.0 ± 1.9
[Gla4E,V18A]gGID	602 ± 75.1	40.8 ± 8.0	7.9 ± 2.9

[a] Where IC_{50} values were unable to be determined, estimations are represented as > the highest concentration tested. NA denotes a nonactive analogue at concentrations ≤ 1μM.

Banerjee *et al.* built a binding mode of the gGID with α4(+)β2(-) interface using the crystal structure of acetylcholine binding protein (AChBP) in complex with [A10L, D14K]PnIA as a template, which was used to design new mutants to selectively and potently inhibit α4β2 nAChR. Out of 22 mutants that have been designed and tested, [V18N]gGID maintained a comparable activity at rat α4β2 nAChR but had no biological activity at the rat α3β2 nAChR, suggesting that the selectivity against different subtypes of this molecule can be improved using a *de novo* design approach (17). Likewise, Leffler *et al.* built the molecular model of gGID interacting with the α4(+)β2(-) binding site based on the crystal structures of AChBPs in complex with α-conotoxins [A10L, D14K]PnIA, ImI, BuIA, and [A10L]TxIA, which was refined using a newly developed docking algorithm ToxDock based on the Rosetta modeling framework (18). The refined molecular model was then used to screen virtually some predicted bioactive peptides that were selected to evaluate their activities against a range of nAChRs.

The [V13Y]gGID displayed reduced activity at the human α7 nAChR from 0.1 μM to 4 μM while maintaining same activity at the α4β2 nAChR (3 μM), but demonstrated increased activity at the α3β2 nAChR from 10 nM to 2 nM (18).

The modification of gGID to selectively and potently block α4β2 nAChRs has been attempted but did not succeed, possibly resulting from imperfect GID/α4β2 complex molecular models. Although the AChBP is a structural homologue to nAChR and is typically considered as a structural surrogate of nAChR ligand binding domain, the low sequence identity (< 30%) possibly prevents from constructing a reliable α4β2 nAChR molecular model using homology modelling only. Recently, the high-resolution 3D crystal structures of $(\alpha4)_2(\beta2)_3$ and $(\alpha4)_3(\beta2)_2$ nAChR have been released (19,20), which provide an opportunity to build a more accurate molecular model of the complex between GID and α4β2 nAChR. The globular [Gla4E]GID ([Gla4E]gGID) mutant was reported to have comparable activity at rat α3β2, α4β2 and α7 nAChR to gGID (Table 5.1), and this variant was used to build the molecular models described below. The [Gla4E]gGID is referred to as the " gGID*" in the literature and this study. Likewise, the ribbon [Gla4E]GID is referred to as the " rGID*".

In this chapter, we report on the development of selective and potent α4β2 nAChR inhibitors based on the globular and ribbon GID, and guided by molecular modelling and energy calculation method. The binding modes of gGID* at α3β2, α4β2 and α7 nAChRs were built by assuming interactions at the α3(+)β2(-), α4(+)β2(-) and α7(+)α7(-) interface. As noted in Chapter 3, the ribbon α-conotoxin can bind at the α(+)α(-) interface, suggesting that the ribbon GID (rGID) could bind the $(\alpha4)_3(\beta2)_2$ nAChR at the α4(+)α4(-) interface. We therefore built a molecular model of the interaction between rGID* and $(\alpha4)_3(\beta2)_2$ nAChR at the interface between two a4 subunits, with the aim of modifying the peptide to selectively and potently inhibit $(\alpha4)_3(\beta2)_2$ nAChR. These molecular models were used to calculate the mutational energies (ΔΔG) of GID* mutants, and this analysis was used to suggest potential α4β2 nAChR inhibitors.

5.2 Materials and methods

5.2.1 Homology modelling and molecular dynamics simulation

Molecular models of the interaction between gGID* and the ECD of rat α3β2, α4β2 and α7 nAChRs were built by homology using Modeller 9v18 (21) and the following crystal structures as templates: the complex between *Aplysia californica* acetylcholine-binding protein (AChBP)

and conotoxin PnIA variant (PDB ID: 2BR8), and the human α4β2 nAChR (PDB ID: 5KXI; 6CNK; 6CNJ). The complexes between gGID* and the ECD of $(\alpha3)_2(\beta2)_3$, $(\alpha4)_2(\beta2)_3$ and $(\alpha7)_5$ nAChR were modelled by assuming an interaction at the α3(+)β2(–), α4(+)β2(–) and α7(+)α7(–) orthosteric binding sites. The complex between rGID* and the ECD of $(\alpha4)_3(\beta2)_2$ nAChR was built by assuming an interaction at the α4(+)α4(–) orthosteric binding site. Modeller 9v18 was set up to create 100 models, and the best model was selected according to the lowest DOPE score (22).

The models were refined by a 50-100 ns molecular dynamics simulation in a solution of discrete water using the GROMACS 5.1.4 package (23) and the Amber99SB-ILDN protein force field (24) using the same methods described in "Material and methods" section in Chapter 3. MD simulations were finished until the last 20 ns of the simulations was stable (60 ns for gGID*/α4β2 complex, 100 ns for gGID*/α3β2, 70 ns for gGID*/α7 complex and 50 ns for rGID*/α4β2 complex). All bonds involving hydrogen atoms were constrained with the LINCS algorithm (25) and the particle-mesh Ewald method (26) was used to compute long-range electrostatic interactions.

5.2.2 Mutational energy calculation

For energy calculation, 100 frames were extracted from each MD simulation, and the resulting structures were optimised using Foldx (http://foldx.crg.es/) *RepairPDB*. The *Buildmodel* command of Foldx was used to mutate the residues and build mutation models. The interaction energy and mutational energy of the complex between GID* and α3β2, α4β2 or α7 nAChR were calculated by the following equations: $\Delta G_{binding} = G_{complex} - (G_{receptor} + G_{ligand})$ and $\Delta\Delta G_{binding} = \Delta G_{binding}$ (mutant) – $\Delta G_{binding}$ (wildtype), which was conducted by the command *Positionscan*. The ΔΔG of each mutation is an automatic output in Foldx and generated in a separate file.

5.2.3 Analysis of energy prediction data

The experimental data and predicted ΔΔGs were divided into three classes. For experimental data, 1) decreased in activity (IC_{50} value of the mutant ≥ 8-fold of IC_{50} value of the wildtype); 2) similar activity (affinity value of the wildtype versus affinity value of a mutant is within 8-fold); 3) improved in activity (8-fold IC_{50} value of the wildtype ≤ IC_{50} value of the mutant). For the predicted ΔΔG, we binned the ΔΔG into three classes: 1) decreased in activity (ΔΔG ≥ 1

kcal/mol); 2) similar activity (-1 kcal/mol < ΔΔG < 1 kcal/mol); improved in activity (ΔΔG ≤ -1 kcal/mol).

A confusion matrix was used to analyse energy prediction data. The terms of Positive (P), Negative (N), True (T) and False (F) were defined as follow: 1) Positive: IC_{50} value of peptides decreased or showed no change in experimental data; 2) Negative: IC_{50} value of peptides increased in experimental data; 3) True: predicted mutational energies are consistent with experimental data; 4) False: predicted mutational energies are not consistent with experimental data. The mutational energy results were classified as true positives (TP), false positives (FP), true negatives (TN) and false positives (FP). By these four values, the accuracy and Matthews correlation coefficient (MCC) were calculated using the equations as below:

$$\text{Accuracy} = \frac{\mathbf{TP + TN}}{\mathbf{TP + TN + FP + FN}} \times 100\%$$

$$\text{MCC} = \frac{\mathbf{TP \times TN - FP \times FN}}{\sqrt{(\boldsymbol{TP+FP})(\boldsymbol{TP+FN})(\boldsymbol{TN+FP})(\boldsymbol{TN+FN})}}$$

5.3 Results

5.3.1 Binding modes of GID*

We here built molecular models of the interaction between the α4(+)β2(–), α3(+)β2(–), and α7(+)α7(–) binding sites and gGID* as well as interaction between the α4(+)α4(–) binding site and rGID*. These models were refined using molecular dynamics simulations and used to propose explanations for the SAR data previously published by Millard *et al.* (16). The backbone RMSD from the starting conformation was stable over the last 20 ns of the simulations and this period was referred to 'simulation time' and was used for analysis.

5.3.1.1 Binding mode of gGID* at the rat α4(+)β2(–) interface

In the previous study, the SAR experimental data of gGID* (Table 5.1) showed that R2A, D3A, N8A, P9A, R12A, N14A, N15A, O16A, H17A and V18A mutants lost activity at α4β2 nAChR by more than 8-fold (16). The molecular model of the complex between gGID* and α4(+)β2(–) binding site can be used to provide rational explanations of these data (Figure 5.2).

In the proposed model, Arg2 and Asp3 form salt bridges with α4 (+)-E191 and α4(+)-R188, respectively. Therefore, substitution of these two residues by Ala could prevent the establishment of the salt bridges, potentially resulting in a change of conformation of the tail,

which could explain why the substitution of these two residues by Ala caused a decrease in activity > 18-fold (Table 5.1). Pro9 (Corresponding to Pro 6 in most other α-conotoxins) is highly conserved among all α-conotoxins, and it is crucial for stabilising the structure of globular α-conotoxins; Substitution of Pro by an Ala typically results in a dramatic decrease in activity (27-35). In the molecular model, Arg12 is buried at the interface with the receptor and forms a salt bridge with β2 (–)-E61. Its side chain interacts within 5 Å of the M36, T59, E61, F119 and L121 of β2 (–) subunit (Distance < 5 Å is considered to be a certain contact in this study). It is therefore not surprising that the substitution of Arg by Ala caused a decrease in activity by > 18-fold (Table 5.1). Residues Asn8, Asn14 and Hyp16 established hydrogen bonds with β2 (–)-D171, α4 (+)-T150 and β2 (–)-K79, respectively. These interactions were present in 85%, 94% and 71% of the molecular dynamics simulation time, respectively. These hydrogen bonds seem to be crucial for the activity of the peptide as experimental data showed that the loss of any of these hydrogen bonds caused a significant drop in activity (Table 5.1). In the molecular model, Asn15 interacts with the C-loop disulfide bond (formed by α4 (+)-C192, and α4 (+)-C193), Glu195 and Y197. His17 contact with the C-loop disulfide bond. The sidechain of Val18 is embedded into a pocket formed by Cys5, Cys6, Arg12, Asn15, Hyp16 and His17 of gGID* as well as the C-loop disulfide bond. Substitution of Asn15, His17 and Val18 by Ala could reduce interaction between the peptide and nAChR, resulting in a decrease

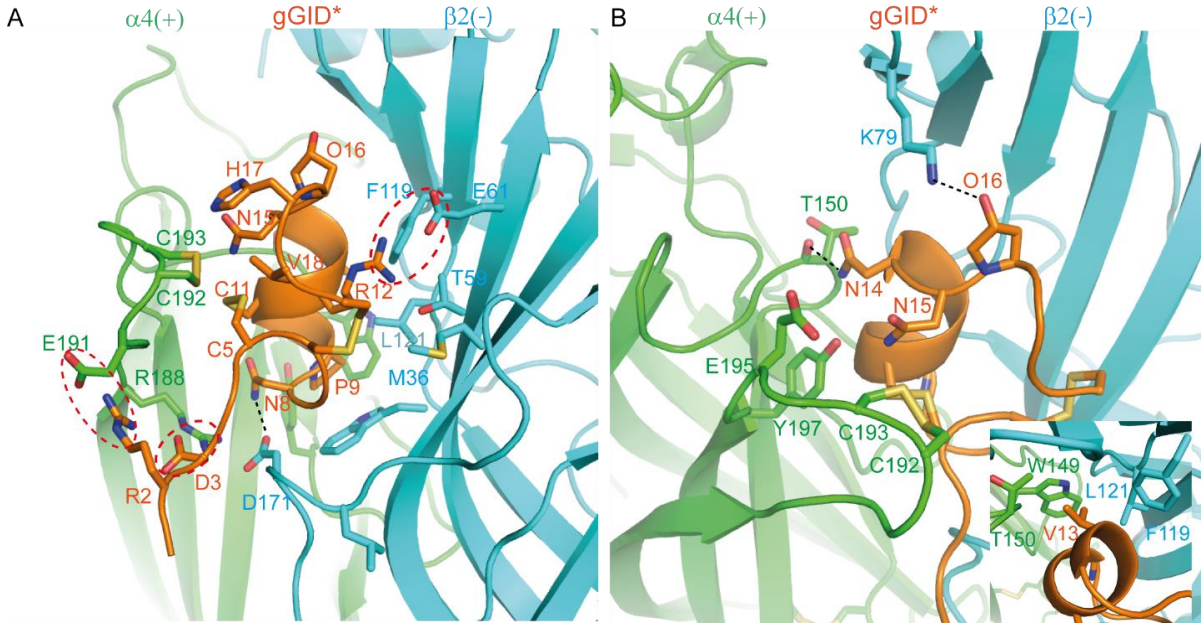

Figure 5.2 Molecular model of the complex between gGID* and α4(+)β2(-) interface. A: Interactions between the receptor and R2, D3, N8, P9, R12, H17, and V18 of gGID*; B: Interactions between the receptor and V13 (inserted figure), N14, N15 and O16 of the gGID*. Hydrogen bonds are displayed as dotted black lines. Interactions between charged side chains are circled with a dotted red line.

in activity. It is in agreement with the experimental data that N15A, H17A and V18A mutants demonstrated reduced activity compared to the parent peptide (Table 5.1). In the molecular model, the side chain of Val13 contacts α4 (+)-W149, α3 (+)-T150, β2 (–)-F119 and β2 (–)-L121, and the substitution of Val13 by Ala should result in less contact between the peptide and α4β2 nAChR, negatively impacting the activity. By contrast, the experimental data showed that the V13A mutant had comparable activity to the gGID*, suggesting that interpreting the mutational data by side chain interactions is not sufficient, as reorientation can occur in the binding pocket of the conotoxin after a side chain replacement.

5.3.1.2 Binding mode of gGID* at the rat α3(+)β2(–) interface

According to experiments (Table 5.1), the R2A, D3A, P9A and V18A mutants display decreased (> 8-fold) potency at rat α3β2 nAChR compared to gGID* (16). The molecular model (Figure 5.3A) suggests that a salt bridge is formed between the Arg2 and D171 of β2 (–) subunit. The oxygen of Asp3 forms a stable hydrogen bond (99% of the simulation time) with the nitrogen of the α3 (+) -N191 as well as consistent contact with the I188, Y190 and N191 of the α3 (+) subunit. The side chain of Val18 interacts with the disulfide bond of the C-loop. In the previously reported SAR study, the E4A, R12A, N14A and N15A mutants had no change in activity compared to gGID* (16). However, our model (Figure 5.3B) shows that Glu4 builds a hydrogen bond with α3 (+)-N191, which was stable for 98% of the simulation time. Arg12

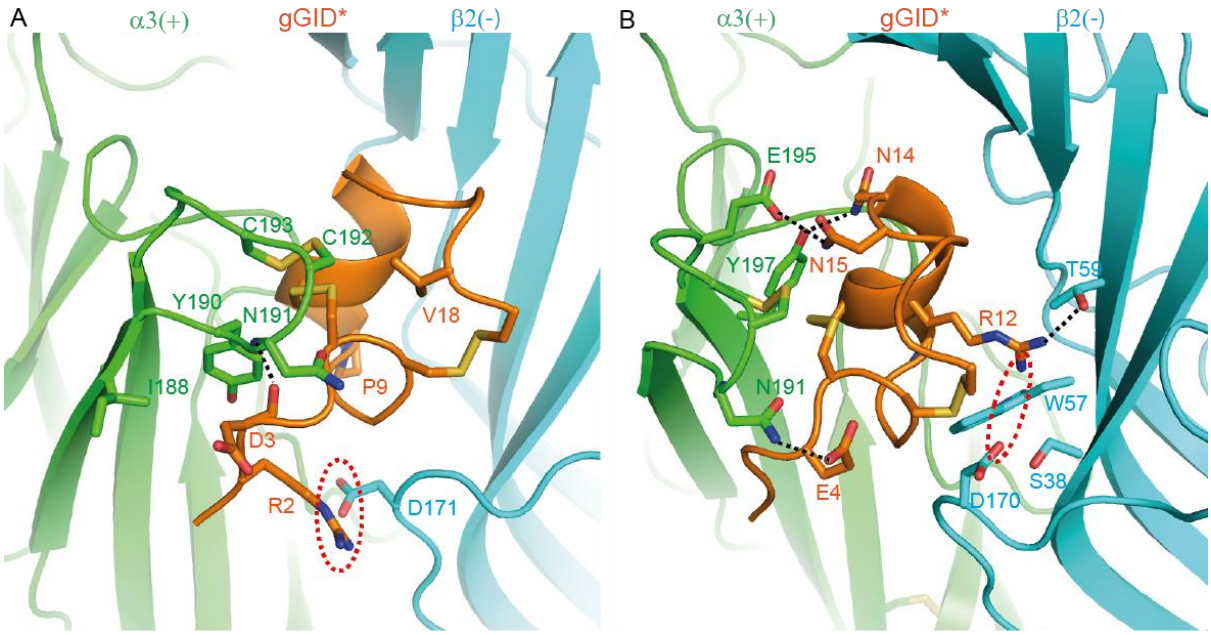

Figure 5.3 Molecular model of the complex between gGID* and α3(+)β2(-) interface. A: Interactions between the receptor and R2, D3, P9, and V18 of gGID*; B: Interactions between the receptor and E4, R12, N14, and N15 of the gGID*. Hydrogen bonds are displayed as dotted black lines. Interactions between charged side chains are circled with a dotted red line.

side chain forms an unstable hydrogen bond with β2 (–)-T59 for 41% of the simulation time and has charge interaction with β2 (–)-D170. It also contacts S38, W57 and T59 of β2 (–) subunit. Asn14 forms hydrogen bonds with α3 (+)-Y197 (94% of the simulation time) and Asn15 forms a hydrogen bond with α3 (+)-E195 (99% of the simulation time).

5.3.1.3 Binding mode of gGID* at the rat α7(+)α7(–) interface

The positions 8, 9, 12 and 14 of gGID* are the main determinants of its interaction with rat α7 nAChR according to experimental data (16). In Figure 5.4A, the molecular model shows that Asn8 constantly contacts with α7 (+)-Y93, α7 (+)-Y188 and α7 (+)-Y195. There is a hydrogen bond established between Arg12 and α7 (–)-Q57 during 79% of the simulation time and the side chain of Arg12 interacts with Q57, S59, Q117, L119 and Q161 of α7 (–) subunit. Asn14 forms two stable hydrogen bonds with α7 (+)-E193 (85% of the simulation time) and α7 (+)-Y195 (91% of the simulation time). Apart from the four positions above, experimental substitution of other positions with Ala had substitution of other positions with Ala had only a minor impact on the inhibition of rat α7 nAChR by gGID*. Nevertheless, the molecular model shows that positions 3, 15, 16 and 18 have substantial interactions with the receptor (Figure 5.4B). Specifically, the Asp3 forms a salt bridge with α7 (+)-K186. The Hyp16 forms hydrogen bonds with α7 (–)-N111 and α7 (–)-H115 during the 66% of the simulation time as well as contacting α7 (–)-N77 and α7 (–)-Q117. The Asn15 and Val18 make contact with the C-loop

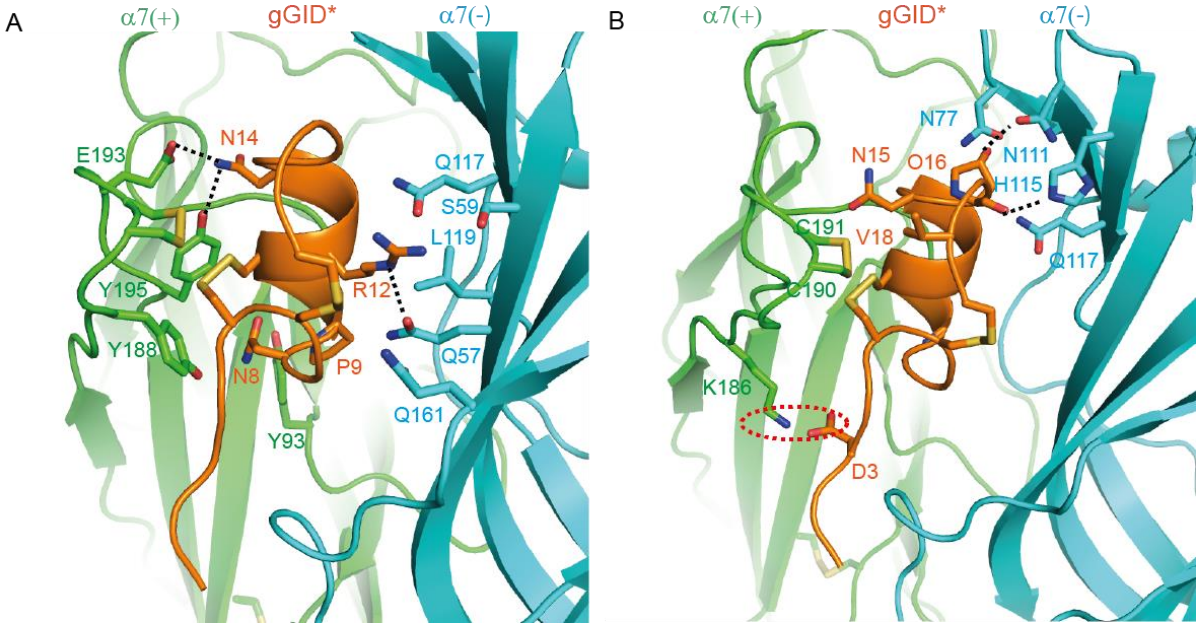

Figure 5.4 Molecular model of the complex between gGID* and α7(+)α7(-) interface. A: Interactions between the receptor and N8, P9, R12 and N14 of gGID*; B: Interactions between the receptor and D3, N15, O16 and V18 of gGID*. Hydrogen bonds are displayed as dotted black lines. Interactions between charged side chains are circled with a dotted red line.

disulfide bond. As mentioned previously, interpreting side-chain mutations using only the wild-type model is limited. The wild-type model does not compensate for energy loss by conformation change or change of binding mode, which can occur in conotoxins mutated during an Alanine scan.

5.3.1.4 Binding mode of rGID* at the human α4(+)α4(–) interface

We proposed a molecular model of the interaction of rGID* with the α4(+)α4(–) binding site to inform the design of variants that could bind at this interface. According to the molecular model of the complex between rGID* and the α4(+)α4(–) binding site (Figure 5.4 A and B), the side chain of Arg2 forms a salt bridge with α4 (–)-D166. However, Arg2 can also have an electrostatic repulsion with Arg12 of rGID*. Arg2 could possibly be used to modulate the activity of rGID* at the α4-α4 binding site. In Loop 1, Glu4 interacts with the C-loop disulfide bond as well as α4 (+)-E191. Ser7 and Asn8 contact with the α4 (–)-L168 and α4 (+)-Y93, respectively.

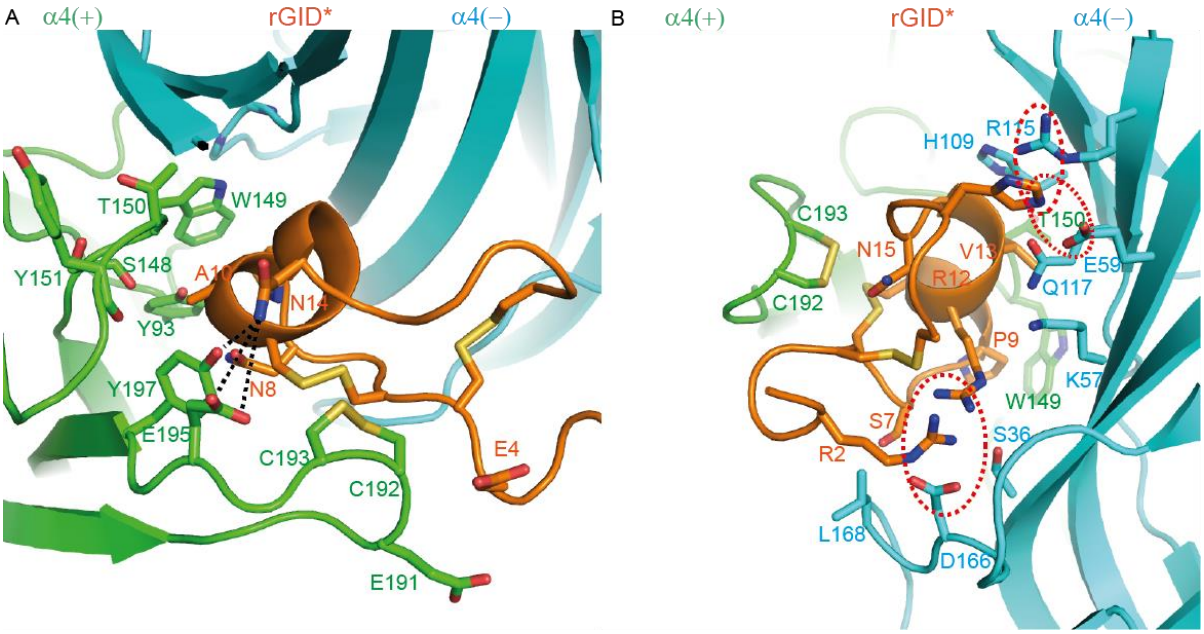

Figure 5.5 Molecular model of the complex between rGID* and α4(+)α4(-) interface. A: Interactions between the receptor and E4, N8, A10, and N14 of rGID*; B: Interactions between the receptor and R2, S7, P9, V13, N15, and H17 of gGID*. Hydrogen bonds are displayed as dotted black lines on the structure. Interactions between charged side chains are circled with a dotted red line.

As mentioned previously, Pro9 is an important compact point for globular α-conotoxins as it binds in a conserved aromatic pocket of the nAChR, which is also the binding site of Ach. Ala10 makes contact with Y93, S148, W149, T150, Y151 and Y197 of the α4 (+) subunit. In the Loop 2 of rGID*, the sidechain of Arg12 establishes attractive charge interactions with α4

(–)-D166 and contacts with α4 (–)-S36 and K57, but it also creates an electrostatic repulsion with Arg2. The sidechain of Val13 contacted α4 (+)-Y149, α4 (+)-T150, α4 (–)-H109, α4 (–)-Q117, α4 (–)-W118 and α4 (–)-T119. Asn14 forms a transient hydrogen bond with α4 (+)-E195 (42% of the simulation time) and a stable hydrogen bond with α4 (+)-Y197 (73% of the simulation time). Asn15 sits at a pocket formed by three disulfide bonds (disulfide bond of C-loop and two disulfide bonds of rGID*) which seems to maintain the conformation of the second loop of rGID* at the binding site. His17 has charge interaction with α4 (–)-E59 and α4 (–)-R115.

5.3.2 ΔΔGs prediction

5.3.2.1 Full sequence amino acid scanning of gGID* on rat α3β2, α4β2 and α7 nAChR

We have shown in Chapter 4 that Foldx gave better energy predictions than other tested methods for the α-conotoxin/AChBP complex. We therefore used Foldx to calculate ΔΔGs for gGID*/nAChR complexes. Since the four conserved cysteines and Pro9 are crucial for maintaining the gGID* structure, ΔΔGs of these five positions were not calculated, except the P9A mutation as reported in the literature (16). The ΔΔGs of 266 gGID* mutants were calculated *in silico* using rat α3β2, α4β2 and α7 nAChRs, and the resulting predicted mutational energy changes are listed in Tables 5.2 to 5.4. We also calculated the accuracy and MCC of the predicted ΔΔGs based on published experimental IC_{50}s using the confusion matrix (Table 5.5). The molecular dynamics simulations suggested that the tail of gGID* was very flexible at three binding sites, but as mentioned in Chapter 4, the core function of Foldx does not simulate backbone movement of the protein. The predictions were particularly inaccurate for mutations of position 13 (Red in Table 5.5), suggesting that the molecular models gave unreliable results at this position. We therefore excluded mutants derived from I1, R2, D3, E4 and V13 when calculating the accuracy and MCC of the predicted ΔΔGs for gGID* mutants. Our data show that the gGID*/α4β2 nAChR, gGID*/α3β2 nAChR and gGID*/α7 nAChR systems obtained an accuracy of 81.3%, 50%, 66.7% and a MCC of 0.46, 0, 0.32, respectively. Three mutants, N15K, O16A and V18N, has their ΔΔGs wrongly predicted at α4β2 nAChR. In contrast, the impact of eight mutants (N8A, A10S, R12A, N14A, N15A, N15K, N15H and O16A) was wrongly predicted for the α3β2 nAChR, and the impact of three mutants (R12A, N14A and O16A) were wrongly predicted for the α7 nAChR system (Table 5.5). These results indicate that the ΔΔGs of the 266 gGID* mutants at α4β2 nAChR, rather than α3β2 and α7 nAChR, can

be potentially used to identify novel peptides with favourable properties. Surprisingly, the mutational energy predictions suggest that the sequence of gGID* seems to be optimal for binding to α4β2 nAChR because activity could not be improved via single amino-acid substitutions. All mutations at positions 7, 8, 10, 12, 14, 15, 16, 17 and 18 in the α4β2 system were predicted to have a decrease or no change in activity compared to the parent peptide (Table 5.2). The results from Foldx suggest that it is difficult to design more selective and potent α4β2 nAChR inhibitors based on gGID, and therefore designing rGID mutants is possibly an alternative way to develop selective and potent α4β2 nAChR inhibitors.

Table 5.2 Predicted mutational energy of full sequence amino acid scanning of gGID* at the rat α4β2 nAChR (266 mutants)

	I1	**R2**	**D3**	**E4**	**S7**	**N8**	**A10**	**R12**	**V13**	**N14**	**N15**	**O16**	**H17**	**V18**
G	0.11	0.96	0.25	-0.25	0.36	2.85	1.33	3.26	2.43	1.66	3.7	0.8	1.59	2.47
A	0.11	0.77	-0.32	-0.52	-0.38	2.17	–	2.09	1.46	1.7	1.98	0.92	1.41	1.84
L	0.04	0.78	-0.29	-1.01	4.75	1.52	1.7	0.32	-0.13	0.33	0.79	0.67	0.63	1.16
V	0.06	0.97	-0.26	-0.27	2.07	2.22	0.86	2.36	–	1.9	1.5	1.45	1.3	–
I	–	0.91	-0.49	-0.54	4.07	2.9	1.51	2.07	0.41	1.56	1.19	1.23	0.83	0.87
T	0.05	0.79	-0.18	-0.3	1.01	1.2	1.17	2.91	1.54	2.12	2	1.33	1.65	2.23
S	0.08	0.8	-0.42	-0.54	–	1.51	0.74	2.58	2.43	1.88	2.43	0.78	1.46	2.9
C	0.01	0.83	-0.29	-0.63	0.63	2	0.73	2.25	1.53	1.4	1.53	1.03	1.31	1.47
M	-0.16	0.87	-0.71	-1.27	4.55	0.54	0.33	0.2	-0.68	0.51	0.42	0.3	0.34	1.1
Q	-0.22	0.43	-0.32	-1.06	6.68	4.45	1.35	1.92	1.96	0.93	1.61	0.63	0.9	2.32
N	-0.04	0.91	-0.26	-0.81	3.22	–	2.51	2.62	1.56	–	–	0.8	1.14	2.8
R	-0.74	–	-0.48	-1.71	8.66	2.15	0.48	–	3.57	1.31	0.4	-0.05	0.23	1.69
K	-0.4	0.46	-0.35	-0.53	7.42	2.55	0.73	1.15	1.3	1.13	0.65	0.37	0.4	1.68
E	0.11	0.92	-0.39	–	8.35	0	1.79	3.82	2.79	2.14	2.82	0.99	1.01	3.22
D	0.31	1.39	–	0.11	5.25	0.29	3.42	4.18	3.11	6.14	3.35	1.08	1.36	4
P	0.08	1.48	-0.89	2.51	1.53	4.45	0.08	9.23	3	3.71	6.14	0.11	2.65	2.42
W	-0.23	0.98	0.38	-1.49	27.43	1.85	7.68	3.07	4.76	1.85	1.86	0.34	0.4	8.15
Y	0.09	0.79	-0.15	-1.4	24.51	0.37	7.99	1.6	0.9	1.26	1.18	0.62	-0.18	8.07
F	0.14	0.72	-0.2	-1.31	18.27	0.06	7.02	0.86	0.1	1.2	0.93	0.2	-0.07	6.71
H	0.25	0.89	0	-1	22.9	1.53	23.7	3.05	1.93	2.05	1.14	0.87	–	8.56

Table 5.3 Predicted mutational energy of full sequence amino acid scanning of gGID* at the rat α3β2 nAChR (266 mutants)

	I1	**R2**	**D3**	**E4**	**S7**	**N8**	**A10**	**R12**	**V13**	**N14**	**N15**	**O16**	**H17**	**V18**
G	0.35	1.3	0.18	1.23	0.47	2.64	1.48	3.32	2.02	2.67	2.89	1.97	0.31	2.25
A	0.4	1.14	-0.31	0.72	0.17	2.03	-	2.16	1.2	2.3	1.52	1.51	0.18	1.34
L	-0.05	0.79	-0.7	0.25	1.38	0.16	4.22	0.34	-0.95	1.65	0.82	1.11	-0.47	0.99
V	0.36	1.19	-0.1	0.67	1.43	1.84	3.99	1.8	-	2.4	1.88	1.05	0.13	-
I	-	1.06	-0.34	0.34	1.66	1.82	5.72	1.54	-0.52	2.49	1.78	2.3	-0.22	0.38
T	0.41	1.06	0.6	0.96	1.07	0.81	3.37	2.48	1.25	2.82	2.92	2.65	0.37	1.39
S	0.47	1.06	0.13	1.14	-	1.49	1.12	2.53	1.96	2.54	2.58	1.52	0.17	1.95
C	0.32	1.06	-0.11	0.77	0.7	1.16	1.83	2.31	1.43	2.16	1.65	1.69	0.05	1.04
M	-0.28	0.72	-1.15	0.4	0.55	0.09	1.63	-0.07	2.95	1.82	0.88	0.71	-0.63	0.59
Q	0.18	0.88	-0.47	0.4	1.39	1.24	3.5	2	1.15	1.87	1.42	1.55	-0.23	1.61
N	0.39	0.64	-0.32	0.25	1.88	-	5.04	2.98	1.99	-	-	1.45	0.03	1.82
R	-0.1	-	-1.15	0.01	0.45	0.49	5.24	-	1.59	2.35	0.32	1.21	-0.61	1.2
K	-0.05	0.44	-0.84	0.19	0.32	0.8	3.49	0.87	0.26	1.75	0.67	1.25	-0.58	1.02
E	0.32	1.51	-0.25	-	2.88	0.22	4.23	3.68	1.49	3.63	3.04	2.2	-0.02	2.57
D	0.51	1.47	-	0.1	4.36	-0.82	5.65	4.81	2.79	2.79	3.95	2.98	0.39	3.9
P	0.48	1.27	-0.17	0.42	1.08	7.56	1.25	8.53	4.07	4.4	5.62	-0.17	1.01	3.39
W	0.16	1.11	-0.09	0.87	4.14	1.17	19.32	0.37	8.28	3.79	1.07	1.05	-0.49	4.72
Y	0.55	1.04	-0.35	0.32	3.16	0.27	14.22	0.54	7.23	2.73	1.37	1.82	-0.77	6.66
F	0.39	0.95	-0.2	0.22	3.24	-0.12	11.47	0.66	2.95	2.43	0.84	1.72	-0.87	4.58
H	0.48	1.21	-0.06	0.76	3.16	0.76	44.71	2.52	2.49	2.98	0.98	2.41	-	4.44

Table 5.4 Predicted mutational energy of full sequence amino acid scanning of gGID* at the rat α7 nAChR (266 mutants)

	I1	**R2**	**D3**	**E4**	**S7**	**N8**	**A10**	**R12**	**V13**	**N14**	**N15**	**O16**	**H17**	**V18**
G	0.1	0.74	1.41	0.16	0.52	2.98	0.87	1.05	2.11	1.88	1.49	1.76	0.5	1
A	0.11	0.66	0.84	-0.02	0.3	1.89	–	0.04	1.57	0.85	0.52	1.66	0.38	0.8
L	-0.03	0.02	0.05	-0.42	0.22	0.75	2.36	-0.6	-0.27	0.19	-0.45	1.26	-0.36	-0.09
V	0.1	0.8	0.62	0.29	0.48	2.69	1.32	0.28	–	2.16	0.46	2.72	0.19	–
I	–	0.4	0.19	-0.01	0.69	1.69	2.01	0.27	-0.43	2.49	0.27	2.74	-0.12	-0.2
T	0.01	0.75	0.72	0.33	0.21	2.55	1.11	1.19	0.78	1.85	1.56	1.4	0.48	0.64
S	0.02	0.64	1.13	-0.04	–	2.16	0.34	0.32	1.82	1.19	1.19	1.93	0.37	0.99
C	0.02	0.65	0.75	0.16	0.23	1.65	1.14	0.27	1.51	1.01	0.42	1.74	0.17	0.58
M	-0.19	-0.1	-0.24	-0.44	-0.3	0.35	-0.12	-0.86	0.2	0.09	-0.61	0.91	-0.58	-0.35
Q	-0.11	0.6	0.82	-0.57	1	1.6	1.53	1.08	0.99	0.62	0.87	2.06	-0.14	0.34
N	-0.08	0.72	1.25	-0.42	0.73	–	3.36	0.87	1.61	–	–	1.82	0.17	0.5
R	-0.63	–	0.93	-0.69	0.27	1.39	0.02	–	2.25	0.21	-0.68	2.99	-0.31	0.02
K	-0.29	0.18	0.73	-0.65	0.38	1.29	1.3	0.16	0.21	0.35	-0.66	2.61	-0.38	-0.07
E	-0.05	0.79	0.45	–	2.83	0.99	2.32	1.85	1.93	1.11	0.86	1.94	-0.23	0.86
D	0.09	1.17	–	0.2	2.91	1.18	3.92	1.95	2.11	2.35	1.11	2.33	0.17	1.3
P	0.11	1.05	0.05	-0.3	1.39	6.66	0.94	5.99	2.69	6.23	5.31	0.35	1.81	2.92
W	-0.11	0.74	2.32	-0.05	1.35	1.5	13.07	0.51	3.76	4.52	0.02	2.21	-0.63	0.78
Y	0.11	0.48	1.55	-0.36	0.7	0.42	11.55	0.74	3.49	4.73	-0.63	2.12	-0.85	0.78
F	0.03	0.43	1.41	-0.49	0.23	-0.15	11.31	-0.19	1.36	3.19	-0.82	1.48	-0.94	0.13
H	-0.14	0.46	5.05	-0.24	1.23	1.1	18.9	1.57	2.31	6.08	0.01	2.87	–	0.35

Table 5.5 Fold change in IC_{50} values of mutants *versus* wild type for gGID* and predicted mutational energy (ΔΔG). IC_{50} values were taken from Millard *et al.* (16) and Banerjee *et al.* (17). The ΔΔGs of gGID* mutants were calculated using Foldx on 100 frames extracted from MD simulations. TP: True positive; TN: True negative; FP: False positive; FN: False negative.

	α4β2 nAChR			α3β2 nAChR			α7 nAChR		
Position	Fold change	Foldx		Fold change	Foldx		Fold change	Foldx	
S7A	7.6	-0.38	TP	0.9	0.17	TP	2.2	0.3	TP
N8A	>17.6	2.17	TN	1.4	2.03	FN	> 10	1.89	TN
P9A	>17.6	2.89	TN	59.5	2.56	TN	15.3	2.53	TN
A10S	0.8	0.74	TP	6.4	1.12	FN	–	–	–
A10T	>20.8	1.17	TN	>2777.8	3.37	TN	–	–	–
R12A	>17.6	2.09	TN	3.6	2.16	FN	8.3	0.04	FP
V13A	2	1.46	FN	0.2	1.21	FN	1.9	1.57	FN
V13F	>20.8	0.1	FP	111.1	2.95	TN	–	–	–
V13W	>20.8	4.76	TN	>2777.8	8.28	TN	–	–	–
V13L	>20.8	-0.13	FP	>2777.8	-0.95	FP	–	–	–
V13I	1.3	0.41	TP	3.6	-0.52	TP	–	–	–
V13S	1	2.43	FN	0.4	1.96	FN	–	–	–
V13T	1.2	1.54	FN	1.3	1.25	FN	–	–	–
N14A	>17.6	1.7	TN	0.4	2.28	FN	8.7	0.85	FP
N15A	>17.6	1.98	TN	1.1	1.52	FN	1	0.52	TP
N15K	>20.8	0.65	FP	>2777.8	0.67	FP	–	–	–
N15H	>20.8	1.14	TN	44.4	0.98	FP	–	–	–
O16A	10.6	0.92	FP	4.7	1.51	FN	2.2	1.66	FN
H17A	10.6	1.41	TN	0.9	0.18	TP	0.8	0.38	TP
V18A	>17.6	1.84	TN	14.1	1.34	TN	1.3	0.8	TP
V18Y	>20.8	8.07	TN	>2777.8	6.66	TN	–	–	–
V18Q	>20.8	2.32	TN	>2777.8	1.61	TN	–	–	–
V18N	0.4	2.8	FN	>2777.8	1.82	TN	–	–	–
Accuracy	81.3%			50%			66.7%		
MCC	0.46			0			0.32		

5.3.2.2 Full sequence amino acid scanning of rGID* on human $(\alpha4)_3(\beta2)_2$ nAChR

Using the molecular model of the complex between rGID* and $(\alpha4)_3(\beta2)_2$ nAChR, the ΔΔGs of a library of 285 rGID* mutants were calculated in silico (Table 5.6). The mutants with ΔΔG values ≤ -1 kcal/mol were assumed to increase activity significantly. The computations suggest that there are no gGID* mutations of positions 4, 17 and 18 that can increase affinity at α4β2 nAChR (Table 5.2). By contrast, these same positions of rGID* have the potential to be mutated to increase affinity at $(\alpha4)_3(\beta2)_2$ nAChR. Specifically, the gGID* ΔΔGs results

Table 5.6 Full sequence amino acid scanning of rGID* at the human α4β2 nAChR

	I1	R2	D3	E4	S7	N8	P9	A10	R12	V13	N14	N15	O16	H17	V18
G	-0.18	0.99	0.09	0.1	0.14	2.19	5.01	1.34	1.6	1.69	0.68	2.05	2.22	0.05	0.5
A	-0.17	0.86	-0.18	-0.27	-0.7	0.99	3.35	–	0.75	0.89	0.25	0.69	1.87	0.11	0.22
L	0.08	0.27	-0.69	-0.8	-1.01	-0.54	7.69	1.99	0.17	-0.38	-0.64	0.33	1.79	0.07	-0.6
V	0.19	1.19	0.4	0.28	-0.8	0.63	4.19	1.62	1.18	–	0.75	0.77	2.36	0.78	0
I	–	0.74	-0.07	-0.14	0.05	0.55	5.68	3.09	0.94	0.03	0.48	1.98	2.09	0.6	-0.4
T	-0.03	1.2	0.59	0.28	0.22	1.06	4.71	2.26	1.66	1.39	0.64	1.63	2.45	0.79	0.27
S	-0.11	1.11	0.05	0.05	–	1.73	4.64	1.04	0.85	1.46	0.47	1.59	2.1	0.21	0.26
C	-0.02	1.1	0.13	-0.01	-0.5	1.08	4.7	1.04	1.01	0.83	0.18	0.77	2.17	0.42	0.06
M	-0.15	0.21	-0.73	-0.77	-1.02	-0.63	5.83	-0.3	-0.4	-0.63	-0.3	-0.5	1.69	-0.1	-0.9
Q	-0.14	0.62	-0.39	-0.25	0.69	0.66	8.09	1.97	1.05	1.2	0.47	1.3	2.02	0.08	-0.2
N	-0.18	0.95	-0.01	0.23	0.62	–	6.52	3.06	1.1	1.48	–	–	2.2	0.12	0.06
R	-0.17	–	-0.7	-0.77	2.54	0.23	9.69	1.03	–	1.52	0.31	2.62	1.74	0.21	-0.4
K	-0.22	0.63	-0.67	-0.87	0.94	0.49	9.5	1.53	0.43	0.82	0.06	1.75	1.68	0.18	-0.5
E	-0.1	0.38	-0.49	–	2.04	0.28	8.1	2.75	1.97	1.83	1.23	2.53	1.87	-0.3	-0.1
D	-0.03	1.21	–	0.72	1.67	-0.13	6.84	4.11	2.39	1.9	0.88	1.37	1.92	-0.1	0.07
P	0.21	0.38	-1.02	0.88	-1.7	-0.25	–	2.18	6.8	0.84	3.12	6.22	0.02	-1.03	0.82
W	0.18	0.54	-0.58	-0.24	9.03	-0.54	20.9	5.79	0.32	3.41	1.91	10	2.18	0.22	-0.4
Y	0.28	0.42	-0.61	-0.65	6.66	-0.42	19.3	5.71	1.09	2.09	0.98	8.18	1.84	0.11	-0.4
F	0.25	0.44	-0.66	-0.82	5.63	-0.54	17.6	4.76	0.56	0.14	0.8	7.01	1.65	0.02	-0.9
H	0.26	1.14	-0.02	0.21	13.4	1.19	27.9	29.2	1.46	1.23	1.49	13.5	2.25	–	0.16

show that the S7L, S7M, S7P, H17P and V18F mutants are 4.75, 4.55, 1.53, 2.65 and 6.71 Kcal/mol (Tble 5.2), indicating these gGID* mutants lose their activity. The corresponding values for rGID* are -1.01, -1.02, -1.7, -1.03 and -0.9 Kcal/mol (Table 5.6), suggesting these rGID*mutants can have significantly improved activity. Therefore, [S7L]rGID*, [S7M]rGID*, [S7P]rGID*, [H17P]rGID* and [V18F]rGID* are valuable candidates for future synthesis and biological activity test. The results here further suggest that optimising rGID could be a potential method to design selective and potent α4β2 nAChR inhibitors.

5.4 Discussion

In this study, we computationally investigated several variants of globular and ribbon GID*, which could be designed to selectively and potently inhibit α4β2 nAChR. Four molecular models of GID* bound to α3β2, α4β2 and α7 nAChRs were built, which were used to calculate mutational energies. Some mutants of rGID* were identified as potential candidates for improving $(\alpha4)_3(\beta2)_2$ nAChR stoichiometry inhibitors according to the ΔΔG results by targeting the α4-α4 binding site.

5.4.1 A suitable template can improve the quality of a molecular model

The molecular models were built using a crystal structure of human α4β2 nAChR as a template. The molecular model of gGID*/rat α4β2 nAChR complex provided reasonable explanations to experimental mutational data. Correlation of Foldx ΔΔG computations with experimental activity was also reasonably good. By contrast, the predictive power of the two other models involving α3β2 and α7 nAChRs was poorer, possibly arising from a lower quality of homology models. Human α4 has 97.61%, 60.77% and 44.93 % sequence identity with rat α4, α3 and α7, respectively, while human β2 has 98.56% sequence identity with rat β2. Accordingly, the crystal structure of human α4β2 nAChR is an ideal template for the construction of rat α4β2 nAChR, but it is not as accurate for building models of the rat α3β2 and α7 nAChR. The human α4 subunit and the rat α3 subunit display some difference of sequence that could lead to a different conformation of the binding site. For example, residues His186, I188, N191, Glu194 and Gln198 of rat α3 (+) correspond to Asn186, Arg188, Glu191, Ala194 and Pro198 of the human α4 (+) subunit, and these positions are located in the C-loop and possibly influence its conformation. Therefore using human α4 subunit as a template to build a homology model of rat α3 subunit likely results in a Loop C with inaccurate conformation, affecting the binding of gGID* at the α3(+)β2(-) pocket. In agreement with this analysis, a previous study also

concluded that selecting a suitable template is crucial for reliable molecular models of the complex between α4β2 nAChR and α-conotoxins (36).

5.4.2 The N- or C-terminal tail of the α-conotoxin can modulate activity on nAChRs

Most α-conotoxins do not bind to α4β2 nAChR (11,37). A previous study found that the α4 (+)-Arg188 (α4 (+)-Arg185 in that study) prevents α-conotoxins binding to α4β2 nAChR (36). Compared with other α-conotoxins, GID has a longer N-terminal tail. As described in the results section, the α4 (+)-Arg188 interacts with the unusual N-terminal tail of gGID* (Figure 5.2A), showing that the N-terminal tail is vital for gGID* activity at α4β2 nAChR (16). Additionally, Ala substitution or deletions in the tail significantly decreased activity at α3β2, α4β2 and α7 nAChRs (16). These observations illustrate that the N-terminal tail is involved in modulating the activity of gGID* on α3β2, α4β2 and α7 nAChRs. Several other α-conotoxins also have an extended N- or C-terminal tail, such as AnIB (15), LsIA (38), and Lo1a (39). Like GID, the tail of these conotoxins was found to be involved in modulating the activity of these peptides (15,38,39). For example, AnIB inhibited the α7 nAChR with IC_{50} of 76 nM, but deletion of a Gly in the N-terminal tail caused a loss of activity (15). The truncation of the N-terminal tail of LsIA resulted in a drop ~10-fold in activity at α3β2 nAChR (38). By contrast, truncation of the C-terminus of Lo1a result in an increased activity by ~ 4000-fold at α7 nAChR (39). Studying the mechanism of how modifications to N- or C- termini affect the activity of these peptides could help design more potent and selective nAChR antagonists.

5.4.3 Potential $(\alpha4)_3(\beta2)_2$ nAChR inhibitors suggested by Foldx

The virtual screen of 266 gGID* point mutants did not indicate any novel peptides with increased binding affinity for the α4β2 nAChR. This result is consistent with experimental mutational studies, which did not create a globular α-conotoxin GID* variant that would potently block α4β2 nAChR (16-18). Alternative methods include mutating gGID* using non-natural amino acids, which has been used to increase the activity of α-conotoxin PnIA at α7 nAChR (40). Design of ribbon α-conotoxins is an underexploited strategy with the potential to influence the inhibition of nAChRs (41).

The ΔΔG results of rGID* indicate that the S7L, S7M, S7P, H17P and V18F mutants are attractive candidates for future studies with human $(\alpha4)_3(\beta2)_2$ nAChR. In the molecular model of rGID*/$(\alpha4)_3(\beta2)_2$ nAChR (Figure 6.5), the Ser7 of rGID* only makes contact with α4 (-)-

L168. Hence the substitution with Leu, Met or Pro would possibly increase interaction with other residues of the α4 (–) subunit. His17 and Val18 are in the second loop, which could result in conformational changes upon mutation of the peptide (42). Substitution of H17 by Pro and Val18 by Phe could result in conformational changes increasing contact of the second loop with the receptor, significantly increasing activity.

In summary, we built a reliable molecular model of the gGID*/rat α4β2 nAChR complex and showed that it is important to choose a suitable template to construct the α-conotoxin/nAChR homology model. We demonstrated how the tail endows gGID* the ability to interact with rat α4β2 nAChR. Additionally, some rGID* mutants were identified, with potential to be developed into more selective and potent inhibitors of the $(\alpha4)_3(\beta2)_2$ nAChR.

5.5 References

1. Gonzales, D., Rennard, S. I., Nides, M., Oncken, C., Azoulay, S., Billing, C. B., Watsky, E. J., Gong, J., Williams, K. E., and Reeves, K. R. (2006) Varenicline, an alpha4beta2 nicotinic acetylcholine receptor partial agonist, vs sustained-release bupropion and placebo for smoking cessation: a randomized controlled trial. *Jama* **296**, 47-55
2. Crunelle, C. L., Miller, M. L., Booij, J., and van den Brink, W. (2010) The nicotinic acetylcholine receptor partial agonist varenicline and the treatment of drug dependence: a review. *Eur. Neuropsychopharmacol.* **20**, 69-79
3. Picciotto, M. R., Caldarone, B. J., Brunzell, D. H., Zachariou, V., Stevens, T. R., and King, S. L. (2001) Neuronal nicotinic acetylcholine receptor subunit knockout mice: physiological and behavioral phenotypes and possible clinical implications. *Pharmacol. Ther.* **92**, 89-108
4. Rueter, L. E., Donnelly-Roberts, D. L., Curzon, P., Briggs, C. A., Anderson, D. J., and Bitner, R. S. (2006) A-85380: A pharmacological probe for the preclinical and clinical investigation of the alpha4beta2 neuronal nicotinic acetylcholine receptor. *CNS. Drug. Rev.* **12**, 100-112
5. Zwart, R., and Vijverberg, H. P. (1998) Four pharmacologically distinct subtypes of alpha4beta2 nicotinic acetylcholine receptor expressed in Xenopus laevis oocytes. *Mol. Pharmacol* **54**, 1124-1131
6. Moroni, M., Zwart, R., Sher, E., Cassels, B. K., and Bermudez, I. (2006) Alpha4beta2 nicotinic receptors with high and low acetylcholine sensitivity: pharmacology, stoichiometry, and sensitivity to long-term exposure to nicotine. *Mol. Pharmacol.* **70**, 755-768
7. Mazzaferro, S., Bermudez, I., and Sine, S. M. (2017) Alpha4beta2 nicotinic acetylcholine receptors: relationship between subunit stoichiometry and function at the single channel level. *J. Biol. Chem.* **292**, 2729-2740
8. Son, C. D., Moss, F. J., Cohen, B. N., and Lester, H. A. (2009) Nicotine normalizes intracellular subunit stoichiometry of nicotinic receptors carrying mutations linked to autosomal dominant nocturnal frontal lobe epilepsy. *Mol. Pharmacol.* **75**, 1137-1148
9. Weltzin, M. M., Lindstrom, J. M., Lukas, R. J., and Whiteaker, P. (2016) Distinctive effects of nicotinic receptor intracellular-loop mutations associated with nocturnal frontal lobe epilepsy. *Neuropharmacology* **102**, 158-173

10. Arthur, D., and Levin, E. D. (2002) Chronic inhibition of alpha4beta2 nicotinic receptors in the ventral hippocampus of rats: impacts on memory and nicotine response. *Psychopharmacology* **160**, 140-145
11. Lebbe, E. K., Peigneur, S., Wijesekara, I., and Tytgat, J. (2014) Conotoxins targeting nicotinic acetylcholine receptors: an overview. *Mar. Drugs.* **12**, 2970-3004
12. Cartier, G. E., Yoshikami, D., Gray, W. R., Luo, S., Olivera, B. M., and McIntosh, J. M. (1996) A new alpha-conotoxin which targets alpha3beta2 nicotinic acetylcholine receptors. *J. Biol. Chem.* **271**, 7522-7528
13. Nicke, A., Loughnan, M. L., Millard, E. L., Alewood, P. F., Adams, D. J., Daly, N. L., Craik, D. J., and Lewis, R. J. (2003) Isolation, structure, and activity of GID, a novel alpha 4/7-conotoxin with an extended N-terminal sequence. *J. Biol. Chem.* **278**, 3137-3144
14. McIntosh, J. M., Dowell, C., Watkins, M., Garrett, J. E., Yoshikami, D., and Olivera, B. M. (2002) Alpha-conotoxin GIC from *Conus geographus*, a novel peptide antagonist of nicotinic acetylcholine receptors. *J. Biol. Chem.* **277**, 33610-33615
15. Loughnan, M. L., Nicke, A., Jones, A., Adams, D. J., Alewood, P. F., and Lewis, R. J. (2004) Chemical and functional identification and characterization of novel sulfated alpha-conotoxins from the cone snail *Conus anemone*. *J. Med. Chem.* **47**, 1234-1241
16. Millard, E. L., Nevin, S. T., Loughnan, M. L., Nicke, A., Clark, R. J., Alewood, P. F., Lewis, R. J., Adams, D. J., Craik, D. J., and Daly, N. L. (2009) Inhibition of neuronal nicotinic acetylcholine receptor subtypes by alpha-conotoxin GID and analogues. *J. Biol. Chem.* **284**, 4944-4951
17. Banerjee, J., Yongye, A. B., Chang, Y. P., Gyanda, R., Medina-Franco, J. L., and Armishaw, C. J. (2014) Design and synthesis of alpha-conotoxin GID analogues as selective alpha4beta2 nicotinic acetylcholine receptor antagonists. *Biopolymers* **102**, 78-87
18. Leffler, A. E., Kuryatov, A., Zebroski, H. A., Powell, S. R., Filipenko, P., Hussein, A. K., Gorson, J., Heizmann, A., Lyskov, S., Tsien, R. W., Poget, S. F., Nicke, A., Lindstrom, J., Rudy, B., Bonneau, R., and Holford, M. (2017) Discovery of peptide ligands through docking and virtual screening at nicotinic acetylcholine receptor homology models. *Proc. Natl. Acad. Sci. U. S. A.* **114**, E8100-E8109
19. Morales-Perez, C. L., Noviello, C. M., and Hibbs, R. E. (2016) X-ray structure of the human alpha4beta2 nicotinic receptor. *Nature* **538**, 411-415

20. Walsh, R. M., Jr., Roh, S. H., Gharpure, A., Morales-Perez, C. L., Teng, J., and Hibbs, R. E. (2018) Structural principles of distinct assemblies of the human alpha4beta2 nicotinic receptor. *Nature* **557**, 261-265
21. Šali, A., and Blundell, T. L. (1993) Comparative protein modelling by satisfaction of spatial restraints. *J. Mol. Biol.* **234**, 779-815
22. Shen, M. y., and Sali, A. (2006) Statistical potential for assessment and prediction of protein structures. *Protein Sci.* **15**, 2507-2524
23. Abraham, M. J., Murtola, T., Schulz, R., Páll, S., Smith, J. C., Hess, B., and Lindahl, E. (2015) GROMACS: High performance molecular simulations through multi-level parallelism from laptops to supercomputers. *SoftwareX* **1-2**, 19-25
24. Lindorff-Larsen, K., Piana, S., Palmo, K., Maragakis, P., Klepeis, J. L., Dror, R. O., and Shaw, D. E. (2010) Improved side-chain torsion potentials for the Amber ff99SB protein force field. *Proteins* **78**, 1950-1958
25. Hess, B., Bekker, H., Berendsen, H. J., and Fraaije, J. G. (1997) LINCS: a linear constraint solver for molecular simulations. *J. Comput. Chem.* **18**, 1463-1472
26. Darden, T., York, D., and Pedersen, L. (1993) Particle mesh Ewald: An N· log (N) method for Ewald sums in large systems. *J. Chem. Phys* **98**, 10089-10092
27. Yu, R., Kompella, S. N., Adams, D. J., Craik, D. J., and Kaas, Q. (2013) Determination of the alpha-conotoxin Vc1.1 binding site on the alpha9alpha10 nicotinic acetylcholine receptor. *J. Med. Chem.* **56**, 3557-3567
28. Grishin, A. A., Cuny, H., Hung, A., Clark, R. J., Brust, A., Akondi, K., Alewood, P. F., Craik, D. J., and Adams, D. J. (2013) Identifying key amino acid residues that affect alpha-conotoxin AuIB inhibition of alpha3beta4 nicotinic acetylcholine receptors. *J. Biol. Chem.* **288**, 34428-34442
29. Servent, D., Thanh, H. L., Antil, S., Bertrand, D., Corringer, P.-J., Changeux, J.-P., and Ménez, A. (1998) Functional determinants by which snake and cone snail toxins block the alpha7 neuronal nicotinic acetylcholine receptors. *J. Physiol.(Paris)* **92**, 107-111
30. Everhart, D., Cartier, G. E., Malhotra, A., Gomes, A. V., McIntosh, J. M., and Luetje, C. W. (2004) Determinants of potency on alpha-conotoxin MII, a peptide antagonist of neuronal nicotinic receptors. *Biochemistry* **43**, 2732-2737
31. Quiram, P. A., and Sine, S. M. (1998) Structural elements in alpha-conotoxin ImI essential for binding to neuronal alpha7 receptors. *J. Biol. Chem.* **273**, 11007-11011
32. Hone, A. J., Ruiz, M., Scadden, M., Christensen, S., Gajewiak, J., Azam, L., and McIntosh, J. M. (2013) Positional scanning mutagenesis of alpha-conotoxin PeIA

identifies critical residues that confer potency and selectivity for alpha6/alpha3beta2beta3 and alpha3beta2 nicotinic acetylcholine receptors. *J. Biol. Chem.* **288**, 25428-25439

33. McIntosh, J. M., Azam, L., Staheli, S., Dowell, C., Lindstrom, J. M., Kuryatov, A., Garrett, J. E., Marks, M. J., and Whiteaker, P. (2004) Analogs of alpha-conotoxin MII are selective for alpha6-containing nicotinic acetylcholine receptors. *Mol. Pharmacol.* **65**, 944-952
34. Jacobsen, R. B., DelaCruz, R. G., Grose, J. H., McIntosh, J. M., Yoshikami, D., and Olivera, B. M. (1999) Critical residues influence the affinity and selectivity of alpha-conotoxin MI for nicotinic acetylcholine receptors. *Biochemistry* **38**, 13310-13315
35. Wu, Y., Zhangsun, D., Zhu, X., Kaas, Q., Zhangsun, M., Harvey, P. J., Craik, D. J., McIntosh, J. M., and Luo, S. (2017) Alpha-conotoxin [S9A]TxID potently discriminates between alpha3beta4 and alpha6/alpha3beta4 nicotinic acetylcholine receptors. *J. Med. Chem.* **60**, 5826-5833
36. Beissner, M., Dutertre, S., Schemm, R., Danker, T., Sporning, A., Grubmuller, H., and Nicke, A. (2012) Efficient binding of 4/7 alpha-conotoxins to nicotinic alpha4beta2 receptors is prevented by Arg185 and Pro195 in the alpha4 subunit. *Mol. Pharmacol.* **82**, 711-718
37. Kaas, Q., Westermann, J. C., Halai, R., Wang, C. K., and Craik, D. J. (2008) ConoServer, a database for conopeptide sequences and structures. *Bioinformatics (Oxford, England)* **24**, 445-446
38. Inserra, M. C., Kompella, S. N., Vetter, I., Brust, A., Daly, N. L., Cuny, H., Craik, D. J., Alewood, P. F., Adams, D. J., and Lewis, R. J. (2013) Isolation and characterization of alpha-conotoxin LsIA with potent activity at nicotinic acetylcholine receptors. *Biochem. Pharmacol.* **86**, 791-799
39. Lebbe, E. K., Peigneur, S., Maiti, M., Devi, P., Ravichandran, S., Lescrinier, E., Ulens, C., Waelkens, E., D'Souza, L., Herdewijn, P., and Tytgat, J. (2014) Structure-function elucidation of a new alpha-conotoxin, Lo1a, from *Conus longurionis*. *J. Biol. Chem.* **289**, 9573-9583
40. Hopping, G., Wang, C. I., Hogg, R. C., Nevin, S. T., Lewis, R. J., Adams, D. J., and Alewood, P. F. (2014) Hydrophobic residues at position 10 of alpha-conotoxin PnIA influence subtype selectivity between alpha7 and alpha3beta2 neuronal nicotinic acetylcholine receptors. *Biochem. Pharmacol.* **91**, 534-542

41. Grishin, A. A., Wang, C. I., Muttenthaler, M., Alewood, P. F., Lewis, R. J., and Adams, D. J. (2010) Alpha-conotoxin AuIB isomers exhibit distinct inhibitory mechanisms and differential sensitivity to stoichiometry of alpha3beta4 nicotinic acetylcholine receptors. *J. Biol. Chem.* **285**, 22254-22263

42. Wu, X., Tae, H.-S., Huang, Y.-H., Adams, D. J., Craik, D. J., and Kaas, Q. (2018) Stoichiometry dependent inhibition of rat α3β4 nicotinic acetylcholine receptor by the ribbon isomer of alpha-conotoxin AuIB. *Biochem. Pharmacol.* **155**, 288-297

Chapter 6: Conclusions and future directions

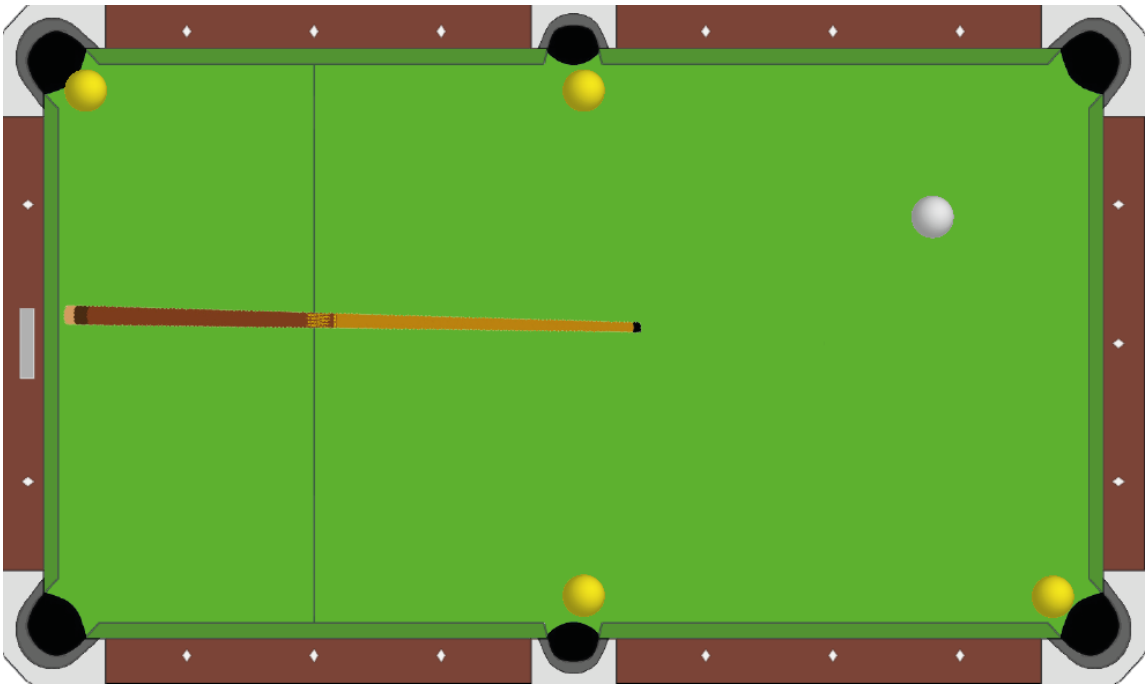

6.1 Conclusions

All subtypes of nAChRs have attracted considerable attention over the last few decades because they are involved in various physiological diseases (1,2). It is essential to understand the physiological roles played by nAChRs, requiring the development of selective molecular probes for each nAChR subtype. In pursuit of this goal, the toxins from marine cone snails are an important resource to discover and develop nAChR selective probes (3,4).

The largest characterised pharmacological class of conotoxins is the α-conotoxin, most of which display a cysteine Framework I. Framework I is characterised by two disulfide bonds with the first two hemi-cysteines (I and II) being adjacent along the sequence. Cysteine Framework I conotoxins can have three different disulfide-connected isomers: globular (Cys I-III, Cys II-IV), ribbon (Cys I-IV, Cys II-III) and bead (Cys I-II, Cys III-IV). The globular and ribbon α-conotoxins inhibit nAChR subtypes, having potential in the development of novel drugs (5-9). This thesis focused on the molecular design of ribbon α-conotoxins for therapeutic applications.

Ribbon αO-conotoxin GeXIVA inhibits the rat and human α9α10 nAChR with IC_{50}s of 7 nM and 47.3 nM, respectively. Despite this high potency, the therapeutic potential of GeXIVA is limited. Like most peptides, it is susceptible to proteolytic degradation and is challenging to synthesise in high yield. Chapter 2 discusses backbone cyclisation as a strategy to improve the folding yield and increase the serum stability, while preserving activity of ribbon GeXIVA at the α9α10 nAChR. Specifically, five cyclisation linkers were designed using molecular modelling. Conotoxin GeXIVA was cyclised using the short linker GG (hereafter named GeXIVA_GG) and synthesised using Fmoc-based solid phase synthesis. The yield through this method (8.6%) was 17-fold higher than the uncyclised ribbon GeXIVA obtained by two-step oxidation. The cyclic ribbon GeXIVA_GG maintained activity (IC_{50}=37.6 ± 4.9 nM) on human α9α10 nAChR compared to the parent peptide (IC_{50}=35.1 ± 2.7 nM). Additionally, cyclic ribbon GeXIVA_GG improved stability by 13% in human serum compared to the three isomers of GeXIVA.

Previous electrophysiological experiments of α-conotoxin AuIB indicated that ribbon AuIB (rAuIB) binds to the α3(+)α3(−) interface at the α3β4 nAChR ligand binding domain. This interface is displayed by the $(\alpha3)_3(\beta4)_2$ nAChR stoichiometry but not by $(\alpha3)_2(\beta4)_3$, which is

not targeted by rAuIB (10). In Chapter 3, The SAR of rAuIB at α3(+)α3(–) interface was investigated by successively mutating each non-Cys residue of rAuIB to Ala. At 1 μM (corresponding to the reported IC_{50} of rAuIB [10]), all rAuIB mutants exhibited activity comparable to the parent peptide except for [S4A] and [F9A]rAuIB, which caused 25% and 20% inhibition, respectively, indicating that positions 4 and 9 are the major determinants of the activity of rAuIB at $(\alpha3)_3(\beta4)_2$ nAChR. Secondary Hα chemical shifts of rAuIB and its mutants suggested that the S4A and F9A mutants have a similar structure to the rAuIB, indicating loss of activity is not due to a change of structure. Interestingly, the [P7A]rAuIB variant adopts a different fold displaying similar secondary Hα chemical shifts to globular AuIB. Globular AuIB has an α-helix between Pro6 and Phe9, therefore it is likely [P7A]rAuIB demonstrates this feature as well.

Chapter 3 discusses the binding mode of rAuIB at α3(+)α3(–) interface using mutational data. This binding mode is similar to that of globular α-conotoxins: the first loop of rAuIB binds to the aromatic box, similar to that of gAuIB. Slight differences occur in the second loop and terminus of rAuIB: these have different orientations and interactions in the binding site to those of gAuIB. According to the model, the substitution of Ser4 by Ala would cause the loss of two weak hydrogen bonds. The F9A mutant has fewer contacts with the receptor compared with the parent peptide, with a decrease of 194 $Å^2$ in the buried surface area. The knowledge obtained from this study can be used to guide the design of ribbon α-conotoxins to inhibit nAChR subtypes. Similar to globular α-conotoxins, residues in the second loop of ribbon α-conotoxins interact with a different area on each nAChR subtype, offering the opportunity to design subtype-selective inhibitors.

Several challenges limit the development of α-conotoxins to become drugs. For example, some α-conotoxins are active at rat nAChRs but not at human nAChRs. The selectivity of wild-type α-conotoxins for a target nAChR subtype also needs to be improved (11-14). The rational design of selective human nAChR subtype inhibitors based on α-conotoxins is challenging (10,15-18). Computational energy calculation methods have been used to design highly selective and potent α-conotoxins inhibiting human nAChR subtypes (16). In Chapter 4, four methods (BeAtMuSic, Foldx, CG_US and MMPBSA/MMGBSA) were benchmarked to discover the optimal computational approach to rationally design α-conotoxins. The recently published crystal structures of the Ls-AChBP/α-conotoxin LsIA and Ac-AChBP/α-conotoxin

LvIA complexes as well as the associated experimental affinities of LsIA and LvIA mutants provide an ideal case scenario for testing these methods (19,20). The best method was Foldx, which reached 87.5% in accuracy and achieved a 0.75 Mathews Correlation Coefficient (MCC). Notably, Foldx was successful at predicting mutations with an increased or a decreased affinity for the receptor (See Chapter 5 for details of Foldx applied to design selective and potent α4β2 nAChR inhibitors). Therefore this method should be useful for designing selective inhibitors of human nAChR subtypes based on α-conotoxins.

The α4β2 nAChR is the most abundant and widely distributed neuronal nAChR. It is involved in nicotine addiction (21,22), epilepsy (23), and Parkinson's and Alzheimer's diseases (24). This receptor exists as two major stoichiometries, $(\alpha4)_3(\beta2)_2$ and $(\alpha4)_2(\beta2)_3$, which have distinct functional properties (25). No conotoxin to date has been identified to selectively block α4β2 nAChR, which would have therapeutic applications for addiction. Nevertheless, some conotoxins, such as α-conotoxin GID, block α4β2 nAChR but are also more potent antagonists of other nAChR subtypes, such as α3β2 and α7 nAChRs. In Chapter 5, globular and ribbon α-conotoxin GID variants are investigated to selectively block the α4β2 nAChR stoichiometries using a combination of molecular modelling and energy calculation methods.

Using the experimental structures of human $(\alpha4)_2(\beta2)_3$ and $(\alpha4)_3(\beta2)_2$ nAChR as templates, we built molecular models of the interaction between the α4(+)β2(−), α3(+)β2(−), and α7(+)α7(−) binding sites and gGID* as well as interaction between the α4(+)α4(−) binding site and rGID*. The molecular model of the gGID*/rat α4β2 nAChR complex seems to correlate with experiments, as it can rationally explain experimental SAR data, suggesting that it has reasonable accuracy. By contrast, the molecular models of gGID* at rat α3β2 and α7 nAChR could only be partially explained using experimental SAR data. Foldx was used to predict the impact of a complete scanning (i.e. mutations in all amino acids of every non-cysteine position) of GID in the context of the four molecular systems mentioned above. The accuracy and MCC of calculated ΔΔGs for the experimentally validated mutants were 81.3% and 0.46 as a function of the published experimental data for the gGID*/rat α4β2 nAChR complex. The corresponding values for the gGID*/rat α3β2 nAChR complex and the gGID*/rat α7 nAChR complex were only 50% and 0, 55.6% and 0.32, respectively, confirming that these models are not accurate enough to predict the impact of mutations using Foldx. Foldx-predicted ΔΔG results showed that the activity of gGID* at α4β2 nAChR cannot be improved using any

mutation, whereas the [S7L]rGID*, [S7M]rGID*, [S7P]rGID*, [H17P]rGID* and [V18F]rGID* were suggested to have favourable properties to inhibit human $(\alpha4)_3(\beta2)_2$ nAChR.

6.2 Future directions

Overall, this project was very successful in providing new insights into conotoxin structure-activity relationships. However, in any project there are always new directions that are identified for future studies and some suggestions for areas worthy of investigation are given below.

6.2.1 To investigate the physiological role of α3β4 nAChR stoichiometries and in disease states

The role of the two stoichiometries of α3β4 nAChR, i.e. $(\alpha3)_3(\beta4)_2$ and $(\alpha3)_2(\beta4)_3$ nAChRs, has not yet been investigated. rAuIB has been reported to only target the $(\alpha3)_3(\beta4)_2$ nAChR. In Chapter 3, the binding mode of rAuIB at $(\alpha3)_3(\beta4)_2$ nAChR was modelled, which could be used to design more potent $(\alpha3)_3(\beta4)_2$ nAChR inhibitors based on rAuIB. The rationally designed more-potent rAuIB variants could then be used to identify α3β4 nAChR stoichiometries and their involvement in diseases.

6.2.2 Biological activity of rGID* variants at nAChR subtypes

In Chapter 5, the ΔΔG results for rGID* indicated that the S7L, S7M, S7P, H17P and V18F mutants should have activity at the α4(+)α4(−) binding site of the human $(\alpha4)_3(\beta2)_2$ nAChR. It would therefore be interesting to measure the biological activity of these rGID* variants at the two main stoichiometries of α4β2 nAChR and other nAChR subtypes.

6.2.3 Biological activity test for ribbon α-conotoxins at different receptors or ion channels

A recent study showed that globular α-conotoxin Lt1.3 blocks α3β2 nAChR but the ribbon Lt1.3 inhibits $GABA_B$ receptor-coupled Cav2.2 (26). Another α-conotoxin, ImI, is a potent inhibitor of α7 nAChR but was also shown to have weak inhibitory activity at the $GABA_A$ receptor (27). Hence, it would be interesting to test rAuIB as well as rGID at different receptors such as $GABA_A$ and $GABA_B$.

6.3 Concluding remarks

In summary, the application of a range of biochemical methods in this thesis has proven that the ribbon α-conotoxin can be engineered with favourable properties. The use of a multi-faceted computational and biochemical approach has assisted in understanding how the ribbon α-conotoxin interacts with nAChRs. The benchmark of energy prediction methods has enabled to design ribbon α-conotoxin mutants rationally. The design of ribbon α-conotoxin GID has shown that the ribbon α-conotoxin has potential to be engineered as specific nAChR inhibitors. The overall findings of this thesis will facilitate for future studies of the establishment of the role of specific nAChR stoichiometries in disease states, and the development of the ribbon scaffold as a drug template for pharmaceutical applications in the future. Ribbon isomers should therefore be more systematically considered in the design of molecular probes and specific inhibitors of nAChR subtypes based on α-conotoxins.

6.4 References

1. Gotti, C., Clementi, F., Fornari, A., Gaimarri, A., Guiducci, S., Manfredi, I., Moretti, M., Pedrazzi, P., Pucci, L., and Zoli, M. (2009) Structural and functional diversity of native brain neuronal nicotinic receptors. *Biochem. Pharmacol.* **78**, 703-711
2. Albuquerque, E. X., Pereira, E. F., Alkondon, M., and Rogers, S. W. (2009) Mammalian nicotinic acetylcholine receptors: from structure to function. *Physiol. Rev.* **89**, 73-120
3. Akondi, K. B., Muttenthaler, M., Dutertre, S., Kaas, Q., Craik, D. J., Lewis, R. J., and Alewood, P. F. (2014) Discovery, synthesis, and structure-activity relationships of conotoxins. *Chem. Rev.* **114**, 5815-5847
4. McIntosh, J. M., Santos, A. D., and Olivera, B. M. (1999) *Conus* peptides targeted to specific nicotinic acetylcholine receptor subtypes. *Annu. Rev. Biochem.* **68**, 59-88
5. Lebbe, E. K., Peigneur, S., Wijesekara, I., and Tytgat, J. (2014) Conotoxins targeting nicotinic acetylcholine receptors: an overview. *Mar. Drugs.* **12**, 2970-3004
6. Dutton, J. L., Bansal, P. S., Hogg, R. C., Adams, D. J., Alewood, P. F., and Craik, D. J. (2002) A new level of conotoxin diversity, a non-native disulfide bond connectivity in alpha-conotoxin AuIB reduces structural definition but increases biological activity. *J. Biol. Chem.* **277**, 48849-48857
7. Wu, Y., Wu, X., Yu, J., Zhu, X., Zhangsun, D., and Luo, S. (2014) Influence of disulfide connectivity on structure and bioactivity of alpha-conotoxin TxIA. *Molecules* **19**, 966-979
8. Kasheverov, I. E., Zhmak, M. N., Fish, A., Rucktooa, P., Khruschov, A. Y., Osipov, A. V., Ziganshin, R. H., D'hoedt, D., Bertrand, D., Sixma, T. K., Smit, A. B., and Tsetlin, V. I. (2009) Interaction of alpha-conotoxin ImII and its analogs with nicotinic receptors and acetylcholine-binding proteins: additional binding sites on Torpedo receptor. *J. Neurochem.* **111**, 934-944
9. Lebbe, E. K., Peigneur, S., Maiti, M., Mille, B. G., Devi, P., Ravichandran, S., Lescrinier, E., Waelkens, E., D'Souza, L., Herdewijn, P., and Tytgat, J. (2014) Discovery of a new subclass of alpha-conotoxins in the venom of *Conus australis*. *Toxicon* **91**, 145-154
10. Grishin, A. A., Wang, C. I., Muttenthaler, M., Alewood, P. F., Lewis, R. J., and Adams, D. J. (2010) Alpha-conotoxin AuIB isomers exhibit distinct inhibitory mechanisms and

differential sensitivity to stoichiometry of alpha3beta4 nicotinic acetylcholine receptors. *J. Biol. Chem.* **285**, 22254-22263

11. Inserra, M. C., Kompella, S. N., Vetter, I., Brust, A., Daly, N. L., Cuny, H., Craik, D. J., Alewood, P. F., Adams, D. J., and Lewis, R. J. (2013) Isolation and characterization of alpha-conotoxin LsIA with potent activity at nicotinic acetylcholine receptors. *Biochem. Pharmacol.* **86**, 791-799
12. Luo, S., Zhangsun, D., Zhu, X., Wu, Y., Hu, Y., Christensen, S., Harvey, P. J., Akcan, M., Craik, D. J., and McIntosh, J. M. (2013) Characterization of a novel alpha-conotoxin TxID from *Conus textile* that potently blocks rat alpha3beta4 nicotinic acetylcholine receptors. *J. Med. Chem.* **56**, 9655-9663
13. Nicke, A., Loughnan, M. L., Millard, E. L., Alewood, P. F., Adams, D. J., Daly, N. L., Craik, D. J., and Lewis, R. J. (2003) Isolation, structure, and activity of GID, a novel alpha 4/7-conotoxin with an extended N-terminal sequence. *J. Biol. Chem.* **278**, 3137-3144
14. Franco, A., Kompella, S. N., Akondi, K. B., Melaun, C., Daly, N. L., Luetje, C. W., Alewood, P. F., Craik, D. J., Adams, D. J., and Mari, F. (2012) RegIIA: an alpha4/7-conotoxin from the venom of *Conus regius* that potently blocks alpha3beta4 nAChRs. *Biochem. Pharmacol.* **83**, 419-426
15. Halai, R., Clark, R. J., Nevin, S. T., Jensen, J. E., Adams, D. J., and Craik, D. J. (2009) Scanning mutagenesis of alpha-conotoxin Vc1.1 reveals residues crucial for activity at the alpha9alpha10 nicotinic acetylcholine receptor. *J. Biol. Chem.* **284**, 20275-20284
16. Yu, R., Kompella, S. N., Adams, D. J., Craik, D. J., and Kaas, Q. (2013) Determination of the alpha-conotoxin Vc1.1 binding site on the alpha9alpha10 nicotinic acetylcholine receptor. *J. Med. Chem.* **56**, 3557-3567
17. Azam, L., and McIntosh, J. M. (2012) Molecular basis for the differential sensitivity of rat and human alpha9alpha10 nAChRs to alpha-conotoxin RgIA. *J. Neurochem.* **122**, 1137-1144
18. Cuny, H., Kompella, S. N., Tae, H. S., Yu, R., and Adams, D. J. (2016) Key structural determinants in the agonist binding loops of human beta2 and beta4 nicotinic acetylcholine receptor subunits contribute to alpha3beta4 subtype selectivity of alpha-conotoxins. *J. Biol. Chem.* **291**, 23779-23792
19. Xu, M., Zhu, X., Yu, J., Yu, J., Luo, S., and Wang, X. (2017) The crystal structure of Ac-AChBP in complex with alpha-conotoxin LvIA reveals the mechanism of its selectivity towards different nAChR subtypes. *Protein Cell.* **8**, 1-11

20. Abraham, N., Healy, M., Ragnarsson, L., Brust, A., Alewood, P. F., and Lewis, R. J. (2017) Structural mechanisms for alpha-conotoxin activity at the human alpha3beta4 nicotinic acetylcholine receptor. *Sci. Rep.* **7**, 45466

21. Gonzales, D., Rennard, S. I., Nides, M., Oncken, C., Azoulay, S., Billing, C. B., Watsky, E. J., Gong, J., Williams, K. E., and Reeves, K. R. (2006) Varenicline, an alpha4beta2 nicotinic acetylcholine receptor partial agonist, *vs* sustained-release bupropion and placebo for smoking cessation: a randomized controlled trial. *Jama* **296**, 47-55

22. Crunelle, C. L., Miller, M. L., Booij, J., and van den Brink, W. (2010) The nicotinic acetylcholine receptor partial agonist varenicline and the treatment of drug dependence: a review. *Eur. Neuropsychopharmacol.* **20**, 69-79

23. Picciotto, M. R., Caldarone, B. J., Brunzell, D. H., Zachariou, V., Stevens, T. R., and King, S. L. (2001) Neuronal nicotinic acetylcholine receptor subunit knockout mice: physiological and behavioral phenotypes and possible clinical implications. *Pharmacol. Ther.* **92**, 89-108

24. Rueter, L. E., Donnelly-Roberts, D. L., Curzon, P., Briggs, C. A., Anderson, D. J., and Bitner, R. S. (2006) A-85380: A pharmacological probe for the preclinical and clinical investigation of the alpha4beta2 neuronal nicotinic acetylcholine receptor. *CNS. Drug. Rev.* **12**, 100-112

25. Mazzaferro, S., Bermudez, I., and Sine, S. M. (2017) Alpha4beta2 nicotinic acetylcholine receptors: relationship between subunit stoichiometry and function at the single channel level. *J. Biol. Chem.* **292**, 2729-2740

26. Chen, J., Liang, L., Ning, H., Cai, F., Liu, Z., Zhang, L., Zhou, L., and Dai, Q. (2018) Cloning, synthesis and functional characterization of a novel alpha-conotoxin Lt1.3. *Mar. Drugs.* **16**, 112

27. Kudryavtsev, D. S., Shelukhina, I. V., Son, L. V., Ojomoko, L. O., Kryukova, E. V., Lyukmanova, E. N., Zhmak, M. N., Dolgikh, D. A., Ivanov, I. A., Kasheverov, I. E., Starkov, V. G., Ramerstorfer, J., Sieghart, W., Tsetlin, V. I., and Utkin, Y. N. (2015) Neurotoxins from snake venoms and alpha-conotoxin ImI inhibit functionally active ionotropic gamma-aminobutyric acid (GABA) receptors. *J. Biol. Chem.* **290**, 22747-22758